Solution Reactivity Studies of Group 15 Zintl Anions Towards Unsaturated Substrates

Robert Turbervill

Wadham College

University of Oxford

A thesis submitted for the degree of

Doctor of Philosophy

Hilary 2014

ABSTRACT

Solution Reactivity Studies of Group 15 Zintl Anions Towards Unsaturated Substrates

Robert Turbervill — Wadham College

DPhil Inorganic Chemistry — Hilary 2014

This thesis describes selected reactivity studies of group 15 Zintl anion $[E_7]^{3-}$ (E = P, As) derived cages towards a series of unsaturated organic molecules. The synthesis and characterization of forty-two compounds derived from $[E_7]^{3-}$ cages are detailed herein.

A high yielding procedure for the synthesis of $[HE_7]^{2-}$ (E = P, As) from the K_3E_7 Zintl phase has been developed. This solves prior issues with poor solubility and variable purity of the Zintl phases. The conditions required for the deprotonation of the phosphorus congener to $[P_7]^{3-}$ are described.

The reactivity of both $[P_7]^{3-}$ and $[HP_7]^{2-}$ towards carbon dioxide and isolobal isocyanates and carbodiimides was explored. This yielded a series of monofunctionalized $[E_7R]^{2-}$ cages, via a net hydropnictination of a C=N double bond of the organic substrate. The protonation chemistry of these anions was further investigated, resulting in the formation of the protic $[HP_7C(NHDipp)(NDipp)]^-$ cluster. This anion is capable of further hydrophosphination chemistry to give a series of difunctionalized heptaphosphide cages.

The reaction of $[E_7]^{3-}$ with alkynes results in the formation of the relatively unusual 1,2,3-tripnictolide anions. A series of such anions have been prepared, encompassing all of the previously reported anions and several novel species. Investigation of the coordination properties of these cyclopentadienyl analogues shows that they are superior π acceptor ligands.

A synthetic route to $[P_5]^-$ as a compositionally pure solid, and some initial studies on its protonation chemistry are also additionally presented.

ACKNOWLEDGEMENTS

The three years that have gone by while I pursued my D.Phil. have been hugely enjoyable, in no small part due to the fantastic people by whom I have been surrounded. Firstly, I want to thank my supervisor, Dr. Jose Goicoechea. It sounds clichéd, but without his boundless enthusiasm, guidance, support, and encouragement the last few years wouldn't have been the same. His taste in music isn't all that awful either.

I must thank my fellow D.Phil. students in the group. It was great to share the lab with you. Dr. Binbin Zhou initially taught me how to do synthetic chemistry during the final year of my undergraduate course. Dr. Mark Irwin couldn't have been a better fumehood neighbour – I have fond memories of late nights spent doing chemistry and listening to loud electronic music. Dr. Caroline Knapp initiated the phosphorus project in the Goicoechea group and we shared several long, delayed journeys to conferences together! Gaby Espinoza Quintero was a breath of fresh air into the lab, and is directly responsible for introducing several "Mexicanisms" into my vocabulary. Andy Jupp deserves an extra acknowledgement for proofreading this thesis in its entirety, but also for being an adequate neighbour this last year. I wish Andy and Gaby the best of luck in the rest of their D.Phil. studies.

Several undergraduate students I supervised contributed work directly to this research, namely Andy, Phil, Doruk and Bethan. Pete, Becca and Jordan worked with me as well, albeit on different projects, which made for a pleasant change of pace. The other undergraduate students I didn't supervise made the lab an enjoyable and lively place to work in, and so I must thank Belinda, CJ, Joe, Amy, Charlie, Laurence, Izzy and Ben for this.

I additionally want to mention and thank the following people outside the Goicoechea group: Dr Nick Rees for his NMR expertise and always entertaining basement radio station. Dr Josh Bates for chats about phosphorus chemistry and many, many lunches. Mike Kelly, Hasna Zaher, and Tobias Krämer for the pub trips and gossip.

I would like to thank my family, and in particular my parents. Despite not knowing much about what I have been up to in the laboratory, they were always interested to hear about it. Their support has been constant and unwavering.

Finally, I need to thank Melissa Raybould for putting up with me when I got grumpy. I'm very glad she stuck around.

LIST OF ABBREVIATIONS

12-crown-4	1,4,7,10-tetraoxacyclododecane
15-crown-5	1,4,7,10,13-pentaoxacyclopentadecane
18-crown-6	1,4,7,10,13,16-hexaoxacyclooctadecane
2,1,1-crypt	4,7,13,18-tetraoxa-1,10-diazabicyclo[8.5.5]eicosane
2,2,1-crypt	4,7,13,16,21-pentaoxa-1,10-diazabicyclo[8.8.5]tricosane
2,2,2-crypt	4,7,13,16,21,24-hexaoxa-1,10-diazabicyclo[8.8.8]hexacosane
Å	angstrom
Ad	1-adamantyl
Ar^F	3,5-bis(trifluoromethyl)phenyl (3,5-$(CF_3)_2C_6H_3$)
av	average (mean)
BDE	bond dissociation energy
Bn	benzyl
CAAC	cyclic (alkyl)(amino)carbene
calc	calculated
CCD	charge-coupled device
CDC	carbonyl-decorated carbene
cm^{-1}	wavenumber
COD	1,5-cyclooctadiene
COSY	correlation spectroscopy
cov	covalent
Cp	cyclopentadienyl or cyclopentadienide
Cy	cyclohexyl
d	doublet

Da	Dalton
DCM	dichloromethane
DFT	density functional theory
Dipp	2,6-diisopropylphenyl (2,6-$^{i}Pr_2C_6H_3$)
DME	dimethoxyethane
DMF	*N*,*N*-dimethylformamide
e^-	electron
Elec	electrophile
en	ethylenediamine
ESI	electrospray-ionization
ESR	electron spin resonance
Et	ethyl
exp	experimental
GPa	gigapascal
Hex	hexyl
HMQC	heteronuclear multiple quantum coherence
HOMO	highest occupied molecular orbital
Hz	hertz
^{i}Bu	isobutyl
^{i}Pr	isopropyl
IPr	1,3-bis(2,6-diisopropylphenyl)-imidazol-2-ylidene
IR	infrared
J	coupling constant
K	kelvin
KHMDS	potassium bis(trimethylsilyl)amide

kJ	kilojoule
LUMO	lowest occupied molecular orbital
M	molar
m	mass
m	multiplet
MAO	methylaluminoxane
Me	methyl
MeCN	acetonitrile
mes	mesityl (2,4,6-$Me_3C_6H_2$)
mes*	supermesityl (2,4,6-$^tBu_3C_6H_2$)
mg	milligram
mL	millilitre
mol	mole
MS	mass spectrometry
^{n}Bu	n-butyl
NHC	*N*-heterocyclic carbene
NICS	nucleus independent chemical shift
NMR	nuclear magnetic resonance
^{n}Pr	n-propyl
Nuc	nucleophile
OTf	trifluoromethanesulfonate (CF_3SO_3)
Ph	phenyl
ppm	parts per million
PXRD	powder X-ray diffraction
py	pyridine

s	singlet
SA	sequestering agent
sept	septet
SIPr	1,3-bis(2,6-diisopropylphenyl)-4,5-dihydroimidazol-2-ylidene
t	triplet
^{t}Bu	tertiary-butyl
THF	tetrahydrofuran
TMEDA	tetramethylethylenediamine
tol	toluene
UV	ultraviolet
z	charge
δ	chemical shift
ε	dielectric constant
μL	microlitre
γ	gyromagnetic ratio

CONTENTS

LIST OF COMPOUNDS

1 $[HP_7]^{2-}$

2 $[HAs_7]^{2-}$

3 $[P_7]^{3-}$

4 $[P_7{-}CO_2]^{3-}$

5 $[P_7C(NHDipp)(NDipp)]^{2-}$

6 $[P_7C(NHCy)(NCy)]^{2-}$

7 $[P_7C(NH^{i}Pr)(N^{i}Pr)]^{2-}$

8 $[P_7C(O)(NHAd)]^{2-}$

9 $[As_7C(NHDipp)(NDipp)]^{2-}$

10 $[As_7C(NHCy)(NCy)]^{2-}$

11 $[As_7C(NH^{i}Pr)(N^{i}Pr)]^{2-}$

12 $[As_7C(O)(NHAd)]^{2-}$

13 $[HP_7C(NHDipp)(NDipp)]^{-}$

14 $[P_7\{C(NHDipp)(NDipp)\}_2\}^{-}$

15 $[P_7\{C(NHDipp)(NDipp)\}\{C(NHCy)(NCy)\}]^{-}$

16 $[P_7\{C(NHDipp)(NDipp)\}\{C(NH^{i}Pr)(N^{i}Pr)\}]^{-}$

17 $[P_3C_2H_2]^{-}$

18 $[As_3C_2H_2]^{-}$

19 $[P_3C_2Ph_2]^{-}$

20 $[As_3C_2Ph_2]^{-}$

21 $[P_3C_2HPh]^{-}$

22 $[As_3C_2HPh]^{-}$

23 $[P_3C_6H_4]^{-}$

24 $[Ru(\eta^5\text{-}P_3C_2H_2)\{\eta^1\text{-}CH_3C(CH_2)_2\}\{\eta^3\text{-}CH_3C(CH_2)_2\}]^-$

25 $[Ru(\eta^5\text{-}As_3C_2H_2)\{\eta^1\text{-}CH_3C(CH_2)_2\}\{\eta^3\text{-}CH_3C(CH_2)_2\}]^-$

26 $[(\eta^5\text{-}P_3C_2H_2)Mo(CO)_3]^-$

27 $[(\eta^5\text{-}As_3C_2H_2)Mo(CO)_3]^-$

28 $[(\eta^5\text{-}P_3C_2Ph_2)Mo(CO)_3]^-$

29 $[(\eta^5\text{-}As_3C_2Ph_2)Mo(CO)_3]^-$

30 $[(\eta^5\text{-}P_3C_2HPh)Mo(CO)_3]^-$

31 $[(\eta^5\text{-}As_3C_2HPh)Mo(CO)_3]^-$

32 $[P_3C_2H(2\text{-pyridyl})]^-$

33 $[\{\eta^5\text{-}P_3C_2H(2\text{-pyridyl})\}Mo(CO)_3]^-$

34 $[\{\kappa^2\text{-}P,N\text{−}P_3C_2H(2\text{-pyridyl})\}Mo(CO)_4]^-$

35 $[\{\mu\text{:}\eta^5\kappa^2\text{-}P,N\text{-}P_3C_2H(2\text{-pyridyl})\}\{Mo(CO)_3\}\{Mo(CO)_4\}]^-$

36 $[P_3C_2H\{Fe(C_5H_4)(C_5H_5)\}]^-$

37 $[As_3C_2H\{Fe(C_5H_4)(C_5H_5)\}]^-$

38 $[P_3C_2H(CH_2NH_2)]^-$

39 $[As_3C_2H(CH_2NH_2)]^-$

40 $[P_5]^-$

41 $[HP_5C_6H_{12}]$

42 $[P_5C_6H_{12}]^-$

CHAPTER ONE

Introduction

1.1 PHOSPHORUS

Phosphorus containing molecules are omnipresent in the world around us. The element has wide ranging applications in all areas of chemistry, and even more importantly is a crucial building block in every known form of life.[1,2] The industrial feedstock for phosphorus containing molecules is the phosphate containing mineral apatite ($Ca_{10}(PO_4)_6(X)_2$, X = OH, F, Cl, Br). Annually, in excess of one million tons of apatite are reduced to white phosphorus, P_4, which represents the major commercial P atom source for food, detergent, speciality chemicals and pharmaceutical applications.[3] The synthesis of organophosphorus compounds typically starts from phosphorus trichloride, formed in turn by the direct chlorination of white phosphorus. Functionalization of phosphorus trichloride can be achieved by reaction with Grignard or organolithium reagents, or by reaction with halogenated organic compounds in the presence of powerful reducing agents.[4,5] As an example, the industrial synthesis of triphenylphosphine involves the high temperature reaction of phosphorus trichloride with chlorobenzene in the presence of molten sodium metal.[6]

From both a sustainability and safety perspective, neither white phosphorus nor phosphorus trichloride are particularly palatable P atom sources for the construction of organophosphorus molecules. White phosphorus is an extremely pyrophoric, toxic substance that is notorious due to its documented use in chemical warfare.[7] Phosphorus trichloride is moisture-sensitive, highly corrosive, and very toxic. Its use as a precursor for the manufacture of chemical weapons has meant that its production is closely regulated.[8] There is therefore interest in exploiting the inherently safer allotropes of phosphorus for the manufacture of organophosphorus compounds.

1.2 Allotropy in Group 15

The lightest element of group 15, nitrogen, is exclusively known in elemental form as the dinitrogen molecule. This triply bonded diatomic features one of the strongest bonds in chemistry (941 kJ mol^{-1}).[9] In contrast, diatomic molecules for the heavier congeners are unknown under standard conditions. Diphosphorus and diarsenic, P_2 and As_2, are formed in an equilibrium process from P_4 and As_4, respectively, however significant concentrations of these species are obtained only under conditions of extreme heat (above 1100 K) or UV irradiation.[10–13] More recently, elegant work by Cummins and co-workers has shown the mild generation and trapping of diphosphorus either from a niobium complex or directly from P_4.[14,15] Carbene supported diphosphorus and diarsenic fragments have been reported by the groups of both Robinson and Bertrand.[16–18]

The reluctance for elements beyond the first row of the p-block to form (p–p)π bonds either with themselves or other elements is referred to as the so-called "double bond rule".[19] This describes the reduced importance of p–π bonding as the group is descended (bond energies N_2: 941 kJ mol^{-1}, P_2 486 kJ mol^{-1}, As_2 348 kJ mol^{-1}).[20,21] As a result, the heavier non-metallic elements of group 15 (phosphorus, arsenic and antimony) display a propensity for catenation into a multitude of interconvertible allotropic forms. Later research has shown that such elements are indeed capable of forming multiply bonded systems, but they remain relatively scarce in comparison to singly bonded systems.[22,23]

The most common, and reactive form of phosphorus is white phosphorus. This consists of discrete molecular P_4 units with a tetrahedral arrangement of singly bonded phosphorus atoms (Figure 1.1).[24] The ring strain (P–P–P angles of approximately 60º, P–P distances of approximately 2.21 Å) results in the increased reactivity relative to the other allotropes. The yellow allotrope of arsenic is known to have an analogous structure, although it is much less

stable than P_4. It is both heat- and photo-sensitive, polymerizing to the more stable grey allotrope.[25] The corresponding antimony allotrope is less stable again.[26] Upon heating white phosphorus to 250 ºC, or upon prolonged exposure to light, the tetrahedral structure is lost. A polymeric amorphous network resulting from the linkage of P_4 units by P–P bonds is formed, known as red phosphorus. Black arsenic and black antimony are thought to possess similar structures.

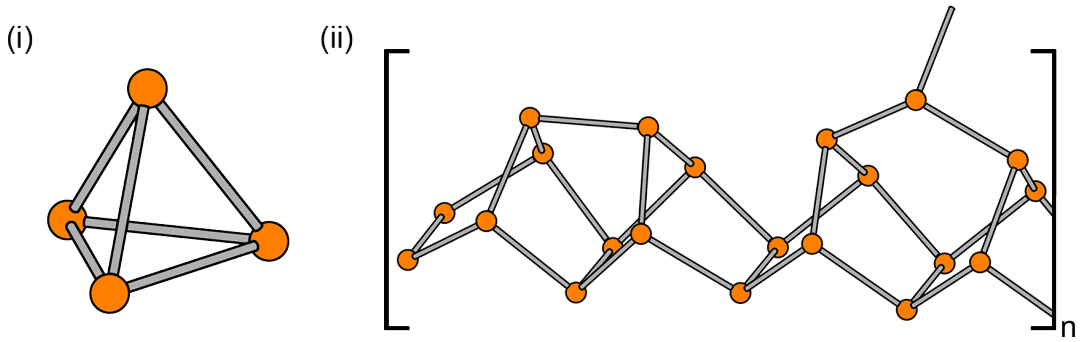

Figure 1.1: Ball and stick representations of one of the molecules found in the crystal structure of white phosphorus (i) and the repeat unit in the crystal structure of Hittorf's phosphorus (ii).[24,27]

Heating samples of red phosphorus further converts them to violet, or Hittorf's phosphorus.[27,28] This consists of alternating $[P_8]$ and $[P_9]$ units linked by pairs of P atoms to give a polymer with an overall $[P_{21}]$ repeat unit (Figure 1.1). These chains are further linked in perpendicularly aligned layers. The most thermodynamically stable allotrope of phosphorus is known as black phosphorus, formed under high pressure and temperature (Figure 1.2). Its structure consists of puckered six-membered rings, stacked in layers somewhat similarly to the structure of graphite.[29] The thermodynamically stable forms of grey arsenic and metallic antimony also adopt this structure.

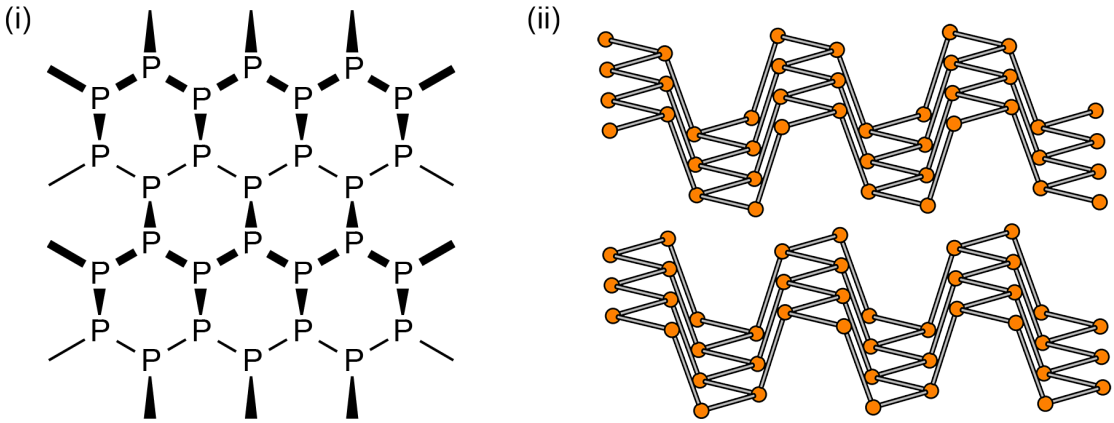

Figure 1.2: Representation of the structure of black phosphorus (i), ball and stick model of the crystal structure of black phosphorus (ii).[29,30]

Of particular note is that only white phosphorus is pyrophoric. Additionally, due to the reduced solubility that results from their polymeric structures, the other forms are much less toxic than the molecular white allotrope. This makes them inherently more attractive sources of phosphorus for synthesis, although much more forcing conditions are required for their chemical activation. Peruzzini and co-workers have recently demonstrated that the reaction of red phosphorus with water under high pressure (>0.1 GPa) and ultraviolet irradiation forms a range of oxy-acids and phosphane.[31]

1.2.1 Related Cages

Insertion of atoms into the P–P bonds of the P_4 tetrahedron gives a series of structures where the four-atom cage has been expanded. Perhaps the best known are the phosphorus oxides. Phosphorus trioxide, P_2O_3, is found as discrete P_4O_6 molecular units reminiscent of adamantane, which are derived from P_4 by insertion of an oxygen atom into each of the four P–P bonds.[28,32] Further oxidation to the pentoxide, P_4O_{10}, caps each of the phosphorus atoms with an oxygen atom.[4,28] In both of these examples, all of the P–P bonds of the tetrahedron have been broken. Many intermediate oxides and indeed chalcogenides are known with varying degrees of cage oxidation. One such compound is phosphorus

sesquisulfide, P_4S_3, with a structure similar to the hydrocarbon nortricyclane.[33,34] Isolobal replacement of S with P^- in this structure gives the heptaphosphide trianion $[P_7]^{3-}$, a polyphosphide and Zintl anion.[35,36]

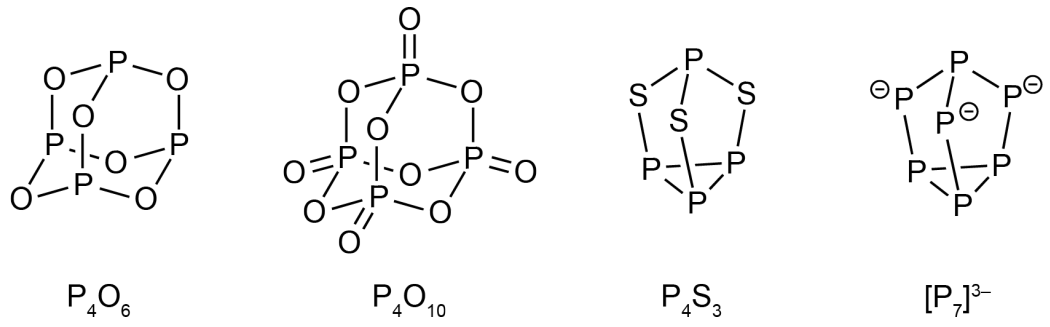

Figure 1.3: Structures adopted by P_4O_6, P_4O_{10}, P_4S_3 and $[P_7]^{3-}$.

1.3 ZINTL ANIONS

1.3.1 Historical Perspective

The first steps in Zintl anion chemistry were taken by Joannis in 1891, who observed that elemental lead could be dissolved into liquid ammonia solutions of sodium, giving rise to intensely coloured, green solutions.[37] He later showed that antimony forms yellow solutions under the same conditions, while Kraus expanded the work to tin.[38–40] The approximate stoichiometries of the solutions were determined by Smyth and Peck (2.24 atoms of Pb per Na, and 2.33 atoms of Sb per Na, respectively),[41,42] however it was not until 1931 that the identities of the anions responsible for the coloration were determined. Eduard Zintl, for whom the so-called Zintl anions would later be named, identified the $[Pb_9]^{4-}$, $[Sn_9]^{4-}$, $[Sb_7]^{3-}$ and $[As_7]^{3-}$ polyatomic anions present in the liquid ammonia solutions by the method of potentiometric titration.[43–46]

Zintl phases, intermetallic alloys formed by the high temperature reaction of s-block metals with p-block elements, contain polyatomic p-block anions. In some cases, these are cluster anions, either the same as or related to those observed in solution by Zintl. In 1970, Kummer and Diehl demonstrated that dissolution of the alloy Na_4Sn_9 into ethylenediamine resulted in the formation of the same $[Sn_9]^{4-}$ homoatomic polyanion observed by Zintl and Joannis.[47] Further advances were made when the work of Corbett and co-workers showed that addition of cation sequestering agents, in particular the cryptand 2,2,2-crypt, stabilized the resulting solutions and also allowed crystallization of the compounds for structural characterization.[48] This route, namely dissolution of precursor Zintl phases into polar, aprotic solvents (typically ammonia, ethylenediamine, pyridine or DMF) in the presence of a cation sequestering agent (cryptands or crown ethers) proved to be the most convenient way to generate stable solutions of the Zintl cluster anions for further study.[49] Initially this allowed crystallization of $[K(2,2,2\text{-crypt})]_3[Sb_7]$, but was later extended to other Zintl phases, allowing the characterization of a wealth of both homoatomic and heteroatomic polyanions (Figure 1.4).[50,51]

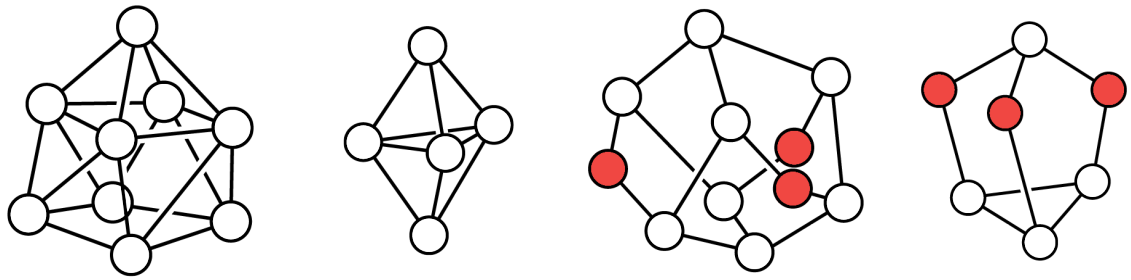

Figure 1.4: Examples of some of the structures found for Zintl anions. Atoms possessing a formal negative charge are shown in red. E′ = Si, Ge, Sn, Pb; E = P, As, Sb.

Since the entirety of the results described in this thesis derive from the reactivity of the $[E_7]^{3-}$ anions (E = P, As), the remainder of this discussion will focus exclusively on them.

There are two major groups of Zintl phases that contain the $[E_7]^{3-}$ polyanion. The A_3E_7 (A = Li, Na, K, Rb, Cs; E = P, As, Sb) phases are formed with group 1 metals,[52–56] and Ae_3E_{14} (Ae = Sr, Ba; E = P, As) are formed with group 2 metals.[57–59] In both cases, the crystal structures of the known phases contain discrete $[E_7]^{3-}$ units linked into an infinite structure by interspersed metal cations. The alkali metal containing phases are more frequently used, in particular the K_3E_7 phases. The reasons for this will be detailed in Chapter Two.

There are other reported synthetic methods to the $[E_7]^{3-}$ anions that do not require solid state chemistry and are instead entirely solution based. The most commonly cited source of $[P_7]^{3-}$ is $[Li(DME)]_3[P_7]$. This is synthesized by the nucleophilic cleavage of P_4 with $LiPH_2$ in dimethoxyethane (DME).[60] Requiring the use of both phosphane and white phosphorus, it is unsurprising that more recent work has exclusively used the Zintl phases as a starting material. An analogous route does not exist for the heavier congeners $[As_7]^{3-}$ and $[Sb_7]^{3-}$, however an alternative route involving thermolysis of heterobimetallic molecules has been detailed by Wright and co-workers.[61,62]

1.3.2 Structure and Bonding of the $[E_7]^{3-}$ Clusters

Most Zintl anions of group 14 are electron deficient, and their structure and bonding requires invocation of the Wade-Mingos rules (or more complex concepts) to rationalize adequately.[63–66] A notable exception is the $[E'_4]^{4-}$ cluster (E = Si, Ge, Sn, Pb), isoelectronic with P_4.[67–69] In contrast, the polyatomic anions of group 15 are electron precise, and their bonding can be described using the simple two-centre, two-electron bonding model.[28] In the solid state, the $[P_7]^{3-}$ cluster anion adopts a C_{3v} symmetric nortricyclane-like structure (Figure 1.5). The basal three-membered ring (P5, P6, P7) is linked by three bridging atoms (P2, P3, P4) to a single apical atom (P1). Each of the bridging atoms can be considered to carry a formal negative charge, giving the cluster an overall three minus charge.

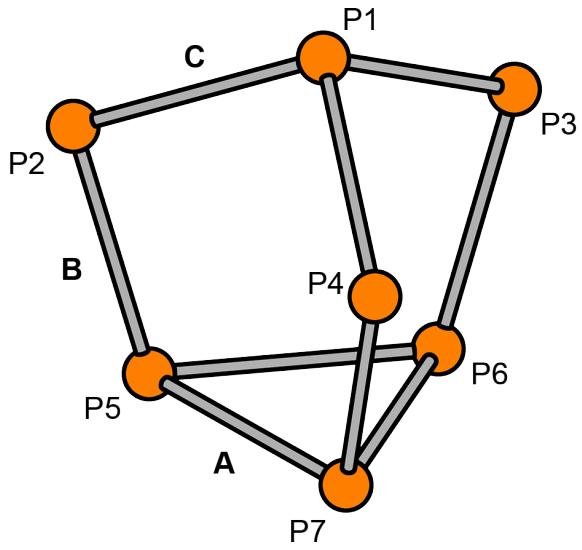

Figure 1.5: Ball and stick representation of the $[P_7]^{3-}$ anion.

Analysis of the bond distances shows that the longest bonds are found in the base of the clusters (Table 1.1). The basal P–P bond distances of 2.255(av) Å and P–P–P angles of approximately 60º in $[Li(TMEDA)]_3[P_7]$ are very similar to those observed for white phosphorus (*vide supra*) and suggest significant ring strain.[35] As would be expected, the arsenic and antimony congeners possess structures that are grossly identical, albeit with substantially lengthened bonds.[48,59]

Table 1.1: Mean bond lengths in the $[E_7]^{3-}$ clusters. Labelling refers to that used in Figure 1.5. Data taken from references 32, 45 and 46.

Bond	Mean length in $[P_7]^{3-}$ (Å)	Mean length in $[As_7]^{3-}$ (Å)	Mean length in $[Sb_7]^{3-}$ (Å)
A	2.255	2.498	2.86
B	2.150	2.399	2.70
C	2.204	2.432	2.78

The structure and dynamics of the $[P_7]^{3-}$ cluster have been extensively probed using ^{31}P NMR spectroscopy, both in solution and the solid state. At room temperature, in solution, only a very broad, non-distinct resonance is observed.[36] On heating to 50 ºC this sharpens to a singlet at –119 ppm, implying the equivalence of all seven atoms on the NMR timescale

via a fluxional process that exchanges them all. Upon cooling to –60 ºC this fluxionality is frozen out, and the spectrum reveals three multiplet resonances at –57, –103 and –162 ppm integrating in the ratio 1:3:3. These were assigned to the apical vertex, bridging vertices and basal vertices, respectively. Similar behaviour is observed in variable temperature solid state ^{31}P NMR spectroscopy on amorphous samples of $[Li(DME)]_3[P_7]$.[70] This has been attributed to a reversible valence tautomerism process analogous to the degenerate Cope rearrangement in the hydrocarbon bullvalene (Figure 1.6).[71–73] The process is undoubtedly driven by the strain inherent within the base of the cluster, and assisted by the presence of easily movable electron pairs on the bridging phosphide vertices. It seems reasonable to assume that there are analogous dynamic processes in the $[As_7]^{3-}$ and $[Sb_7]^{3-}$ clusters, although neither element has a suitable NMR active nucleus that would allow for this phenomenon to be investigated.

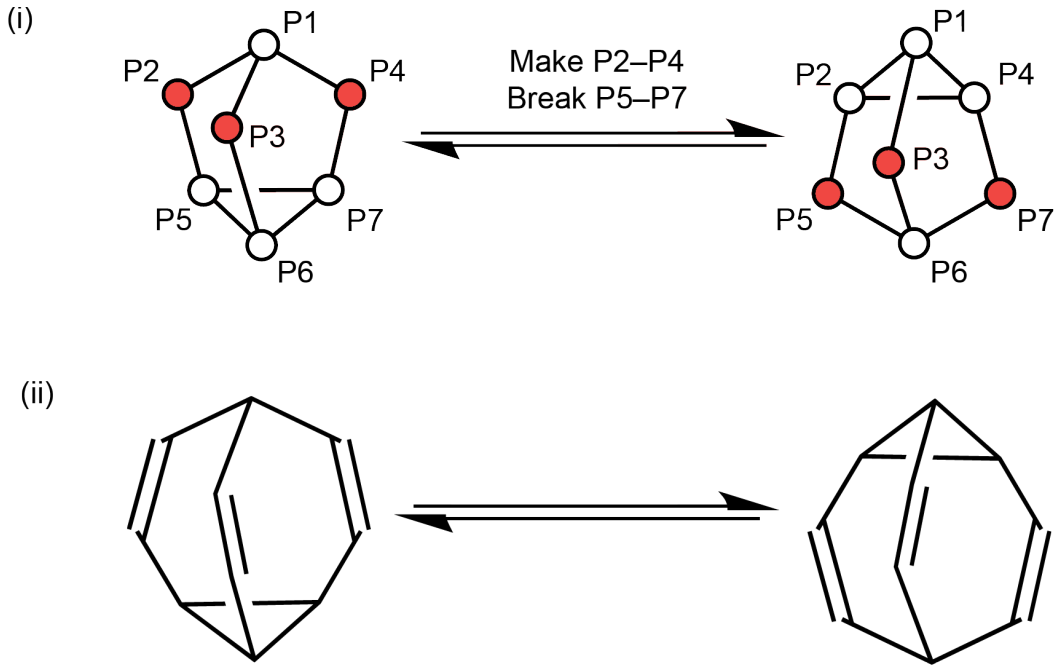

Figure 1.6: The valence tautomerism processes occurring in $[P_7]^{3-}$ (i) and the hydrocarbon bullvalene (ii). Only one such interconversion is shown – for $[P_7]^{3-}$ there are 7!/3 = 1680 valence tautomeric forms, and for bullvalene there are 10!/3 = 1,209,600.

1.4 Other Polyphosphides

The rich chain and cage chemistry of polyphosphanes and polyphosphides has been extensively studied and reviewed, primarily by the groups of Baudler and von Schnering.[36,74–76] There are two principal routes that have been taken for their synthesis: the direct combination of an alkali metal with elemental phosphorus either in solution or the solid state; or the reaction of phosphanes with elemental phosphorus under reducing or basic conditions. Depending on the exact reaction conditions and stoichiometries used, a plethora of unique polyphosphides can be synthesized, either as binary solids or solvated molecular systems. The binary systems and molecular anions are inextricably linked by both shared structural motifs and indeed the ability to extract solvated molecules from the binary phases themselves. The sheer number of known polyphosphides means that any detailed discussion is beyond the scope of this introduction, which will be limited to known polyphosphides that are frequently observed in, or derived from the chemistry of the $[P_7]^{3-}$ anion.

The synthesis of polyphosphides by the reaction of white phosphorus with alkali metals in ammonia can be considered an activation of the P_4 cage. It seems reasonable to assume that the first step is a one- or two-electron transfer, leading to the formation of an anionic or dianionic P_4 moiety. This cannot be isolated, but Baudler and co-workers reported the synthesis of $[HP_4]^-$, the first isolable reduction product, by reaction of P_4 with K/naphthalene in DME.[77] This is only stable at low temperature, decomposing to higher polyphosphides on warming. The $[HP_4]^-$ anion is likely the building block for the more aggregated polyphosphides. Using this method a wide range of polyphosphides can be synthesized and characterized. Frequently it is not possible to achieve isolation of a single polyphosphide, but instead a mixture of polyphosphides is obtained that can be enriched in

a particular species by careful tuning of reaction conditions.[78] The product distribution is particularly dependent on stoichiometry, temperature, and solvent. Low boiling point, highly polar solvents such as ammonia tend to favour the formation of relatively small polyphosphides, whereas higher boiling point or less polar solvents tend to favour the formation of more highly aggregated polyphosphides.

In addition to these reductive routes, the formation of higher nuclearity polyphosphides from the mild oxidative coupling of $[P_7]^{3-}$ is often seen. As such, it becomes useful to define an "average reduction state" of the anion simply by dividing the overall cluster charge by the number of phosphorus atoms. These are given for the anions discussed here in Table 1.2. It is important to note that these numbers should not be taken as indicative of any charge delocalization throughout these anions, which possess isolated anionic charges on the two-coordinate phosphorus atoms. Polyphosphides with charge delocalization do, however, exist and will be discussed in a later section.

Table 1.2: Charge per P atom for the anions discussed in this section shown in order of increasing cage oxidation state.

Anion	Charge per P atom
$[P_7]^{3-}$	–0.429
$[P_{14}]^{4-}$	–0.286
$[P_{21}]^{3-}$	–0.143
$[P_{16}]^{2-}$	–0.125

The hypothetical dimerization (or oxidative coupling) of two $[P_7]^{3-}$ cages by formation of a single bond between two bridging atoms gives rise to the $[P_{14}]^{4-}$ anion (Figure 1.7). Although the cage geometry is clearly related to that of $[P_7]^{3-}$, the known synthetic routes do not start from $[P_7]^{3-}$. Instead, it is formed by the reaction of lithium with white phosphorus in liquid ammonia or sodium with red phosphorus in ethylenediamine in the appropriate stoichiometric ratio.[79,80] The structure reveals the linking of two nortricyclane-

like P_7 cages in an "up-down" fashion to form the polyphosphide $[P_{14}]^{4-}$. No definitive ^{31}P NMR data exists for this anion.

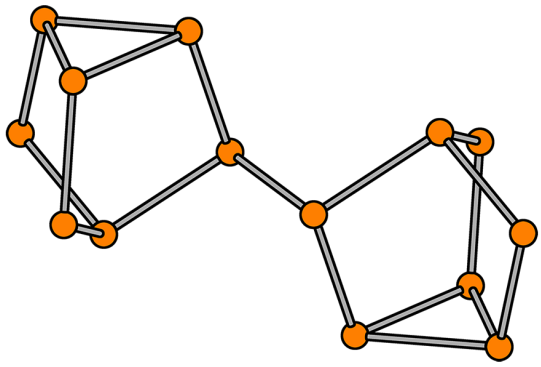

Figure 1.7: Ball and stick representation of the $[P_{14}]^{4-}$ anion.

The coupling of three $[P_7]$ cages gives rise to the $[P_{21}]^{3-}$ anion (Figure 1.8). The published synthetic route involves the reduction of white phosphorus with substoichiometric sodium in DME, although it is frequently observed in $[P_7]^{3-}$ chemistry through a mild cage oxidation process.[81] The structure is reminiscent of Hittorf's phosphorus, with linking P_2 fragments between P_7 and P_3 units. The anion possesses an extremely characteristic ^{31}P NMR spectrum, with resonances at 72, 61, –15, –108, –118, –146 and –169 ppm integrating in the ratio 2:8:2:1:2:2:4.

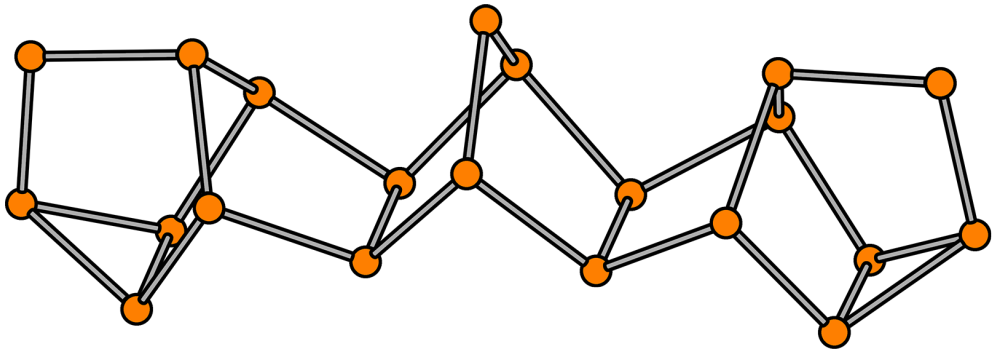

Figure 1.8: Ball and stick representation of the $[P_{21}]^{3-}$ anion.

The most oxidized polyphosphide observed in $[P_7]^{3-}$ chemistry before the ultimate oxidation to elemental phosphorus is $[P_{16}]^{2-}$. This consists of two P_7 fragments linked in an "up-up" fashion by a P_2 unit (Figure 1.9). In contrast to $[P_{14}]^{4-}$ and $[P_{21}]^{3-}$, this was first prepared by the mild oxidation of $[P_7]^{3-}$ with $[PPh_4][Cl]$.[82] Baudler and co-workers later reported the synthesis via the disproportionation of $[Li]_2[HP_7]$ and its ^{31}P NMR spectrum.[83,84]

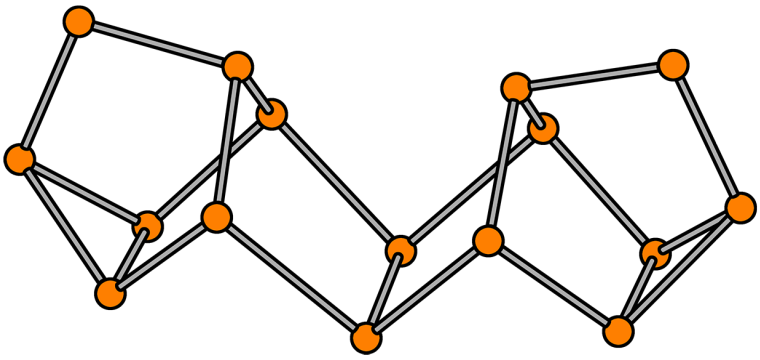

Figure 1.9: Ball and stick representation of the $[P_{16}]^{2-}$ anion.

The redox interconversion of $[P_{16}]^{2-}$ and $[P_{21}]^{3-}$ has been reported by Guerrin and Richeson.[85] Upon dissolving a pure sample of K_2P_{16} in THF, ^{31}P NMR and X-ray fluorescence measurements showed conversion to $[P_{21}]^{3-}$ and elemental phosphorus. Removing the THF from such solutions and redissolving the residue in ethanol restored the ^{31}P NMR spectrum of $[P_{16}]^{2-}$.

1.5 Chemical Activation of Pnictide Cages

As mentioned in Section 1.1, the main industrial source of P atoms for synthesis is PCl_3. There is significant interest in seeking to avoid the conversion of the P_4 feedstock into PCl_3, and instead directly convert P_4 itself into commodity chemicals. A variety of main group and transition metal mediated transformations (or activations) have been described, some representative examples of which will be detailed here. Related to this is the chemical

reactivity and transformation of alternative phosphorus cages, for example $[P_7]^{3-}$, which have been much less explored.

1.5.1 White Phosphorus

The reactivity of P_4 is frequently attributed to the high degree of bond strain present in the tetrahedron.[86] It mainly reacts with nucleophiles through attack on a σ^* orbital, although reactions with electrophiles both through the lone pairs and σ bonds are known. These result in P–P bond cleavage(s), or "activation" of the cage. Accompanying these is the redox activation by group 1 metals discussed in Section 1.4. It is frequently difficult to classify a particular reaction as occurring by electrophilic, nucleophilic, or redox activation pathways especially since frequently combinations of these operate in tandem (Scheme 1.1).

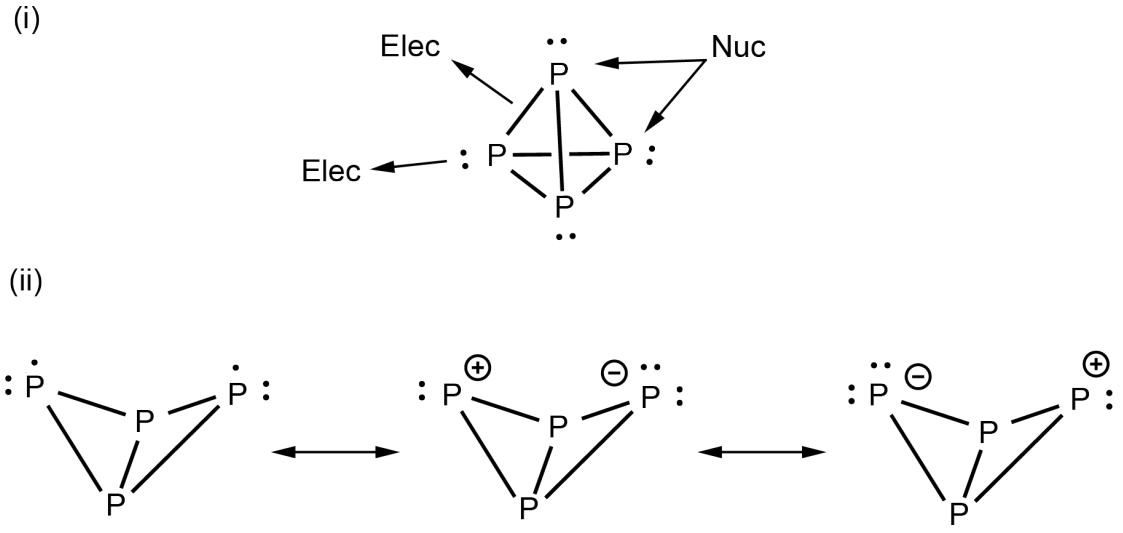

Scheme 1.1: The electrophilic and nucleophilic (i), and redox (ii) chemistry of the P_4 tetrahedron. Scheme adapted from Scheer et al.[87]

A multitude of P_4 activation reactions have been reported using reagents from across the periodic table, from transition metals to main group compounds. Such activations are known to give rise to a range of phosphorus containing fragments from P_1 up to P_{29} moieties.[88] This reactivity has been extensively reviewed in recent years.[87,89,90] The

reactivity of the arsenic homologue, As_4, has not been as extensively studied due to the synthetic challenges incurred in its production and handling. Specialized equipment is required for the generation of yellow arsenic, and the cage is rather unstable with respect to polymerization (*vide supra*).[91] Nevertheless, the research that has been performed on it shows that it possesses similar reactivity to white phosphorus.[92–95]

Since the work described in this thesis results primarily in the synthesis of compounds with new P–C bonds (and As–C bonds), only P_4 activations that result in the formation of P–C bonds by reaction with organic compounds will be discussed in any depth here.

1.5.1.1 Reaction With Anionic Carbon Nucleophiles

The initial degradation of P_4 by nucleophiles occurs via the cleavage of a P–P bond and subsequent opening of the tetrahedral cage to give a "butterfly-like" bicyclo[1.1.0]tetraphosphabutane moiety. Using the bulky aryl 2,4,6-^{t}Bu$_3$C$_6$H$_2$Li in the presence of the corresponding aryl bromide allowed this to be trapped as a neutral molecule (Figure 1.10).[96] A similar phosphorus skeleton is observed for the $[HP_4]^-$ anion discussed earlier, and also in a terphenyl substituted analogue reported by Power and co-workers.[97]

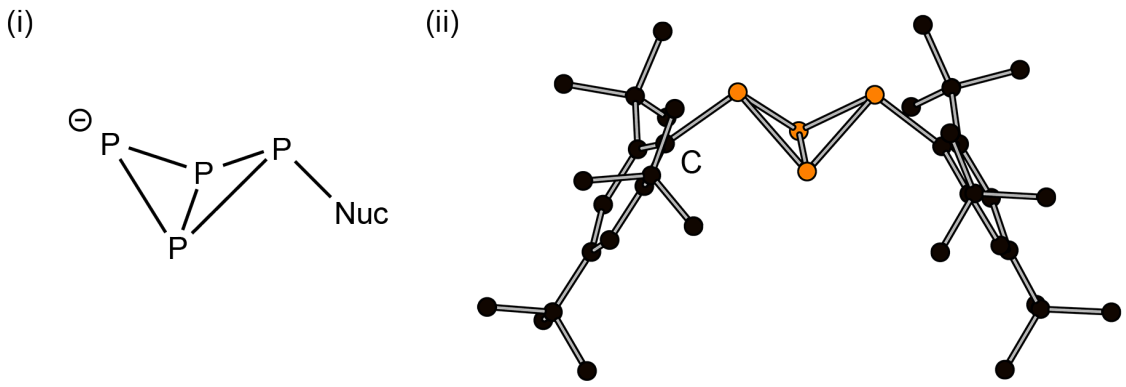

Figure 1.10: The initial step of nucleophilic attack on P_4 (i). Ball and stick representation of the molecular structure of (2,4,6-^{t}Bu$_3$C$_6$H$_2$)$_2$P$_4$ (ii), with hydrogen atoms omitted for clarity.[96]

The reaction of P_4 with organolithium reagents results in deep red solutions, which contain a complex mixture of organophosphides.[98] Upon quenching with alkyl halides tertiary phosphines are formed, whereas quenching with water gives mainly primary phosphines.[99,100] Use of organomagnesium reagents in place of organolithium reagents favours the formation of the tetrameric $(RP)_4$ cyclic phosphanes under similar conditions. A similar method has been used to synthesize acetylenic tertiary phosphines via reaction of P_4 with alkali metal acetylides.[101]

The cyanide anion is sufficiently nucleophilic to cause disproportionation of P_4 upon reaction.[102] The isolated product is the $[P(CN)_2]^-$ anion alongside a mixture of polyphosphides.

1.5.1.2 Reaction With Stable Carbenes

Since the discovery and crystallographic characterization of the first stable singlet carbenes over twenty years ago,[103,104] there has been much research dedicated to studying their structure and reactivity.[105] Singlet carbenes are strongly nucleophilic but more intriguingly possess a formally vacant p orbital, which hints at the possibility of transition metal-like reactivity. Indeed this is experimentally realized in the reaction of cyclic (alkyl)(amino)carbenes (CAACs) with H_2 and NH_3.[106] Following the wealth of transition metal mediated activation reactions of P_4,[87,90] in recent years there have been multiple reports of P_4 fragmentation and aggregation by stable carbenes with concomitant P–C bond formation. An overview of the reactivity and carbenes used is shown in Scheme 1.1.

The N-heterocyclic carbene (NHC) SIPr (**A**) reacts with P_4 to form a neutral P_{12} cluster stabilized by two NHC ligands, **VII** (Scheme 1.2, Figure 1.11).[107] A tetraphosphatriene intermediate **VI** is observed by ^{31}P NMR spectroscopy during the course of the reaction.

This can be trapped, along with the initial triphosphirene **IV**, by a [4+2] cycloaddition of 2,3-dimethylbutadiene with the P=P bonds. Switching from an NHC to a more basic CAAC ligand (**D**) allowed the isolation of the carbene stabilized tetraphosphatriene **VI**.[108] The CAACs possess a smaller singlet-triplet gap and a higher energy HOMO, which makes them both more electrophilic and more nucleophilic than the NHCs. The increased basicity relative to the NHCs disfavours the [3+2] cycloaddition that aggregates the triene into a P_{12} cluster, since the CAAC is a poorer leaving group.

The initial triphosphirene **IV** resulting from attack of a carbene at a phosphorus vertex could be isolated by the use of an extremely electrophilic acyclic (alkyl)(amino)carbene (**C**).[18] The transient triphosphirene **IV** formed by reaction with the carbene undergoes a cyclopropanation reaction with a second equivalent of the carbene to give a bis(carbene)adduct of P_4, **V**.

Cleavage of further P–P bonds can be accomplished by using a greater stoichiometric excess of the carbene. Accordingly, addition of three equivalents of CAAC (**B**), or a carbonyl-decorated carbene (CDC) (**E**) to a suspension of P_4 in diethyl ether results in the cleavage of further P–P bonds to result in the formation of carbene supported P_4 and P_2 fragments **II** and **III**, respectively.[18,109] The total fragmentation of P_4 into P_1 and P_3 (identified by an ABX ^{31}P NMR spectrum) moieties is achieved with the least sterically demanding stable carbene known, bis(diisopropylamino)cyclopropylidene (**F**). The P_1 cation, **I**, could be isolated as the chloride salt from chloroform, while the structutally unidentified P_3 anion decomposes during workup.[18]

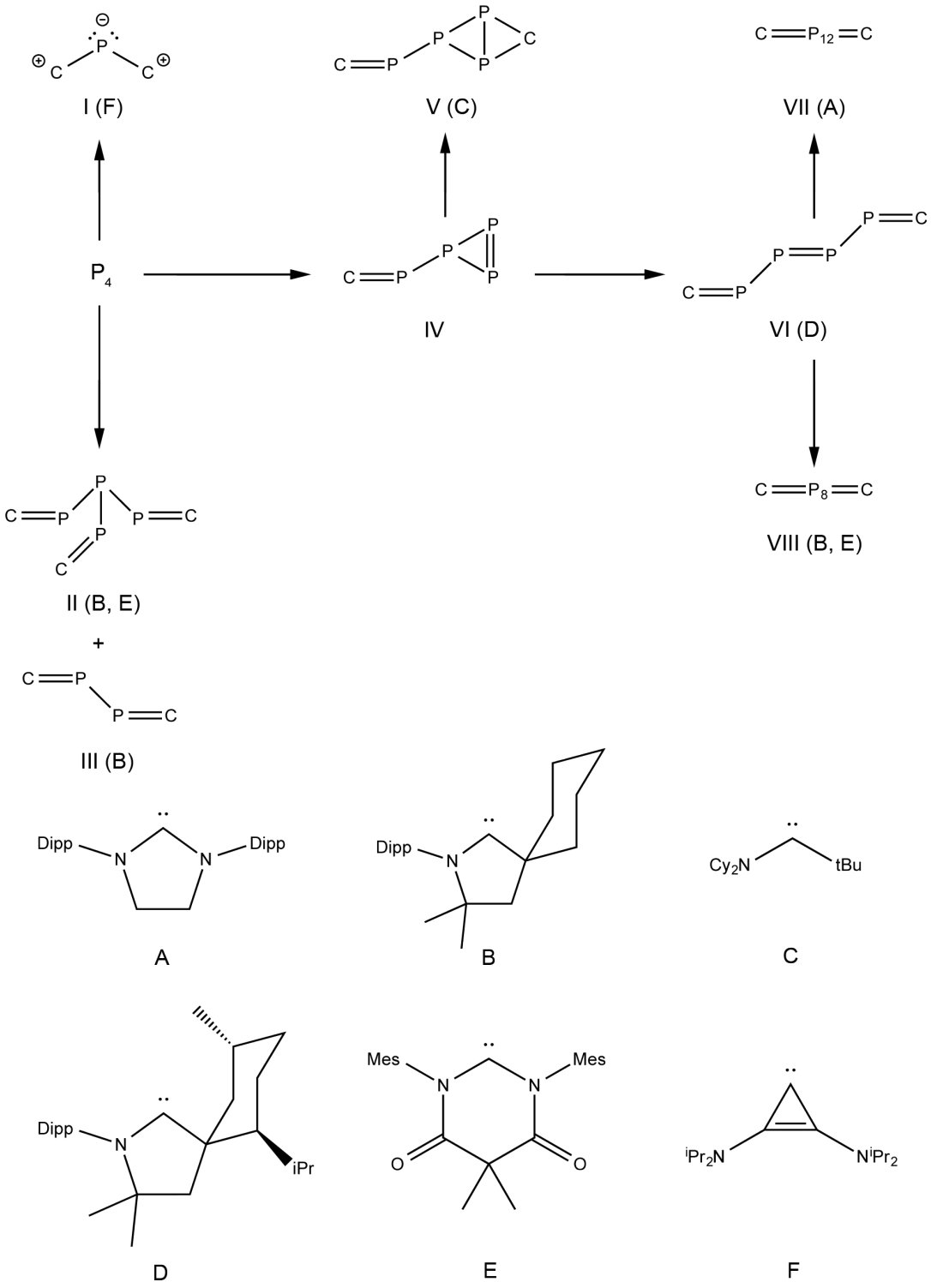

Scheme 1.2: Scheme for the reactivity of the carbenes A–F with P_4. Figure adapted from Scheer et al.[87]

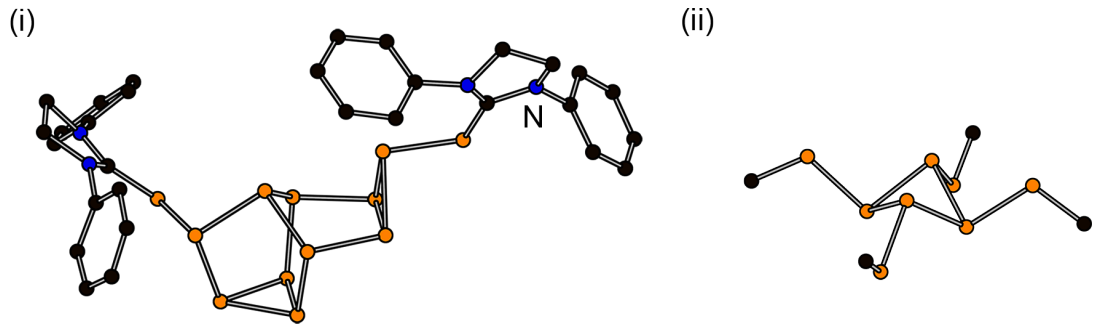

Figure 1.11: (i) Ball and stick representation of the P_{12} cluster. Hydrogen atoms and ligand isopropyl groups omitted for clarity. (ii) Ball and stick representation of the P_8 moiety. Only carbenic carbon atoms are shown for clarity.

More recently, coterminous reports from the groups of Bertrand and Hudnall have shown the formation of P_8 clusters **VIII** by the CDC (**E**) or CAAC (**B**) activation of P_4 (Figure 1.11).[109,110] This is highly sensitive to both the nature of carbene and solvent used. The CAAC mediated activation and aggregation to the P_8 cluster was achieved simply by switching solvents to benzene, and lies in contrast to the previously discussed reactivity performed in diethyl ether. This is rationalized by the relative solubility of P_4 in the solvent – it is only sparingly soluble in diethyl ether, so the carbene is present in large excess and favours the P_4 cleaved product.

1.5.1.3 Radical Based P–C bond Formation

P–P bonds are known to be an excellent trap for carbon based radicals under mild conditions, resulting in the formation of new P–C bonds.[111] Despite this, there are not many reported examples of the direct radical functionalization of P_4. Barton and co-workers reported the synthesis of phosphonic acids by reaction of *O*-acyl derivatives of *N*-hydroxy-2-thiopyridone (PTOC esters) with P_4 upon irradiation with UV light.[112,113] Further work by Cossairt and Cummins has demonstrated the radical synthesis of tertiary phosphines directly from P_4 and an aryl, alkyl, silyl or stannyl halides.[114] The titanium (III) trisanilide complex

$Ti[N(^tBu)(Ar)]_3$ (Ar = 3,5-$Me_2C_6H_3$) is used as a radical initiator, abstracting a halide to form a carbon-based radical which subsequently cleaves P_4 (Scheme 1.3).

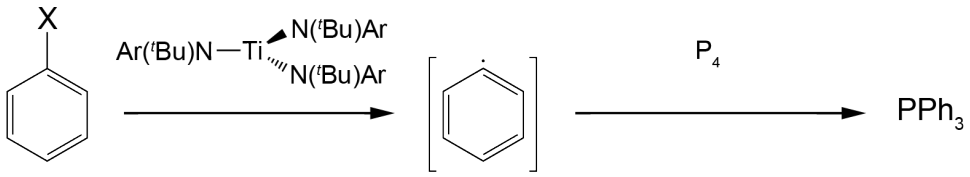

Scheme 1.3: The radical synthesis of PPh_3 from phenyl halides. X = Br, I; Ar = 3,5-$Me_2C_6H_3$.

1.5.2 Reactivity of $[E_7]^{3-}$

In contrast to the reactivity of P_4, for which some pertinent P–C bond forming reactions have been described above, the reactivity of other soluble phosphorus cages has been much less investigated. Amongst the other cages is the $[P_7]^{3-}$ cluster. Since its discovery, the reactivity of both $[P_7]^{3-}$ and the heavier arsenic and antimony cages has been somewhat explored, although the synthetic potential remains relatively untapped. The most commonly used contemporary synthesis of $[E_7]^{3-}$ cages (E = P, As, Sb) starts from the (relatively) innocuous red phosphorus, grey arsenic and metallic antimony allotropes. Formation of P–C bonds (or indeed As–C and Sb–C bonds) from these cages can therefore be regarded as a safer (though circuitous) route to the activation and functionalization of the elements.

The reactivity of $[E_7]^{3-}$ seems to be best described by considering several factors. The presence of three pnictide vertices imbues the cluster with a potent nucleophilicity and basicity, while the triply negative charge results in significant reductive power. In addition, the three-membered basal ring is highly strained, analogous to P_4, resulting in the potential for bond cleavage, which is particularly observed for the arsenic and antimony congeners. With this in mind, the reactivity of the clusters can be broadly split into two categories:

reactions where the nuclearity and (approximate) geometry of the cage is retained, and reactions where the nuclearity and geometry of the cage is significantly altered.

1.5.2.1 Reactions in Which the $[E_7]^{3-}$ Cage is Retained

The nucleophilic nature of the pnictide vertices allows the synthesis of a series of mono-, di-, and tri-substituted cages where a two-centre, two-electron *exo*-bond is formed between the phosphorus atom and the substituent. Examples are known for organic, main group and transition metal substituents. In the latter case the cage is described as coordinating in an η^1 mode, and is formally considered a two-electron donor to the metal centre.

Monosubstituted cages, with the general formula $[E_7R]^{2-}$, are rare. There are no examples of arsenic and antimony cages, and only a handful of $[P_7R]^{2-}$ cages are known. Arguably the simplest of these examples, with R = H, is well documented in the literature. A variety of methods have been used to synthesize it ranging from disproportionation of P_2H_4 with ^{n}BuLi,[115] to simple protonation reactions of the naked $[P_7]^{3-}$ cage.[116,117] A general structural feature of the $[P_7R]^{2-}$ cages is their chirality, due to the pyramidalization of the substituted phosphorus vertex (Figure 1.12). All known examples exist as a racemic mixture since no attempts have been made to separate the enantiomers.

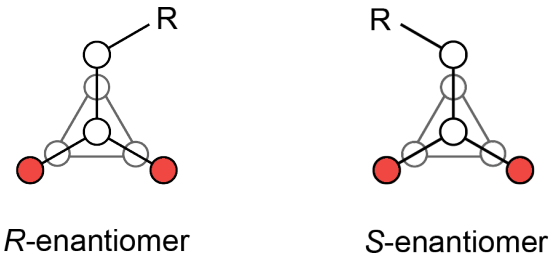

Figure 1.12: The two enantiomers of a monosubstituted heptapnictide cage viewed from the apical vertex. Atoms coloured in red carry a formal negative charge.

The other result of this pyramidalization is that in the static structure there are no equivalent phosphorus atoms. All of the known $[P_7R]^{2-}$ anions report the observation of fluxionality in the ^{31}P NMR spectra. The ^{31}P NMR spectrum of $[HP_7]^{2-}$ exemplifies this behaviour. At room temperature two broad resonances are seen as a result of a degenerate Cope-like rearrangement similar to that observed for $[P_7]^{3-}$ (a more detailed discussion can be found in Chapter Two). Only on cooling to –60 ºC is the fluxional process frozen out, with seven resonances corresponding to the seven inequivalent phosphorus environments being observed at –9.0, –67.5, –83.7, –119.4, –134.8, –145.2 and –215.9 ppm.

Fritz et al. reported the observation of $[P_7{}^tBu]^{2-}$ cage as a product of the reaction of ^{t}BuLi with a cyclic tetraphosphane, but did not report characterization data.[118] The $[P_7(SiMe_3)]^{2-}$ cage can be synthesized by a ligand redistribution reaction between $[P_7(SiMe_3)_3]$ and $[P_7]^{3-}$ in the stoichiometric ratio 1:2.[119] The only non-hydrogen substituted crystallographically characterized cage, which clearly shows the racemic mixture of enantiomers formed, is with R = $SiMe(SiMe_3)_2$.[120] This crystallizes in the centrosymmetric space group $P2_1/n$ (and is thus necessarily a racemate).

The most convenient synthesis of the disubstituted $[E_7R_2]^-$ cages involves the transfer of an R group from a tetraalkylammonium salt, as reported by Eichhorn and co-workers.[121,122] This has been used to synthesize $[E_7R_2]^-$ anions (E = P: R = Me, Et, Bu, $PhCH_2$, $EtOCOCH_2$, EtOCOCHMe; E = As: R = $PhCH_2$) from $[RR'_3N][X]$ salts (R = R′ = Me, Et, Bu; R = $PhCH_2$, $EtOCOCH_2$, EtOCOCHMe: R′ = Me; X = Cl, Br, I). The reaction is proposed to be a nucleophilic attack of a pnictide vertex of the cage at the α-carbon atom of the most electrophilic group of the ammonium salt. No evidence for a radical process was observed.

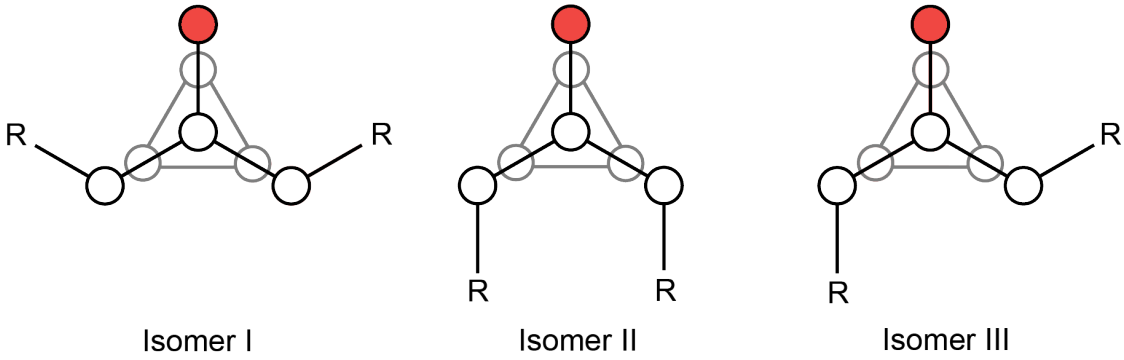

Figure 1.13: Representation of the three possible isomers of $[E_7R_2]^-$ viewed from the apical vertex. Atoms possessing a formal negative charge are shown in red.

There are three possible isomers of a disubstituted cage with two identical R groups (Figure 1.13). Two (isomers I and II) possess C_s symmetry, with a mirror plane bisecting the cage between the two R groups, giving them two pairs of equivalent E atoms and three unique E atoms. The third isomer (III) has seven inequivalent E atoms. The ^{31}P NMR spectra of the $[P_7R_2]^-$ anions prepared by Eichhorn and co-workers displayed five resonances, which ruled out the presence of isomer III. On steric grounds it seems reasonable to assume that the formation of isomer I would be favoured, and this was confirmed crystallographically. It is worth noting that no evidence of fluxionality was observed in the ^{31}P NMR spectra, in contrast to the monosubstituted $[P_7R]^{2-}$ cages.

Reaction of $[P_7]^{3-}$ with alkyl tosylates has also been used to form $[P_7R_2]^-$ (R = ^{i}Pr, ^{i}Bu), and ^{31}P NMR studies suggest the formation of either isomer I or II.[123]

Trisubstituted, neutral cages are known for carbon, p-block, and transition metal substituents, all prepared by salt metathesis with an appropriate element halide. Accordingly the alkyl substituted $[P_7R_3]$ (R = Me, Et, ^{i}Pr, Bu, ^{i}Bu),[124–126] main group substituted $[E_7R_3]$ (E = P: R = SiH_3, SiH_2Me, $SiMe_3$, $SiMe_2PEt_2$, $SiPh_3$, $GeMe_3$, $SnMe_3$, P^tBu_2, Sb^tBu_2; E = As: R = $SiMe_3$),[125–128] and metalated $[P_7\{Fe(Cp)(CO)_2\}_3]$ are known.[129] The isomerism seen for the mono- and disubstituted cages is also possible in the trisubstituted cages, with two

distinct arrangements of the R groups termed the symmetrical and unsymmetrical isomers (Figure 1.14).

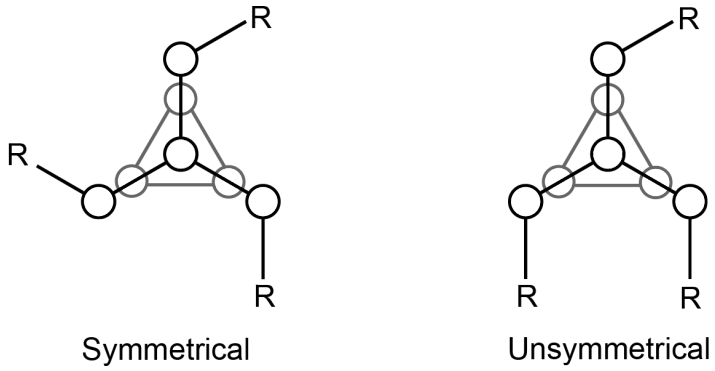

Figure 1.14: The two possible isomers of $[R_3E_7]$ viewed from the apical E atom.

Smaller R groups allow the formation of both isomers, but upon increasing the steric demands of the R group the less hindered, and thermodynamically favourable symmetrical isomer is increasingly favoured. For the largest R groups, such as in $[P_7\{Fe(Cp)(CO)_2\}_3]$, exclusive formation of the symmetrical isomer is observed. This has been argued as an example of kinetic versus thermodynamic reaction control. Since the groups are likely added sequentially, $[P_7R_2]^-$ is a probable intermediate. Only alkylation of isomer III will give the symmetrical isomer of $[P_7R_3]$ and this requires an inversion of a substituted E atom in isomer I or II, a process with a high activation barrier. Accordingly, the symmetric isomer forms more slowly than the unsymmetrical isomer, despite being thermodynamically preferential, and its formation is only favoured by bulky R groups.

So far, only examples where the cage acts as a two-electron donor through one pnictide vertex have been described. There are two other coordination modes available to the $[E_7]^{3-}$ anion: η^2, where it acts as a four-electron donor; and η^4, where it acts as a six-electron donor (Figure 1.15). Examples are known for both coordination modes from the metalation chemistry of the clusters. Only a few examples for each mode will be discussed since the

primary focus of this thesis is the P–C bond forming chemistry of the cages. The metalation chemistry of the cages has recently been reviewed in depth.[130]

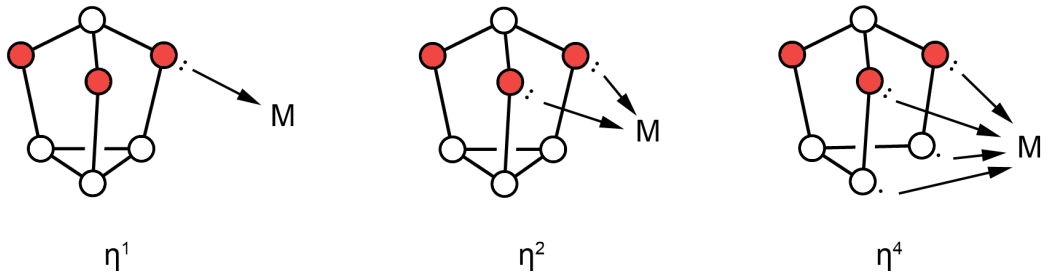

Figure 1.15: Diagram showing the three possible bonding modes of $[E_7]^{3-}$. Atoms possessing a formal negative charge are shown in red.

An archetypal example of the η^2 mode is found in the $[M(\eta^2\text{-}E_7)]^{4-}$ (E = P, M = Zn, Cd; E = As, M = Zn) anions.[131] These heterometallic clusters are synthesized by reaction of $[E_7]^{3-}$ with MPh_2 reagents in ethylenediamine. An M–C reductive bond cleavage is proposed, illustrating the reductive potential of the naked cluster anion (Scheme 1.4). The structure consists of a tetrahedral M(II) d^{10} metal centre coordinated in a tetrahedral fashion by two $[E_7]^{3-}$ cages (Figure 1.16).

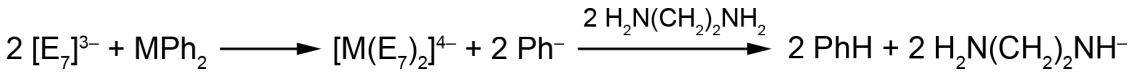

Scheme 1.4: Formation of $[M(\eta^2\text{-}E_7)_2]^{4-}$ from $[E_7]^{3-}$ and MPh_2.

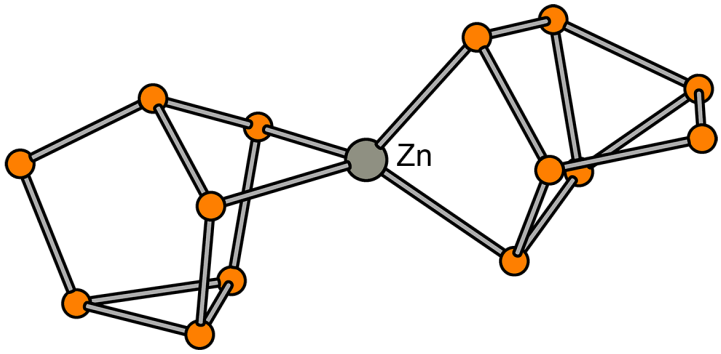

Figure 1.16: Ball and stick representation of the $[Zn(\eta^2\text{-}P_7)_2]^{4-}$ cluster anion.

Other examples where the cage displays the η^2 coordination mode are $[(\eta^2\text{-}P_7)Mo(CO)_4]^{3-}$,[132] $[(\eta^2\text{-}E_7)PtH(PPh_3)]^{2-}$ (E = P, As),[133,134] $[Pd_2(\eta^2\text{-}As_7)_2]^{4-}$,[135] $[Zn(\eta^2\text{-}As_7)]^{4-}$,[136,137] $[(\eta^2\text{-}E_7)InPh_2]^{2-}$ (E = P, As),[131] $[In(\eta^2\text{-}E_7)_2]^{3-}$ (E = P, As) and $[Tl(\eta^2\text{-}E_7)]^{2-}$ (E = P, As).[138] These are all prepared by the reaction of a suitable metal precursor compound with $[E_7]^{3-}$ in ethylenediamine.

Numerous examples of the η^4 coordination mode are known. The cage undergoes mild activation when coordinated in this fashion, resulting in the homolytic cleavage of an E–E bond in the basal plane to give a norbornadiene-like geometry (Figure 1.17). This results in the cage being considered a six-electron donor to the metal centre, through two vertices and two phosphinyl donors. This is, however, not a good descriptor of the bonding between such cages and metal centres. Fenske-Hall molecular orbital calculations on the $[(\eta^4\text{-}E_7)Cr(CO)_3]^{3-}$ complexes synthesized by the group of Eichhorn show significant similarities between $[\eta^4\text{-}E_7]^{3-}$ and the cyclobutadiendiide anion.[139,140]

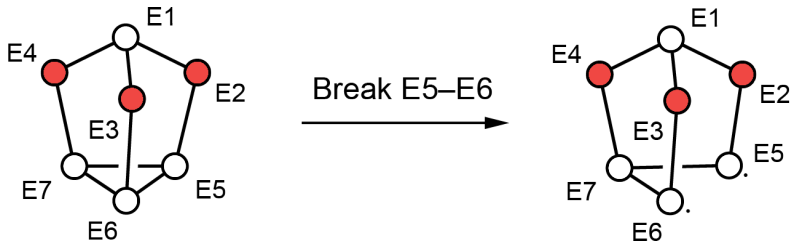

Figure 1.17: Diagram showing the nortricyclane- to norbornadiene-like transition in $[E_7]^{3-}$ via homolytic cleavage of the E5–E6 bond. Atoms possessing a formal negative charge are shown in red.

The $[(\eta^4\text{-}E_7)M(CO)_3]^{3-}$ anions (E = P, As: M = Cr, W; E = Sb: M = Cr, Mo, W) are formed by reaction of $[E_7]^{3-}$ with metal carbonyl complexes possessing a labile ligand (mesitylene, cycloheptatriene or 2,2′-bipyridine).[139–141] The further chemistry of these anions has been explored to yield a series of protonated anions of the form $[(\eta^4\text{-}HP_7)M(CO)_3]^{2-}$ (M = Cr, W),[142] bimetallic anions $[(en)(CO)_3W(\eta^1,\eta^4\text{-}P_7)M(CO)_3]^{3-}$ (M = Cr, W) and $[(\eta^4\text{-}$

$P_7R)W(CO)_3]^{2-}$ (R = Me_3Si, $^nBu_3Si$, Hex_3Si, Ph_3Si, Et_3Ge, Ph_3Ge, Et_3Sn, $^nBu_3Sn$, Cy_3Sn, Ph_3Sn, Ph_3Pb),[143,144] and reversible CO binding accompanied by a change of cage hapticity from η^4 to η^2.[132]

The other crystallographically characterized examples of η^4 coordination are $[(\eta^4\text{-}P_7)Ni(CO)_3]^{3-}$ and the "inorganometallic" metallocene analogues $[M(\eta^4\text{-}HP_7)_2]^{2-}$ (M = Fe, Ru) (Figure 1.18).[133,145,146]

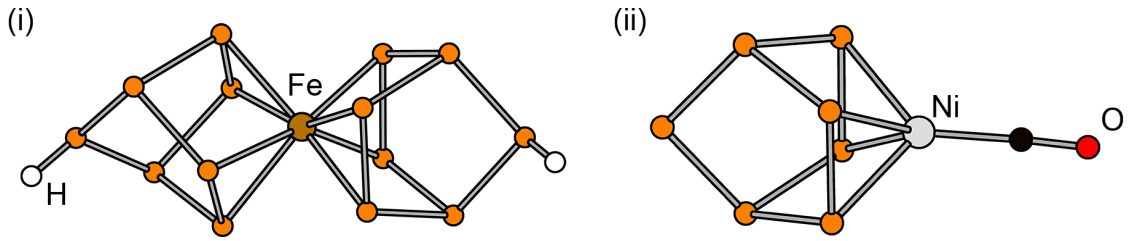

Figure 1.18: Ball and stick representations of the $[Fe(\eta^4\text{-}HP_7)_2]^{2-}$ (i) and $[(\eta^4\text{-}P_7)Ni(CO)]^{3-}$ (ii) anions.

1.5.2.2 Reactions in Which the $[E_7]^{3-}$ Cage Is Fragmented

While η^4 coordination of the cluster can be considered a mild activation of the cage, there are also examples known where the geometry or indeed the nuclearity of the cage is significantly altered. Until recently all known examples were for the heavier arsenic and antimony congeners. This behaviour is likely attributable to the necessary requirement for bond cleavage on cluster dissociation and reassembly. On descending group 15 the E–E bond dissociation energies are known to decrease, allowing for more facile cluster rearrangements.[9] This is taken to its logical conclusion in the chemistry of the homoatomic bismuth polyanions $[Bi_4]^{2-}$ and $[Bi_2]^{2-}$ (no $[Bi_7]^{3-}$ cluster is known in either the solid state or solution), both of which give rise to large heterometallic systems on reaction with transition metal reagents.[147–151]

The reaction mechanisms that lead to formation of higher nuclearity clusters are poorly understood, yet occasionally well defined products can be isolated. A series of $[ME_8]^{n-}$ (M = Nb, Cr, Mo; M = As, Sb; n = 2, 3) are synthesized either by reaction of $[E_7]^{3-}$ with M(arene) complexes or in a solid state synthesis.[152–155] These comprise a crown-like E_8 ring possessing a formal 8– charge, isolectronic with S_8 and centred by a metal cation (Figure 1.19).

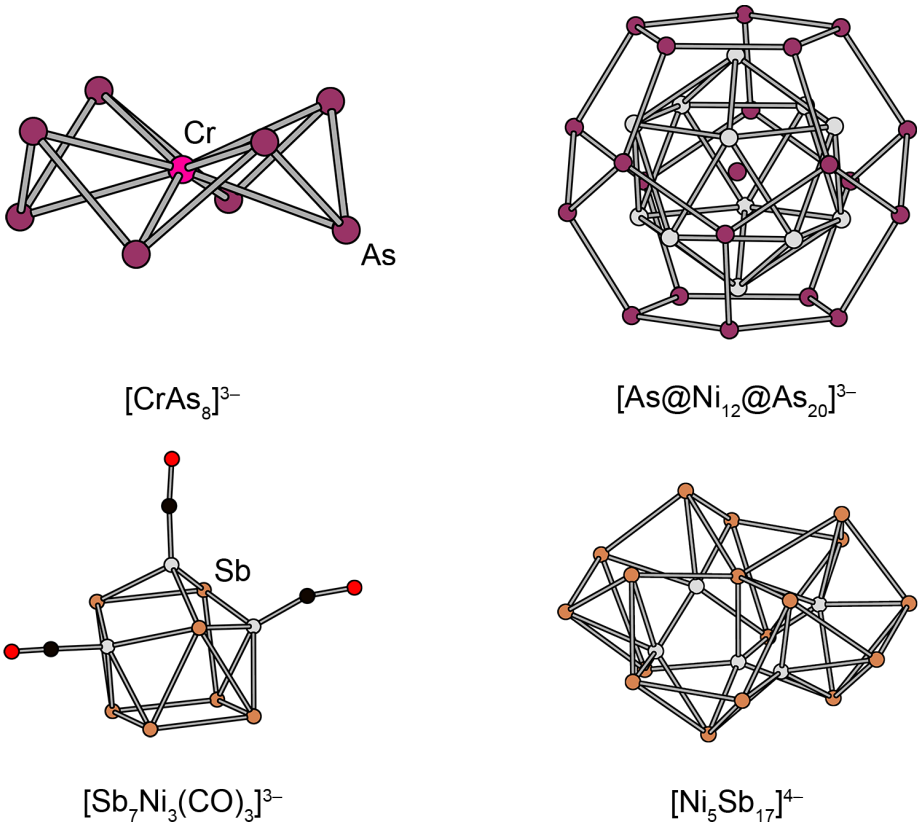

Figure 1.19: Ball and stick representation of the $[CrAs_8]^{3-}$, $[As@Ni_{12}@As_{20}]^{3-}$, $[Sb_7Ni_3(CO)_3]^{3-}$ and $[Ni_5Sb_{17}]^{4-}$ anions.

The $[As@Ni_{12}@As_{20}]^{3-}$ cluster is synthesized by reaction of $Ni(COD)_2$ with $[As_7]^{3-}$, and consist of an icosahedral $[Ni_{12}(\mu_{12}\text{-As})]^{3-}$ core encapsulated in a fullerene-like As_{20} unit.[156] An analogous reaction between $Ni(COD)_2$ with $[Sb_7]^{3-}$ gives rise to $[Ni_5Sb_{17}]^{4-}$, which possesses an entirely different structure.[157] Despite very similar reaction conditions entirely disparate products are obtained, demonstrating that attempting to predict the chemistry of

the heptapnictide clusters is somewhat challenging. A further example can be found in the reaction of $Ni(CO)_2(PPh_3)_2$ with $[Sb_7]^{3-}$. Earlier, the reaction of this transition metal compound with $[P_7]^{3-}$ was detailed and gave rise to the $[(\eta^4\text{-}P_7)Ni(CO)_3]^{3-}$ cluster. In contrast, the reaction with $[Sb_7]^{3-}$ results in the formation of the electron deficient ten vertex $[Sb_7Ni_3(CO)_3]^{3-}$ cluster.[158]

As mentioned above, cluster fragmentation reactions are virtually unknown for $[P_7]^{3-}$. The cobalt organometallic compound $Co(mes)_2(PPhEt_2)_2$ has recently been reported to activate both the $[P_7]^{3-}$ and $[As_7]^{3-}$ cages.[159,160] The products resulting from this transformation are $[Co(\eta^5\text{-}P_5)\{\eta^2\text{-}P_2H(mes)\}]^{2-}$ and $[Co(\eta^3\text{-}As_3)\{\eta^4\text{-}As_4(mes)_2\}]^{2-}$, respectively. In both cases, the nuclearity (i.e. seven) of the parent cluster has been maintained, but extensive cage rearrangement has occurred. These molecules contain pnictide analogues of organic ligands; namely $[P_5]^-$ (cyclopentadienide, Cp, $[C_5H_5]^-$), [HP=P(mes)] (alkenes, $R_2C{=}CR_2$) and $[As_4R_2]^{2-}$ (butadienediide, $[C_4R_6]^{2-}$). This analogy between carbon chemistry and pnictogen chemistry has been widely explored, particularly in phosphorus chemistry, and warrants further discussion.

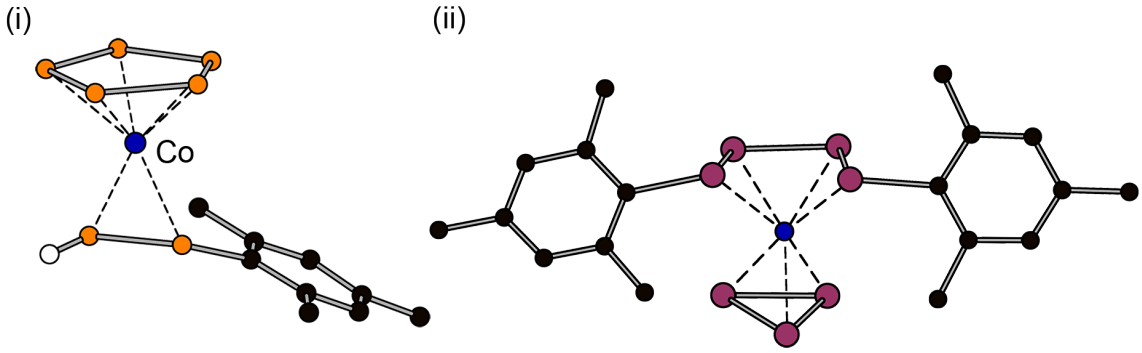

Figure 1.20: Ball and stick representations of the $[Co(\eta^5\text{-}P_5)\{\eta^2\text{-}P_2H(mes)\}]^{2-}$ (i) and $[Co(\eta^3\text{-}As_3)\{\eta^4\text{-}As_4(mes)_2\}]^{2-}$ (ii) anions.

1.6 PHOSPHORUS AS A "CARBON-COPY"

1.6.1 The Isolobal Principle

The principle of isolobality is used to relate seemingly unrelated fragments of molecules. The concept is best popularized by Hoffmann, who stated that two fragments are isolobal if the *"...number, symmetry properties, approximate energy and shape of the frontier orbitals are similar – not identical, but similar"*.[161,162] There is no necessity for the fragments to be either isoelectronic or isostructural. The concept was initially used to relate transition-metal moieties to known organic moieties,[163] but has since been extended to the rest of the periodic table. Of particular note for this work is the isolobal analogy between the P and CH fragments (Scheme 1.5).

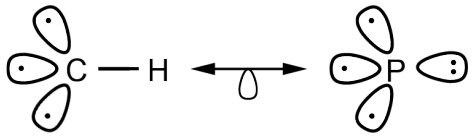

Scheme 1.5: The isolobal relationship between CH and P, showing the frontier orbitals and their occupation.

The isolobal principle is most useful in relating the structures of unusual or complex molecules to better known, perhaps simpler, molecules. This may offer insight into bonding or reactivity, and allow parallels to be drawn between related molecules. Like any simple (albeit useful) model, it has drawbacks. An isolobal relationship does not imply anything more than that, and both electronic and gross structural features can vary. More importantly, it makes absolutely no prediction as to kinetic or thermodynamic stability of a molecule within an "isolobal pair". There are many examples of carbon based molecules that have no inorganic parallel, and vice-versa.[164]

1.6.2 Phospha-organic Chemistry

As mentioned above, the methine fragment and phosphorus atom are isolobal. The relationship between the two elements goes deeper, however. The diagonal relationship (a well noted result of the competing effects of both descending and traversing the periodic table from left to right) means that the two elements are also chemically similar. The ability of phosphorus to accept or release electrons is somewhat similar to that of carbon. While the σ electronegativity of carbon is higher than phosphorus (X_C = 2.55, X_P = 2.19),[165] the π electronegativity of phosphorus is very similar, or perhaps even higher than carbon.[166] Accordingly, despite the chemistry of phosphines resembling that of the amines, phosphorus in low-coordinate environments far more closely resembles that of carbon (Scheme 1.6).[167] This parallel has lead to the emergence of a subfield of organophosphorus chemistry known as "phospha-organic" chemistry, and phosphorus being nicknamed "the carbon copy".[168,169]

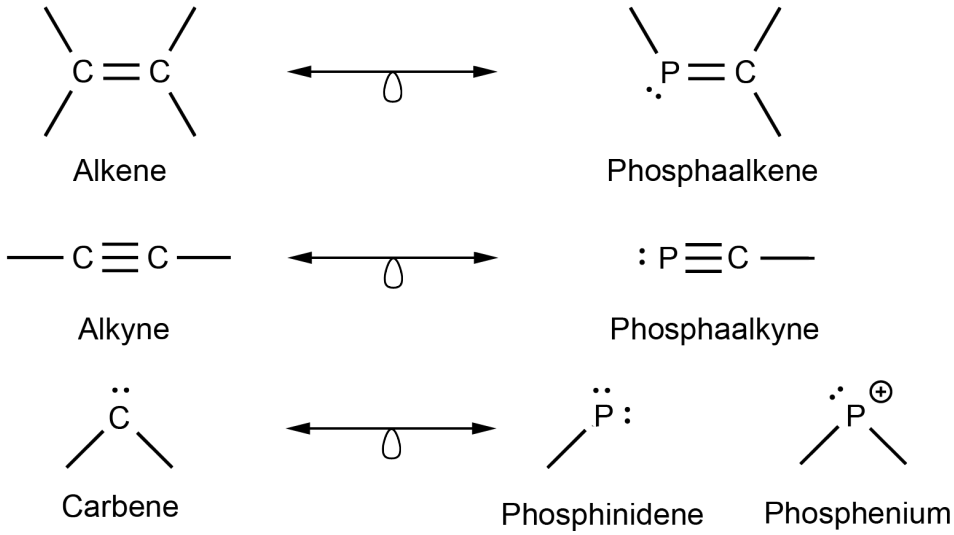

Scheme 1.6: Common low-coordinate carbon species and their isolobal phosphorus analogues. Figure adapted from Bates et al.[170]

The synthesis of these phosphorus analogues of organic molecules is frequently challenging however, due in part to the reticence of heavier p-block elements to form multiple bonds (the "double-bond rule" discussed above).[19] Strategies for the stabilization of these species typically involve stabilization (which is a combination of both kinetic and thermodynamic effects) by the use of bulky substituents,[171] stabilization in the coordination sphere of a metal,[172] or delocalization of multiple bond character into an extended π system (of which a multitude of examples are known).[173]

1.6.2.1 Phosphaalkenes

A widely studied series of compounds that well illustrates the analogy between carbon and phosphorus chemistry are the phosphaalkenes. These feature a formal (3p–2p)π bond between P and C. The bond lengths typically lie in the range 1.60 to 1.70 Å (for example, the P=C bond length in (mes)P=CPh_2 is 1.69 Å),[174] which is significantly shorter than typical P–C bond distances of around 1.83 Å.[175] Calculations have shown that the P=C bond is somewhat weaker than C=C bonds (180 kJ mol^{-1} compared to 272 kJ mol^{-1}).[176,177] UV photoelectron spectroscopy has been used to probe the electronic structure of the parent phosphaethylene, HP=CH_2.[178] This shows that the HOMO at –10.3 eV is the π bond (by comparison the π bond of ethylene has an ionization potential of –10.5 eV), with the phosphorus lone pair sitting lower in energy at –10.7 eV.

The bond is effectively apolar,[179] with reactivity studies showing that the regiochemistry of addition reactions can be influenced by both substituent effects and thermal or photochemical means.[180] The conjugative ability of P=C bonds is very similar to that of C=C bonds,[181] a phenomenon that has recently been used to design π-conjugated phosphorus polymers for potential electronic applications.[182,183] The P=C bond is, however, extremely reactive and has a propensity for oligomerization reactions which can result in

the isolation of well defined oligomers or polymers.[184,185] Sufficient stabilization for isolation of the species requires conjugation,[186] steric hindrance,[174,187] or complexation to a metal centre (Figure 1.21).[188]

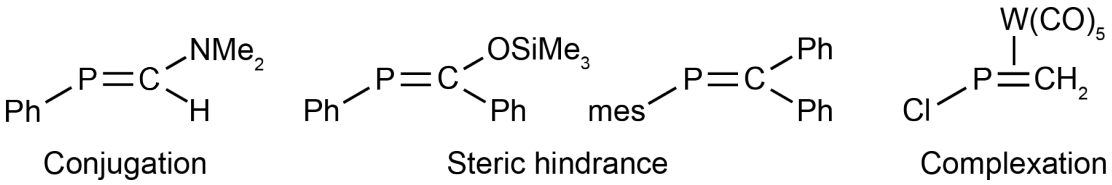

Figure 1.21: Some examples of stable, isolable phosphaalkenes and their method of achieving stability.

The synthesis and reactivity of phosphaalkenes has been described and reviewed comprehensively, and lies beyond the scope of this introduction.[168,189,190] Since their initial discovery they have developed from being mere chemical curiosities into molecules that are of particular interest for their applications from ligands in catalysis to materials chemistry.[170,191] Their use as ligands is particularly intriguing because although they mainly coordinate through the phosphorus lone pair, the sp^2 hybridized phosphorus atom makes them poor σ donors and good π acceptors. This lies in contrast to phosphines, which are generally good σ donors and poor π acceptors. The concept of phospha-organic molecules as π acceptor ligands will be revisited later in this thesis.

1.6.2.2 Phosphaalkynes

The chemistry of P–C multiply bonded systems can be extended beyond phosphaalkenes, to the triply bonded phosphaalkynes. Phosphaacetylene, HCP, was first detected using IR spectroscopy and mass spectrometry by Gier in 1961 by an unusual synthesis involving the decomposition of PH_3 in an electric arc between graphite electrodes.[192] An improved synthesis involving the double dehydrohalogenation of CH_3PCl_2 allowed further information to be gleaned on the compound, but did not permit isolation of a

phosphaalkyne.[193] The isolation of a compound containing a triple bond between phosphorus and carbon was not realized until 1981 by Becker, who prepared ^{t}BuCP.[194] This molecule is surprisingly stable, and the original method has been improved and generalized to give a host of known compounds of the form RCP.

The P–C triple bond is remarkably short (^{t}BuCP: 1.548(1) Å),[195] supporting its formulation as a true triple bond. Unlike phosphaalkenes, which are essentially apolar, the bond is usually strongly polarized towards carbon. Phosphaalkynes are therefore protonated exclusively at carbon.[196] UV photoelectron spectroscopy of ^{t}BuCP shows the π bonds lie at –9.61 eV, whereas the phosphorus lone pair lies much lower in energy at –11.44 eV.[197] As such, the lone pair would be expected to be much less reactive than in phosphaalkenes, and as such the chemistry π bond should be the predominant feature of reactivity in the class of molecules. This is indeed observed experimentally, with the cycloaddition chemistry being well developed.[189,198] Of relevance in developing the analogy between carbon and phosphorus chemistry is the observation of "side-on" η^2 coordination modes between phosphaalkynes and metal centres, comparable to that for alkynes.[199,200]

1.6.2.3 Phosphinidenes

The final set of acyclic compounds to discuss are the phosphinidenes, which are isolobal analogues of carbenes. While an extensive range of stable, free carbenes is known, phosphinidenes have only been observed as transient species in gas or matrix phases.[201] Both theoretical and experimental methods have shown that the triplet state is generally preferred over the singlet state, although this is dependent on the nature of the single σ bonded substituent.[202,203] Despite their instability, they can be trapped by suitable moieties (typically unsaturated organic molecules), and indeed have been implicated as intermediates in a variety of synthetic transformations.[204,205]

In parallel with carbon chemistry, for which the first examples of isolable carbenes were found in transition metal complexes, the stabilization of phosphinidenes by complexation to transition metals is well established. Examples of both nucleophilic and electrophilic metal-phosphinidenes are known,[206–208] similar to the well known Schrock and Fischer carbene complexes found in carbon chemistry.[209,210] Both bent, two-electron donor and linear, four-electron coordination (where the phosphorus lone pair acts as a donor) modes are known for terminal metal-phosphinidene complexes.[211,212] Computational and experimental studies confirm the presence of genuine metal-phosphorus double bond character.[213]

1.6.3 Cyclic Phospha-organic Molecules

Of the multitude of inorganic heterocycles,[173] phosphorus has a particularly well developed heterocyclic chemistry.[214,215] Of particular interest are the 6π electron planar aromatic systems that show extensive electronic delocalization. Two such series of compounds are known, both formed by a hypothetical replacement of CH with P in organic molecules. The phosphinenes are formally derived from benzene,[216] while the phospholides are analogues of the ubiquitous cyclopentadienyl ligand.[217]

1.6.3.1 Phospholides

All of the possible phospholides, with the general formula $[(CR)_nP_{(5-n)}]^-$ (n = 1–5), are known.[217] There are seven total members of the family taking into account the isomerism inherent to the di- and tri-phospholides (Figure 1.22), however, not all are isolable as free anions. Even the members of the family that are isolable do not always have generally applicable synthetic procedures that are tolerant of different R groups on carbon.

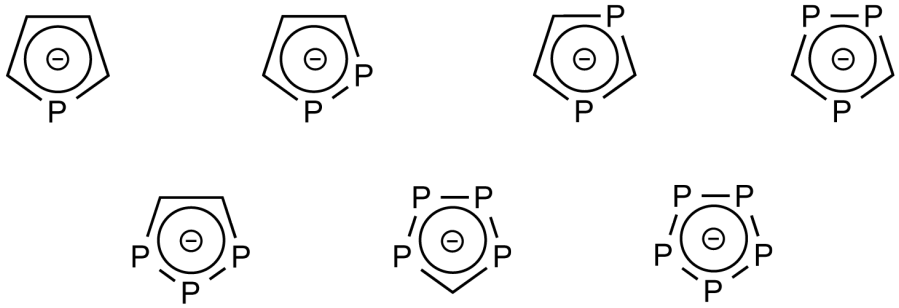

Figure 1.22: The range of possible phospholide anions.

1.6.3.1.1 Properties

Crystal structures of the free anions (i.e. as alkali or alkaline earth metal salts) are known for all of the isomers except the pentaphospholide. Representative examples of these are [Li(TMEDA)][PC_4Me_4],[218] [Na(diglyme)][1,2-$P_2C_3Ph_3$],[219] [K][1,3-$P_2C_3{}^tBu_3$],[220] {[Mg_2(μ-Cl)$_3$(THF)$_6$][1,3,4-$P_3C_2{}^tBu_2$]$_2$,[221] [Li(12-crown-4)$_2$][1,2,3-$P_3C_6H_4$],[222,223] and [Cs][P_4C-(mes*)].[224] In all cases, similar structural features are observed. The anions are essentially planar rings, with significant contractions of the C–C, P–C and P–P bond distances from those typically observed for single bonds. The C–C bonds lie in the approximate range 1.39–1.42 Å, C–P bonds in the range 1.69–1.75 Å, and P–P bonds in the range 2.07–2.11 Å. This implies partial multiple bond character within the ring, as would be expected for a delocalized aromatic system. Where the cation is not fully sequestered, η^5 coordination of the anion to the metal is observed.

The ^{31}P NMR spectra of the phospholide anions show generally low field chemical shifts compared to typical phosphides.[225] This deshielding effect has been attributed to a coupling between the phosphorus lone pairs and the electrons of the ring π system.[226] The downfield shift generally increases with the number of phosphorus atoms in the ring, from around 70 ppm for the monophospholides up to 470 ppm for $[P_5]^-$. These are very substituent dependent, with the phosphorus atom in $[PC_4H_4]^-$ resonating at 77 ppm while that in 3,4-

dimethyl-2,5-dibenzoylmonophospholide resonates at 210 ppm.[227,228] There are very few known examples of phospholides with CH groups in the ring, and even fewer with reported ^{1}H NMR spectra, but $[PC_4H_4]^-$ displays proton resonances at 6.78 and 6.62 ppm. The two other known examples with CH units, $[1,2,3\text{-}P_3C_2H_2]^-$ and $[P_4CH]^-$ have both only been characterized by in situ ^{31}P NMR spectroscopy. All of the known species display very large $^{1}J_{P–C}$ and $^{1}J_{P–P}$ (where applicable) coupling constants, which is strongly indicative of multiple bond character within the ring.

The electronic structure of the pentaphospholide anion has been investigated by UV and photoelectron spectroscopy.[229,230] The UV spectrum shows π– π* transitions at 260 and 320 nm. A combined theoretical and photoelectron spectroscopic investigation, showed orbitals of π symmetry comparable to those in $[C_5H_5]^-$.

The aromaticity of the phospholides has been confirmed and studied computationally using a variety of methods. Early semi-empirical work suggested that the anions have from 86–101% of the aromaticity of $[C_5H_5]^-$, increasing with the number of phosphorus atoms in the ring.[231] More recently, the nucleus-independent chemical shift (NICS) at the centre of the rings (NICS(0)) have been calculated.[232,233] The aromatic stabilization energies of the anions have also been calculated.[234] These support the earlier work, and suggest that the level of aromaticity in the phospholides is comparable to that of the cyclopentadienide anion.

1.6.3.1.2 Synthesis

The monophospholides, $[PC_4R_4]^-$, have the most established and general routes to their synthesis. The first developed synthesis involves the reductive cleavage of the P–Ph bond in *P*-phenylphospholes with alkali metals, eliminating MPh (M = Li, Na, K) (Scheme 1.7).[235]

This proceeds via a detectable phosphole radical anion.[236] The method has been used to prepare a wide range of monophospholides. Mathey and co-workers developed an alternative method for preparing α-functionalized anions, or for phospholides bearing groups sensitive to reductive conditions.[237]

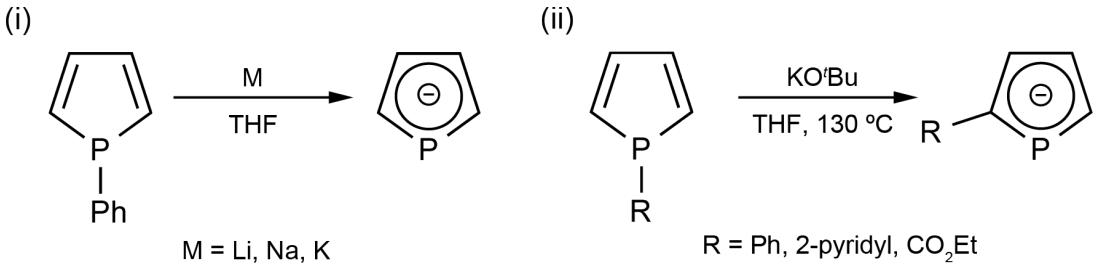

Scheme 1.7: The Braye (i) and Mathey (ii) syntheses of monophospholide anions.

The initial route to 1,2-diphospholides was devised by Mathey, and proceeds in low yields to give lithium salts of $[1,2\text{-}P_2\text{-}3,4\text{-}(CR)_2CH]^-$ (R = Et, Ph) anions.[238] These were not isolated, but instead identified by their ^{31}P NMR spectra and mass spectrometry. The isolation and structural verification of $[1,2\text{-}P_2C_3Ph_3]^-$ by single crystal X-ray structural analysis was achieved by reaction of solutions of NaP_5 with a nickel organometallic compound (Scheme 1.8).

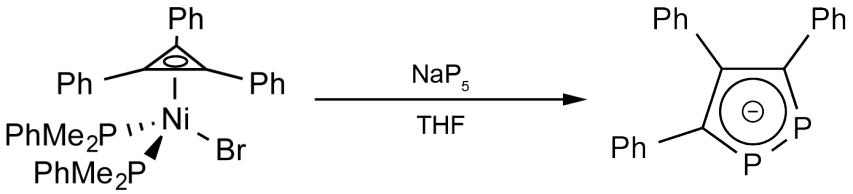

Scheme 1.8: Nickel promoted synthesis of a 1,2-diphospholide.

The 1,3-isomer is relatively more accessible. The $[1,3\text{-}P_2C_3{}^tBu_3]^-$ anion was initially synthesized by reaction of the phosphaalkyne with $LiP(SiMe_3)_2$,[239] but was later discovered to be one of the products resulting from the chemical reduction of phosphaalkynes with alkali metals.[240–242] A more selective synthesis from phosphaalkynes proceeds through

trimerization of phosphaalkynes into triphosphabenzene followed by reaction with potassium or a lithium amide.[220,243] Another route starts from dihydrophosphetenes and proceeds through a ring expansion/reduction methodology but does not allow isolation of the free anions.[244]

The other product resulting from the reduction of phosphaalkynes are the 1,3,4-triphospholides.[240,241,245–247] The best known, due to the relative accessibility of the requisite phosphaalkyne, is the di-^{t}Bu substituted anion. The synthesis of this particular anion has since been refined by Russell and co-workers who prepared exclusively this isomer from phosphaalkynes, uncontaminated by the 1,2-diphospholide (Scheme 1.9).[221,248]

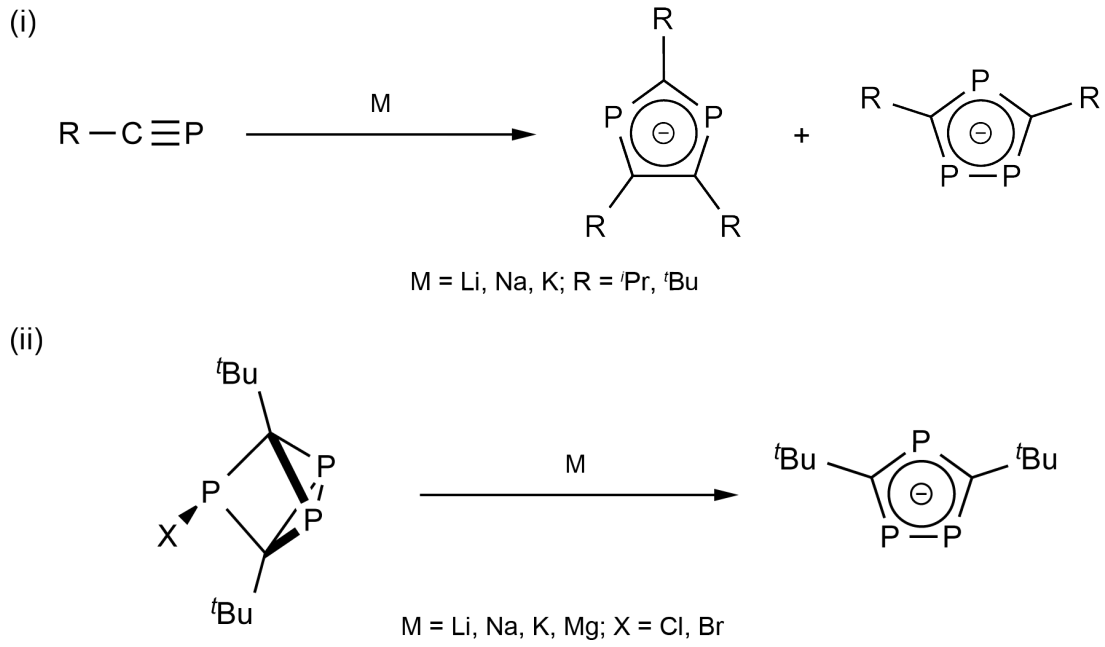

Scheme 1.9: The chemical reduction of phosphaalkynes (i) and a selective synthesis of the [1,3,4-$P_3C_2{}^tBu_2]^-$ anion (ii).

1,2,3-triphospholide anions are considerably rarer. Spectroscopic observation of the parent [1,2,3-$P_3C_2H_2]^-$ anion by reaction of P_4 and sodium in refluxing diglyme was reported by Baudler in 1987,[249,250] and an extremely laborious, low-yielding synthesis to [1,2,3-$P_3C_2R_2]^-$ (R = Ph, ^{t}Bu) by Mathey in 1995.[251] More recently, two reports of the 1,2,3-

triphosphaindenide anion were independently reported by the groups of Russell and Wright (Scheme 1.10).[222,223]

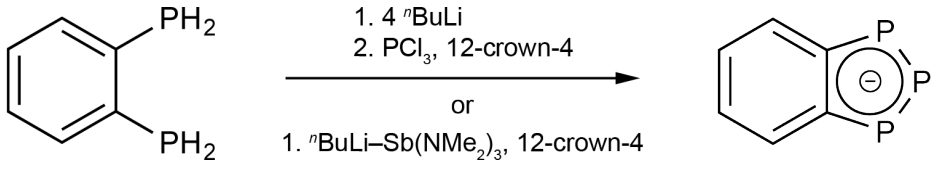

Scheme 1.10: The Russell (top) and Wright (bottom) syntheses of the 1,2,3-triphosphaindenide anion.

Alongside the report of $[1,2,3\text{-}P_3C_2H_2]^-$, Baudler also observed the $[P_4CH]^-$ anion by ^{31}P NMR spectroscopy.[249] The only other known example, $[P_4C(mes^*)]^-$, is isolated via fractional crystallization amongst a host of other phosphorus containing products from the reaction of $P(SiMe_3)_3$, 2,4,6-tri-tert-butylbenzoyl chloride and CsF.[224]

Replacement of all CH units within the cyclopentadienide anion with P gives the *cyclo*-$[P_5]^-$ anion. This is an excellent example of a polyphosphide exhibiting charge delocalization. It is also of particular interest for its potential in the formation of entirely inorganic metallocenes. The remarkable $[Ti(\eta^5\text{-}P_5)_2]^{2-}$ anion synthesized by Ellis and co-workers is to date the only reported example of such a molecule, and will be discussed later.[252] Despite this, and several other examples of η^5-coordinated $[P_5]^-$ moieties, the isolation of a salt of $[P_5]^-$ as a compositionally pure solid has thus far eluded chemists. Solutions of the anion as the Na^+ or K^+ salt can be prepared in low yield (~15% based on phosphorus) alongside other polyphosphides by the reaction of the alkali metal with P_4 in ethereal solvents,[229,249] or alternatively by the action of KPH_2 on red phosphorus in refluxing DMF.[253] All attempts to isolate a solid are reported to result in decomposition of the anion to red phosphorus and higher polyphosphides.

Predictably, due to the reduced propensity of the elements to engage in π bonding, there are far fewer reported examples of the heavier pnictolides (arsolides and stibolides). The monoarsolides are known as both free anions and coordinated to transition metals,[254–260] while the pentaarsolide anion has only been observed coordinated to and created in the sphere of a transition metal.[261–267] Stibolides are rarer still, with only a small handful of monostibolides known.[256,260,268,269] The group of Jones has additionally reported the synthesis of a 2,4-diphosphastibolide anion by reaction of [Li][$Sb(SiMe_3)_2$] with a phosphaalkyne.[270]

1.6.3.1.3 Reactivity Towards Organic Molecules

Exploration of the chemistry of the pnictolides has mostly been restricted to the chemistry of the phospholides. The monophospholides react exclusively at phosphorus, whereas the polyphospholides show a more diverse, albeit less controllable, reactivity.

The addition of electrophiles to the monophospholides can give a range of products. Alkylation with alkyl halides forms the 1-alkylphospholes, which has been exploited to form macrocyclic polyphosphole ligands.[271–274] The initial product of protonation is similarly a 1*H*-phosphole, but these are unstable and rapidly undergo [1,5] sigmatropic shifts to give 2*H*-phospholes (Scheme 1.11). These are in turn also unstable and dimerize, with the end product being dependent on the level of steric bulk on the ring. Unhindered phospholes undergo a [4+2] cycloaddition, while hindered phospholes react by addition of a P–H bond to a P=C bond.[275–277]

The electrophilic reactivity of the monophospholides has been used to effect cyanation, silylation and stannylation.[278] Oxidation by chalcogens and oxidative coupling using halogens has also been reported.[278,279]

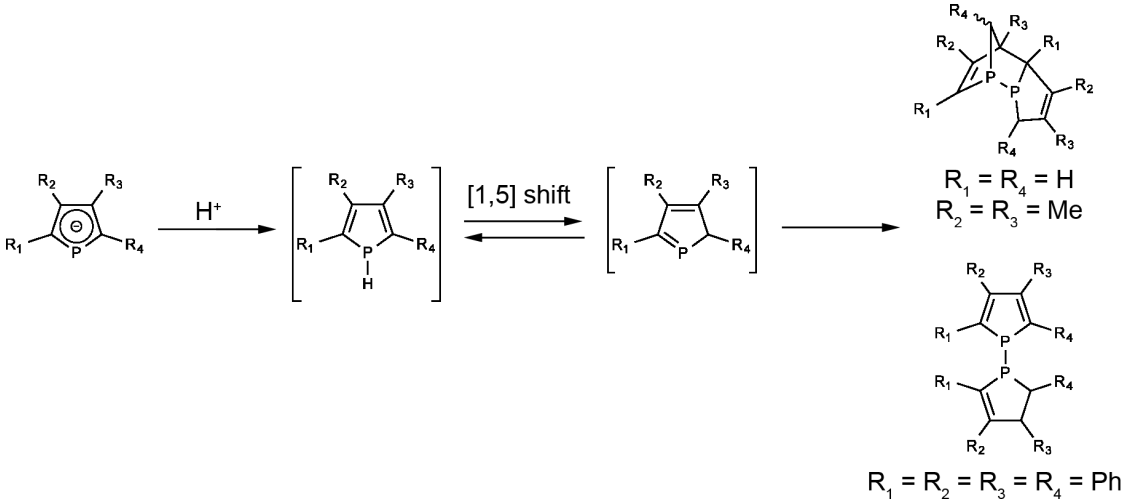

Scheme 1.11: The contrasting results of protonation of the monophospholides.

Polyphospholides show a rather more interesting pattern of reactivity. Due to the presence of multiple phosphorus atoms in the ring, any reaction with electrophiles inevitably results in initial products with isolated P=P or P=C double bonds. These generally dimerize, polymerize, or decompose. The only known exception to this are the triphospholes prepared by Nixon and co-workers through alkylation of 1,3,4-triphospholides (Scheme 1.12).[280,281] The stability is attributed to the extreme bulk of the alkyl group and presence of electron accepting groups on the ring that impose electron delocalization, and indeed aromaticity, upon the system.

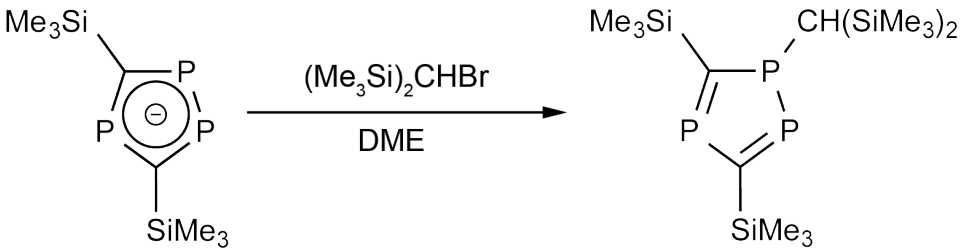

Scheme 1.12: *P*-alkylation of a 1,3,4-triphospholide to give an aromatic triphosphole.

The usual products of electrophilic addition to the ring are unstable. Protonation of the 4,5-diphenyl-1,3-diphospholide occurs at the P–C–P unit, and results in a ring system with two

P=C bonds.[282] These can be trapped by either MeSH or *N*-phenylmaleimide. The protonation of the [1,3,4-$P_3C_2{}^tBu_2$]$^-$ anion similarly occurs at phosphorus, but the resulting species undergoes sequential [4+2] and [2+2] cycloadditions to give a remarkable [$P_6C_4{}^tBu_4H_2$] cage (Scheme 1.13).[283] Addition of H^+ to equimolar quantities of the [1,3-$P_2C_3{}^tBu_3$]$^-$ and [1,3,4-$P_3C_2{}^tBu_2$]$^-$ anions also effects a [4+2] cycloaddition.[284]

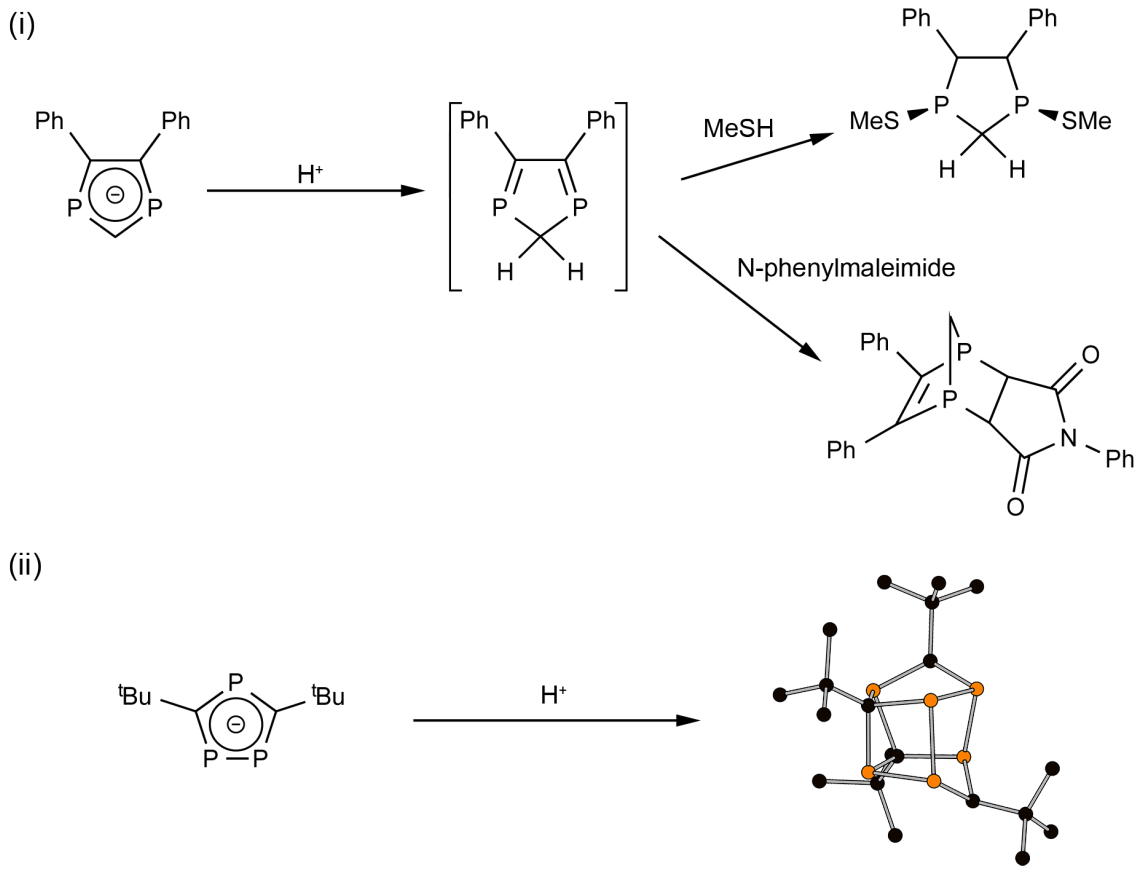

Scheme 1.13: The trapped products resulting from the protonation of a 1,3-diphospholide (i). Ball and stick representation of the cage compound resulting from the protonation of a 1,3,4-triphospholide (ii).

Attempts to alkylate the [P_5]$^-$ anion result in the formation of the aforementioned nortricyclane-like [P_7R_3] compounds, amongst others.[229] Apparently the initial product is so unstable that a complex series of rearrangement reactions occurs.

Finally, the oxidative coupling of polyphospholides with transition metal halides has been observed. The reaction of $[Ru(COD)Cl_2]_x$ with $[1,3\text{-}P_2C_3{}^tBu_3]^-$ results in P–P coupling,[285] while a mixture of $[1,3\text{-}P_2C_3{}^tBu_3]^-$ and $[1,3,4\text{-}P_3C_2{}^tBu_2]^-$ is oxidatively coupled into a phosphorus-carbon cage by $FeCl_3$ or $CoBr_2$.[286]

1.6.3.1.4 Pnictolides as Ligands

The close resemblance of the phospholides to cyclopentadienide means that there is considerable interest in exploiting them as ligands for metals. The presence of phosphorus atoms within the five-membered anionic ring results in two major differences in the coordination chemistry of the phospholides compared to cyclopentadienides.

The first difference is the relative lowering of the ligand π orbitals. The presence of low-lying unoccupied π orbitals means that the phospholides are good π acceptor ligands. As a result, they are capable of stabilizing unusual low oxidation state, electron rich metal centres. Two excellent examples of this can be found within titanium chemistry. The first inorganic metallocene, $[Ti(\eta^5\text{-}P_5)_2]^{2-}$, is formed by reaction of P_4 with a naphthalene-stabilized titanate (Figure 1.23).[252] The strongest metal-ligand interaction in the sandwich complex is found to be a back-bonding contribution from the filled metal e_2' orbitals into the ring e_2' π orbitals, which strongly stabilize the formally Ti(0) metal centre. This confers unusual stability – in contrast to other Ti(0) species, $[Ti(\eta^5\text{-}P_5)_2]^{2-}$ is air stable in the solid state and solution.

Co-condensation of ^{t}BuCP and Ti vapour leads to the formation of the hexaphosphatitanocene $[Ti(1,3,4\text{-}P_3C_2{}^tBu_2)_2]$.[287] This is found to be diamagnetic, and stable in both the solid state and solution under a dinitrogen atmosphere. In contrast, $[Ti(C_5Me_5)_2]$ is paramagnetic, undergoes reversible C–H activation in solution, and binds dinitrogen.[288]

Theoretical and photoelectron spectroscopic studies upon the hexaphosphatitanocene show that there is extensive metal–ligand backbonding, resulting in the formation of a δ bond.[289]

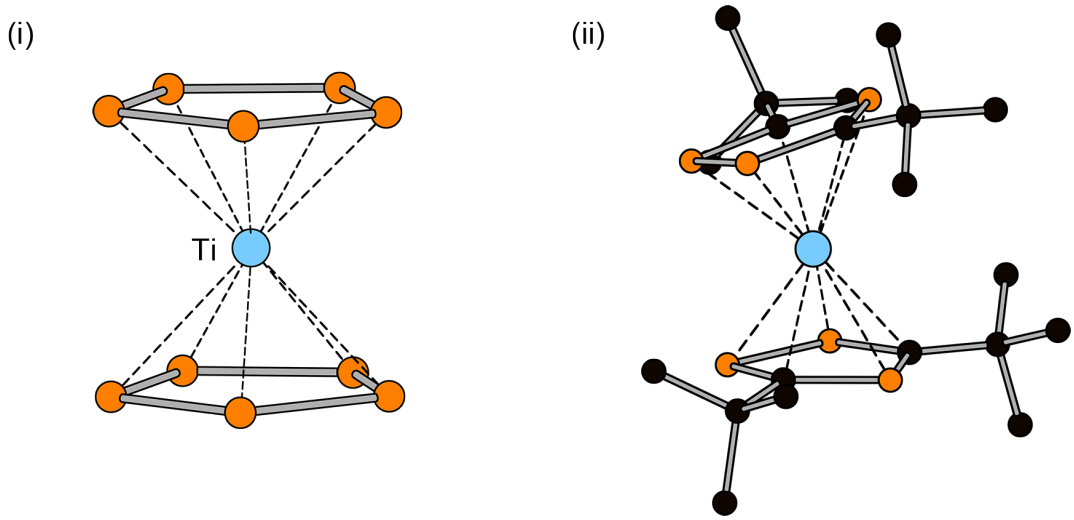

Figure 1.23: Ball and stick representations of $[Ti(\eta^5\text{-}P_5)_2]^{2-}$ (i) and $[Ti(1,3,4\text{-}P_3C_2{}^tBu_2)_2]$ (ii). Hydrogen atoms have been omitted for clarity.

There are other examples of unusual oxidation states, or ground electronic states that are stabilized by the π acceptor character of the phospholyl ligands. They have been used to stabilize the Tm(II) oxidation state in homoleptic bis(phospholyl) and bis(arsolyl) complexes.[258] Zenneck and co-workers have reported the synthesis of $[Mn(1,3,4\text{-}P_3C_2{}^tBu_2)_2]$, which is found to have an unusual low spin ^2A ground state by ESR spectroscopy, compared to the more usual ^2E ground state found for $[Mn(C_5Me_5)_2]$.[290] This is caused by the reversal of the frontier orbital ordering in the phosphorus-containing compound. They attribute this not only to the strong π acceptor properties of the triphospholyl ligand, but also to the increased size of the ring.

The enhanced π acceptor abilities suggest that phospholides should be considered as ligands for chemical processes where a Lewis acidic metal centre is required. The archetypal example of this in catalysis is the polymerization of olefins using homogeneous Ziegler-

Natta zirconium and titanium metallocenes. The prototypical catalyst for this is $[Cp_2ZrMe]^+$, formed by the reaction of $(MeAlO)_n$ (MAO) with $[Cp_2ZrCl_2]$.[291] Several Ti and Zr phospholyl complexes have been synthesized and tested in the polymerization of alkenes. The most notable are shown in Figure 1.24.[292,293] In both cases, activity is comparable to the all-carbon catalysts, but coordination of excess MAO to the phosphorus lone pair can retard reactivity. In this specific case, it is a major drawback, but illustrates the second major difference between the phospholides and the cyclopentadienides, namely the presence of lone pairs on phosphorus allowing additional coordination modes to metals.

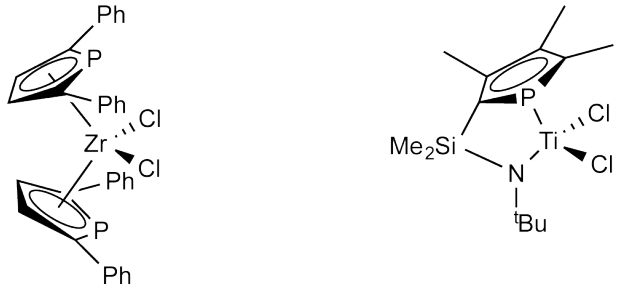

Figure 1.24: Two of the reported phospholide based polymerization catalysts.

The lone pair chemistry is perhaps best illustrated by the 1,3,4-triphospholide anion, for which at least five coordination modes are known and crystallographically characterized (Figure 1.25).[294–297]

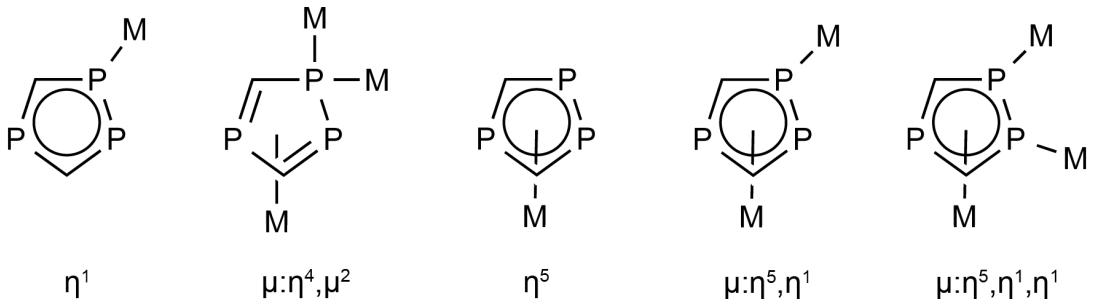

Figure 1.25: Crystallographically characterized coordination modes of 1,3,4-triphospholides.

This additional coordination chemistry available beyond the simple η^5, six-electron donor mode has been exploited to design unusual molecules. Of particular note is the work of Scheer on supramolecular systems, and Fu on asymmetric catalysis.

The group of Scheer has used the metallocenes $[Fe(\eta^5\text{-}C_5Me_5)(\eta^5\text{-}P_5)]$ to form one- or two-dimensional coordination polymers by reaction with copper(I) halides.[298] Under the right conditions, however, a three-dimensional fullerene-like cage of the formula $[\{Cp^*Fe(\eta^5{:}\eta^1{:}\eta^1{:}\eta^1{:}\eta^1\text{-}P_5)\}_{12}\{CuCl\}_{10}\{Cu_2Cl_3\}_5\{Cu(CH_3CN)_2\}_5]$ is formed (Figure 1.25).[299] This process has been elaborated upon to create spherical molecules of varying nuclearities that can form a variety of host-guest complexes.[300–302]

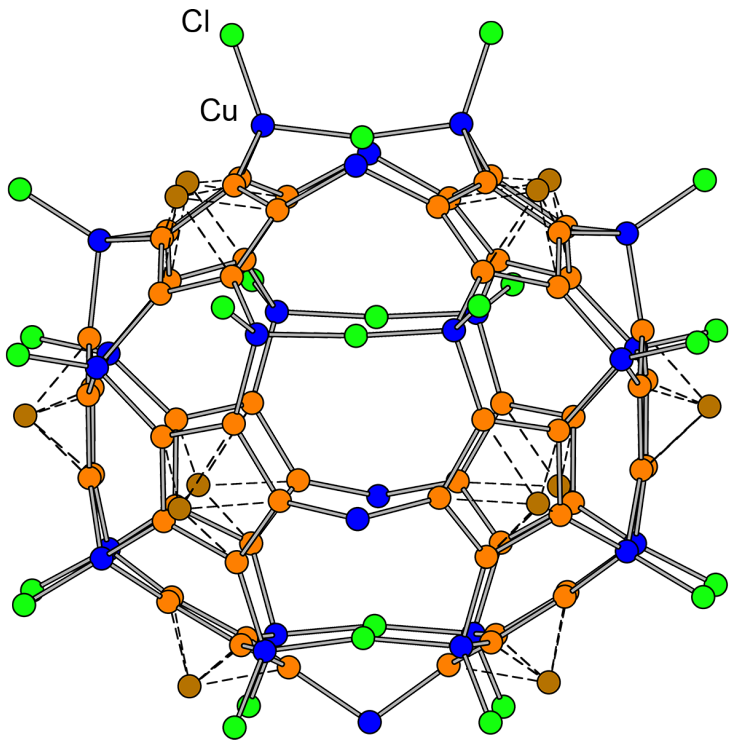

Figure 1.26: Ball and stick model of the inorganic core of $[\{Cp^*Fe(\eta^5{:}\eta^1{:}\eta^1{:}\eta^1{:}\eta^1\text{-}P_5)\}_{12}\{CuCl\}_{10}\{Cu_2Cl_3\}_5\{Cu(CH_3CN)_2\}_5]$. All carbon atoms and solvent molecules have been omitted for clarity.

Fu and co-workers have used the planar chirality inherent to disymmetrically substituted monophosphaferrocenes alongside the coordinating ability of the phosphorus lone pair in

asymmetric catalysis. A variety of enantioselective rhodium catalyzed transformations supported by a planar chiral chelating phosphaferrocene have been reported, including hydrogenations and isomerizations.[303–305]

1.7 Project Objectives

In 2010, when this work commenced, the reactivity of group 15 Zintl anions was underdeveloped compared to their neighbours in group 14. The literature existing on the reactivity of heptapnictide clusters focused almost exclusively on metalation reactions, with only simple alkylations known.

The initial aim of this work was to investigate the binding and reduction of carbon dioxide using the $[P_7]^{3-}$ cluster anion. This required the synthesis of a well-characterized, soluble precursor to the $[P_7]^{3-}$ anion in solution, which will be described in Chapter Two. The research on the reactivity of heptaphosphide clusters towards both carbon dioxide and the isolobal isocyanantes and carbodiimides will then be discussed in Chapter Three.

Building on the results obtained and detailed in Chapters Two and Three, the reactivity studies were extended to other unsaturated organic molecules, particularly alkynes. The chemistry stemming from these investigations will be described in Chapters Four to Six.

1.8 References

(1) Filippelli, G. M. *Elements* **2008**, *4*, 89–95.

(2) Westheimer, F. H. *Science* **1987**, *235*, 1173–1178.

(3) Emsley, J. *The Shocking History of Phosphorus: a Biography of the Devil's Element*; Pan: London, 2001.

(4) Corbridge, D. E. . *Phosphorus: Chemistry, Biochemistry and Technology*; CRC Press: Boca Raton, 2013.

(5) Engel, R. *Synthesis of Carbon–Phosphorus Bonds*; 2nd ed.; CRS Press: Boca Raton, 2004.

(6) Quin, L. D. *A Guide to Organophosphorus Chemistry*; Wiley: New York, 2000.

(7) MacLeod, I. J.; Rogers, A. P. V. *Yearbook of International Humanitarian Law* **2007**, *10*, 75–97.

(8) Schedule 3, C. W. C., Organisation for the Prohibition of Chemical Weapons, last reviewed April 2008.

(9) Huheey, J. E. *Inorganic Chemistry: Principles of Structure and Reactivity*; 4th ed.; Harper Collins: New York, 1993.

(10) Bock, H.; Mueller, H. *Inorg. Chem.* **1984**, *23*, 4365–4368.

(11) Stevenson, D. P.; Yost, D. M. *J. Chem. Phys.* **1941**, *9*, 403.

(12) Rathenau, G. *Physica* **1937**, *4*, 503–514.

(13) *Gmelins Handbuch der Anorganischen Chemie, Arsen*; Verlag Chemie: Weinheim, 1952; Vol. 17.

(14) Piro, N. A.; Figueroa, J. S.; McKellar, J. T.; Cummins, C. C. *Science* **2006**, *313*, 1276–1279.

(15) Tofan, D.; Cummins, C. C. *Angew. Chem., Int. Ed.* **2010**, *49*, 7516–7518.

(16) Wang, Y.; Xie, Y.; Wei, P.; King, R. B.; Schaefer, I.; Schleyer, P. von R.; Robinson, G. H. *J. Am. Chem. Soc.* **2008**, *130*, 14970–14971.

(17) Abraham, M. Y.; Wang, Y.; Xie, Y.; Wei, P.; Schaefer, H. F.; Schleyer, P. von R.; Robinson, G. H. *Chem. Eur. J.* **2010**, *16*, 432–435.

(18) Back, O.; Kuchenbeiser, G.; Donnadieu, B.; Bertrand, G. *Angew. Chem., Int. Ed.* **2009**, *48*, 5530–5533.

(19) Jutzi, P. *Angew. Chem. Int. Ed. Engl.* **1975**, *14*, 232–245.

(20) Dasent, W. E. *Inorganic Energetics: An Introduction*; 2nd ed.; Cambridge University Press: Cambridge, 1982.

(21) Mochizuki, Y.; Tanaka, K. *Chem. Phys. Lett.* **1997**, *274*, 264–268.

(22) Power, P. P. *Chem. Rev.* **1999**, *99*, 3463–3504.

(23) Fischer, R. C.; Power, P. P. *Chem. Rev.* **2010**, *110*, 3877–3923.

(24) Simon, A.; Borrmann, H.; Craubner, H. *Phosphorus and Sulfur and the Related Elements* **1987**, *30*, 507–510.

(25) Rodionov, A.; Kalendarev, R.; Eiduss, J.; Zhukovskii, Y. *J. Mol. Struct.* **1996**, *380*, 257–266.

(26) Norman, N. C. *Chemistry of Arsenic, Antimony, and Bismuth*; 1st ed.; Blackie Academic & Professional: London, 1998.

(27) Thurn, H.; Krebs, H. *Acta. Cryst. B* **1969**, *25*, 125–135.

(28) Greenwood, N. N.; Earnshaw, A. *Chemistry of the Elements*; 2nd ed.; Butterworth Heinemann: Oxford, 1997.

(29) Hultgren, R.; Gingrich, N. S.; Warren, B. E. *J. Chem. Phys.* **1935**, *3*, 351.

(30) Lange, S.; Schmidt, P.; Nilges, T. *Inorg. Chem.* **2007**, *46*, 4028–4035.

(31) Ceppatelli, M.; Bini, R.; Caporali, M.; Peruzzini, M. *Angew. Chem., Int. Ed.* **2013**, *52*, 2313–2317.

(32) Jansen, M.; Moebs, M. *Inorg. Chem.* **1984**, *23*, 4486–4488.

(33) Leung, Y. C.; Waser, J.; Houten, S. v.; Vos, A.; Wiegers, G. A.; Wiebenga, E. H. *Acta. Cryst.* **1957**, *10*, 574–582.

(34) Schleyer, P. von R. *J. Am. Chem. Soc.* **1958**, *80*, 1700–1704.

(35) Hönle, W.; von Schnering, H. G.; Schmidpeter, A.; Burget, G. *Angew. Chem. Int. Ed. Engl.* **1984**, *23*, 817–818.

(36) Baudler, M. *Angew. Chem., Int. Ed.* **1982**, *21*, 492–512.

(37) Joannis, A. *C. R. Hebd. Seances Acad. Sci.* **1891**, *113*, 795.

(38) Joannis, A. *C. R. Hebd. Seances Acad. Sci.* **1892**, *114*, 585–587.

(39) Joannis, A. *Ann. Chim. Phys.* **1906**, *7*, 5–118.

(40) Kraus, C. A. *J. Am. Chem. Soc.* **1907**, *29*, 1557–1571.

(41) Smyth, F. H. *J. Am. Chem. Soc.* **1917**, *39*, 1299–1312.

(42) Peck, E. B. *J. Am. Chem. Soc.* **1918**, *40*, 335–347.

(43) Zintl, E.; Goubeau, J.; Dullenkopf, W. *Z. Phys. Chem., Abt. A* **1931**, *154*, 1.

(44) Zintl, E.; Dullenkopf, W. *Z. Phys. Chem., Abt. B* **1932**, *16*, 183–212.

(45) Zintl, E.; Harder, A. *Z. Phys. Chem., Abt. A* **1931**, *154*, 47–96.

(46) Zintl, E.; Kaiser, H. *Z. Anorg. Allg. Chem.* **1933**, *211*, 113–131.

(47) Kummer, D.; Diehl, L. *Angew. Chem. Int. Ed. Engl.* **1970**, *9*, 895–895.

(48) Corbett, J. D.; Adolphson, D. G.; Merryman, D. J.; Edwards, P. A.; Armatis, F. J. *J. Am. Chem. Soc.* **1975**, *97*, 6267–6268.

(49) Fässler, T. F.; Hoffmann, R. *Angew. Chem., Int. Ed.* **1999**, *38*, 543–546.

(50) Corbett, J. D. *Chem. Rev.* **1985**, *85*, 383–397.

(51) Corbett, J. D. *Angew. Chem., Int. Ed.* **2000**, *39*, 670–690.

(52) Manriquez, V.; Hönle, W.; von Schnering, H. G. *Z. Anorg. Allg. Chem.* **1986**, *539*, 95–109.

(53) Santandrea, R. P.; Mensing, C.; von Schnering, H. G. *Thermochim. Acta* **1986**, *98*, 301–311.

(54) Meyer, T.; Hönle, W.; von Schnering, H. G. *Z. Anorg. Allg. Chem.* **1987**, *552*, 69–80.

(55) Emmerling, F.; Rohr, C. *Z. Naturforsch., B: J. Chem. Sci.* **2002**, *57*, 963–975.

(56) Hirschle, C.; Röhr, C. *Z. Anorg. Allg. Chem.* **2000**, *626*, 1992–1998.

(57) Dahlmann, W.; von Schnering, H. G. *Naturwissenschaften* **1972**, *59*, 420–420.

(58) Dahlmann, W.; von Schnering, H. G. *Naturwissenschaften* **1973**, *60*, 429–429.

(59) Schmettow, W.; von Schnering, H. G. *Angew. Chem. Int. Ed. Engl.* **1977**, *16*, 857–857.

(60) Baudler, M.; Glinka, K. *Inorg. Synth.* **1990**, *27*, 227–235.

(61) Beswick, M. A.; Choi, N.; Harmer, C. N.; Hopkins, A. D.; McPartlin, M.; Wright, D. S. *Science* **1998**, *281*, 1500–1501.

(62) Bashall, A.; Beswick, M. A.; Choi, N.; Hopkins, A. D.; Kidd, S. J.; Lawson, Y. G.; Mosquera, M. E. G.; McPartlin, M.; Raithby, P. R.; Wheatley, A. A. E. H.; Wood, J. A.; Wright, D. S. *J. Chem. Soc., Dalton Trans.* **2000**, 479–486.

(63) Fässler, T.; Armatas, G. S. *Zintl Ions: Principles and Recent Developments*; Structure and Bonding; Springer: Heidelberg ; New York, 2011.

(64) Wade, K. *J. Chem. Soc. D* **1971**, 792–793.

(65) Mingos, D. M. P. *Nature* **1972**, *236*, 99–102.

(66) Mingos, D. M. P. *Acc. Chem. Res.* **1984**, *17*, 311–319.

(67) Waibel, M.; Kraus, F.; Scharfe, S.; Wahl, B.; Fässler, T. F. *Angew. Chem. Int. Ed.* **2010**, *49*, 6611–6615.

(68) Stegmaier, S.; Waibel, M.; Henze, A.; Jantke, L.-A.; Karttunen, A. J.; Fässler, T. F. *J. Am. Chem. Soc.* **2012**, *134*, 14450–14460.

(69) Wiesler, K.; Brandl, K.; Fleischmann, A.; Korber, N. *Z. Anorg. Allg. Chem.* **2009**, *635*, 508–512.

(70) Sen, T.; Poupko, R.; Fleischer, U.; Zimmermann, H.; Luz, Z. *J. Am. Chem. Soc.* **2000**, *122*, 889–896.

(71) Schröder, G. *Angew. Chem. Int. Ed. Engl.* **1963**, *2*, 481–482.

(72) Oth, J. F. M.; Müllen, K.; Gilles, J.-M.; Schröder, G. *Helv. Chim. Acta.* **1974**, *57*, 1415–1433.

(73) Poupko, R.; Zimmermann, H.; Müller, K.; Luz, Z. *J. Am. Chem. Soc.* **1996**, *118*, 7995–8005.

(74) Baudler, M.; Glinka, K. *Chem. Rev.* **1993**, *93*, 1623–1667.

(75) Baudler, M. *Angew. Chem., Int. Ed.* **1987**, *26*, 419–441.

(76) Von Schnering, H. G.; Hönle, W. *Chem. Rev.* **1988**, *88*, 243–273.

(77) Baudler, M.; Adamek, C.; Opiela, S.; Budzikiewicz, H.; Ouzounis, D. *Angew. Chem. Int. Ed. Engl.* **1988**, *27*, 1059–1061.

(78) Baudler, M.; Düster, D.; Germeshausen, J. *Z. Anorg. Allg. Chem.* **1986**, *534*, 19–26.

(79) Hanauer, T.; Aschenbrenner, J. C.; Korber, N. *Inorg. Chem.* **2006**, *45*, 6723–6727.

(80) Miluykov, V.; Kataev, A.; Sinyashin, O.; Lönnecke, P.; Hey-Hawkins, E. *Z. Anorg. Allg. Chem.* **2006**, *632*, 1728–1732.

(81) Baudler, M.; Düster, D.; Langerbeins, K.; Germeshausen, J. *Angew. Chem. Int. Ed. Engl.* **1984**, *23*, 317–318.

(82) Von Schnering, H. G.; Manriquez, V.; Hönle, W. *Angew. Chem. Int. Ed. Engl.* **1981**, *20*, 594–595.

(83) Baudler, M.; Exner, O. *Chem. Ber.* **1983**, *116*, 1268–1270.

(84) Baudler, M.; Heumüller, R.; Hahn, J. *Z. Anorg. Allg. Chem.* **1985**, *529*, 7–14.

(85) Guerin, F.; Richeson, D. *Inorg. Chem.* **1995**, *34*, 2793–2794.

(86) Schoeller, W. W.; Staemmler, V.; Rademacher, P.; Niecke, E. *Inorg. Chem.* **1986**, *25*, 4382–4385.

(87) Scheer, M.; Balázs, G.; Seitz, A. *Chem. Rev.* **2010**, *110*, 4236–4256.

(88) Dielmann, F.; Sierka, M.; Virovets, A. V.; Scheer, M. *Angew. Chem., Int. Ed.* **2010**, *49*, 6860–6864.

(89) Cossairt, B. M.; Piro, N. A.; Cummins, C. C. *Chem. Rev.* **2010**, *110*, 4164–4177.

(90) Caporali, M.; Gonsalvi, L.; Rossin, A.; Peruzzini, M. *Chem. Rev.* **2010**, *110*, 4178–4235.

(91) Spinney, H. A.; Piro, N. A.; Cummins, C. C. *J. Am. Chem. Soc.* **2009**, *131*, 16233–16243.

(92) Tan, R. P.; Comerlato, N. M.; Powell, D. R.; West, R. *Angew. Chem. Int. Ed. Engl.* **1992**, *31*, 1217–1218.

(93) Fanta, A. D.; Tan, R. P.; Comerlato, N. M.; Driess, M.; Powell, D. R.; West, R. *Inorg. Chim. Acta.* **1992**, *198–200*, 733–739.

(94) Scherer, O. J.; Sitzmann, H.; Wolmershäuser, G. *Angew. Chem. Int. Ed. Engl.* **1989**, *28*, 212–213.

(95) Schwarzmaier, C.; Noor, A.; Glatz, G.; Zabel, M.; Timoshkin, A. Y.; Cossairt, B. M.; Cummins, C. C.; Kempe, R.; Scheer, M. *Angew. Chem., Int. Ed.* **2011**, *50*, 7283–7286.

(96) Riedel, R.; Hausen, H.-D.; Fluck, E. *Angew. Chem. Int. Ed. Engl.* **1985**, *24*, 1056–1057.

(97) Fox, A. R.; Wright, R. J.; Rivard, E.; Power, P. P. *Angew. Chem., Int. Ed.* **2005**, *44*, 7729–7733.

(98) Fritz, G.; Härer, J. *Z. Anorg. Allg. Chem.* **1983**, *504*, 23–37.

(99) Rauhut, M. M.; Semsel, A. M. *J. Org. Chem.* **1963**, *28*, 471–473.

(100) Rauhut, M. M.; Semsel, A. M. *J. Org. Chem.* **1963**, *28*, 473–477.

(101) Trofimov, B. A.; Brandsma, L.; Arbuzova, S. N.; Gusarova, N. K. *Russ. Chem. Bull.* **1997**, *46*, 849–850.

(102) Schmidpeter, A.; Burget, G.; Zwaschka, F.; Sheldrick, W. S. *Z. Anorg. Allg. Chem.* **1985**, *527*, 17–32.

(103) Igau, A.; Grützmacher, H.; Baceiredo, A.; Bertrand, G. *J. Am. Chem. Soc.* **1988**, *110*, 6463–6466.

(104) Arduengo, A. J.; Harlow, R. L.; Kline, M. *J. Am. Chem. Soc.* **1991**, *113*, 361–363.

(105) Bourissou, D.; Guerret, O.; Gabbaï, F. P.; Bertrand, G. *Chem. Rev.* **2000**, *100*, 39–92.

(106) Frey, G. D.; Lavallo, V.; Donnadieu, B.; Schoeller, W. W.; Bertrand, G. *Science* **2007**, *316*, 439–441.

(107) Masuda, J. D.; Schoeller, W. W.; Donnadieu, B.; Bertrand, G. *J. Am. Chem. Soc.* **2007**, *129*, 14180–14181.

(108) Masuda, J. D.; Schoeller, W. W.; Donnadieu, B.; Bertrand, G. *Angew. Chem., Int. Ed.* **2007**, *46*, 7052–7055.

(109) Dorsey, C. L.; Squires, B. M.; Hudnall, T. W. *Angew. Chem., Int. Ed.* **2013**, *52*, 4462–4465.

(110) Martin, C. D.; Weinstein, C. M.; Moore, C. E.; Rheingold, A. L.; Bertrand, G. *Chem. Commun.* **2013**, *49*, 4486–4488.

(111) Sato, A.; Yorimitsu, H.; Oshima, K. *J. Am. Chem. Soc.* **2006**, *128*, 4240–4241.

(112) Barton, D. H. R.; Zhu, J. *J. Am. Chem. Soc.* **1993**, *115*, 2071–2072.

(113) Barton, D. H. .; Vonder Embse, R. A. *Tetrahedron* **1998**, *54*, 12475–12496.

(114) Cossairt, B. M.; Cummins, C. C. *New J. Chem.* **2010**, *34*, 1533–1536.

(115) Baudler, M.; Heumüller, R.; Langerbeins, K. *Z. Anorg. Allg. Chem.* **1984**, *514*, 7–17.

(116) Aschenbrenner, A. C.; Korber, N. *Z. Anorg. Allg. Chem.* **2004**, *630*, 31–32.

(117) Dai, F. R.; Xu, L. *Inorg. Chim. Acta.* **2006**, *359*, 4265–4273.

(118) Fritz, G.; Biastoch, R.; Stoll, K.; Vaahs, T.; Hanke, D.; Schneider, H. W. *Phosphorus and Sulfur and the Related Elements* **1987**, *30*, 385–388.

(119) Fritz, G.; Harer, J.; Matern, E. *Z. Anorg. Allg. Chem.* **1983**, *504*, 38–46.

(120) Noblet, P.; Cappello, V.; Tekautz, G.; Baumgartner, J.; Hassler, K. *Eur. J. Inorg. Chem.* **2011**, *2011*, 101–109.

(121) Charles, S.; Fettinger, J. C.; Eichhorn, B. W. *J. Am. Chem. Soc.* **1995**, *117*, 5303–5311.

(122) Mattamana, S. P.; Promprai, K.; Fettinger, J. C.; Eichhorn, B. W. *Inorg. Chem.* **1998**, *37*, 6222–6228.

(123) Milyukov, V. A.; Kataev, A. V.; Hey-Hawkins, E.; Sinyashin, O. G. *Russ. Chem. Bull.* **2007**, *56*, 298–303.

(124) Baudler, M.; Faber, W.; Hahn, J. *Z. Anorg. Allg. Chem.* **1980**, *469*, 15–21.

(125) Fritz, G.; Hoppe, K. D.; Hönle, W.; Weber, D.; Mujica, C.; Manriquez, V.; von Schnering, H. G. *J. Organomet. Chem.* **1983**, *249*, 63–80.

(126) Fritz, G.; Schneider, H.-W. *Z. Anorg. Allg. Chem.* **1990**, *584*, 12–20.

(127) Von Schnering, H. G.; Fenske, D.; Hönle, W.; Binnewies, M.; Peters, K. *Angew. Chem. Int. Ed. Engl.* **1979**, *18*, 679–679.

(128) Fritz, G.; Layher, E.; Goesmann, H.; Hanke, D.; Persau, C. *Z. Anorg. Allg. Chem.* **1991**, *594*, 36–46.

(129) Ahlrichs, R.; Fenske, D.; Fromm, K.; Krautscheid, H.; Krautscheid, U.; Treutler, O. *Chem. Eur. J.* **1996**, *2*, 238–244.

(130) Scharfe, S.; Kraus, F.; Stegmaier, S.; Schier, A.; Fässler, T. F. *Angew. Chem., Int. Ed.* **2011**, *50*, 3630–3670.

(131) Knapp, C.; Zhou, B.; Denning, M. S.; Rees, N. H.; Goicoechea, J. M. *Dalton Trans.* **2009**, *39*, 426–436.

(132) Charles, S.; Fettinger, J. C.; Eichhorn, B. W. *Inorg. Chem.* **1996**, *35*, 1540–1548.

(133) Charles, S.; Fettinger, J. C.; Bott, S. G.; Eichhorn, B. W. *J. Am. Chem. Soc.* **1996**, *118*, 4713–4714.

(134) Kesanli, B.; Charles, S.; Lam, Y.-F.; Bott, S. G.; Fettinger, J.; Eichhorn, B. *J. Am. Chem. Soc.* **2000**, *122*, 11101–11107.

(135) Moses, M. J.; Fettinger, J.; Eichhorn, B. *J. Am. Chem. Soc.* **2002**, *124*, 5944–5945.

(136) Qian, M.; Reber, A. C.; Ugrinov, A.; Chaki, N. K.; Mandal, S.; Saavedra, H. M.; Khanna, S. N.; Sen, A.; Weiss, P. S. *ACS Nano* **2010**, *4*, 235–240.

(137) Mandal, S.; Reber, A. C.; Qian, M.; Liu, R.; Saavedra, H. M.; Sen, S.; Weiss, P. S.; Khanna, S. N.; Sen, A. *Dalton Trans.* **2012**, *41*, 12365–12377.

(138) Knapp, C. M.; Large, J. S.; Rees, N. H.; Goicoechea, J. M. *Dalton Trans.* **2010**, *40*, 735–745.

(139) Eichhorn, B. W.; Haushalter, R. C.; Huffman, J. C. *Angew. Chem. Int. Ed. Engl.* **1989**, *28*, 1032–1033.

(140) Charles, S.; Eichhorn, B. W.; Rheingold, A. L.; Bott, S. G. *J. Am. Chem. Soc.* **1994**, *116*, 8077–8086.

(141) Bolle, U.; Tremel, W. *J. Chem. Soc., Chem. Commun.* **1994**, 217–219.

(142) Charles, S.; Danis, J. A.; Mattamana, S. P.; Fettinger, J. C.; Eichhorn, B. W. *Z. Anorg. Allg. Chem.* **1998**, *624*, 823–829.

(143) Charles, S.; Danis, J. A.; Fettinger, J. C.; Eichhorn, B. W. *Inorg. Chem.* **1997**, *36*, 3772–3778.

(144) Kesanli, B.; Mattamana, S. P.; Danis, J.; Eichhorn, B. *Inorg. Chim. Acta.* **2005**, *358*, 3145–3151.

(145) Knapp, C. M.; Large, J. S.; Rees, N. H.; Goicoechea, J. M. *Chem. Commun.* **2011**, *47*, 4111–4113.

(146) Knapp, C. M. Solution Reactivity Studies of Group 15 Zintl Ions, University of Oxford, 2013.

(147) Goicoechea, J. M.; Hull, M. W.; Sevov, S. C. *J. Am. Chem. Soc.* **2007**, *129*, 7885–7893.

(148) Goicoechea, J. M.; Sevov, S. C. *Angew. Chem., Int. Ed.* **2006**, *45*, 5147–5150.

(149) Bobev, S.; Sevov, S. C. *Inorg. Chem.* **1999**, *38*, 2672–2675.

(150) Xu, L.; Sevov, S. C. *Inorg. Chem.* **2000**, *39*, 5383–5389.

(151) Weinert, B.; Weigend, F.; Dehnen, S. *Chem. Eur. J.* **2012**, *18*, 13589–13595.

(152) Von Schnering, H. G.; Wolf, J.; Weber, D.; Ramirez, R.; Meyer, T. *Angew. Chem. Int. Ed. Engl.* **1986**, *25*, 353–354.

(153) Eichhorn, B. W.; Mattamana, S. P.; Gardner, D. R.; Fettinger, J. C. *J. Am. Chem. Soc.* **1998**, *120*, 9708–9709.

(154) Kesanli, B.; Fettinger, J.; Eichhorn, B. *J. Am. Chem. Soc.* **2003**, *125*, 7367–7376.

(155) Kesanli, B.; Fettinger, J.; Scott, B.; Eichhorn, B. *Inorg. Chem.* **2004**, *43*, 3840–3846.

(156) Moses, M. J.; Fettinger, J. C.; Eichhorn, B. W. *Science* **2003**, *300*, 778–780.

(157) Moses, M. J.; Fettinger, J. C.; Eichhorn, B. W. *Inorg. Chem.* **2007**, *46*, 1036–1038.

(158) Charles, S.; Eichhorn, B. W.; Bott, S. G. *J. Am. Chem. Soc.* **1993**, *115*, 5837–5838.

(159) Knapp, C. M.; Westcott, B. H.; Raybould, M. A. C.; McGrady, J. E.; Goicoechea, J. M. *Angew. Chem., Int. Ed.* **2012**, *51*, 9097–9100.

(160) Knapp, C. M.; Westcott, B. H.; Raybould, M. A. C.; McGrady, J. E.; Goicoechea, J. M. *Chem. Commun.* **2012**, *48*, 12183–12185.

(161) Elian, M.; Chen, M. M. L.; Mingos, D. M. P.; Hoffmann, R. *Inorg. Chem.* **1976**, *15*, 1148–1155.

(162) Hoffmann, R. *Angew. Chem. Int. Ed. Engl.* **1982**, *21*, 711–724.

(163) Albright, T. A. *Tetrahedron* **1982**, *38*, 1339–1388.

(164) Chandrasekhar, J.; Schleyer, P. von R.; Schlegel, H. B. *Tetrahedron Lett.* **1978**, *19*, 3393–3396.

(165) *Quantities, Units and Symbols in Physical Chemistry*; Royal Society of Chemistry: Cambridge, 2002.

(166) Waluk, J.; Klein, H. P.; Ashe, A. J.; Michl, J. *Organometallics* **1989**, *8*, 2804–2808.

(167) *Multiple Bonds and Low Coordination in Phosphorus Chemistry*; Thieme: Stuttgart, 1990.

(168) Mathey, F. *Angew. Chem., Int. Ed.* **2003**, *42*, 1578–1604.

(169) Dillon, K. B. *Phosphorus: the Carbon Copy: From Organophosphorus to Phospha-organic Chemistry*; Wiley: Chichester, 1998.

(170) Bates, J. I.; Dugal-Tessier, J.; Gates, D. P. *Dalton Trans.* **2010**, *39*, 3151–3159.

(171) Norman, N. C. *Polyhedron* **1993**, *12*, 2431–2446.

(172) Green, J. C.; Green, M. L. H.; Morris, G. E. *J. Chem. Soc., Chem. Commun.* **1974**, 212–213.

(173) Haiduc, I. *The Chemistry of Inorganic Homo- and Heterocycles*; Academic Press: London, 1987.

(174) Klebach, T. C.; Lourens, R.; Bickelhaupt, F. *J. Am. Chem. Soc.* **1978**, *100*, 4886–4888.

(175) Allen, F. H.; Kennard, O.; Watson, D. G.; Brammer, L.; Orpen, A. G.; Taylor, R. *J. Chem. Soc., Perkin Trans. 2* **1987**, S1–S19.

(176) Schleyer, P. von R.; Kost, D. *J. Am. Chem. Soc.* **1988**, *110*, 2105–2109.

(177) Schmidt, M. W.; Truong, P. N.; Gordon, M. S. *J. Am. Chem. Soc.* **1987**, *109*, 5217–5227.

(178) Lacombe, S.; Gonbeau, D.; Cabioch, J. L.; Pellerin, B.; Denis, J. M.; Pfister-Guillouzo, G. *J. Am. Chem. Soc.* **1988**, *110*, 6964–6967.

(179) Schoeller, W. W. *J. Chem. Soc., Chem. Commun.* **1985**, 334–335.

(180) Navech, J.; Majoral, J. P.; Meriem, A.; Kramer, R. *Phosphorus and Sulfur and the Related Elements* **1983**, *18*, 27–30.

(181) Nyulászi, L.; Veszpremi, T.; Reffy, J. *J. Phys. Chem.* **1993**, *97*, 4011–4015.

(182) Wright, V. A.; Patrick, B. O.; Schneider, C.; Gates, D. P. *J. Am. Chem. Soc.* **2006**, *128*, 8836–8844.

(183) Hissler, M.; Dyer, P. W.; Réau, R. *Coordination Chemistry Reviews* **2003**, *244*, 1–44.

(184) Appel, R.; Casser, C.; Knoch, F. *Chem. Ber.* **1984**, *117*, 2693–2702.

(185) Tsang, C.-W.; Yam, M.; Gates, D. P. *J. Am. Chem. Soc.* **2003**, *125*, 1480–1481.

(186) Oehme, H.; Leissring, E.; Meyer, H. *Tetrahedron Lett.* **1980**, *21*, 1141–1144.

(187) Becker, G. *Z. Anorg. Allg. Chem.* **1976**, *423*, 242–254.

(188) Deschamps, B.; Mathey, F. *J. Chem. Soc., Chem. Commun.* **1985**, 1010–1012.

(189) Gaumont, A. C.; Denis, J. M. *Chem. Rev.* **1994**, *94*, 1413–1439.

(190) Mathey, F. *Acc. Chem. Res.* **1992**, *25*, 90–96.

(191) Floch, P. L. *Coord. Chem. Rev.* **2006**, *250*, 627–681.

(192) Gier, T. E. *J. Am. Chem. Soc.* **1961**, *83*, 1769–1770.

(193) Hopkinson, M. J.; Kroto, H. W.; Nixon, J. F.; Simmons, N. P. C. *J. Chem. Soc., Chem. Commun.* **1976**, 513–515.

(194) Becker, G.; Gresser, G.; Uhl, W. *Z. Naturforsch., B: J. Chem. Sci.* **1981**, *36*, 16–19.

(195) Antipin, M. Y.; Chernega, A. N.; Lysenko, K. A.; Struchkov, Y. T.; Nixon, J. F. *J. Chem. Soc., Chem. Commun.* **1995**, 505–506.

(196) Laali, K. K.; Geissler, B.; Regitz, M.; Houser, J. J. *J. Org. Chem.* **1995**, *60*, 6362–6367.

(197) Laurent, J. C. T. R. B.-S.; King, M. A.; Kroto, H. W.; Nixon, J. F.; Suffolk, R. J. *J. Chem. Soc., Dalton Trans.* **1983**, 755–759.

(198) Regitz, M. *Chem. Rev.* **1990**, *90*, 191–213.

(199) Laurent, J. C. T. R. B.-S.; Hitchcock, P. B.; Kroto, H. W.; Nixon, J. F. *J. Chem. Soc., Chem. Commun.* **1981**, 1141–1143.

(200) Nixon, J. F. *Coord. Chem. Rev.* **1995**, *145*, 201–258.

(201) Lammertsma, K. In *New Aspects in Phosphorus Chemistry III*; Majoral, J.-P., Ed.; Topics in Current Chemistry; Springer Berlin Heidelberg, 2003; pp. 95–119.

(202) Cade, P. E. *Can. J. Phys.* **1968**, *46*, 1989–1991.

(203) Li, X.; Weissman, S. I.; Lin, T.-S.; Gaspar, P. P.; Cowley, A. H.; Smirnov, A. I. *J. Am. Chem. Soc.* **1994**, *116*, 7899–7900.

(204) Schmidt, U. *Angew. Chem. Int. Ed. Engl.* **1975**, *14*, 523–528.

(205) Velian, A.; Cummins, C. C. *J. Am. Chem. Soc.* **2012**, *134*, 13978–13981.

(206) Aktaş, H.; Slootweg, J. C.; Lammertsma, K. *Angew. Chem., Int. Ed.* **2010**, *49*, 2102–2113.

(207) Cowley, A. H.; Barron, A. R. *Acc. Chem. Res.* **1988**, *21*, 81–87.

(208) Cowley, A. H. *Acc. Chem. Res.* **1997**, *30*, 445–451.

(209) Fischer, E. O.; Maasböl, A. *Angew. Chem. Int. Ed. Engl.* **1964**, *3*, 580–581.

(210) Schrock, R. R. *J. Am. Chem. Soc.* **1974**, *96*, 6796–6797.

(211) Hitchcock, P. B.; Lappert, M. F.; Leung, W.-P. *J. Chem. Soc., Chem. Commun.* **1987**, 1282–1283.

(212) Cowley, A. H.; Pellerin, B.; Atwood, J. L.; Bott, S. G. *J. Am. Chem. Soc.* **1990**, *112*, 6734–6735.

(213) Ehlers, A. W.; Baerends, E. J.; Lammertsma, K. *J. Am. Chem. Soc.* **2002**, *124*, 2831–2838.

(214) Mathey, F. *Phosphorus-Carbon Heterocyclic Chemistry: the Rise of a New Domain*; 1st ed.; Elsevier Science Ltd: Amsterdam ; New York, 2001.

(215) Mathey, F. In *Modern Heterocyclic Chemistry*; Alvarez-Builla, J.; Vaquero, J. J.; Barluenga, J., Eds.; Wiley-VCH Verlag GmbH & Co. KGaA, 2011; pp. 2071–2116.

(216) Müller, C.; Vogt, D. *Dalton Trans.* **2007**, 5505–5523.

(217) Mathey, F. *Coord. Chem. Rev.* **1994**, *137*, 1–52.

(218) Douglas, T.; Theopold, K. H. *Angew. Chem. Int. Ed. Engl.* **1989**, *28*, 1367–1368.

(219) Miluykov, V.; Kataev, A.; Sinyashin, O.; Lönnecke, P.; Hey-Hawkins, E. *Organometallics* **2005**, *24*, 2233–2236.

(220) Cloke, F. G. N.; Hitchcock, P. B.; Nixon, J. F.; Wilson, D. J. *Organometallics* **2000**, *19*, 219–220.

(221) Fish, C.; Green, M.; Jeffery, J. C.; Kilby, R. J.; Lynam, J. M.; Russell, C. A.; Willans, C. E. *Organometallics* **2005**, *24*, 5789–5791.

(222) Butts, C. P.; Green, M.; Hooper, T. N.; Kilby, R. J.; McGrady, J. E.; Pantazis, D. A.; Russell, C. A. *Chem. Commun.* **2008**, 856–858.

(223) García, F.; Less, R. J.; Naseri, V.; McPartlin, M.; Rawson, J. M.; Tomas, M. S.; Wright, D. S. *Chem. Commun.* **2008**, 859–861.

(224) Ionkin, A. S.; Marshall, W. J.; Fish, B. M.; Marchione, A. A.; Howe, L. A.; Davidson, F.; McEwen, C. N. *Eur. J. Inorg. Chem.* **2008**, *2008*, 2386–2390.

(225) Quin, L. D.; Orton, W. L. *J. Chem. Soc., Chem. Commun.* **1979**, 401–402.

(226) Chesnut, D. B.; Quin, L. D. *J. Am. Chem. Soc.* **1994**, *116*, 9638–9643.

(227) Charrier, C.; Mathey, F. *Tetrahedron Lett.* **1987**, *28*, 5025–5028.

(228) Toullec, P.; Mathey, F. *Synlett* **2001**, *2001*, 1977–1979.

(229) Baudler, M.; Akpapoglou, S.; Ouzounis, D.; Wasgestian, F.; Meinigke, B.; Budzikiewicz, H.; Münster, H. *Angew. Chem., Int. Ed.* **1988**, *27*, 280–281.

(230) Zhai, H.-J.; Wang, L.-S.; Kuznetsov, A. E.; Boldyrev, A. I. *J. Phys. Chem. A* **2002**, *106*, 5600–5606.

(231) Malar, E. J. P. *J. Org. Chem.* **1992**, *57*, 3694–3698.

(232) Schleyer, P. von R.; Jiao, H.; Hommes, N. J. R. van E.; Malkin, V. G.; Malkina, O. L. *J. Am. Chem. Soc.* **1997**, *119*, 12669–12670.

(233) Dransfeld, A.; Nyulászi, L.; Schleyer, P. von R. *Inorg. Chem.* **1998**, *37*, 4413–4420.

(234) Cyrañski, M. K.; Krygowski, T. M.; Katritzky, A. R.; Schleyer, P. von R. *J. Org. Chem.* **2002**, *67*, 1333–1338.

(235) Braye, E. H.; Caplier, I.; Saussez, R. *Tetrahedron* **1971**, *27*, 5523–5537.

(236) Thomson, C.; Kilcast, D. *Angew. Chem. Int. Ed. Engl.* **1970**, *9*, 310–311.

(237) Holand, S.; Jeanjean, M.; Mathey, F. *Angew. Chem. Int. Ed. Engl.* **1997**, *36*, 98–100.

(238) Maigrot, N.; Avarvari, N.; Charrier, C.; Mathey, F. *Angew. Chem. Int. Ed. Engl.* **1995**, *34*, 590–592.

(239) Becker, G.; Becker, W.; Kuebl, R.; Schmidt, H.; Webber, U.; Westerhausen, M. *Nova Acta Leopold.* **1985**, *59*, 55–67.

(240) Bartsch, R.; Nixon, J. F. *Polyhedron* **1989**, *8*, 2407.

(241) Bartsch, R.; Nixon, J. F. *J. Organomet. Chem.* **1991**, *415*, C15–C18.

(242) Cowley, A. H.; Hall, S. W. *Polyhedron* **1989**, *8*, 849–850.

(243) Clendenning, S. B.; Hitchcock, P. B.; Lappert, M. F.; Merle, P. G.; Nixon, J. F.; Nyulászi, L. *Chem. Eur. J.* **2007**, *13*, 7121–7128.

(244) Maigrot, N.; Ricard, L.; Charrier, C.; Mathey, F. *Angew. Chem. Int. Ed. Engl.* **1990**, *29*, 534–535.

(245) Mansell, S. M.; Green, M.; Kilby, R. J.; Murray, M.; Russell, C. A. *C. R. Chim.* **2010**, *13*, 1073–1081.

(246) Ionkin, A. S.; Marshall, W. J.; Fish, B. M.; Schiffhauer, M. F.; Davidson, F.; McEwen, C. N. *Organometallics* **2009**, *28*, 2410–2416.

(247) Callaghan, C.; Clentsmith, G. K. B.; Cloke, F. G. N.; Hitchcock, P. B.; Nixon, J. F.; Vickers, D. M. *Organometallics* **1999**, *18*, 793–795.

(248) Lynam, J. M.; Copsey, M. C.; Green, M.; Jeffery, J. C.; McGrady, J. E.; Russell, C. A.; Slattery, J. M.; Swain, A. C. *Angew. Chem., Int. Ed.* **2003**, *42*, 2778–2782.

(249) Baudler, M.; Düster, D.; Ouzounis, D. *Z. Anorg. Allg. Chem.* **1987**, *544*, 87–94.

(250) Hahn, J.; Baudler, M. *Z. Naturforsch. B* **1990**, *45*, 1139–1142.

(251) Maigrot, N.; Sierra, M.; Charrier, C.; Mathey, F. *Bull. Soc. Chim. Fr.* **1994**, *131*, 397–399.

(252) Urnėžius, E.; Brennessel, W. W.; Cramer, C. J.; Ellis, J. E.; Schleyer, P. von R. *Science* **2002**, *295*, 832–834.

(253) Baudler, M.; Etzbach, T. *Chem. Ber.* **1991**, *124*, 1159–1160.

(254) Westerhausen, M.; Digeser, M. H.; Gückel, C.; Nöth, H.; Knizek, J.; Ponikwar, W. *Organometallics* **1999**, *18*, 2491–2496.

(255) Ashe, A. J.; Mahmoud, S.; Elschenbroich, C.; Wünsch, M. *Angew. Chem. Int. Ed. Engl.* **1987**, *26*, 229–230.

(256) Ashe, A. J.; Kampf, J. W.; Pilotek, S.; Rousseau, R. *Organometallics* **1994**, *13*, 4067–4071.

(257) Chiche, L.; Galy, J.; Thiollet, G.; Mathey, F. *Acta. Cryst. B* **1980**, *36*, 1344–1347.

(258) Nief, F.; Turcitu, D.; Ricard, L. *Chem. Commun.* **2002**, 1646–1647.

(259) Westerhausen, M.; Birg, C.; Piotrowski, H. *Eur. J. Inorg. Chem.* **2000**, *2000*, 2173–2178.

(260) Westerhausen, M.; Ossberger, M. W.; Mayer, P.; Piotrowski, H.; Nöth, H. *Organometallics* **2004**, *23*, 3417–3424.

(261) Krauss, H.; Balázs, G.; Bodensteiner, M.; Scheer, M. *Chem. Sci.* **2010**, *1*, 337–342.

(262) Scherer, O. J.; Blath, C.; Heckmann, G.; Wolmershäuser, G. *J. Organomet. Chem.* **1991**, *409*, C15–C18.

(263) Scherer, O. J.; Blath, C.; Wolmershäuser, G. *J. Organomet. Chem.* **1990**, *387*, C21–C24.

(264) Scherer, O. J.; Wiedemann, W.; Wolmershäuser, G. *Chem. Ber.* **1990**, *123*, 3–6.

(265) Scherer, O. J.; Wiedemann, W.; Wolmershäuser, G. *J. Organomet. Chem.* **1989**, *361*, C11–C14.

(266) Rink, B.; Scherer, O. J.; Heckmann, G.; Wolmershauser, G. *Chem. Ber.* **1992**, *125*, 1011–1016.

(267) Detzel, M.; Friedrich, G.; Scherer, O. J.; Wolmershäuser, G. *Angew. Chem. Int. Ed. Engl.* **1995**, *34*, 1321–1323.

(268) Ashe III, A. J.; Al-Ahmad, S. In *Advances in Organometallic Chemistry*; F. Gordon, A. S. and R. W., Ed.; Academic Press, 1996; Vol. Volume 39, pp. 325–353.

(269) Sierra, M. L.; Charrier, C.; Ricard, L.; Mathey, F. *Bull. Soc. Chim. Fr.* **1993**, *130*, 521–526.

(270) Francis, M. D.; Hibbs, D. E.; Hursthouse, M. B.; Jones, C.; Malik, K. M. A. *J. Organomet. Chem.* **1997**, *527*, 291–293.

(271) Deschamps, B.; Mathey, F. *Tetrahedron Lett.* **1985**, *26*, 3461–3462.

(272) Holand, S.; Mathey, F. *J. Org. Chem.* **1981**, *46*, 4386–4389.

(273) Charrier, C.; Maigrot, N.; Mathey, F. *Organometallics* **1987**, *6*, 586–591.

(274) Laporte, F.; Mercier, F.; Ricard, L.; Mathey, F. *J. Am. Chem. Soc.* **1994**, *116*, 3306–3311.

(275) Charrier, C.; Bonnard, H.; De Lauzon, G.; Mathey, F. *J. Am. Chem. Soc.* **1983**, *105*, 6871–6877.

(276) De Lauzon, G.; Charrier, C.; Bonnard, H.; Mathey, F. *Tetrahedron Lett.* **1982**, *23*, 511–514.

(277) Lauzon, G. de; Charrier, C.; Bonnard, H.; Mathey, F.; Fischer, J.; Mitschler, A. *J. Chem. Soc., Chem. Commun.* **1982**, 1272–1273.

(278) Holand, S.; Mathey, F. *Organometallics* **1988**, *7*, 1796–1801.

(279) Holand, S.; Charrier, C.; Mathey, F.; Fischer, J.; Mitschler, A. *J. Am. Chem. Soc.* **1984**, *106*, 826–828.

(280) Caliman, V.; Hitchcock, P. B.; Nixon, J. F. *J. Chem. Soc., Chem. Commun.* **1995**, 1661–1662.

(281) Cloke, F. G. N.; Hitchcock, P. B.; Hunnable, P.; Nixon, J. F.; Nyulászi, L.; Niecke, E.; Thelen, V. *Angew. Chem., Int. Ed.* **1998**, *37*, 1083–1086.

(282) Sierra, M. L.; Maigrot, N.; Charrier, C.; Ricard, L.; Mathey, F. *Organometallics* **1991**, *10*, 2835–2838.

(283) Bartsch, R.; Hitchcock, P. B.; Nixon, J. F. *J. Chem. Soc., Chem. Commun.* **1989**, 1046–1048.

(284) Bartsch, R.; Hitchcock, P. B.; Nixon, J. F. *J. Chem. Soc., Chem. Commun.* **1990**, 1307–1308.

(285) Al-Juaid, S. S.; Hitchcock, P. B.; Matos, R. M.; Nixon, J. F. *J. Chem. Soc., Chem. Commun.* **1993**, 267–269.

(286) Bartsch, R.; Hitchcock, P. B.; Nixon, J. F. *J. Organomet. Chem.* **1989**, *375*, C31–C34.

(287) Cloke, F. G. N.; Hanks, J. R.; Hitchcock, P. B.; Nixon, J. F. *Chem. Commun.* **1999**, 1731–1732.

(288) Sanner, R. D.; Duggan, D. M.; McKenzie, T. C.; Marsh, R. E.; Bercaw, J. E. *J. Am. Chem. Soc.* **1976**, *98*, 8358–8365.

(289) Cloke, F. G. N.; Green, J. C.; Hanks, J. R.; Nixon, J. F.; Suter, J. L. *J. Chem. Soc., Dalton Trans.* **2000**, 3534–3536.

(290) Clark, T.; Elvers, A.; Heinemann, F. W.; Hennemann, M.; Zeller, M.; Zenneck, U. *Angew. Chem., Int. Ed.* **2000**, *39*, 2087–2091.

(291) Bochmann, M. *J. Chem. Soc., Dalton Trans.* **1996**, 255–270.

(292) De Boer, E. J. .; Gilmore, I. J.; Korndorffer, F. M.; Horton, A. D.; van der Linden, A.; Royan, B. W.; Ruisch, B. J.; Schoon, L.; Shaw, R. W. *J. Mol. Catal. A: Chem* **1998**, *128*, 155–165.

(293) Brown, S. J.; Gao, X.; Harrison, D. G.; Koch, L.; Spence, R. E. v. H.; Yap, G. P. A. *Organometallics* **1998**, *17*, 5445–5447.

(294) Bartsch, R.; Carmichael, D.; Hitchcock, P. B.; Meidine, M. F.; Nixon, J. F.; Sillett, G. J. D. *J. Chem. Soc., Chem. Commun.* **1988**, 1615–1617.

(295) Nixon, J. F.; Sillett, G. J. D. *J. Organomet. Chem.* **1993**, *461*, 237–245.

(296) Hitchcock, P. B.; Meidine, M. F.; Nixon, J. F.; Sillett, G. J. D. *J. Chem. Soc., Chem. Commun.* **1990**, 317–319.

(297) Heinemann, F. W.; Pritzkow, H.; Zeller, M.; Zenneck, U. *Organometallics* **2001**, *20*, 2905–2915.

(298) Bai, J.; Virovets, A. V.; Scheer, M. *Angew. Chem., Int. Ed.* **2002**, *41*, 1737–1740.

(299) Bai, J.; Virovets, A. V.; Scheer, M. *Science* **2003**, *300*, 781–783.

(300) Welsch, S.; Gröger, C.; Sierka, M.; Scheer, M. *Angew. Chem., Int. Ed.* **2011**, *50*, 1435–1438.

(301) Schindler, A.; Heindl, C.; Balázs, G.; Gröger, C.; Virovets, A. V.; Peresypkina, E. V.; Scheer, M. *Chem. Eur. J.* **2012**, *18*, 829–835.

(302) Scheer, M.; Schindler, A.; Bai, J.; Johnson, B. P.; Merkle, R.; Winter, R.; Virovets, A. V.; Peresypkina, E. V.; Blatov, V. A.; Sierka, M.; Eckert, H. *Chem. Eur. J.* **2010**, *16*, 2092–2107.

(303) Tanaka, K.; Qiao, S.; Tobisu, M.; Lo, M. M.-C.; Fu, G. C. *J. Am. Chem. Soc.* **2000**, *122*, 9870–9871.

(304) Qiao, S.; Fu, G. C. *J. Org. Chem.* **1998**, *63*, 4168–4169.

(305) Fu, G. C. *Acc. Chem. Res.* **2006**, *39*, 853–860.

CHAPTER TWO

The Brønsted Acid-Base Chemistry of Heptapnictide Anions

2.1 INTRODUCTION

Of all the elements, only carbon has more known hydrides than phosphorus.[1] Individual polyphosphanes (P_mH_n) can be detected by their mass spectra, but more detailed analysis of their structure, particularly for the complex polyphosphorus cages found in hydrogen-poor phosphanes, can only be determined by a combination of ^{31}P NMR spectroscopy and diffraction methods.[2] Due to their low solubility and tendency to form as amorphous solids or liquids, many of the known polyphosphanes are not well characterized. The polyphosphides, however, are well explored and are frequently structurally related to the parent polyphosphanes.[3,4] Despite the sole difference between the two series being the loss or gain of protons through Brønsted acid-base chemistry, this concept is not well explored experimentally. The synthesis of these compounds is not as simple as the above thought experiment might suggest, however. There is a marked tendency for disproportionation upon protonation of polyphosphides, resulting in the formation of higher polyphosphide species and phosphane, PH_3. As such, there are a dearth of intermediate hydrogen polyphosphides bridging the gap between polyphosphides and polyphosphanes. One exception to this are those derived from the $[P_7]^{3-}$ Zintl anion, forming the homologous series $[HP_7]^{2-}$, $[H_2P_7]^{-}$, and $[H_3P_7]$ upon sequential protonation.

2.1.1 $[HP_7]^{2-}$

The hydrogenheptaphosphide anion, $[HP_7]^{2-}$, was first reported by Baudler and co-workers in solution in 1984 by the disproportionation reaction of diphosphane with ^{n}BuLi at low temperature.[5] They report the ^{31}P NMR spectrum at –60 ºC, which suggests the formation of a protonated nortricyclane-like C_1 symmetric cage, with seven inequivalent phosphorus environments. Upon warming, the cage atoms undergo an exchange process that renders

two sets of them equivalent on the NMR timescale, in a manner analogous to the parent $[P_7]^{3-}$ cage (Figure 2.1).

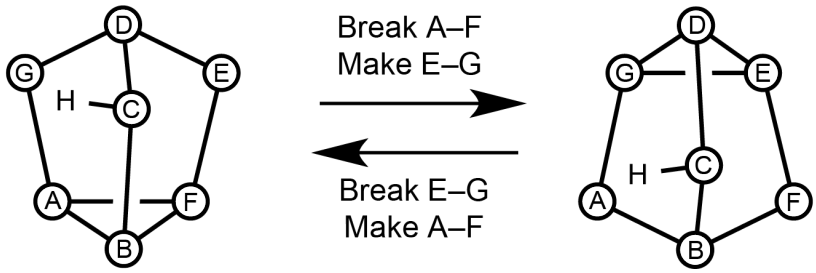

Figure 2.1: Ball and stick diagram showing the interconversion fluxional process within $[HP_7]^{2-}$. Figure adapted from Baudler and co-workers.[5]

It was not until 2004 that the anion was isolated and X-ray structural study performed, confirming the connectivity of the anion proposed by Baudler. Aschenbrenner and Korber synthesized $[PPh_4]_2[HP_7]\cdot 3NH_3$ through the reaction of K_3P_7, Amberlyst® 15 proton exchange resin and $[PPh_4][Br]$ in liquid ammonia.[6] Further crystal structures were reported for the $[K(18\text{-crown-6})]^+$, $[K(2,2,2\text{-crypt})]^+$, and $[K(\text{dibenzo-18-crown-6})]^+$ salts in 2006.[7]

2.1.2 $[H_2P_7]^-$

The only report of the monoanionic $[H_2P_7]^-$ cage in the literature arises from the reaction of K_3P_{11} with wet $[PPh_4][Cl]$ in liquid ammonia.[8] It was structurally characterized as the $[PPh_4]^+$ salt, however orientational disorder within the cluster prevented the location of the hydrogen atoms, which is a known issue with X-ray diffraction data. This precludes the identification of the isomer(s) formed. NMR data were not reported due to the compound decomposing into higher polyphosphorus species upon dissolution into dimethyl sulfoxide or acetonitrile. The presence of a P–H bond was inferred from the presence of a strong, sharp band at 2250 cm^{-1} in the IR spectrum, and the cluster charge from the X-ray crystal structure obtained.

2.1.3 [H_3P_7]

The neutral heptaphosphane, [H_3P_7], is available through the methanolysis of the tris(trimethylsilyl)substituted cage, [$(Me_3Si)_3P_7$] in the absence of solvent (Scheme 2.1).[9]

$$(TMS)_3P_7 + 3\ MeOH \longrightarrow H_3P_7 + 3\ TMSOMe$$

Scheme 2.1: The synthesis of H_3P_7.

When prepared in this manner, the substance is amorphous to X-rays and highly insoluble in the majority of laboratory solvents. ^{31}P NMR studies were carried out on solutions formed directly in benzene, 1-methylnaphthalene, or 1-methylnaphthalene/phenanthrene mixtures, which have to be performed rapidly to avoid the decomposition of the compound into PH_3 and elemental phosphorus.[10] Nine apparent multiplet resonances were observed, which suggests the formation of two isomers of the nortricyclane-like cage compound (Figure 2.2). The symmetrical isomer would give rise to three resonances in a 1:3:3 intensity ratio, whereas seven equal intensity resonances would be expected for the unsymmetrical isomer. It is likely that two of the resonances overlap, giving rise to the observed nine resonances in the ^{31}P NMR spectrum.

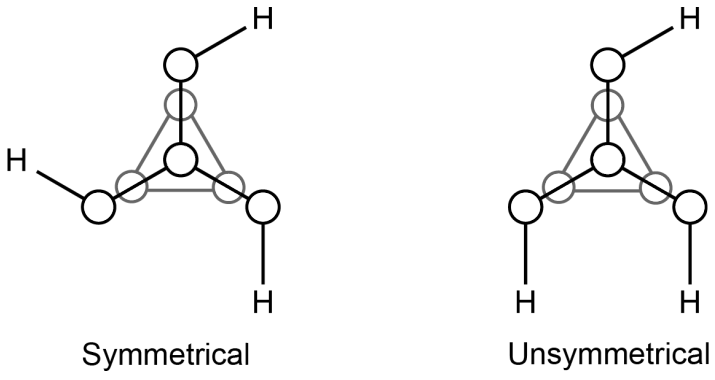

Figure 2.2: The two possible isomers of [H_3P_7] as viewed from the apical phosphorus atom.

2.2 OBJECTIVES

Prior to this work, studies on the reactivity of the $[P_7]^{3-}$ cage had started from the compound $[Li(DME)]_3[P_7]$, synthesized via the nucleophilic cleavage of P_4 with $LiPH_2$,[11] or by direct reactions with the Zintl phases A_3P_7 (A = Li, Na, K, Rb, Cs).[12] The heavier congeners, $[As_7]^{3-}$ and $[Sb_7]^{3-}$, are known through a variety of synthetic routes. Notable are those from the corresponding Zintl phases,[13–15] or from thermolysis of heterobimetallic complexes exemplified by the work of Wright and co-workers.[16–20]

Potassium is typically used in the preparation of the $[P_7]^{3-}$ containing Zintl phases. This is mainly attributable to the reduced cost of the specific cation sequestering agents 2,2,2-crypt and 18-crown-6 relative to those specific for the other alkali metals.[21] The K_3P_7 Zintl phase is synthesized by the high temperature fusion of stoichiometric mixtures of potassium metal and red phosphorus sealed in niobium tubes, which are subsequently jacketed in silica ampoules prior to heating.[22,23] In our hands, the synthesis of the K_3P_7 Zintl phase contains approximately 10% of an unidentified black compound that is completely insoluble in common laboratory solvents. Both the phase and impurity are amorphous to X-ray diffraction experiments, precluding the identification of this impurity. We postulate that it arises due to a side reaction of either potassium or phosphorus with the niobium tubes used in the synthesis. Dissolution of this intermetallic alloy into appropriate solvents (ethylenediamine, pyridine or DMF) in the presence of a cation sequestering agent is slow, and the ^{31}P NMR spectra of these solutions reproducibly reveal the presence of both the $[P_7]^{3-}$ and $[HP_7]^{2-}$ anions due to protonation of the cage by adventitious moisture.

We sought to circumvent these problems and target a well-defined, soluble source of heptaphosphide anions from the K_3P_7 Zintl phase. This chapter will detail the synthesis and characterization of the $[HP_7]^{2-}$ (**1**) and $[HAs_7]^{2-}$ (**2**) anions as the $[K(18\text{-crown-6}]^+$ or

$[K(2,2,2\text{-crypt})]^+$ salts. In addition, it will discuss the specific conditions required for the deprotonation of $[HP_7]^{2-}$ to the $[P_7]^{3-}$ anion (**3**).

2.3 Protonation of the Zintl Phases

2.3.1 Synthesis of $[HP_7]^{2-}$ and $[HAs_7]^{2-}$

Treatment of a stirred slurry of K_3P_7 in pyridine with a measured amount of deionized water, then subsequent addition of two equivalents of either 18-crown-6 or 2,2,2-crypt as a cation sequestering agent, results in a dark orange-brown mixture. Filtration affords a bright orange solution from which the product, $[HP_7]^{2-}$ (**1**), can be precipitated by addition of toluene. The product is isolated by filtration as a bright yellow (as the $[K(18\text{-crown-6})]^+$ salt) or light orange (as the $[K(2,2,2\text{-crypt})]^+$ salt) powder in excellent yields (85–89%). Although the reaction stoichiometry would suggest the necessity for one equivalent of water (Scheme 2.2), crude optimization showed that the best yields were obtained when approximately two equivalents of water were used. The exact reason for this is unclear, although it is possible that the aforementioned unknown impurity in the Zintl phase reacts with water, requiring the addition of a further stoichiometric equivalent to achieve the best yields.

$$K_3P_7 + 2\,H_2O + 2\,(SA) \xrightarrow{\text{Pyridine}} [K(SA)]_2[HP_7] + KOH$$

Scheme 2.2: The formation of $[HP_7]^{2-}$ from K_3P_7. SA: sequestering agent, either 18-crown-6 or 2,2,2-crypt.

This methodology was extended to the arsenic phase to produce the $[K(18\text{-crown-6})]^+$ salt of arsenic analogue $[HAs_7]^{2-}$ (**2**) as an orange solid, albeit in slightly reduced yield (79%). Attempts were made to synthesize $[HSb_7]^{2-}$, but these only resulted in cluster

decomposition and the formation of metallic precipitates. This is not entirely surprising, since the oxidation of the clusters becomes increasingly facile as the group is descended due in part to the lower E–E bond dissociation enthalpies (BDEs: P–P: 201 kJ mol^{-1}; As–As: 146 kJ mol^{-1}; Sb–Sb: 121 kJ mol^{-1}).[24,25] This is obviously not the only factor involved, since the redox process will also depend on both anion solvation effects and the enthalpy of atomization of the elements themselves.

2.3.2 Structures of 1 and 2

Crystals of the $[K(18\text{-crown-6})]^+$ salts of **1** and **2** suitable for single crystal X-ray diffraction could be grown by diffusion of toluene into a pyridine solution, or hexane into a 1:1 THF/pyridine solution of the compounds, respectively. The structure of $[K(18\text{-crown-6})]_2$[**1**] has previously been reported by Dai and Xu, but the dataset is not of high quality, which appears to prevent a sensible analysis of the rotational disorder present in one of the 18-crown-6 units.[7] We have redetermined the structure with a better quality dataset and what we believe to be a more satisfactory model of the disorder present within the 18-crown-6 moiety.

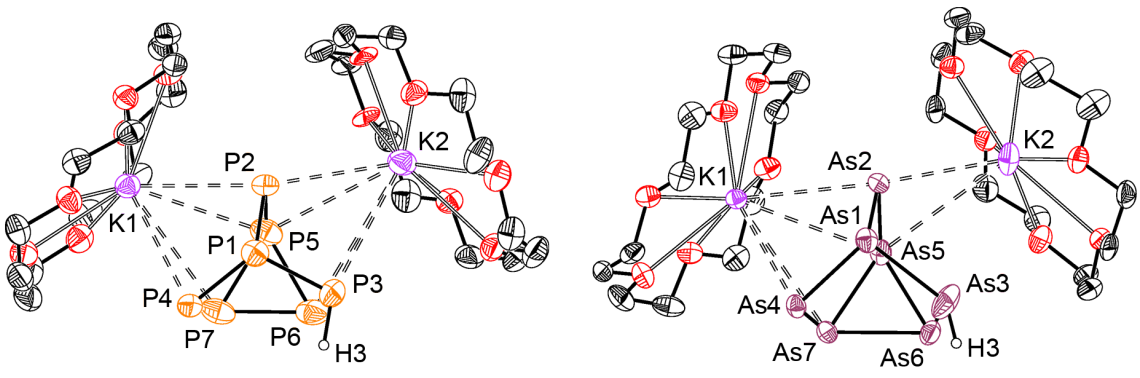

Figure 2.3: Thermal ellipsoid plot of the crystal structures of $[K(18\text{-crown-6})]_2$[**1**] (left) and $[K(18\text{-crown-6})]_2$[**2**] (right). Thermal ellipsoids are shown at the 50% probability level, and hydrogen atoms on the 18-crown-6 moieties have been omitted for clarity. Only the major components of the disordered 18-crown-6 units are shown.

The crystal structures of $[K(18\text{-crown-}6)]_2[\mathbf{1}]$ and $[K(18\text{-crown-}6)]_2[\mathbf{2}]$ are isomorphous, displaying a single crystallographically unique anion accompanied by two charge-balancing $[K(18\text{-crown-}6)]^+$ cations (Figure 2.3). Both of the cations display close contacts to the charged pnictide vertices (E2 and E4), due to the planar nature of the $[K(18\text{-crown-}6)]^+$ complex that exposes the potassium cation. This allows the stabilization of the formally negatively charged pnictide vertices of the cluster. The location of the cage proton could be determined in the residual electron density after anisotropic refinement of the non-hydrogen atoms and placing all hydrogen atoms on the 18-crown-6 molecules.

Table 2.1: Selected bond distances for **1** and **2**.

Bond	Bond distance in 1 (Å)	Bond distance in 2 (Å)	$d_{As} - d_P$ (Å)
E1–E2	2.168(1)	2.376(1)	0.208
E1–E3	2.197(1)	2.438(1)	0.241
E1–E4	2.151(1)	2.385(1)	0.234
E2–E5	2.142(1)	2.363(1)	0.221
E3–E6	2.180(1)	2.400(1)	0.220
E4–E7	2.118(1)	2.357(1)	0.239
E5–E6	2.255(1)	2.469(1)	0.214
E5–E7	2.260(1)	2.482(1)	0.222
E6–E7	2.255(1)	2.475(1)	0.220
K1–E2	3.388(1)	3.492(1)	0.104
K1–E4	3.526(1)	3.562(1)	0.036
K1–E5	3.643(1)	3.846(1)	0.203
K1–E7	3.743(1)	3.876(1)	0.133
K2–E2	3.363(1)	3.462(1)	0.099
K2–E5	3.856(1)	3.818(1)	–0.038
K2–E3	3.771(1)	–	–

Selected bond distances for **1** and **2** are summarized in Table 2.1. The E–E bond lengths lie in the range 2.118(1)–2.260(1) Å for **1** and 2.357(1)–2.482(1) Å for **2**. On average, the equivalent As–As bonds in **2** are 0.22 Å longer than the equivalent P–P bonds in **1**. This is in line with the increased single bond covalent radius of As compared to P (r_P = 1.11 Å; r_{As} = 1.21 Å).[26] The longest bonds are found in the three-membered ring at the base of the cage (those between E5, E6 and E7), which would be expected due to the greater degree of ring

strain. Bonds to the protonated E3 vertex are elongated relative to equivalent bonds to the formally negative E2 and E4. This is likely due to a reduced ionic component to the bonding between the two vertices. The bonds are comparable in length to known $[E_7]^{3-}$ cages, for instance those found in $[Li(TMEDA)]_3[E_7]$ (E = P, 2.150(av)–2.255(av) Å; E = As, 2.360(2)−2.498(2)Å) and $[PPh_4]_2[HP_7]\cdot 3NH_3$ (2.127(3)–2.246(3) Å).[6,17,27]

2.3.3 NMR Spectroscopic Studies on 1 and 2

NMR studies were performed on d_7-DMF solutions of $[K(18\text{-crown-6})]_2[\mathbf{1}]$ and d_5-pyridine solutions of $[K(18\text{-crown-6})]_2[\mathbf{2}]$. Both the ^1H and ^{31}P NMR spectra of **1** support the previously observed fluxionality in solution.[5] At 25 ºC, the ^1H NMR spectrum shows an extremely broad resonance, centred at 0.47 ppm. On cooling to –50 ºC this is resolved as a doublet of multiplets, with a coupling constant of 160 Hz, which is in the expected range for $^1J_{H-P}$ couplings.[28] Broadband ^{31}P decoupling results in the observation of this resonance as a singlet, confirming that it is unequivocally the cage proton (Figure 2.4). The work of Baudler and co-workers does not report the ^1H NMR spectrum, and that of Dai and Xu erroneously assigns an impurity resonance at 7.25–7.17 ppm.[7] In order to confirm this assignment the deuterium labelled version of **1**, **1–D** was prepared by replacing H_2O with D_2O in the synthetic procedure. ^2H NMR studies performed on $[K(18\text{-crown-6}]_2[\mathbf{1–D}]$ in DMF corroborated those performed on **1**. At room temperature a singlet at 0.33 ppm is observed, and on lowering the temperature to –50 ºC this is resolved as a doublet with $^1J_{D-P}$ = 22 Hz. This is very similar to the coupling constant that is calculated by multiplying the $^1J_{H-P}$ coupling constant measured for **1** by the ratio of the nuclear gyromagnetic ratios for ^1H and ^2H ($\gamma_D/\gamma_H \times 160$ Hz = 25 Hz).[29]

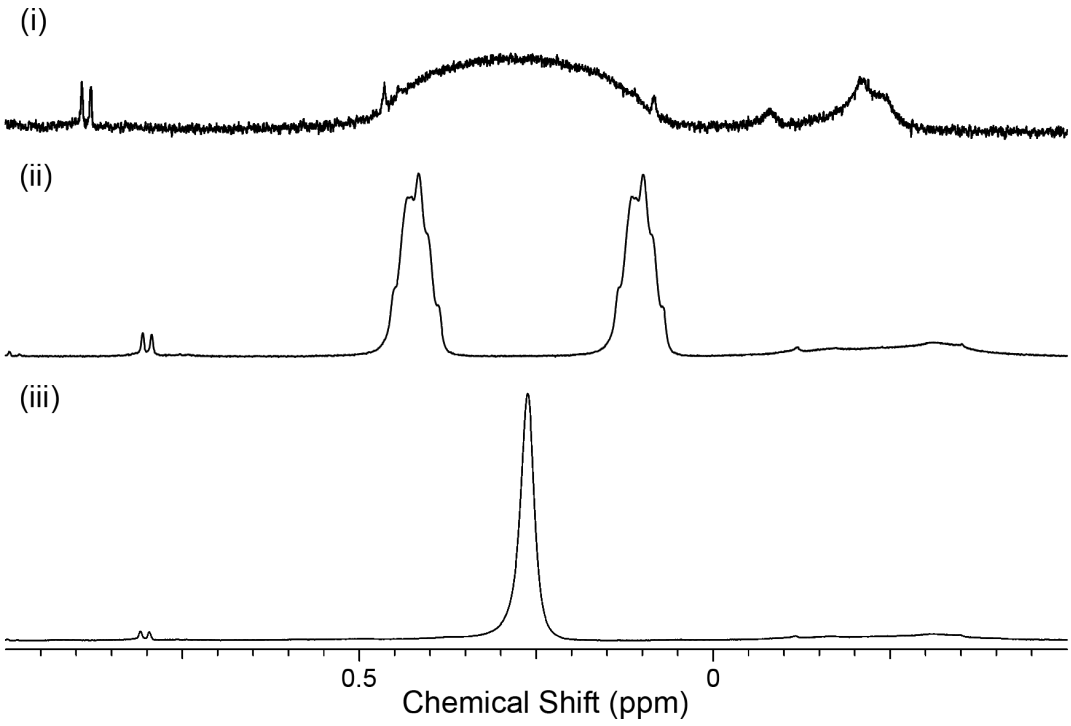

Figure 2.4: ^{1}H NMR spectrum of a d_7-DMF solution of [K(18-crown-6)]$_2$[**1**] at 25 ºC (i) and –50 ºC (ii). $^{1}H\{^{31}P\}$ NMR spectrum of [K(18-crown-6)]$_2$[**1**] at –50 ºC (iii).

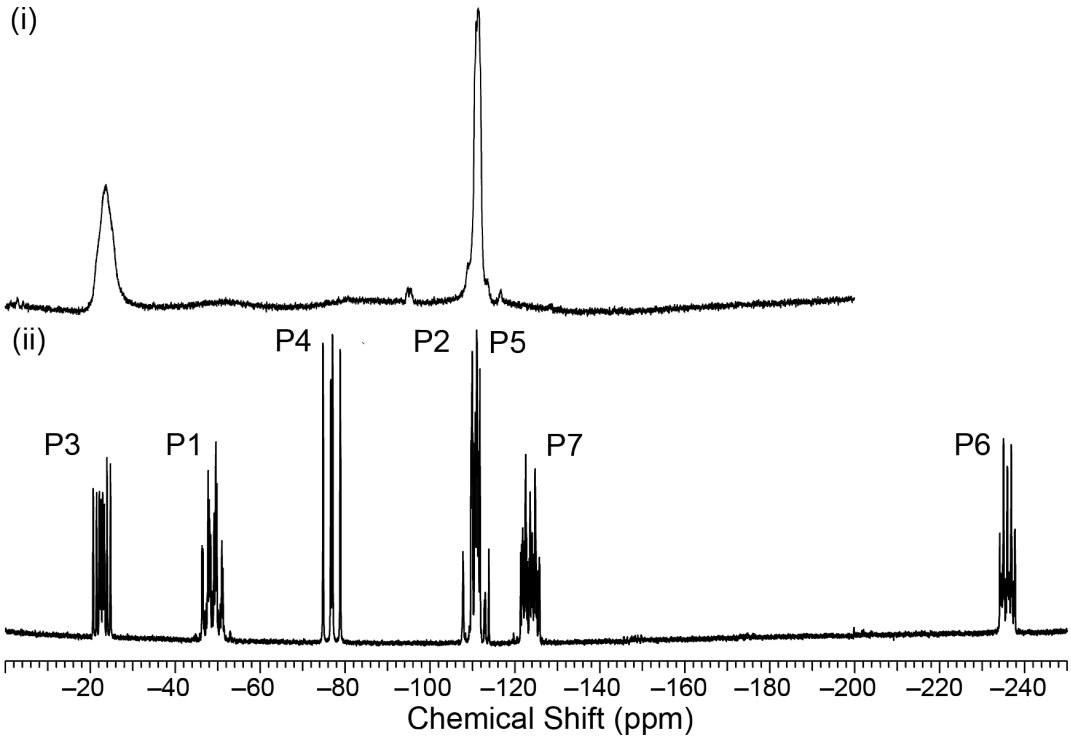

Figure 2.5: $^{31}P\{^{1}H\}$ NMR spectrum of a d_7-DMF solution of [K(18-crown-6)]$_2$[**1**] at 25 ºC (i) and –50 ºC (ii).

The ^{31}P NMR spectrum of **1** in d_7-DMF at room temperature shows broad resonances at –18.4 and –112.4 ppm that do not give integer integrals (Figure 2.5). Upon cooling to –50 ºC the fluxional process is frozen out and seven equal intensity resonances corresponding to the seven inequivalent phosphorus environments are observed at –22.7 (P3), –48.8 (P1), –76.8 (P4), –110.0 (P2), –111.3 (P5), –123.5 (P6) and –235.9 (P7) ppm (according to the atom numbering scheme used in Figure 2.3). These could be assigned with the assistance of a ^{31}P–^{31}P COSY experiment, and the spectrum was simulated to confirm the assignment and extract the ^{31}P–^{31}P coupling constants.

Tabulated values for the results of the simulation can be found in Appendix A. The most upfield shifted resonances are those in the strained triangular base of the cluster. This seems intuitive, since the upfield end of the ^{31}P NMR chemical shift range is defined by P_4 (–488 ppm), an electron rich cluster with P–P–P bond angles of 60º. The ^{31}P NMR spectrum of **1–D** is essentially identical to that of **1**, and does not warrant a detailed discussion.

NMR studies on d_7-DMF solutions of $[K(2,2,2\text{-crypt})]^+$ salt of [**1**] were performed and the spectra obtained are extremely similar to those obtained for the $[K(18\text{-crown-6})]^+$ salt. As a result, they will not be discussed.

The ^{1}H NMR spectrum of a d_7-DMF solution of $[K(18\text{-crown-6})]_2$[**2**] shows a singlet resonance at 1.17 ppm for the cage proton, which is unusually sharp compared to the equivalent resonance in **1**. Deuterium labelling confirms this assignment, with a corresponding resonance observed at 1.21 ppm in the ^{2}H NMR spectrum of a DMF solution of $[K(18\text{-crown-6})]_2$[**2–D**]. This downfield shift compared to **1** appears counterintuitive based purely on a comparison of electronegativities (Pauling electronegativities X_H = 2.20, X_P = 2.19, X_{As} = 2.18).[29] The decreased electronegativity of As compared to P should lead to a bond that is more polarized towards H, and thus a more hydridic upfield chemical shift

in **2** compared to **1**. However, another consideration might be the relative H–E bond strengths (BDEs H–P: 322 kJ mol^{-1}; H–As 247 kJ mol^{-1}).[24] The decreased H–As bond strength may result in the hydrogen atom in **2** being more acidic (in the basic DMF solvent used) than that in **1** (or alternatively, the conjugate base of **1** is stronger than that of **2**). This would result in the observed downfield shift observed for **2**. A similar argument can be used to account for the unexpected sharpness of the resonance. In **1**, the proton is rapidly exchanged between the phosphide vertices leading to the extreme broadness seen at room temperature. An equivalent process may not be operative in **2** due to the reduced basicity of arsenide compared to phosphide, and a correspondingly sharper resonance. Unfortunately, the unfavourable nuclear properties of ^{75}As preclude the variable temperature NMR studies that would allow the investigation of fluxional processes in **2** to be studied.

2.3.4 Mass Spectrometric Studies

DMF solutions of $[K(18\text{-crown-6})]_2[\mathbf{1}]$ and $[K(18\text{-crown-6})]_2[\mathbf{2}]$ were studied by electrospray mass spectrometry in both the positive and negative ion modes. The negative ion mode mass spectra show peaks for the molecular ions at *m/z* values of 216.0 and 526.7 corresponding to **1** and **2**, respectively. The clusters are observed with reduced charges due to oxidation during the ionization process. In both cases this oxidation is also accompanied by extensive decomposition to higher order polypnictide anions. In the positive ion mode mass spectra, a peak corresponding to the cation-paired $\{[K(18\text{-crown-6})]_3[HP_7]\}^+$ species is observed at 1129.1 Da for **1**, and at 1170.1 Da for **2** which can be assigned to $\{K[K(18\text{-crown-6})]_2[HAs_7]\}^+$.

2.3.5 Electronic Structure of 1 and 2

Calculations at the DFT level of theory were performed on **1** and **2** to investigate their electronic structure. Bond distances for the optimized structure were in excellent agreement with those determined experimentally (Table 2.2). The observed slight elongation (by approximately 0.05 Å) for the calculated bond lengths presumably results from the simplistic continuum dielectric model used to simulate the presence of cations in the crystal lattice. While generally applicable, it is incapable of replicating the close contacts between the cation and anion that is observed in the structures of both $[K(18\text{-crown-6})]_2[\mathbf{1}]$ and $[K(18\text{-crown-6})]_2[\mathbf{2}]$. For both **1** and **2**, the HOMO and HOMO–1 are mostly localized p orbitals on the pnictide (E2 and E4) vertices as would be expected for the formally negative charged atoms. The calculated Hirshfeld and Mulliken charges reflect this distribution of charge, with the largest partial negative charges found on E2 and E4 (Table 2.3). The computed HOMO–LUMO gaps are 2.77 and 2.24 eV for **1** and **2**, respectively.

Table 2.2: Comparison of experimentally determined (**1** and **2**) and calculated ($\mathbf{1}_{calc}$ and $\mathbf{2}_{calc}$) bond distances for **1** and **2**.

Bond	Distance in 1 (Å)	Distance in $\mathbf{1}_{calc}$ (Å)	Distance in 2 (Å)	Distance in $\mathbf{2}_{calc}$ (Å)
E1–E2	2.168(1)	2.212	2.376(1)	2.444
E1–E3	2.197(1)	2.257	2.438(1)	2.510
E1–E4	2.151(1)	2.201	2.385(1)	2.432
E2–E5	2.142(1)	2.186	2.363(1)	2.413
E3–E6	2.180(1)	2.227	2.400(1)	2.453
E4–E7	2.118(1)	2.172	2.357(1)	2.394
E5–E6	2.255(1)	2.294	2.469(1)	2.537
E5–E7	2.260(1)	2.305	2.482(1)	2.543
E6–E7	2.255(1)	2.309	2.475(1)	2.549
E3–H3	–	1.446	–	1.547

Table 2.3: Calculated Mulliken and Hirshfeld spin densities for **1** and **2**.

Atom	Mulliken density (1)	Hirshfeld density (1)	Mulliken density (2)	Hirshfeld density (2)
E1	–0.200	–0.209	–0.186	–0.190
E2	–0.562	–0.483	–0.579	–0.494
E3	0.047	–0.138	0.044	–0.133
E4	–0.537	–0.470	–0.553	–0.481
E5	–0.197	–0.227	–0.177	–0.214
E6	–0.203	–0.191	–0.201	–0.191
E7	–0.202	–0.233	–0.184	–0.220
H3	–0.146	–0.050	–0.165	–0.077

2.4 DEPROTONATION OF $[HP_7]^{2-}$

Armed with a high yielding synthesis of **1**, as either the $[K(18\text{-crown-6})]^+$ or $[K(2,2,2\text{-crypt})]^+$ salt we set out to identify the conditions for deprotonation of the cluster to form the parent anion $[P_7]^{3-}$ (**3**). Preliminary experiments were performed in gas-tight NMR tubes using $[K(18\text{-crown-6})]_2[\mathbf{1}]$ in d_5-pyridine and were monitored by ^1H and ^{31}P NMR spectroscopy. Potassium *tert*-butoxide had been used within the group to deprotonate the $[Fe(HP_7)_2]^{2-}$ anion to form the $[Fe(P_7)]^{4-}$ anion, and so formed a reasonable starting point for investigation.[30] However, it proved to be insufficiently basic to deprotonate the cage, which is unsurprising considering the potent basicity associated with multiple free phosphide vertices on the same molecule.

Stronger bases were then tried. Initial experiments with potassium hydride appeared promising, with the disappearance of the resonances arising from **1**, and the appearance of a broad singlet resonance at –120 ppm. Further investigation showed that potassium hydride by itself was incapable of deprotonating **1** and the reaction only proceeded in the presence of a small amount of an amine impurity (ethylenediamine), which presumably acts as a "hydride transfer" agent to circumvent the insolubility of potassium hydride. This was present in early batches of $[K(18\text{-crown-6})]_2[\mathbf{1}]$, when the synthesis was carried out in

ethylenediamine. The trace amount of ethylenediamine left in the material was detrimental to the chemistry that will be described in Chapter Three, and so the synthesis of [K(18-crown-6)]$_2$[**1**] was refined to be carried out in pyridine as described above. Batches of [K(18-crown-6)]$_2$[**1**] made in this fashion were inert to potassium hydride.

Since the amide derived from the deprotonation of ethylenediamine, $[NH_2(CH_2)_2NH]^-$, was competent at the transformation of $[HP_7]^{2-}$ to $[P_7]^-$, we reasoned that other amide bases might also be able to afford the desired deprotonation. Potassium bis(trimethylsilyl)amide (KHMDS) proved to be an excellent base. Treatment of pyridine solutions of [K(18-crown-6)]$_2$[**1**] with a slight excess of KHMDS and 18-crown-6 results in a colour change to a deep orange-brown. Subsequent removal of volatiles under reduced pressure and washing sequentially with THF and diethyl ether to remove the excess base and amine byproduct allows for the isolation of the $[K(18\text{-crown-6})]^+$ salt of $[P_7]^{3-}$ (**3**) as a bright yellow powder in 90% yield (Scheme 2.3).

$$[K(18\text{-c-6})]_2[HP_7] + KHMDS + 18\text{-c-6} \xrightarrow{\text{Pyridine}} [K(18\text{-c-6})]_3[HP_7] + HHMDS$$

Scheme 2.3: The deprotonation of **1** to form **3**. 18-c-6: 18-crown-6.

When the deprotonation of the $[K(2,2,2\text{-crypt})]^+$ salt of **1** was attempted, the ^{31}P NMR spectrum showed conversion to **3**, but solutions changed colour to a deep purple accompanied by a decrease in the signal:noise ratio of the ^{31}P NMR spectrum over the course of several hours. A plausible explanation for this is the reduction of the pyridine solvent by **3**, which is likely to be highly reducing due to the large negative charge it possesses. Dissolution of alkali metals into pyridine is known to give rise to intensely coloured purple solutions containing bipyridyl radical anions.[31,32]

A potential reason for the stability of $[K(18\text{-crown-6})]_3[\mathbf{3}]$ can be found in the crystal structures of $[K(18\text{-crown-6})]_2[\mathbf{1}]$ (*vide supra*) and $[K(18\text{-crown-6})]_3[\mathbf{3}]$ (*vide infra*). Extensive cation-anion pairing is observed due to the open nature of the $[K(18\text{-crown-6})]^+$ cation. It is proposed that these close cation-anion pairings also exist to some extent in solution, stabilizing the anion **3**. By comparison, the potassium cation within the $[K(2,2,2\text{-crypt})]^+$ complex is completely encapsulated, and unable to interact with additional donor atoms. As a result, the anion **3** is destabilized by a lack of cation-anion interactions in solution and thus able to reduce the solvent.

Attempts were made to form $[K(2,2,2\text{-crypt})]_3[\mathbf{3}]$ in alternative solvents such as DMF, but these lead only to non-reproducible solvent activation by the cage or a lack of reaction.

2.4.1 Structure of 3

Crystals of $[K(18\text{-crown-6})]_3[\mathbf{3}]$ suitable for single crystal X-ray diffraction were grown by the slow diffusion of hexane into a THF/pyridine solution of the compound. While the dataset is of good quality, a combination of high symmetry (the best solution is obtained in the hexagonal space group *P*–6), disorder (the asymmetric unit contains three partial clusters, two of which are disordered over two positions), and a high solvent content (there are at least 6 pyridine molecules in the asymmetric unit) preclude a publishable solution. Nevertheless, the composition and connectivity of the anion can be confirmed, and the gross structural features discussed (Figure 2.6).

The $[K(18\text{-crown-6})]^+$ cations display close contacts to the phosphide vertices and those in the basal plane (K101–P2: 3.337(2) Å, K101–P2A: 3.368(2) Å; K101–P3: 3.646(2) Å, K101–P3B: 3.659(2) Å) to form a closely associated cation-anion pair in the solid state. This arrangement is very similar to the closely related $[Rb(18\text{-crown-6})]_3[P_7]\cdot 5NH_3$

reported by Kraus and Korber, which has two different modes of $[Rb(18\text{-crown-6})]^+$ coordination to the cage.[33] Two cations coordinate to the phosphide and basal atoms through four close electrostatic contacts, similar to that seen in the structure of $[K(18\text{-crown-6})]_3$[**3**], with Rb–P distances in the range 3.340(1) to 3.743(2) Å. The third cation displays three close contacts to the apical phosphorus and two phosphides, with Rb– distances between 3.510(1) and 3.790(2) Å.

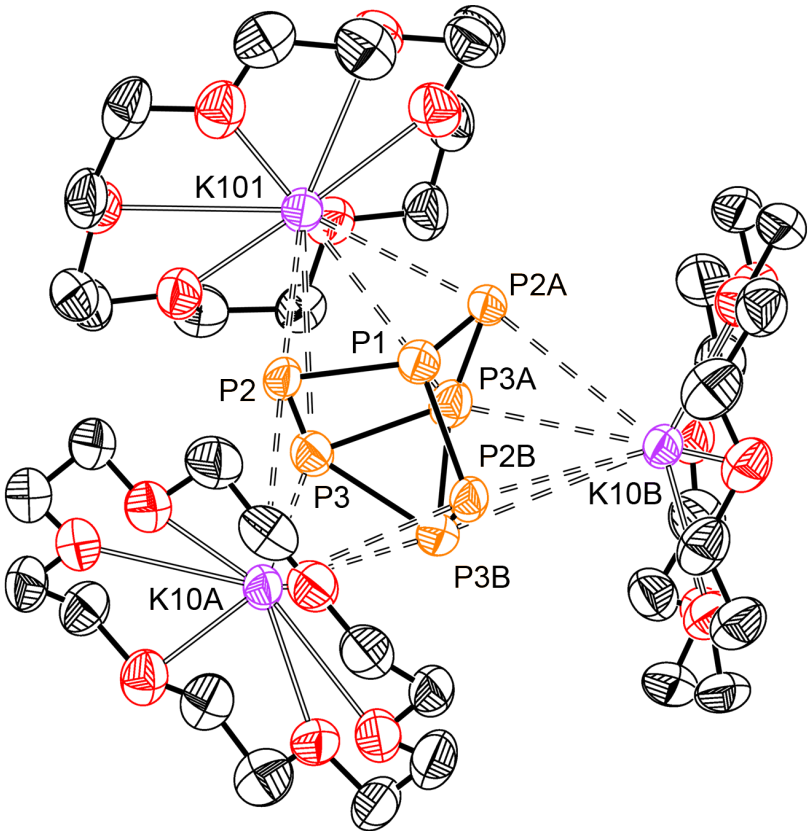

Figure 2.6: Thermal ellipsoid plot of part of the crystal structure of $[K(18\text{-crown-6})]_3$[**3**]. Only one third of the asymmetric unit is shown, expanded to form a complete cluster anion. Thermal ellipsoids are set at the 50% probability level. All hydrogen atoms and solvent molecules have been omitted for clarity.

2.4.2 NMR Spectroscopic Studies on 3

At 25 ºC the ^{31}P NMR spectrum of a d_5-pyridine solution of $[K(18\text{-crown-6})]_3$[**3**] shows only a broad singlet resonance at –120 ppm, due to an exchange process that renders all of

the phosphorus atoms equivalent on the NMR timescale.[2,9] The dynamics of this interconversion process were discussed in Chapter One. On cooling to the limit of the solvent (–40 ºC on the spectrometer), this fluxionality is still present. Exchanging the solvent for a 1:1 mixture of THF/pyridine allows the acquisition of a spectrum at –85 ºC which shows three distinct resonances with integrals 1:3:3 at –30, –115 and –170 ppm, although the multiplet structure is still not resolved even at this temperature. These values agree reasonably well with those previously reported for **3** (–57, –103 and –162 ppm for $[Li(DME)]_3[\mathbf{3}]$).

2.4.3 Mass Spectrometric Studies

Electrospray mass spectrometry was performed on DMF solutions of $[K(18\text{-crown-6})]_3[\mathbf{3}]$. The negative ion mode mass spectrum shows a peak for the molecular ion at an *m/z* value of 217.5, while the positive ion mode mass spectrum shows a mass envelope at 1129.1 Da arising from the cation-paired species $\{[K(18\text{-crown-6})]_3[P_7]\}^+$.

2.5 Conclusion

This chapter has described a high yielding synthesis of $[HE_7]^{2-}$ (E = P (**1**), As (**2**)) as the $[K(18\text{-crown-6})]^+$ or $[K(2,2,2\text{-crypt})]^+$ salts, which can be used to purify the K_3E_7 Zintl phases. The compounds are well soluble in DMF or pyridine and have been extensively characterized in the solid state using single crystal X-ray diffraction, and in solution using multielement NMR spectroscopy and electrospray mass spectrometry. The electronic structures of the anions have been investigated using computational methods. These salts of **1** and **2** allow for further chemistry that is not possible with the crude Zintl phases, which will be described in later chapters.

The specific conditions required to deprotonate **1** to the $[P_7]^{3-}$ (**3**) anion have been detailed, and a synthetic procedure for the $[K(18\text{-crown-6})]^+$ salt described. $[K(18\text{-crown-6})]_3[\mathbf{3}]$ has been characterized by single crystal X-ray diffraction, NMR spectroscopy, and electrospray mass spectrometry.

2.6 REFERENCES

(1) Baudler, M. *Angew. Chem., Int. Ed.* **1987**, *26*, 419–441.

(2) Baudler, M. *Angew. Chem., Int. Ed.* **1982**, *21*, 492–512.

(3) Baudler, M.; Glinka, K. *Chem. Rev.* **1993**, *93*, 1623–1667.

(4) Von Schnering, H. G.; Hönle, W. *Chem. Rev.* **1988**, *88*, 243–273.

(5) Baudler, M.; Heumüller, R.; Langerbeins, K. *Z. Anorg. Allg. Chem.* **1984**, *514*, 7–17.

(6) Aschenbrenner, J. C.; Korber, N. *Z. Anorg. Allg. Chem.* **2004**, *630*, 31–32.

(7) Dai, F. R.; Xu, L. *Inorg. Chim. Acta.* **2006**, *359*, 4265–4273.

(8) Korber, N.; von Schnering, H. G. *J. Chem. Soc., Chem. Commun.* **1995**, 1713–1714.

(9) Baudler, M.; Ternberger, H.; Faber, W.; Hahn, J. *Z. Naturforsch. B* **1979**, *34*, 1690–1697.

(10) Baudler, M.; Riekehofbohmer, R. *Z. Naturforsch. B* **1985**, *40*, 1424–1429.

(11) Baudler, M.; Glinka, K. *Inorg. Synth.* **1990**, *27*, 227–235.

(12) Scharfe, S.; Kraus, F.; Stegmaier, S.; Schier, A.; Fässler, T. F. *Angew. Chem., Int. Ed.* **2011**, *50*, 3630–3670.

(13) Corbett, J. D. *Chem. Rev.* **1985**, *85*, 383–397.

(14) Adolphson, D. G.; Corbett, J. D.; Merryman, D. J. *J. Am. Chem. Soc.* **1976**, *98*, 7234–7239.

(15) Critchlow, S. C.; Corbett, J. D. *Inorg. Chem.* **1984**, *23*, 770–774.

(16) Beswick, M. A.; Choi, N.; Harmer, C. N.; Hopkins, A. D.; McPartlin, M.; Wright, D. S. *Science* **1998**, *281*, 1500–1501.

(17) Bashall, A.; Beswick, M. A.; Choi, N.; Hopkins, A. D.; Kidd, S. J.; Lawson, Y. G.; Mosquera, M. E. G.; McPartlin, M.; Raithby, P. R.; Wheatley, A. A. E. H.; Wood, J. A.; Wright, D. S. *J. Chem. Soc., Dalton Trans.* **2000**, 479–486.

(18) Bashall, A.; Bond, A. D.; Hopkins, A. D.; Kidd, S. J.; McPartlin, M.; Steiner, A.; Wolf, R.; Woods, A. D.; Wright, D. S. *J. Chem. Soc., Dalton Trans.* **2002**, 343–351.

(19) Driess, M.; Merz, K.; Pritzkow, H.; Janoschek, R. *Angew. Chem. Int. Ed. Engl.* **1996**, *35*, 2507–2510.

(20) Hübler, K.; Becker, G. *Z. Anorg. Allg. Chem.* **1998**, *624*, 483–496.

(21) Prices of lithium, sodium, and potassium specific cation sequestering agents (per mmol). Li specific 12-crown-4: £2.14; 2,1,1-crypt: £294.15. Na specific 15-crown-5: £0.76; 2,2,1-crypt: £116.02. K specific 18-crown-6: £0.59; 2,2,2-crypt: £38.97. Prices from Sigma-Aldrich and are correct as of September 2013.

(22) Santandrea, R. P.; Mensing, C.; von Schnering, H. G. *Thermochim. Acta* **1986**, *98*, 301–311.

(23) Emmerling, F.; Rohr, C. *Z. Naturforsch., B: J. Chem. Sci.* **2002**, *57*, 963–975.

(24) Huheey, J. E. *Inorganic Chemistry: Principles of Structure and Reactivity*; 4th ed.; Harper Collins: New York, 1993.

(25) Greenwood, N. N.; Earnshaw, A. *Chemistry of the Elements*; 2nd ed.; Butterworth Heinemann: Oxford, 1997.

(26) Pyykkö, P.; Atsumi, M. *Chem. Eur. J.* **2009**, *15*, 186–197.

(27) Hönle, W.; von Schnering, H. G.; Schmidpeter, A.; Burget, G. *Angew. Chem. Int. Ed. Engl.* **1984**, *23*, 817–818.

(28) Kühl, O. *Phosphorus-31 NMR Spectroscopy: A Concise Introduction for the Synthetic Organic and Organometallic Chemist*; Springer: Berlin, 2008.

(29) *Quantities, Units and Symbols in Physical Chemistry*; Royal Society of Chemistry: Cambridge, 2002.

(30) Knapp, C. M. Solution Reactivity Studies of Group 15 Zintl Ions, University of Oxford, 2013.

(31) Zahlan, A.; Heineken, F. W.; Bruin, M.; Bruin, F. *J. Chem. Phys.* **1962**, *37*, 683–684.

(32) Carrington, A.; dos Santos-Veiga, J. *Mol. Phys.* **1962**, *5*, 21–29.

(33) Kraus, F.; Korber, N. *Chem. Eur. J.* **2005**, *11*, 5945–5959.

CHAPTER THREE

Reactivity of Heptapnictide Anions

Towards Heteroallenes

3.1 INTRODUCTION

3.1.1 Organic Chemistry of $[E_7]^{3-}$

The metallation chemistry of $[E_7]^{3-}$ (E = P, As, Sb) has been extensively studied, however exploration of the reactivity of the clusters towards organic molecules has focused only on simple alkylation reactions.[1] These have typically been performed with the $[P_7]^{3-}$ cage due to the wealth of information that can be gained using ^{31}P NMR spectroscopy.

Reactions with alkyl chlorides or tosylates have been used to form neutral, trisubstituted cages $[P_7R_3]$ (R = Me, Et, ^{i}Pr, ^{n}Bu, ^{i}Bu, Hex).[2–4] The same methodology has also been used to prepare the group 14 and 15 trisubstituted cages, $[E_7(E'R_3)]$ (E = P: $E'R_3$ = $SiPh_3$, SiH_3, $SiMe_3$, $SiMeH_2$, $GeMe_3$, $SnMe_3$, $PbMe_3$; E = As: $E'R_3$ = $SiMe_3$) and $[P_7(E'Bu_3)_3]$ (E = P, Sb).[5–7] In these cases one of two isomers, either symmetric (thermodynamic product) or asymmetric (kinetic product) can be formed, with the ratio of symmetric:asymmetric isomer increasing with the increasing steric bulk of the R group. For extremely bulky groups, such as $\{Fe(Cp)(CO)_2\}$, found in $[\{Fe(Cp)(CO)_2\}_3P_7]$ the symmetric isomer is formed exclusively.[8]

Of interest is the synthesis of $[P_7(P'Bu_3)_3]$ using the fluorophosphine $^{t}Bu_2PF$. Attempts were made to form $[P_7(PMe_2)_3]$ by reaction of $[Li(DME)]_3[P_7]$ with the less bulky Me_2PCl, however the only isolable product was the reductively coupled diphosphane P_2Me_4. This exemplifies the fine balance between the nucleophilic and redox (where the cage acts as a reducing agent) chemistry of the $[E_7]^{3-}$ anions (Scheme 3.1). This was encountered in Chapter Two, where the $[K(18\text{-crown-6})]^{+}$ salt of $[P_7]^{3-}$ (**3**) was found to be stable in pyridine, but the $[K(2,2,2\text{-crypt})]^{+}$ salt was not.

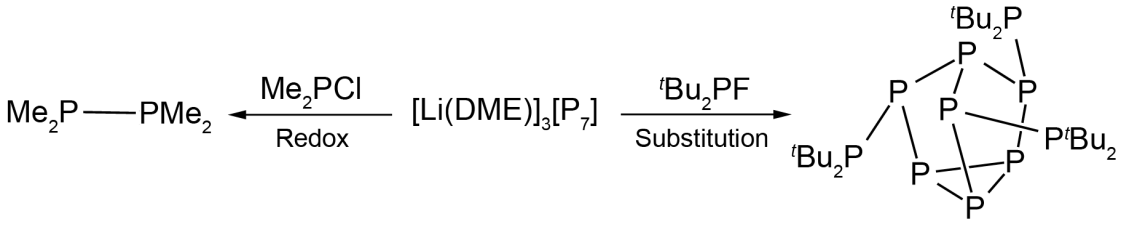

Scheme 3.1: The synthesis of a tri(phosphine) substituted cage, illustrating the balance between redox chemistry and nucleophilic chemistry of the heptaphosphide trianion.

The alkyl groups on these trisubstituted clusters are known to undergo exchange reactions. The monosubstituted $[P_7(SiMe_3)]^{2-}$ and disubstituted $[P_7(SiMe_3)_2]^-$ are synthesized by the reaction of $[P_7(SiMe_3)_3]$ with $[Li(DME)]_3[P_7]$ in the molar ratios 1:2 and 2:1, respectively.[9] This is further illustrated by the reaction of $[P_7(SiMe_3)_2]^-$ with EtBr, which gives rise mixtures of $[P_7(SiMe_3)_2Et]$, $[P_7(SiMe_3)Et_2]$, $[P_7(SiMe_3)_3]$ and $[P_7Et_3]$.[10]

A more convenient route to disubstituted clusters uses tetraalkylammonium salts. Reaction of the halide salts with K_3E_7 results in the stereospecific transfer of the most electrophilic alkyl group to the cage, to form the least sterically hindered isomer of $[E_7R_2]^-$ (E = P, As; R = Me, Et, ^{n}Bu, Bn, *N*-methylated amino acid esters).[11,12]

The only crystallographically characterized monosubstituted cage, $[P_7R]^{2-}$ (R = $(SiMe_3)_2MeSi$) was reported in 2011 by Noblet et al. via the cleavage of two R groups from the neutral $[P_7R_3]$.[13] The ^{31}P NMR spectrum of the anion displays fluxional behaviour that is resolved on cooling, analogous to $[HP_7]^{2-}$ (**1**).[14]

3.1.2 Heteroallenes

Allenes are "Hydrocarbons ... having two double bonds from one carbon atom to two others".[15] Replacement of one of the terminal carbon atoms of the functional group with an isolobal heteroatom gives a so-called heteroallene. This gives a series of compounds, two of which are the isocyanates RN=C=O and carbodiimides RN=C=NR. Carbon dioxide, which

replaces both CR_2 groups with oxygen, is also a heteroallene and related to the carbodiimides and isocyanates by the isolobal principle discussed in Chapter One (Scheme 3.2).

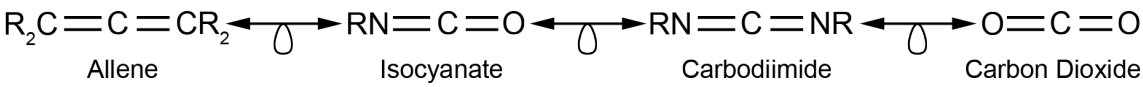

Scheme 3.2: The isolobal principle as applied to allenes and heteroallenes.

Allenes (and by extension heteroallenes) possess a linear sp hybridized central carbon atom. It makes two separate π bonds, which are necessarily orthogonal and non-conjugated.[16] They tend to react as nucleophiles, as would be expected for alkenes. Changing the identity of the terminal atoms to electron withdrawing heteroatoms also changes the reactivity of the group and causes the central carbon acts as an electrophile, subject to nucleophilic attack.[17]

3.2 OBJECTIVES

The account above summarizes the state of the art in the reactivity of organic molecules with heptapnictide cages as of 2010. The initial aim of this project was to investigate the reactivity of $[P_7]^{3-}$ with small molecules, particularly carbon dioxide, to try to exploit the high nucleophilicity and reductive potential of the cages. This chapter will describe the reactivity of **1** and **3** towards carbon dioxide. It will additionally extend the reactivity towards a series of isolobal analogues, which have resulted in the discovery of a new mode of cluster reactivity. A family of amidine and amide functionalized cages could be obtained by reaction of protic heptapnictide cages with carbodiimides and isocyanates, respectively.[18,19] Their synthesis and structures will be discussed. The conditions required for protonation will be described, as will the subsequent reactivity of the protic cages towards further functionalization.[20]

3.3 Reactivity Towards Carbon Dioxide

We postulated that the nucleophilic phosphide vertices of the heptaphosphide cage might be able to trap carbon dioxide. This has been observed in the reaction of $[Ph_2P]^-$ with CO_2 to form $[Ph_2P–CO_2]^-$,[21] and other related transformations can be found in the insertion of carbon dioxide into metal–phosphide bonds,[22] and frustrated Lewis pair chemistry.[23] The reductive nature of the cage might then be able to liberate the trapped carbon dioxide, giving an oxidized polyphosphide cluster and a reduced carbon fragment. A theoretical reduction of the cage back to $[P_7]^{3-}$ would close the envisaged catalytic cycle (Scheme 3.3).

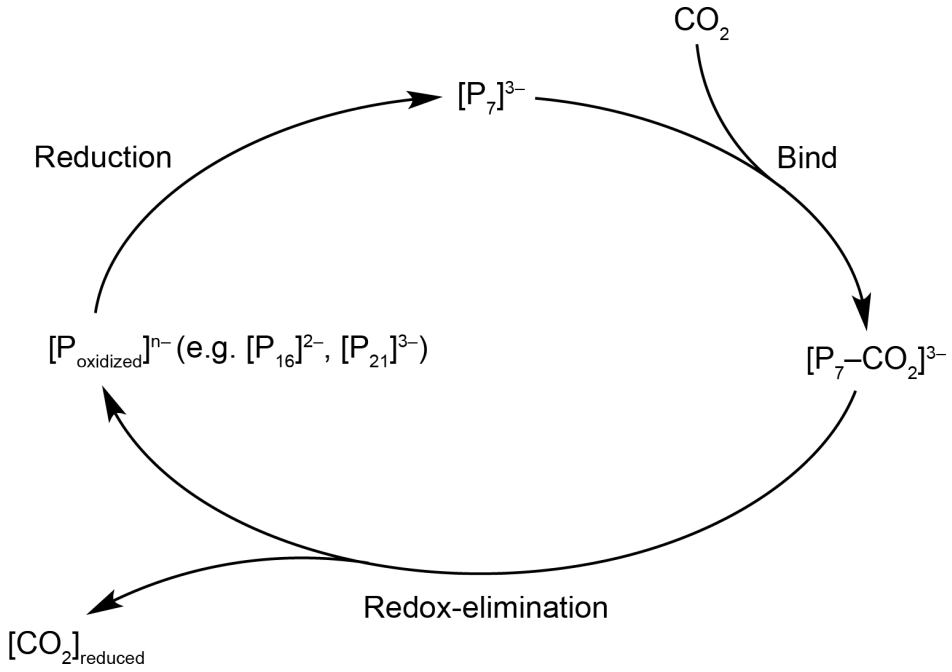

Scheme 3.3: The theorized possible catalytic cycle for the activation and reduction of CO_2 by $[P_7]^{3-}$.

3.3.1 Reactivity of $[P_7]^{3-}$ Towards Carbon Dioxide

Exposure of THF/pyridine solutions of $[K(18\text{-crown-6})]_3$[**3**] to one atmosphere of carbon dioxide resulted in an instantaneous colour change from a dark orange to bright yellow. These solutions were immediately transferred to an NMR spectrometer and analyzed by ^{31}P

NMR spectroscopy (Figure 3.1). The ^{31}P NMR spectrum at 25 °C shows broad resonances at –10 and –68 ppm, with an overall appearance similar to the room temperature ^{31}P NMR spectrum of **1** (*vide supra*). Cooling to –65 °C allows the resolution of six distinct, but broad resonances at 117, 63, 30, –94, –140 and –194 ppm with relative integrals 1:1:1:1:2:1:1. The observation of seven phosphorus environments is consistent with the monofunctionalization of the cage. We tentatively assign this as the 1:1 Lewis acid-base adduct, $[P_7–CO_2]^{3–}$ (**4**), where the functionalization has occurred at one of the phosphide vertices.

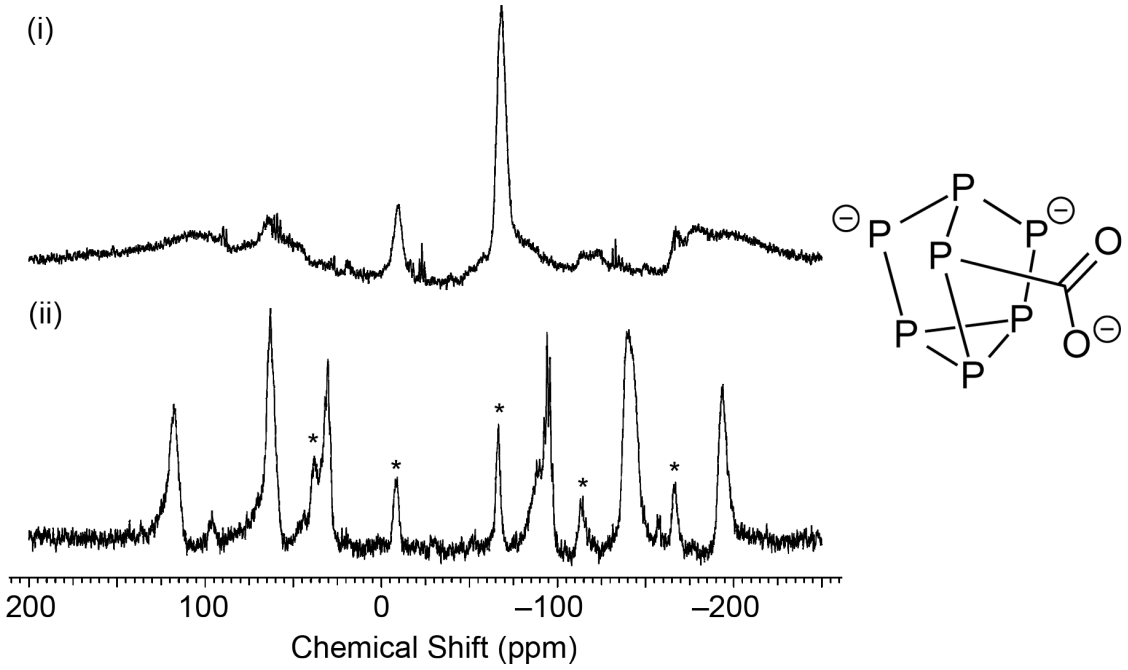

Figure 3.1: 25 ºC (i) and –65 ºC (ii) ^{31}P NMR spectra of **4** recorded immediately after exposure of a 1:1 THF/pyridine solution of $[K(18\text{-crown-6})]_3$[**3**] to carbon dioxide. The proposed structure of **4** is shown on the right. There is a minor product observable in (ii) indicated by *.

Over the course of hours, the NMR tube changes colour to give an intense orange solution, which is indicative of polyphosphide formation. Monitoring the reaction by ^{31}P NMR spectroscopy shows the gradual disappearance of the resonances attributable to **4**, with the

concomitant appearance of resonances attributable to the oxidized polyphosphides $[P_{16}]^{2-}$ and $[P_{21}]^{3-}$.[24,25] This reaction is complete after approximately 48 hours (Figure 3.2).

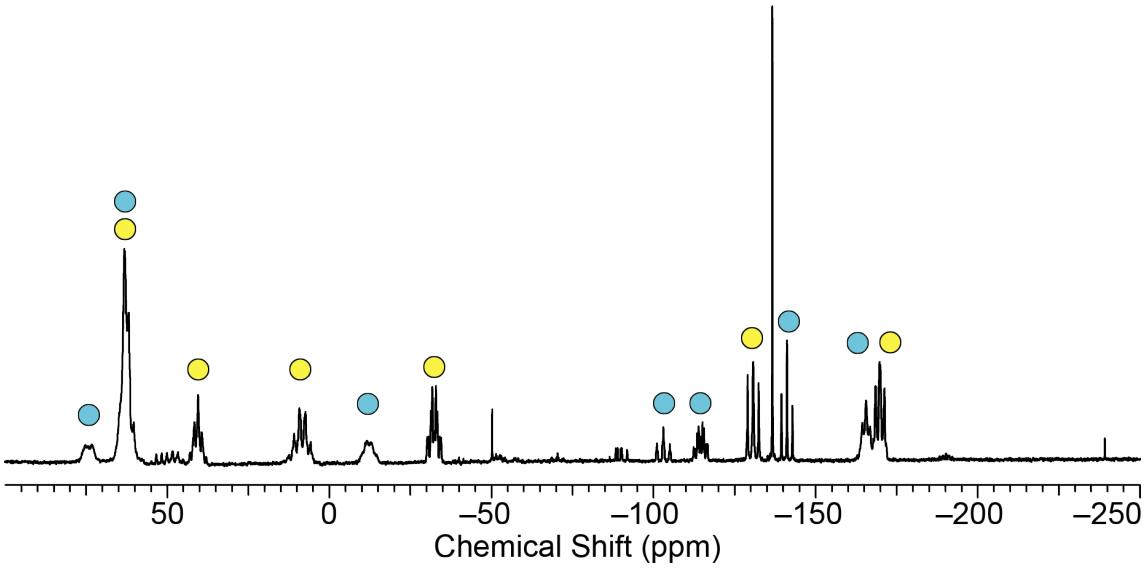

Figure 3.2: ^{31}P NMR spectrum of the reaction between [K(18-crown-6)]$_3$[**3**] and carbon dioxide after 48 hours. Resonances marked with a yellow circle correspond to $[P_{16}]^{2-}$, while those with a blue circle correspond to $[P_{21}]^{3-}$. The identity of the singlet at –140 ppm is unclear, but it does not integrate to significant quantities.

Exhaustive attempts were made to crystallize **4** at low temperature (–35 °C), where the yellow colour persisted for days. These yielded only intractable oils or very small and weakly diffracting crystals. Electrospray mass spectrometry of DMF solutions of [K(18-crown-6)]$_3$[**4**] generated in situ from [K(18-crown-6)]$_3$[**3**] and carbon dioxide showed only mass envelopes arising from **3** and higher polyphosphides ($[P_{16}]^{2-}$ and $[P_{21}]^{3-}$). This is presumably due to a combination of the weak nature of the $CO_2/[P_7]^{3-}$ interaction, and the high temperatures utilized during the ionization process.

3.3.2 Reactivity of $[HP_7]^{2-}$ Towards Carbon Dioxide

Experiments analogous to those described in Section 3.3.1 were performed using **1**. In contrast, exposure of DMF solutions of [K(18-crown-6)]$_2$[**1**] to carbon dioxide results in a

darkening of the solution. Immediate analysis by ^{31}P NMR spectroscopy shows extremely complex spectra with evidence for the formation of multiple unknown polyphosphides. Over the course of 24 hours the colour changes to give an orange solution. The ^{31}P NMR spectrum of such solutions shows that cluster oxidation and fragmentation to the known polyphosphides $[P_{16}]^{2-}$ and $[P_{21}]^{3-}$ has occurred,[24,25] and the ultimate fate of the cage proton is PH_3 (Figure 3.3).

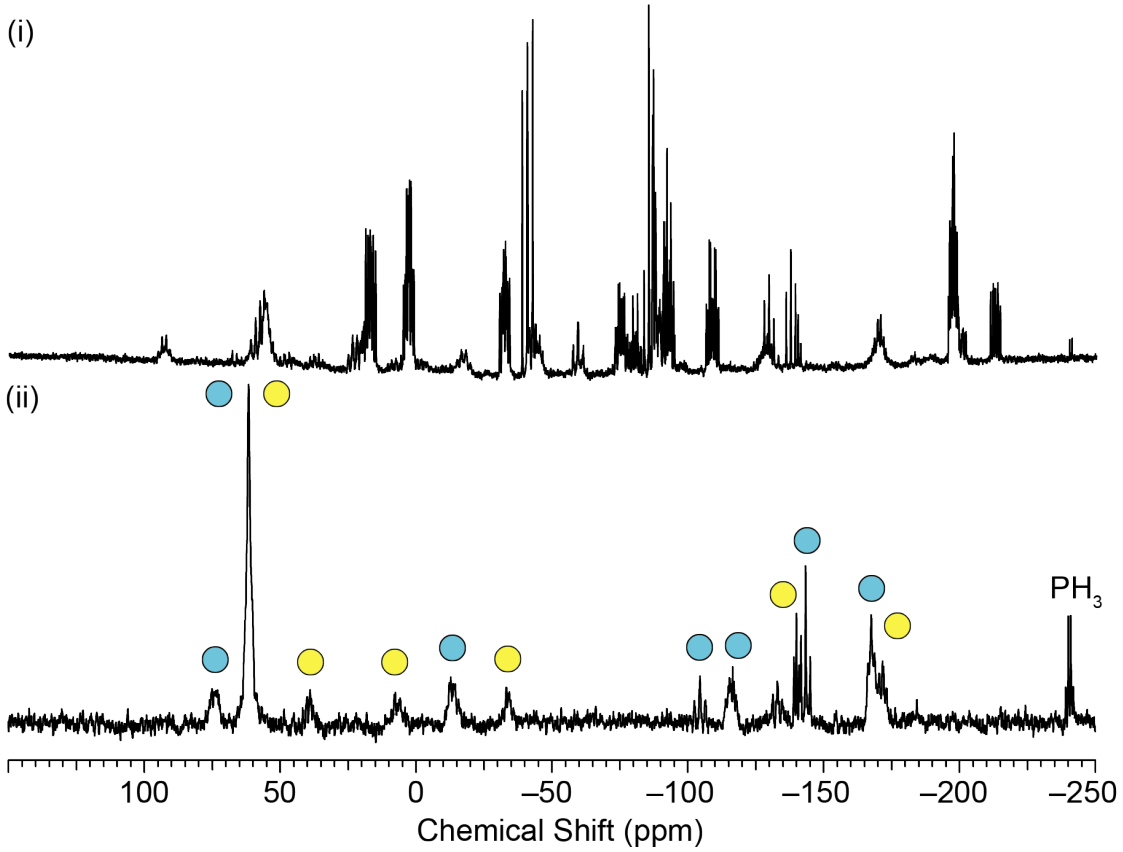

Figure 3.3: $^{31}P\{^{1}H\}$ NMR spectrum of the reaction between $[K(18\text{-crown-6})]_2$[**1**] and carbon dioxide immediately after reaction (i). ^{31}P NMR spectrum of the reaction mixture after one day. Resonances marked with a blue circle correspond to $[P_{21}]^{3-}$ and those with a yellow circles to $[P_{16}]^{2-}$. The PH_3 resonance is clearly resolved as a 1:3:3:1 quartet at –246 ppm.

The observation of oxidized polyphosphides for the reaction of both **1** and **3** with carbon dioxide suggests that the proposed cycle in Scheme 3.3 may be viable. However, due to the rapid decomposition and inability to crystallize any of the intermediate species this avenue

of investigation was not pursued further. The identity of the carbon containing product remains unclear due to the large quantities of **1** and **3** that would be needed to isolate an appreciable quantity of the putative reduction product (RMM of $[K(18\text{-crown-6})]_2[\mathbf{1}]$: 824.7 Da; $[K(18\text{-crown-6})]_3[\mathbf{3}]$: 1127.1 Da ; CO_2 44.0 Da). We turned instead to isocyanates and carbodiimides, isolobal analogues of carbon dioxide possessing sterically tuneable groups that we postulated would be able to hinder cage aggregation processes that are intermediate steps to cage oxidation.

3.4 Hydropnictination of Heteroallenes

Initial studies focused on the reaction of the protic heptaphosphide cage, **1**, due to the ability to monitor cage substitution processes by both ^{1}H and ^{31}P NMR spectroscopy. Accordingly, one equivalent of a carbodiimide or sufficiently bulky isocyanate was added to a d_7-DMF solution of **1**, as either the $[K(18\text{-crown-6})]^+$ or $[K(2,2,2\text{-crypt})]^+$ salt. This gives access to a new heptaphosphide anion, via a net hydrophosphination of a C=N double bond to give an amidine (carbodiimide) or amide (isocyanate) (Scheme 3.4).

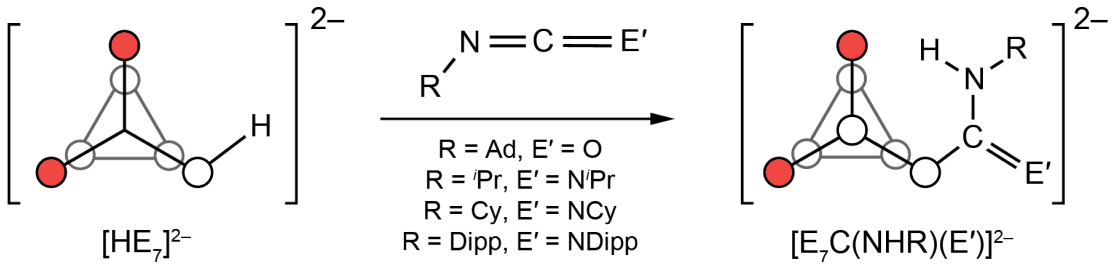

Scheme 3.4: Synthesis of the anions **5**–**12** through the hydropnictination of carbodiimides and isocyanates. Vertices coloured in red carry a formal negative charge.

The reaction is extremely rapid at room temperature, being complete by the time the sample is transferred to the NMR spectrometer for analysis (typically less than five minutes), and is

quantitative. The anions can be isolated as compositionally pure compounds as the $[K(18\text{-crown-6})]^+$ or $[K(2,2,2\text{-crypt})]^+$ salts by removal of solvent under reduced pressure and washing with diethyl ether. It was found that the methodology could also be extended to the arsenic congener, **3**. These reactions gave rise to a family of related amidine $[E_7C(NHR)(NR)]^{2-}$ (E = P, R = Dipp (**5**), Cy (**6**), ^{i}Pr (**7**); E = As, R = Dipp (**9**), Cy (**10**), ^{i}Pr (**11**)) and amide $[E_7C(NHR)(O)]^{2-}$ (E = P, R = Ad (**8**); E = As, R = Ad (**12**)) monosubstituted cages via a "self-catalyzed" hydropnictination process.

The clusters **5**–**7** and **8** can be considered heptaphosphaamidines and heptaphosphaamides, respectively; while **9**–**11** and **12** are heptaarsaamidines and heptaarsaamides, respectively. Previous routes in the literature to phosphaguanidines involve the stepwise deprotonation of secondary phosphines, nucleophilic addition to carbodiimides, and finally protonation of the phosphaguanidinate to give the corresponding phosphaguanidine.[26–28] The same synthetic route can be used to make arsaamidines and arsaamides from secondary arsines.[29,30] The bimodal character of **1** and **2**, which possess both nucleophilic phosphide (arsenide) and phosphine (arsine) vertices, allow for the one step hydropnictination of carbodiimides and isocyanates. This reaction is quantitative, and no protic workup is required since the proton originates from the cage. Related catalytic additions of secondary phosphines to carbodiimides and isocyanates have been reported using alkali-metal and lanthanide catalysis.[31–33]

The deprotonated $[P_7]^{3-}$ (**3**) cluster does not react with carbodiimides, even with extended reaction times or at elevated temperatures. The presence of a proton to transfer to the heteroallene is clearly crucial for reaction to occur. This would suggest a concerted addition of the P–H bond across a C=N double bond, or even an initial proton transfer to the

substrate prior to cluster coordination by analogy to the mechanism for the synthesis of amidine esters from carboxylic acids and carbodiimides.[34]

Interestingly, while even the relatively sterically unprotected carbodiimide bis(isopropyl)carbodiimide forms a stable derivative, the bulky (albeit, and perhaps crucially, only at one end) 1-adamantyl substituted isocyanate was required to form a stable anion. Smaller isocyanates such as phenyl isocyanate resulted in rapid cluster oxidation processes to form $[P_{16}]^{2-}$ and $[P_{21}]^{3-}$, analogously to the work on carbon dioxide described in section 3.2. This suggests that cluster aggregation might be one of the first steps in the cluster oxidation and decomposition process observed with carbon dioxide.

3.4.1 Structures of Hydropnictination Products

Crystals of the $[K(18\text{-crown-6})]^+$ salts of the dianions **5** and **7–12** suitable for single crystal X-ray diffraction could be grown in most cases by diffusion of hexane into THF or THF/pyridine (the addition of pyridine increases cluster solubility where it is otherwise low in neat THF) solutions. It did not prove possible to grow crystals of **6**, and extensive crystallographic disorder and/or inherent issues with the sample prevented us from obtaining satisfactory solutions for $[K(18\text{-crown-6})]_2[\mathbf{9}]\cdot 2.5THF$ and $[K(18\text{-crown-6})]_2[\mathbf{10}]\cdot 2THF\cdot py$ suitable for discussion of bond metric data. Nevertheless, they do confirm the composition and connectivity of the anions. Since the structures are very similar, a general discussion of the structural features will be made before a brief note on the specific details of a particular structure.

Selected bond metric data for the anions **5**, **7**, **8**, **11** and **12** are presented in Table 3.1. The E–E bond lengths within the cluster anions are unremarkable and comparable to literature values for related cages, lying in the range 2.135(av) to 2.264(1) Å for the phosphorus

clusters and 2.350(1) to 2.495(1) Å for the arsenic analogues (see Figure 3.4 for atom labelling scheme used).[8,11,12,35] As expected the E–E bond lengths within the arsenic analogues are longer by approximately 0.22 Å, which was observed for the $[HE_7]^{2-}$ clusters **1** and **3**. Bonds within the base of the cluster are again elongated relative to the other cluster bonds due to the inherent ring strain of this triangular moiety. Functionalization of the cluster at the E3 position results in a moderate lengthening of the E–E bonds to this atom. As a result, the E1–E3 and E3–E6 bond distances are longer than the related bonds involving E2 and E4.

Table 3.1: Comparison of bond metric data for **5**, **7**, **8**, **11** and **12**. E′ = N2 (**5**, **7**, **11**); O1 (**8**, **12**).

Bond Distance (Å)	**5**	**7**	**8**	**11**	**12**
E1–E2	2.164(av)	2.168(1)	2.162(1)	2.387(1)	2.379(1)
E1–E3	2.229(av)	2.221(1)	2.205(1)	2.455(1)	2.438(1)
E1–E4	2.164(av)	2.167(1)	2.161(1)	2.379(1)	2.376(1)
E2–E5	2.157(av)	2.164(1)	2.155(1)	2.376(1)	2.367(1)
E3–E6	2.188(av)	2.186(1)	2.196(1)	2.399(1)	2.410(1)
E4–E7	2.135(av)	2.139(1)	2.136(1)	2.350(1)	2.351(1)
E5–E6	2.244(av)	2.236(1)	2.238(1)	2.464(1)	2.465(1)
E5–E7	2.246(av)	2.264(1)	2.264(1)	2.495(1)	2.495(1)
E6–E7	2.241(av)	2.248(1)	2.231(1)	2.475(1)	2.458(1)
C1–E3	1.893(av)	1.891(2)	1.899(2)	2.030(2)	2.021(3)
C1–N1	1.356(av)	1.356(3)	1.337(2)	1.354(3)	1.346(4)
C1–E′	1.282(av)	1.287(3)	1.232(2)	1.281(3)	1.222(4)
N1–R	1.432(av)	1.452(3)	1.467(3)	1.454(3)	1.473(4)
E′–R	1.404(av)	1.454(3)	-	1.457(3)	-
Deviation from plane E3–C1–E′–N1–C2	0.002	0.014	0.018	0.013	0.011
Bond Angle (°)					
E3–C1–N1	115.8(av)	114.9(2)	119.15(15)	113.76(16)	117.9(2)
E3–C1–E′	125.1(av)	125.4(2)	117.62(15)	125.46(17)	118.6(2)
N1–C1–E′	119.1(av)	119.5(2)	123.2(2)	120.6(2)	123.5(3)
Sum of angles at C1	360(av)	359.8	360.0	359.8	360.0

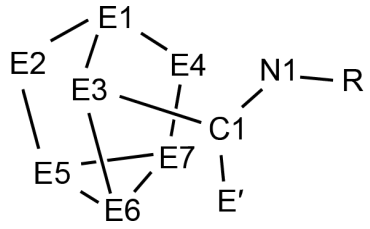

Figure 3.4: Numbering scheme used for discussion of the anions **5**–**12**.

Transfer of the cage proton to the N1 position of the carbodiimide or isocyanate is supported by a number of geometrical features. The sum of bond angles around C1 are all approximately 360°, as expected for an sp^2 hybridized carbon atom. The E3–C1–N1–E′ core of the amidines or amides are essentially coplanar, with only small deviations from planarity observed. Most importantly, the C1–N1 and C1–E distances are indicative of localized single and double bond character, respectively. The amidine functionalized cages **5**, **7** and **11** possess an average Δ_{CN} of 0.07 Å. The bond lengths observed agree well with previously reported phosphaguanidines.[26–28,36–38] The situation is more obvious for the amide functionalized cages **8** and **12** with C1–O1 bond distances of 1.232(2) and 1.222(4) Å, and C1–N1 distances of 1.337(2) and 1.346(4) Å, respectively. These agree well with values taken from the Cambridge Structural Database for related amide fragments.[39] Taken together, these data strongly support the transfer of the proton from the cage to the organic fragment to form amidines and amides.

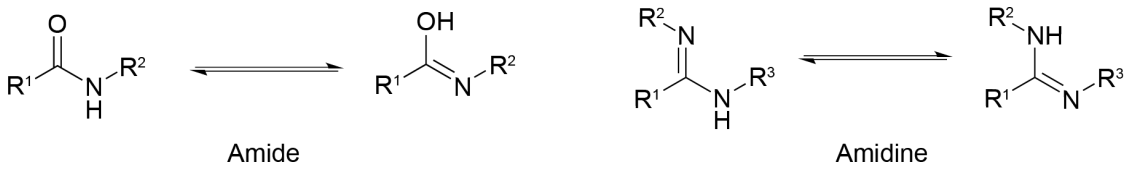

Scheme 3.5: Tautomerism of amides and amidines. In the case of amides, a new functional group is obtained, for amidines the "iminic" and "aminic" residues exchange.

In some cases the hydrogen atom could be located in the difference map after all non-hydrogen atoms were refined anistopically and all other hydrogen positions geometrically positioned. Interestingly, the proton is pointed towards the E4 pnictide vertex, which perhaps suggests the possibility of an intramolecular interaction between the hydrogen and the negatively charged vertex. No spectroscopic evidence for this intramolecular interaction was observed though, and it is likely a packing effect. However, it might also explain why no evidence of amidine or amide functional group tautomerism was observed (Scheme 3.5).[40]

The geometry at E3 is distorted pyramidal in all cases. This precludes any significant π-interactions between the pnictogen atom and the amidine or amide functionality. This is common in guanidines due to better energetic matching and overlap of the nitrogen lone pair with the amidine π system. Stemming from this pyramidalization is the chirality of the anion at E3. In all cases a mixture of enantiomers was observed by single crystal X-ray diffraction. In some cases this was inherent to the space group (compounds that crystallize in a centrosymmetric space group are necessarily racemates), whereas others crystallized as racemic twins in chiral space groups. Since there is no reason for one enantiomer to be favoured over the other during the hydropnictination reaction, this is expected. The *N*-substituents in all crystallographically characterized cages have E_{syn} configurations.[41]

The cluster anion **5** was crystallographically characterized in $[K(18\text{-crown-6})]_2[\mathbf{5}]$. The asymmetric unit contains three anions and six $[K(18\text{-crown-6})]^+$ cations, three of which display rotational disorder (Figure 3.5). Bond metric data have been presented for an average of the three anions.

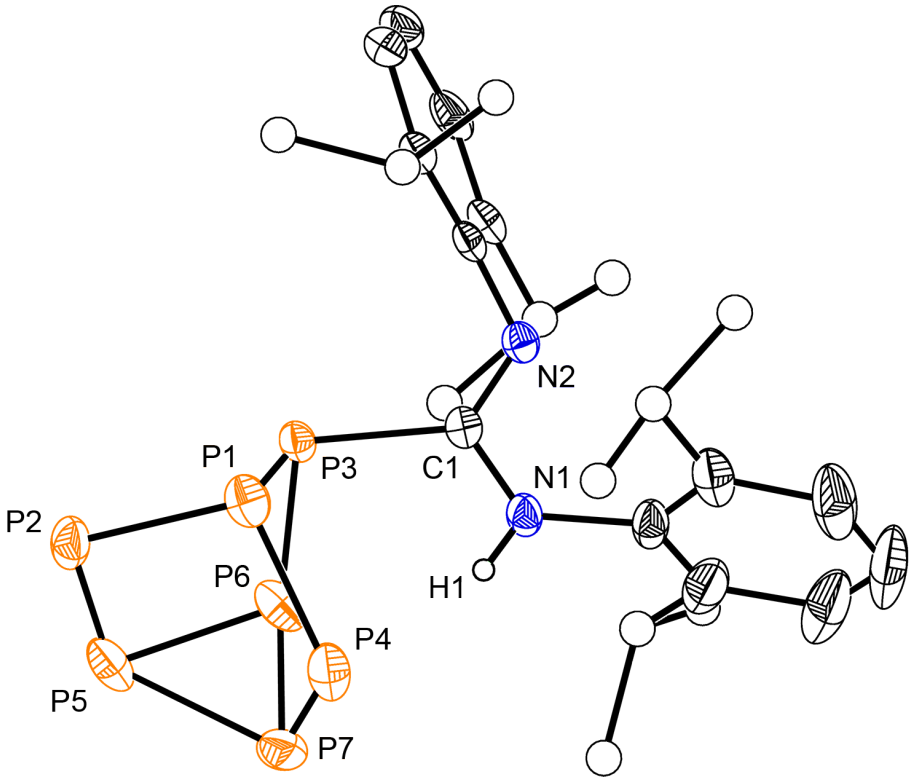

Figure 3.5: Thermal ellipsoid plot of **5**. Thermal ellipsoids are shown at the 50% probability level and all hydrogen atoms have been omitted for clarity with the exception of the amidine proton. Carbon atoms of the isopropyl groups are shown as spheres of arbitrary radius.

The structure of the anion **7** is shown in Figure 3.6. It crystallizes as a racemic mixture in the centrosymmetric *C*2/*c* space group, and the unit cell contains a single crystallographically unique anion accompanied by two $[K(18\text{-crown-6}]^+$ cations.

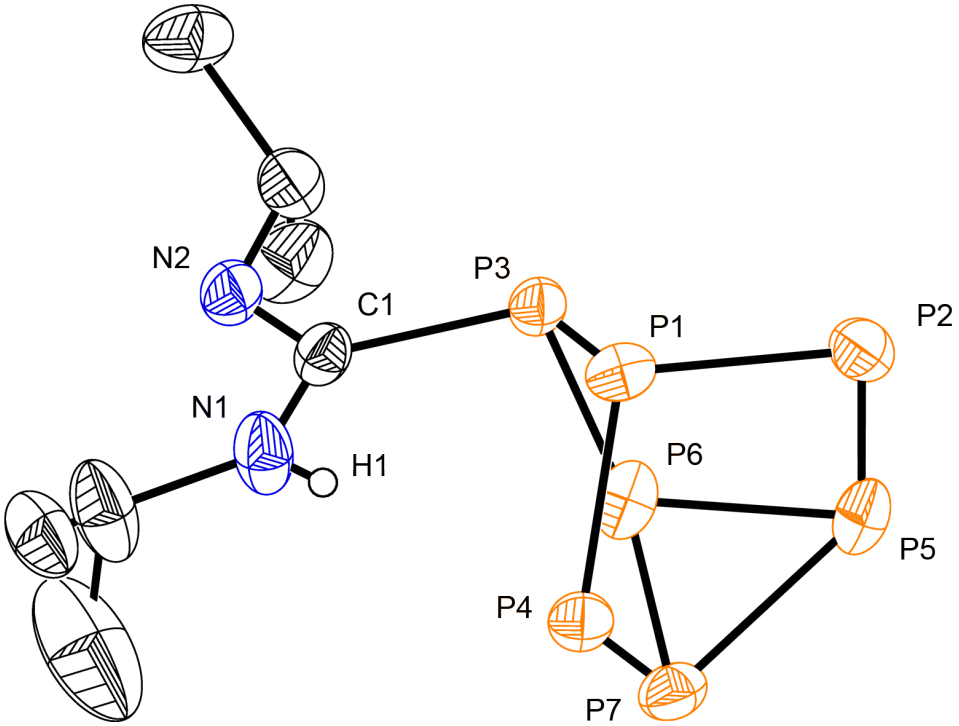

Figure 3.6: Thermal ellipsoid plot of **7**. Thermal ellipsoids are shown at the 50% probability level, and all hydrogen atoms have been omitted for clarity with the exception of the amidine proton.

The anion **8** is shown in Figure 3.7. It was crystallographically characterized in [K(18-crown-6)]$_2$[**8**]·py. One of the [K(18-crown-6)]$^+$ cations forms a close contact (2.655(2) Å) with O1 (Figure 3.6).

Anion **11** was similarly structurally characterized in [K(18-crown-6)]$_2$[**11**], clearly showing the hydroarsination product (Figure 3.8). It crystallizes in *C*2/*c* and is isomorphic with the phosphorus congener **7**.

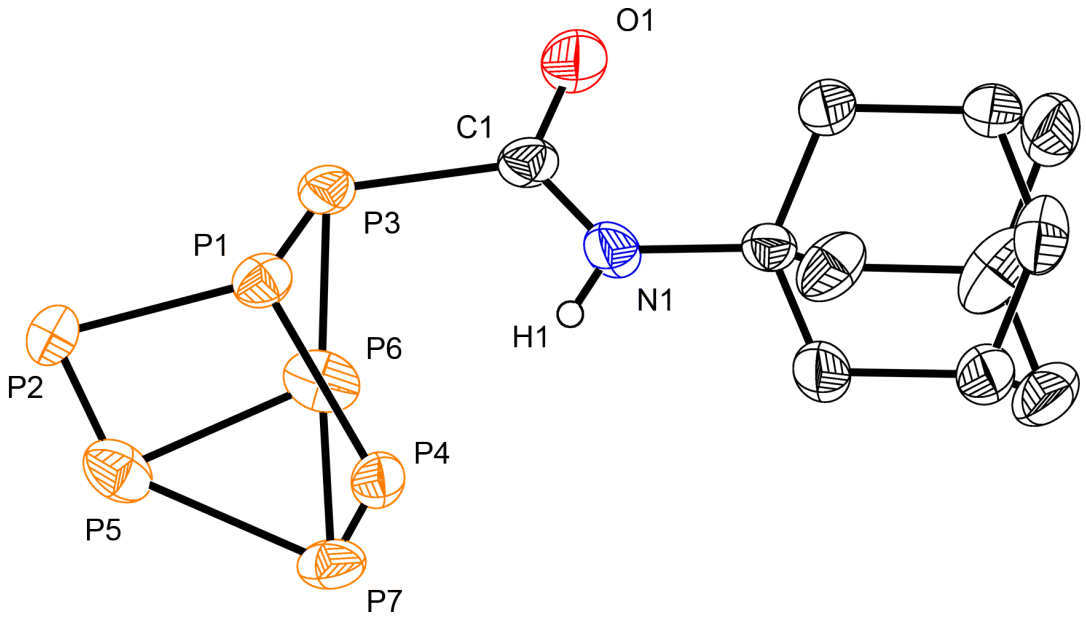

Figure 3.7: Thermal ellipsoid plot of **8**. Thermal ellipsoids are shown at the 50% probability level, and all hydrogen atoms have been omitted for clarity with the exception of the amide proton.

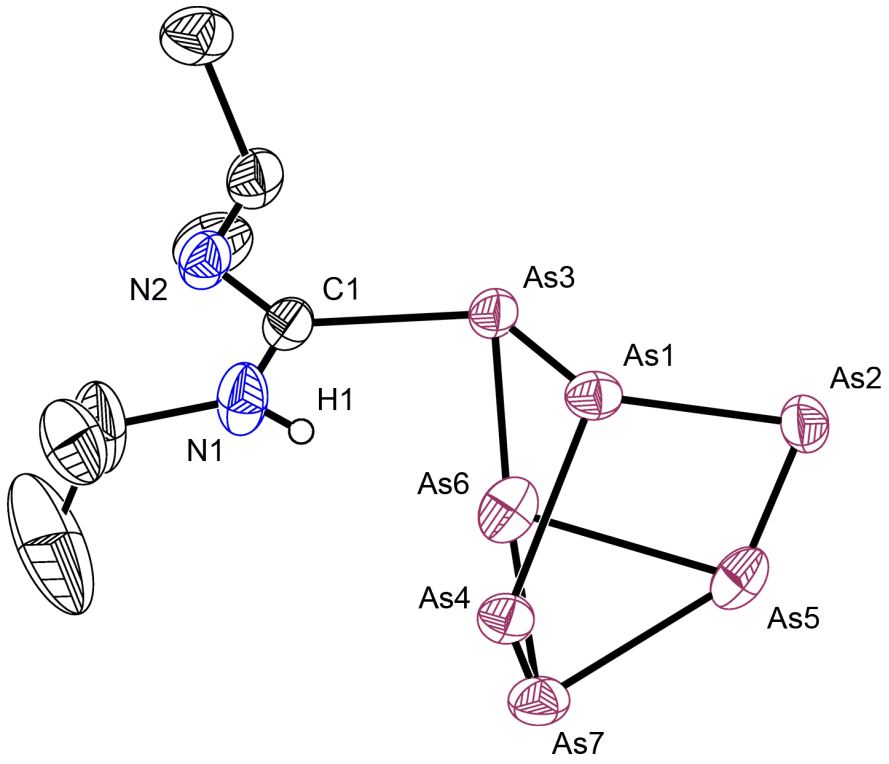

Figure 3.8: Thermal ellipsoid plot of **11**. Thermal ellipsoids are shown at the 50% probability level, and all hydrogen atoms have been omitted for clarity with the exception of the amidine proton. One of the isopropyl groups is disordered over two positions, only the major component (78%) is shown.

Finally, the amide substituted heptaarsenide cage, **12**, was crystallographically characterized as the $[K(18\text{-crown-6})]^+$ salt (Figure 3.9). It is isomorphous with the phosphorus analogue, **8**. The K1–O1 distance is 2.705(3) Å.

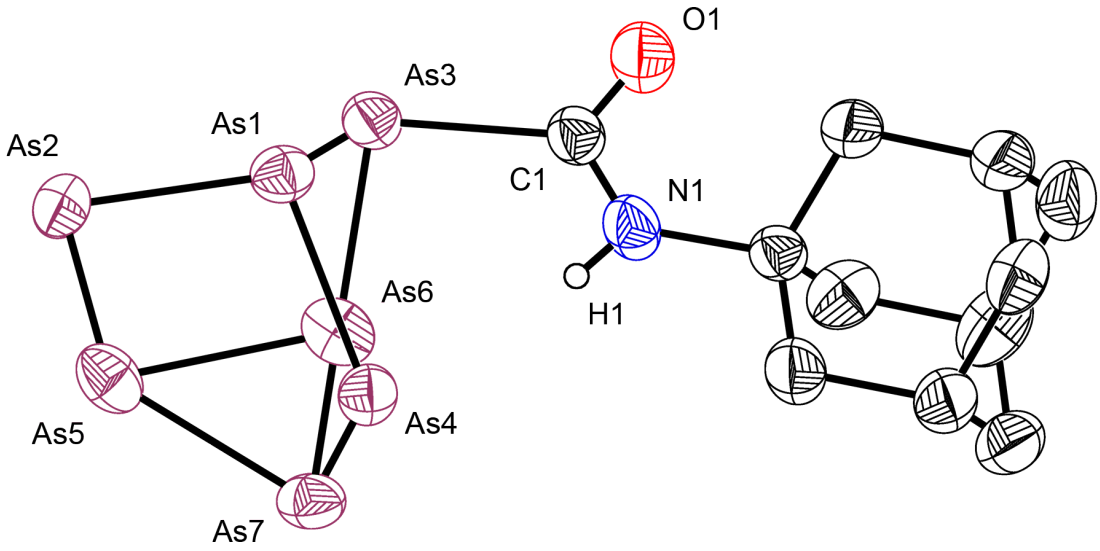

Figure 3.9: Thermal ellipsoid plot of **12**. Thermal ellipsoids are shown at the 50% probability level, and all hydrogen atoms have been omitted for clarity with the exception of the amidine proton.

DFT level calculations were performed on the anions **5**–**12**. The computed optimized structures are generally in very good agreement with those observed by single crystal X-ray diffraction (**5**, **7**, **8**, **11**, **12**). The computed bond lengths are typically longer than those observed experimentally (by approximately 0.05 Å) due to the oversimplifications used in modelling the presence of cations in the crystal lattice (Table 3.2).

The HOMO and HOMO–1 are predominantly lone pair character on the phosphide vertices E2 and E4, as expected. A Mulliken charge decomposition analysis show the greatest degree of negative partial charge on these atoms, which supports the pnictide nature of the vertices (Table 3.3).

Table 3.2: Computationally determined bond lengths and angles for the optimized computed geometries of **5**–**12**. E′ = N2 (**5**–**7**, **9**–**11**), O1 (**8**, **12**).

Bond distance (Å)	**5**$_{calc}$	**6**$_{calc}$	**7**$_{calc}$	**8**$_{calc}$	**9**$_{calc}$	**10**$_{calc}$	**11**$_{calc}$	**12**$_{calc}$
E1–E2	2.200	2.205	2.204	2.203	2.433	2.434	2.437	2.437
E1–E3	2.271	2.270	2.265	2.268	2.523	2.534	2.521	2.521
E1–E4	2.203	2.201	2.202	2.198	2.435	2.431	2.433	2.427
E2–E5	2.190	2.191	2.190	2.191	2.425	2.425	2.423	2.418
E3–E6	2.228	2.222	2.225	2.228	2.462	2.452	2.455	2.456
E4–E7	2.172	2.168	2.170	2.173	2.398	2.395	2.395	2.397
E5–E6	2.290	2.291	2.290	2.290	2.534	2.532	2.531	2.534
E5–E7	2.299	2.305	2.302	2.303	2.538	2.543	2.542	2.542
E6–E7	2.293	2.303	2.302	2.301	2.53	2.541	2.540	2.536
E3–C1	1.924	1.928	1.931	1.933	2.072	2.086	2.088	2.080
C1–N1	1.366	1.372	1.374	1.346	1.366	1.386	1.371	1.344
C1–E′	1.297	1.295	1.294	1.252	1.292	1.290	1.290	1.248
N1–H1	1.042	1.031	1.034	1.040	1.038	1.031	1.032	1.038
Bond angle (º)								
N1–C1–E3	116.2	116.1	115.2	118.0	115.6	114.0	114.2	117.5
N1–C1–E'	120.9	120.8	120.1	125.2	122.9	124.4	124.6	125.5
E′–C1–E3	122.9	123.0	124.0	116.8	121.5	121.5	121.0	117.0

Table 3.3: Selected Mulliken spin densities for **5**–**12**. E′ = N2 (**5**–**7**, **9**–**11**), O1 (**8**, **12**).

Atom	**5**$_{calc}$	**6**$_{calc}$	**7**$_{calc}$	**8**$_{calc}$	**9**$_{calc}$	**10**$_{calc}$	**11**$_{calc}$	**12**$_{calc}$
E1	–0.145	–0.232	–0.225	–0.190	–0.145	–0.207	–0.219	–0.185
E2	–0.549	–0.546	–0.548	–0.532	–0.605	–0.586	–0.585	–0.572
E3	0.020	–0.038	–0.027	–0.074	–0.024	–0.072	–0.047	–0.094
E4	–0.530	–0.502	–0.523	–0.503	–0.548	–0.546	–0.553	–0.540
E5	–0.230	–0.199	–0.206	–0.184	–0.203	–0.185	–0.187	–0.172
E6	–0.152	–0.213	–0.156	–0.178	–0.153	–0.202	0.174	–0.183
E7	–0.200	–0.193	–0.205	–0.192	–0.195	–0.184	–0.183	–0.175
C1	0.104	0.174	0.183	0.404	0.149	0.189	0.204	0.420
N1	–0.187	–0.112	–0.153	–0.095	–0.202	–0.130	–0.152	–0.086
E′	–0.355	-0.362	–0.359	–0.686	–0.371	–0.364	–0.366	–0.685

3.4.2 NMR Spectroscopic Studies on 5–12

NMR studies were performed on d_7-DMF solutions of either the $[K(18\text{-crown-6})]^+$ or $[K(2,2,2\text{-crypt})]^+$ solutions of the anions **5**–**8**. Since all are monosubstituted heptaphosphide cages, the obtained ^{31}P NMR spectra are remarkably similar, with only some minor

chemical shift variations observed for the substituted P3 vertex. At room temperature, the ^{31}P NMR spectra all show a multiplet resonance around 0 ppm, depending on the nature of the R group, and two extremely broad resonances centred at approximately –85 and –111 ppm (Figure 3.10). Chemical shifts for the resonances are given in Table 3.4. The observation of only three resonances at room temperature suggests that a fluxional process that interconverts non-functionalized cage vertices is operating, analogous to that observed for $[HP_7]^{2-}$ (*vide supra*).[14]

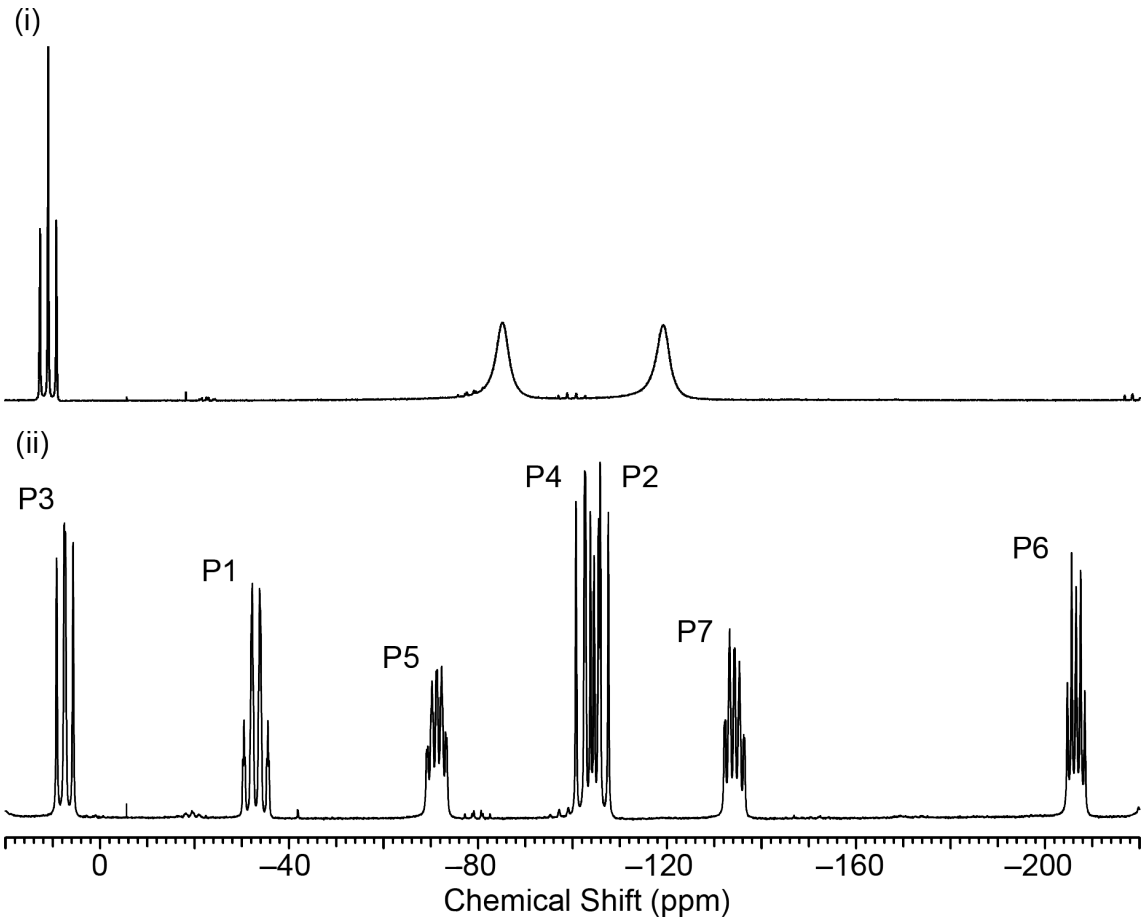

Figure 3.10: ^{31}P NMR spectra of a d_7-DMF solution of [K(18-crown-6)]$_2$[**8**] recorded at 25 ºC (i) and –50 ºC (ii). The atom numbering scheme is the same as that used for the crystal structure of **8**.

Table 3.4: ^{31}P chemical shifts for **5**–**8** recorded at room temperature.

Anion	^{31}P chemical shifts (δ)
5	–6.4, –83.2, –111.9
6	–18.5, –87.5, –111.7
7	–18.3, –87.6, –111.8
8	10.9, –85.2, –119.2

Upon cooling to –50 °C, the fluxional process is retarded and seven distinct resonances can be observed in the NMR spectrum, which arise from the seven magnetically inequivalent phosphorus nuclei (Table 3.5 and Figure 3.10). The most downfield resonances correspond to the functionalized P3 vertex, presumably because it possesses the smallest partial negative charge (and is thus the least shielded) as a result of the functionalization. It is also the resonance that is most perturbed by the nature of the substituent. The two amidines with alkyl groups, **6** and **7** are found significantly upfield shifted from the aryl amidine **5**. The low temperature ^{31}P NMR spectrum of **5** was assigned based on a ^{31}P–^{31}P COSY experiment performed at –50 °C on a d_7-DMF solution of [K(18-crown-6)]$_2$[**5**]. The remaining anions **6**–**8** were assigned by a comparison of chemical shifts. In all cases the spectra could be simulated to extract the ^{31}P–^{31}P coupling constants and confirm the assignment. Tabulated results for these can be found in Appendix A. The coupling constants do not vary much with the identity of the R group, and fall in the approximate range $^{1}J_{P–P}$ = 180–440 Hz, with the smallest couplings found in the base of the cluster and the largest between the phosphide vertices and those in the base. This can be attributed to the increased s orbital character in the bonds made by the phosphide vertices (the basal vertices are approximately sp^3 hydridized, while the phosphide vertices are sp^2 hybridized). The larger s orbital character results in a larger Fermi contact term and hence larger coupling constants. The invariance observed for **5**–**8** reflects the relative electronic remoteness of the substituent from the cage. The ^{31}P and ^{31}P{^{1}H} NMR spectra for each individual compound are identical, which further confirms the lack of a P–H bond.

Table 3.5: ^{31}P chemical shifts (δ) for **5**–**8** recorded at –50 °C.

Nucleus	5	6	7	8
P1	–28.3	–28.2	–28.9	–33.8
P2	–100.0	–103.8	–105.0	–105.6
P3	–6.3	–18.7	–17.7	7.4
P4	–91.6	–95.7	–96.2	–102.7
P5	–68.7	–73.5	–73.0	–71.3
P6	–211.7	–222.4	–224.9	–206.6
P7	–134.1	–130.3	–130.3	–134.2

The ^{1}H and ^{13}C{^{1}H} NMR spectra further support the formulation of the anions **5**–**12** as amidine or amide functionalized cages. Functionalization of the cage results in the disappearance of the diagnostic proton resonances of **1** and **2**, and the appearance of a new, downfield shifted resonance corresponding to the NH proton. Tabulated values are shown in Table 3.6. The chemical shift of this resonance proves to be extremely sensitive to the chemical environment of the amidine or amide proton and can shift substantially depending on the nature of the nitrogen substituent. There is an additional, smaller downfield shift on moving from phosphorus to arsenic. This is consistent with previously reported related compounds.[26,29,30,33] The amidine-functionalized cages **5**–**7** and **9**–**11** display the expected number of resonances for two inequivalent R groups on nitrogen.

Table 3.6: ^{1}H and ^{13}C{^{1}H} chemical shifts (δ) for **5**–**12**.

	5	6	7	9	10	11	8	12
H1	6.29	3.14	4.05	6.6	4.38	4.39	5.88	6.18
C1	165.7	161.3	161.8	168.9	163.9	165.9	182.8	186

The ^{13}C{^{1}H} NMR shifts lie in the expected region of the spectrum. Those for the phosphorus cages **5**–**8** appear as doublets due to coupling to P3, with coupling constants of approximately 80 Hz, although the doublet is partially obscured by the intense DMF solvent resonance in **6** and **7**, which precludes precise measurement of the coupling constant. This lies in the expected range for a $^{1}J_{C–P}$ coupling.[42]

To confirm that the proton transferred during the hydropnictination reaction originates from the protic cage, isotopic labelling studies were performed. The reaction of **1–D** with bis(2,6-diisopropylphenyl)carbodiimide in protic solvent shows the exclusive formation of the labelled **5–D**. The ^{2}H NMR spectrum of **5–D** displays a broad singlet at 6.92 ppm, which corresponds to the ND hydrogen. There is a very small (<5%) amount of the protic analogue, due to incomplete deuterium labelling of the **1–D** starting material. The ^{31}P NMR spectrum is identical to that of **5**, further confirming the lack of a P–H(D) bond.

3.4.3 Mass Spectrometric Studies

DMF solutions of the $[K(18\text{-crown-6})]^{+}$ or $[K(2,2,2\text{-crypt})]^{+}$ salts of **5**–**12** were studied by electrospray ionization mass spectrometry in both the positive and negative ion modes (Table 3.7). All of the anions are observed in the negative ion mode spectra as the $[M+H]^{-}$ ions. The positive ion mode spectra generally show mass envelopes corresponding to the cation-paired $\{[K(SA)]_3[M]\}^{+}$ ions, although no evidence for **5**, **9** or **12** can be observed in their positive ion mode mass spectra. In general the phosphorus clusters are more robust, and less air- and moisture-sensitive than the arsenic analogues, which is reflected in the quality of the spectra obtained. In all cases, however, the parent ion is that the functionalized cluster anion.

Table 3.7: Electrospray mass spectrometry data for **5**–**12**.

Anion	Negative ion mode	Positive ion mode
5	581.3 $[M+H]^{-}$	Nothing observed
6	424.9 $[M+H]^{-}$	1668.7 $\{M+[K(2,2,2\text{-crypt})]_3\}^{+}$
7	344.7 $[M+H]^{-}$	1588.3 $\{M+[K(2,2,2\text{-crypt})]_3\}^{+}$
8	396.1 $[M+H]^{-}$	1306.2 $\{M+[K(18\text{-crown-6})]_3\}^{+}$
9	889.1 $[M+H]^{-}$	Nothing observed
10	732.7 $[M+H]^{-}$	1643.1 $\{M+[K(18\text{-crown-6})]_3\}^{+}$
11	652.2 $[M+H]^{-}$	1562.9 $\{M+[K(18\text{-crown-6})]_3\}^{+}$
12	704.5 $[M+H]^{-}$	Nothing observed

3.5 PROTONATION OF MONOFUNCTIONALIZED CAGES

We next sought to explore the protonation chemistry of the anions, envisaging a situation where one of the remaining phosphide vertices could be protonated to form an anion of the general formula $[HP_7(R)]^-$. This putative anion would still possess bimodal character, and be capable of undergoing further hydrophosphination to allow for the synthesis of bifunctionalized cages. We chose to focus exclusively on the heptaphosphide cages due to the convenient ^{31}P NMR handle.

Initial reactivity screening was performed using the weak acid ammonium tetraphenylborate. The solid acid was added portionwise to stirring d_7-DMF solutions of the $[K(2,2,2\text{-crypt})]^+$ salts of **5**–**8** (prepared in situ from $[K(2,2,2\text{-crypt})]_2$[**1**] and the appropriate heteroallene). The crude reaction mixture was then transferred to an NMR tube and analyzed by ^1H and ^{31}P NMR spectroscopy. In the case of **6**–**8**, the ^{31}P NMR spectrum showed cluster oxidation and decomposition to $[P_{16}]^{2-}$, while the ^1H NMR spectrum was consistent with the formation of the free formamidine or formamide. However, protonation of **5** was reproducibly found to give rise to the protonated monoanionic species $[HP_7C(NHDipp)(NDipp)]^-$ (**13**) (Scheme 3.6). It is worth noting that this is the cage carrying the most sterically demanding substituents, and this is presumably the reason for its stability.

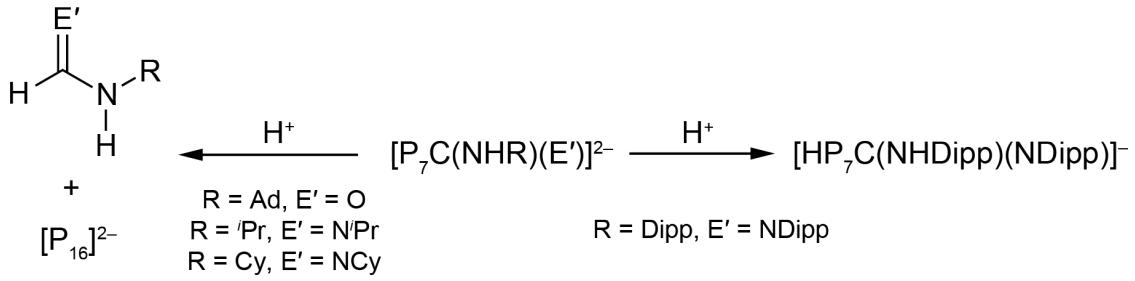

Scheme 3.6: Protonation reactions of **5**–**12**.

All attempts to obtain a compositionally pure sample of [K(2,2,2-crypt)][**13**] from solutions prepared in this fashion were unsuccessful due to its extremely similar solubility to the byproduct, [K(2,2,2-crypt)][BPh_4]. Protonation using Brookhart's acid, [$H(OEt_2)_2$][$BAr^F{}_4$], allowed for the resulting [K(2,2,2-crypt)][$BAr^F{}_4$] byproduct to be removed by washing the bulk sample with diethyl ether, since [K(2,2,2,-crypt)][**13**] is only very sparingly soluble in the solvent.[43] This allowed the synthesis of compositionally pure samples of [K(2,2,2-crypt)][**13**] where no evidence of the [$BAr^F{}_4$]$^-$ anion was visible in the ^{1}H or ^{19}F NMR spectra and an accurate elemental microanalysis could be obtained.

3.5.1 Structure of 13

Crystals of [K(2,2,2-crypt)][**13**] suitable for single crystal X-ray diffraction could be grown by diffusion of hexane into THF solutions of the product at 5 °C. It crystallizes in the space group *Pna*2$_1$, with the asymmetric unit containing one cluster anion and one accompanying [K(2,2,2-crypt)]$^+$ cation, consistent with the formulation of **13** as a monoanionic cluster (Figure 3.11). The anion exhibits "up-down" disorder, as a result of both enantiomers of the [P_7C(NHDipp)(NDipp)] core occupying the same site in a 54:46 occupancy ratio. The amidine functionality in both components of the disorder occupies the same site in the lattice and consequently only the heptaphosphide moiety is disordered. This reduces the precision of the P–P distances, and a detailed discussion of the bond metric data is not possible. For comparative purposes, Table 3.8 summarizes the relevant bond metric data of the two components of the disorder for **13**. There are some anomalously short bond distances (P3–P6 component 2, P6–P7 component 1) that very likely arise as a result of the disorder, illustrating the caution that should be used in their interpretation. The bond distances within the amidine moiety are very similar to those observed for **5**. The C1–N1 and C1–N2 distances are 1.366(5) and 1.273(5) Å, respectively (Δ_{CN} = 0.09 Å). This

supports the formulation of the anion and suggests that the amidine moiety is left unaffected by cluster protonation.

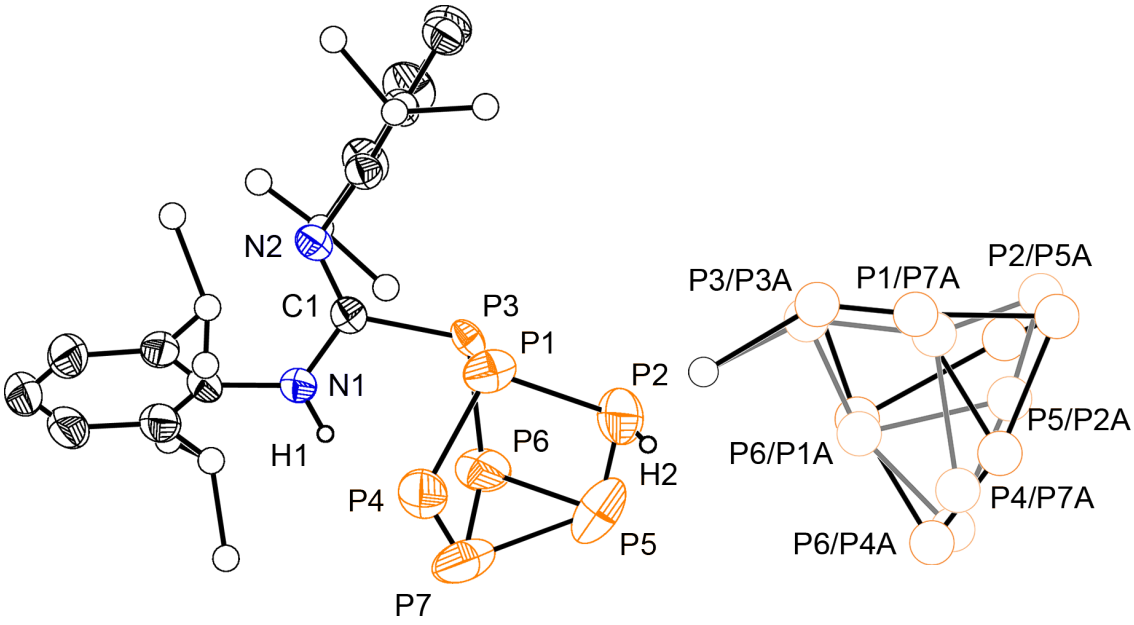

Figure 3.11: Thermal ellipsoid plot of **13** (left). Thermal ellipsoids are set at the 50% probability level. Only the major component of the cage disorder is displayed. Isopropyl groups are shown as spheres of arbitrary radius and all hydrogen atoms have been omitted for clarity with the exception of the amidine proton. Ball and stick representation of the two components of the disorder in the cage (right). Major component is shown in transparency.

It did not prove possible to locate the position of the cluster proton by studying the residual electron density map after anisotropic refinement of non-hydrogen atoms and geometrical positioning of all other hydrogen atoms. This is challenging in non-disordered systems using X-ray data, and owing to the disorder it becomes impossible in this system. The unfortunate result of this is that it is not possible to definitively state which of the conceivable isomers of **13** are present in the solid state (Figure 3.12). This will be discussed in more depth in the following sections.

Table 3.8: Bond lengths (Å) and angles (°) for the two components of the disorder of **13**.

Bond Distance	**Component 1**	**Component 2**
P1–P2	2.147(14)	2.282(9)
P1–P3	2.367(16)	2.234(18)
P1–P4	2.137(10)	2.342(12)
P2–P5	2.149(9)	2.215(8)
P3–P6	2.128(15)	2.002(19)
P4–P7	2.133(9)	2.142(10)
P5–P6	2.093(9)	2.244(14)
P5–P7	2.251(12)	2.232(10)
P6–P7	2.053(12)	2.207(9)
P3–C1	1.844(14)	1.945(16)
C1–N1	1.366(5)	
C1–N2	1.273(5)	
N1–C2	1.423(5)	
N2–C14	1.423(4)	
Bond Angle		
C1–P3–P1	98.8(6)	97.8(5)
P1–P3–P6	96.1(6)	107.3(8)
P6–P3–C1	107.2(5)	101.3(8)
N1–C1–P3	114.0(5)	116.7(5)
N1–C1–N2	121.2(3)	
N2–C1–P3	124.7(5)	121.8(5)

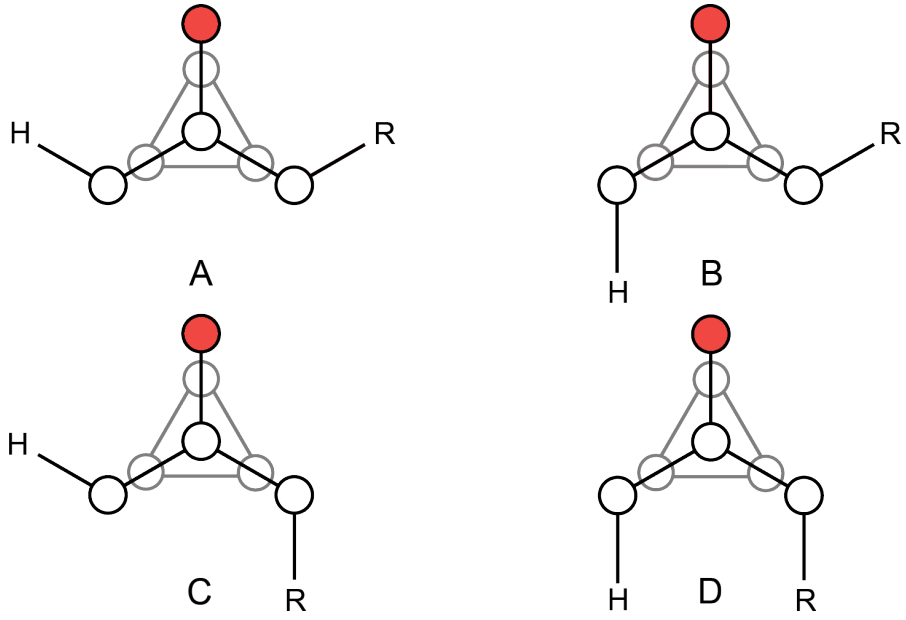

Figure 3.12: The four possible isomers of **13** (or, replacing R′ for H, any disubsituted cage). Vertices coloured in red carry a formal negative charge.

3.5.2 NMR Spectroscopic Studies on 13

Solutions of [K(2,2,2-crypt)][**13**] in d_5-pyridine have been extensively studied using multielement NMR spectroscopy. The $^{31}P\{^{1}H\}$ NMR spectrum of **13** shows fourteen major multiplet resonances, which we assign as arising from two different phosphorus species (Figure 3.13). These are likely two of the four possible isomers of **13**. Integration of the resonances shows that the two species are formed in approximately equal quantities.

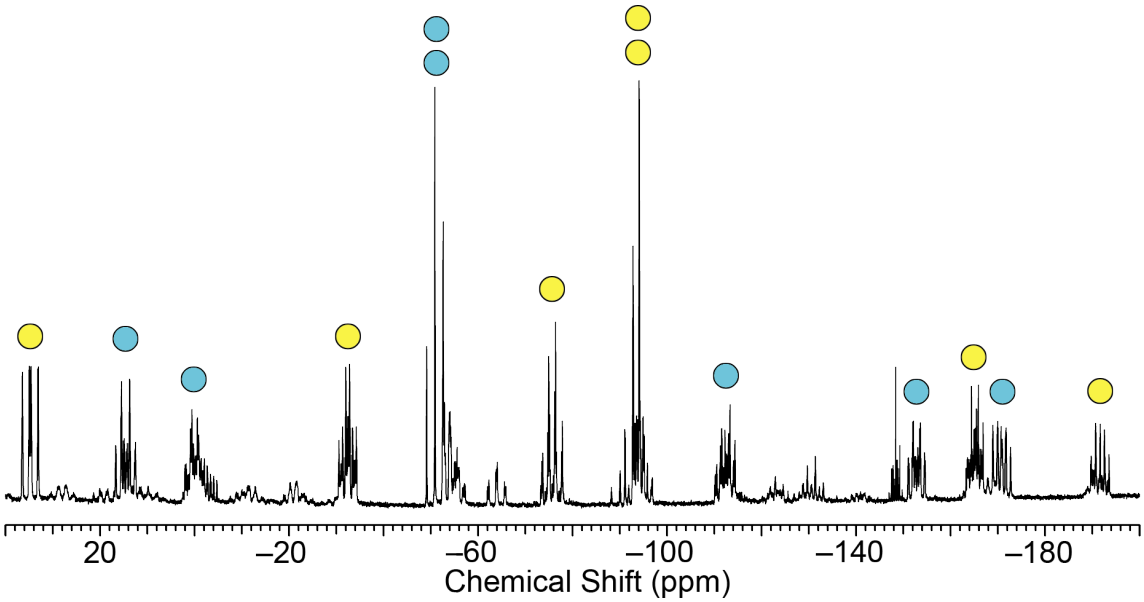

Figure 3.13: ^{31}P NMR spectrum of a d_5-pyridine solution of [K(2,2,2-crypt)][**13**]. Resonances corresponding to the two major isomers as determined by a ^{31}P–^{31}P COSY experiment are marked with blue and yellow circles.

A ^{31}P–^{31}P COSY experiment allows for the resonances to be correlated and tentatively assigned with one species found at 34.8, –32.4, –75.6, –92.7, –95.0, –165.3 and –191.7 ppm, while the second species is found at 14.6, 0.0, –50.8, –54.0, –112.2, –152.9 and –170.6 ppm. The spectrum remains unchanged on standing for several weeks, ruling out the presence of an interconversion process between the two species. Due to extensive overlap of the resonances and the presence of other phosphorus containing products in the baseline

(conceivably minor isomers of **13**) it did not prove possible to satisfactorily simulate the spectrum to obtain the coupling constants.

It is conceivable that the observed spectrum is simply an average spectrum caused by the presence of four interconverting isomers in solution. Isomers A and B (Figure 3.12) are both formed by protonation of **5** at the P2 position, while C and D are formed by protonation at P4. A pyramidal inversion process at P2 interconverts A and B, while the same inversion at P4 relates C and D (Figure 3.14). Such processes have previously been observed in related substituted heptaphosphide anion complexes of transition metals.[11,44,45] In these cases, however, the fluxionality can be frozen out on the NMR timescale by cooling. Variable temperature NMR studies on **13** show no change to the spectrum on cooling, suggesting that if there is a pyramidal inversion process operating to interconvert the isomer pairs A/B and C/D then it has an extremely low energy barrier and is correspondingly very rapid on the NMR timescale.

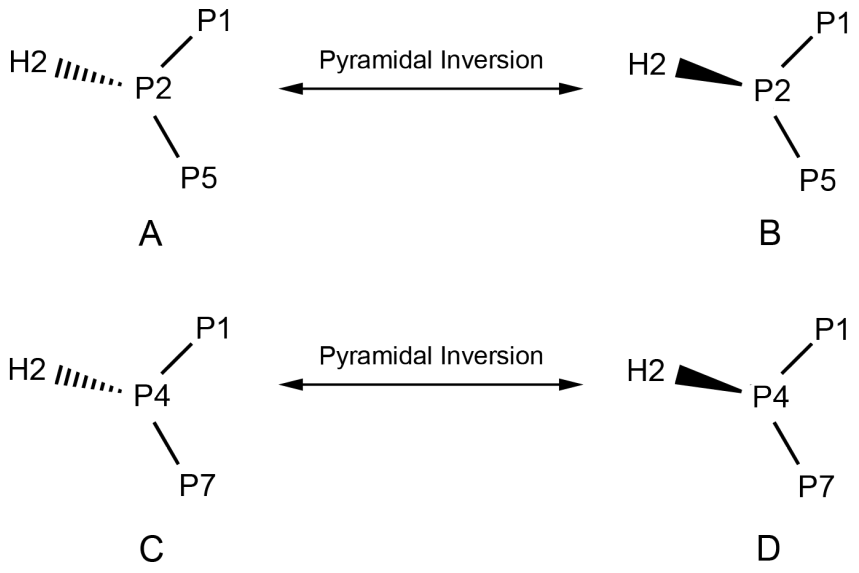

Figure 3.14: The potential pyramidal inversion process in **13** that would lead to two sets of isomer pairs. Rapid interconversion on the NMR timescale would lead to the observation of a set of resonances for A/B and C/D.

It is impossible to definitively assign the isomers of **13** that are present in solution, indeed the ^{31}P NMR spectrum suggests that there may be additional minor isomers, however a simplistic interpretation suggests that A and B are likely to be lowest in energy. Both still have the correct spatial arrangement to allow a potential favourable phosphide–H1 interaction (missing in C and D), and minimize (albeit small) steric clashes between the amidine substituent and the cage proton (particularly in D). This is corroborated by a computational analysis (*vide infra*).

The ^{1}H{^{31}P} NMR spectrum shows two broad resonances at 6.57 and 6.27 ppm which are assigned to the amidine protons of the two isomers. The PH proton resonates as a singlet at 0.92 ppm, and the three resonances integrate in the approximate ratio 1:1:2, suggesting that the PH protons of the two isomers are coincident. The doublet structure of the PH resonance that can be seen in the ^{31}P coupled ^{1}H NMR spectrum overlaps with the methyl resonances of the Dipp groups. A 1D ^{1}H–^{31}P HMQC experiment was performed, so that only resonances arising from protons that couple to a ^{31}P nucleus were observed (Figure 3.15). Both ^{31}P coupled and broadband decoupled experiments were run. Optimizing the ^{31}P coupled experiment for different coupling constants shows that there are two coincident doublet resonances with distinctive $^{1}J_{H–P}$ coupling constants. One has $^{1}J_{H–P}$ = 117 Hz, and the other $^{1}J_{H–P}$ = 254 Hz. The observation of sixteen resonances corresponding to the diastereotopic methyl groups of the Dipp group supports the presence of two major isomers of **13** in solution. The ^{13}C{^{1}H} NMR spectrum is also consistent with this interpretation.

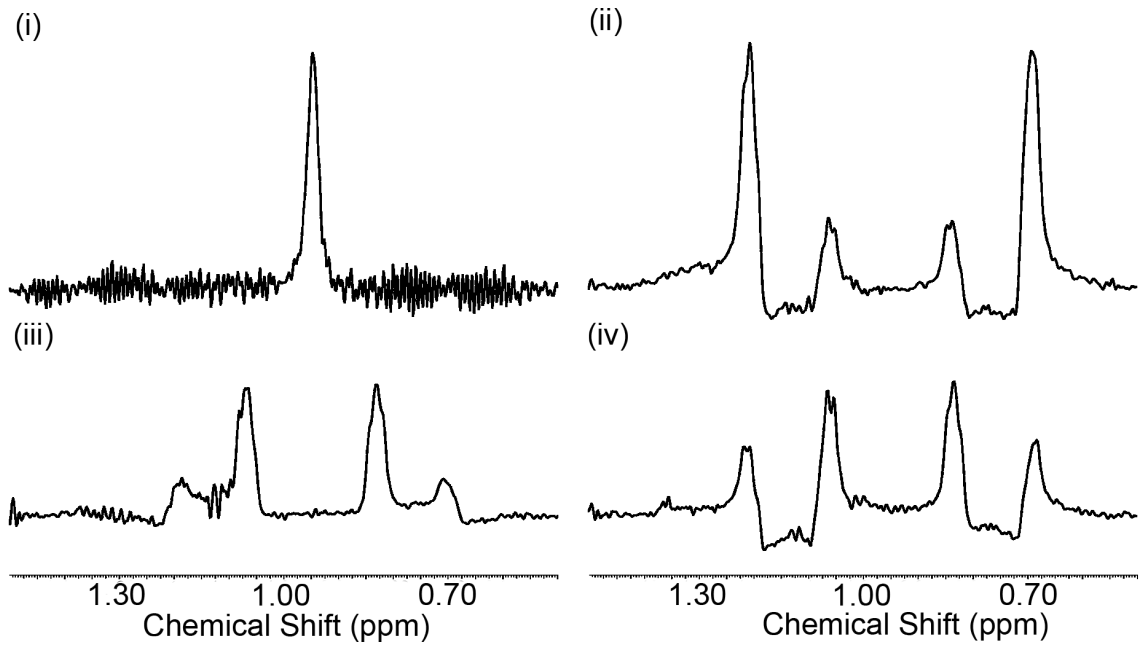

Figure 3.15 1D $^{1}H-^{31}P$ HMQC NMR spectra of [K(2,2,2-crypt)][**13**] (^{1}H observed) showing the results of broadband $\{^{31}P\}$ decoupling (i), optimizing the experiment for a $^{1}J_{H-P}$ value of 250 Hz (ii), optimizing the experiment for a $^{1}J_{H-P}$ value of 116 Hz (iii), optimizing the experiment for a $^{1}J_{H-P}$ value of 180 Hz (iv).

3.5.3 Computational Studies on 13

Calculations at the DFT level of theory were performed on the four possible isomers of **13** (A–D in Figure 3.11). Selected bond lengths and angles for the isomers are given in Table 3.9. In general, these agree very well with the experimentally observed and expected geometries.

Analysis of the total bonding energies for each isomer shows that A and B are lower in energy than C and D. The absolute difference in energy between highest and lowest is only approximately 25 kJ mol^{-1} however, which is insufficient to definitively state which of the isomers have been formed in the course of the reaction. In all cases the HOMO resembles a lone pair orbital on the remaining phosphide vertex (P2 or P4), as expected.

Table 3.9: Selected data for the optimized computed geometries of the four possible isomers of **13**. Atom numbering in brackets refers to isomers C and D.

Bond length (Å)	$\mathbf{13A_{calc}}$	$\mathbf{13B_{calc}}$	$\mathbf{13C_{calc}}$	$\mathbf{13D_{calc}}$
P1–P2	2.250	2.225	2.176	2.183
P1–P3	2.265	2.267	2.242	2.253
P1–P4	2.178	2.185	2.255	2.265
P2–P5	2.258	2.262	2.200	2.219
P3–P6	2.248	2.232	2.258	2.227
P4–P7	2.181	2.197	2.217	2.228
P5–P6	2.268	2.264	2.276	2.265
P5–P7	2.278	2.274	2.283	2.281
P6–P7	2.277	2.274	2.267	2.284
P3–C1	1.917	1.926	1.931	1.926
C1–N1	1.366	1.366	1.370	1.376
C1–N2	1.292	1.291	1.291	1.289
N1–H1	1.035	1.037	1.024	1.020
H2–P2(P4)	1.438	1.443	1.436	1.441
Bond angle (°)				
P1–P3–P6	100.6	101.2	101.9	102.3
P1–P3–C1	105.4	105.1	111.0	110.2
C1–P3–P6	100.4	99.8	103.0	101.4
P1–P2(P4)–P5(P7)	101.1	102.1	102.9	102.9
P1–P2(P4)–H2	95.6	98.1	97.6	101.4
H2–P2(P4)–P5(P7)	94.1	96.2	98.6	96.4
Total bonding energy (kJ mol^{-1})	–39,315.07	–39,311.43	–39,294.11	–39,289.58

3.5.4 Mass Spectrometric Studies

Electrospray mass spectrometry in the negative and positive ion modes was performed on DMF solutions of [K(2,2,2-crypt)][**13**]. The negative ion mode mass spectrum shows a peak for the molecular ion at an *m/z* value of 581.3, and the positive ion mode shows a mass envelope for the cation-paired species $\{[K(2,2,2\text{-crypt})]_2[HP_7C(NHDipp)(NDipp)]\}^+$ at 1414.0, confirming the charge on the anion in solution.

3.6 Further Hydrophosphination

The presence of both phosphane and phosphide vertices on **13** hinted at the possibility of further functionalization. Solutions of [K(2,2,2-crypt)][**13**] prepared in situ were reacted

with an additional equivalent of a carbodiimide RN=C=NR (R = Dipp, Cy, ^{i}Pr). After workup to remove the [K(2,2,2-crypt)][BAr$^{F}_{4}$] byproduct in the same manner as for **13**, the [K(2,2,2-crypt)]$^{+}$ salts of the [P_7{C(NHDipp)(NDipp)}{C(NHR)(NR)}]$^{-}$ (R = Dipp (**14**), Cy (**15**), ^{i}Pr (**16**)) anions could be isolated in good yields (Scheme 3.6). The reactions proceed cleanly to form exclusively **14–16** at room temperature over approximately 24 hours. The increased reaction time presumably results from a combination of the increased steric bulk and decreased nucleophilicity of the remaining phosphide vertex.

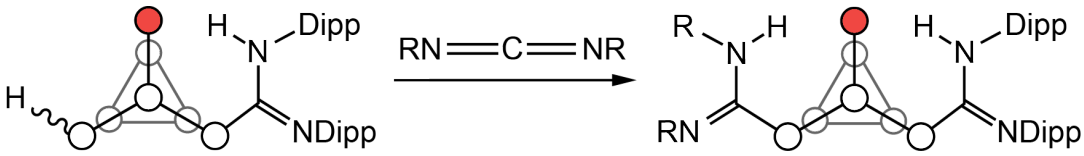

Scheme 3.9: Synthesis of **14–16** (R = Dipp (**14**), Cy (**15**), ^{i}Pr (**16**)).

This allows for the stepwise and controlled synthesis of a family of both symmetrically (**14**) and unsymmetrically (**15**, **16**) disubstituted heptaphosphide anions, something that has previously not been possible. One could envisage making a mixed amidine-amide substituted cage, but this was not realized experimentally.

3.6.1 Structures of 14–16

Crystals of the [K(2,2,2-crypt)]$^{+}$ salts of **14–16** suitable for analysis by single crystal X-ray diffraction could be grown by diffusion of hexane into a THF solution of the products at 5 °C. The crystal structures obtained confirm the formulation of the anions as bis(amidine)functionalized monoanions.

The reaction to form **14–16** is stereospecific and only one of the four possible isomers is observed by single crystal X-ray diffraction, corresponding to A in Figure 3.12 (in the case of the symmetrically substituted cage, **14**, B and C are the same resulting in three possible

isomers). The large steric bulk of the amidine functionalities apparently precludes the formation of the other possible isomers, and indicates that the reaction proceeds under thermodynamic control. In the case of **14**, only one stereosisomer is possible because the cage is symmetrically substituted. The two functionalized vertices P3 and P4 are both chiral and have *R*- and *S*-configurations, respectively, according to the Cahn-Ingold-Prelog priority rules.[46] The unsymmetrically substituted cages **15** and **16** are formed as a racemic mixture of enantiomers, where again one of P3 and P4 has an *R*-configuration while the other has an *S*-configuration.

The bond metric data for the P–P bonds of the heptaphosphide cage are unremarkable, and comparable to that observed for related bisfunctionalized clusters (Table 3.8).[11,12] They lie in the range 2.139(3)–2.228(3) Å, 2.126(2)–2.252(2) Å and 2.115(2)–2.225(3) Å for **14**, **15** and **16**, respectively. Of note is that the bonds involving the unsubstituted phosphide vertex P2 are significantly shorter than the equivalent bonds involving P3 and P4. For example in **14**, the P1–P2 bond distance is 2.145(2) Å compared to the P1–P3 and P1–P4 bond distances of 2.217(2) and 2.225(2) Å, respectively. This was remarked upon previously and can be attributed to an increased ionic component to the bonding. This trend is observed for both **15** and **16**, although the presence of cage disorder in the crystal structure of **15** means that bond metric data should be interpreted with caution.

Differences in the lengths of the *exo*-bonds to the substituents (P3–C1 and P4–C26) are not statistically significant and should be regarded as identical within experimental error. The observed distances are very similar to those observed for the mono-functionalized anions **5**–**7** and **13**. Analysis of the bond metric data allows the differentiation of single and double bonds within the amidine moiety in all cases. Bond angles around the central carbon atoms sum up to approximately 360°, and the amidine cores P3–C1–N1–N2 are virtually planar.

No evidence of amidine tautomerism was observed, and the nitrogen atom substituents have an E_{syn} configuration. Interestingly, the amidine NH (which was positioned geometrically in **14**–**16**) is directed towards the formally negatively charged P2 vertex of the cage, hinting at an interaction.

Table 3.8: Comparison of bond lengths (Å) and angles (°) for **14**–**16**. Data for **15A** and **15B** are for the major (65% occupancy) and minor (35% occupancy) disordered components of the cluster anion, respectively.

Bond Distance	**14**	**15A**	**15B**	**16**
P1–P2	2.145(2)	2.150(2)	2.123(4)	2.139(2)
P1–P3	2.217(2)	2.230(3)	2.210(6)	2.200(1)
P1–P4	2.225(2)	2.252(2)	2.252(4)	2.213(2)
P2–P5	2.139(3)	2.140(2)	2.126(3)	2.115(2)
P3–P6	2.201(2)	2.193(4)	2.176(8)	2.199(2)
P4–P7	2.190(2)	2.198(1)	2.211(2)	2.171(3)
P5–P6	2.223(3)	2.236(3)	2.188(6)	2.222(2)
P5–P7	2.228(3)	2.231(1)	2.224(3)	2.225(3)
P6–P7	2.230(2)	2.189(3)	2.165(7)	2.208(2)
P3–C1	1.879(5)	1.873(3)	1.892(5)	1.874(3)
C1–N1	1.354(5)	1.361(2)		1.363(4)
C1–N2	1.292(6)	1.281(2)		1.277(5)
N1–R	1.425(8)	1.435(2)		1.428(5)
N2–R	1.414(6)	1.418(2)		1.398(4)
P4–C26	1.892(5)	1.893(2)	1.876(5)	1.893(6)
C26–N3	1.342(6)	1.365(3)	1.368(6)	1.412(8)
C26–N4	1.280(7)	1.277(3)	1.278(6)	1.281(9)
N3–R	1.437(7)	1.467(3)	1.468(6)	1.480(8)
N4–R	1.417(7)	1.459(3)	1.456(6)	1.455(13)
Bond Angle				
C1–P3–P1	105.1(2)	105.0(1)	98.2(3)	106.5(1)
P1–P3–P6	101.1(1)	100.3(1)	101.0(3)	100.6(1)
P6–P3–C1	98.6(2)	99.5(2)	101.8(3)	98.1(1)
N1–C1–P3	119.0(4)	116.2(1)	117.2(2)	116.7(2)
N1–C1–N2	119.3(4)	120.6(1)		121.2(3)
N2–C1–P3	121.7(3)	123.1(1)	122.1(2)	122.1(2)
C26–P4–P1	103.9(2)	108.6(1)	105.2(2)	101.6(2)
P1–P4–P7	101.2(1)	101.3(1)	100.6(1)	102.3(1)
P7–P4–C26	99.4(2)	95.3(1)	100.6(2)	103.1(2)
N3–C26–P4	116.0(4)	115.7(2)	114.6(3)	113.1(4)
N3–C26–N4	121.5(4)	121.2(2)	120.6(4)	121.7(7)
N4–C26–P4	122.5(3)	123.5(2)	124.4(4)	125.0(6)
Sum of angles at C1	360.0	359.9	359.9	360.0
Sum of angles at C26	360.0	360.4	359.6	359.8

The anion **14** was crystallographically characterized in [K(2,2,2-crypt)][**14**]·THF (Figure 3.16). There is a single anion in the asymmetric unit accompanied by a $[K(2,2,2\text{-crypt})]^+$ cation and a THF molecule. The cryptand complex displays some rotational disorder. The anion is effectively C_s symmetric due to a virtual mirror plane relating the two halves of the molecule.

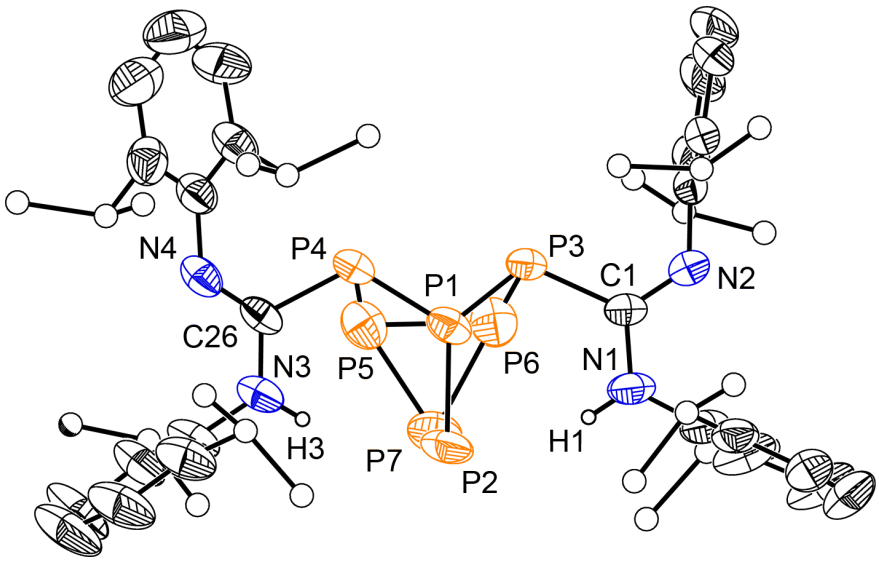

Figure 3.16: Thermal ellipsoid plot of **14**. Thermal ellipsoids are shown at the 50% probability level. Isopropyl groups are shown as spheres of arbitrary radius and all hydrogen atoms have been omitted for clarity with the exception of the amidine protons.

The structure of the difunctionalized cage **15** was determined in [K(2,2,2-crypt)][**15**]·0.65THF·0.35hexane (Figure 3.17). The single $[K(2,2,2\text{-crypt})]^+$ cation is accompanied by a cluster anion, which displays "up-down" disorder of the nortricyclane-like core. This could be modelled as two components, with the major component having 65% occupancy. Despite the high quality of the diffraction data collected, this has an effect on the accuracy of the bond metric data described above. The bis(Dipp) amidine functionality of both components share the same atomic positions, similar to **13**. In one orientation of the rest of the anion it is accompanied by a THF molecule, whereas in the

other it is accompanied by a hexane molecule. The solvent molecule is located at the site of a cyclohexyl group in the other component of the disorder.

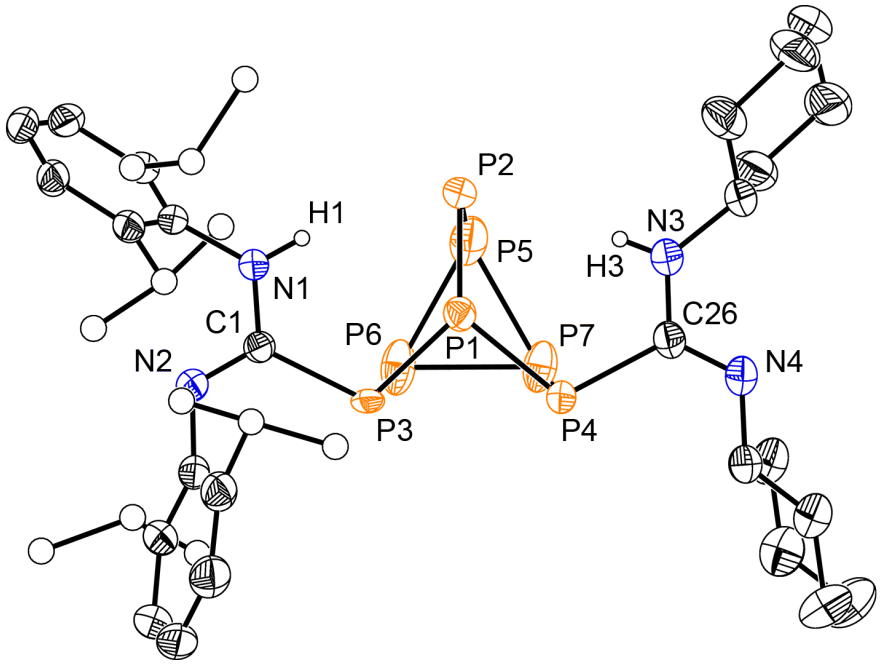

Figure 3.17: Thermal ellipsoid plot of **15**. Thermal ellipsoids are shown at the 50% probability level. Isopropyl groups are shown as spheres of arbitrary radius and all hydrogen atoms have been omitted for clarity with the exception of the amidine protons. Only the major component (65%) of the disorder is shown.

The structure of **16** is very similar to that of **14** and **15**. The compound [K(2,2,2-crypt)][**16**]·hexane crystallizes in the chiral space group $P2_12_12_1$. The asymmetric unit contains a single crystallographically unique anion, which initially hints at the possibility of an enantiopure crystal (Figure 3.18). On refinement it becomes apparent that the structure is inversion twinned, with a batch scale factor of 0.501 making it effectively a racemic mixture of the two enantiomers. The bis(isopropyl) amidine moiety displays rotational disorder which was modelled as two components in a 78:22 ratio.

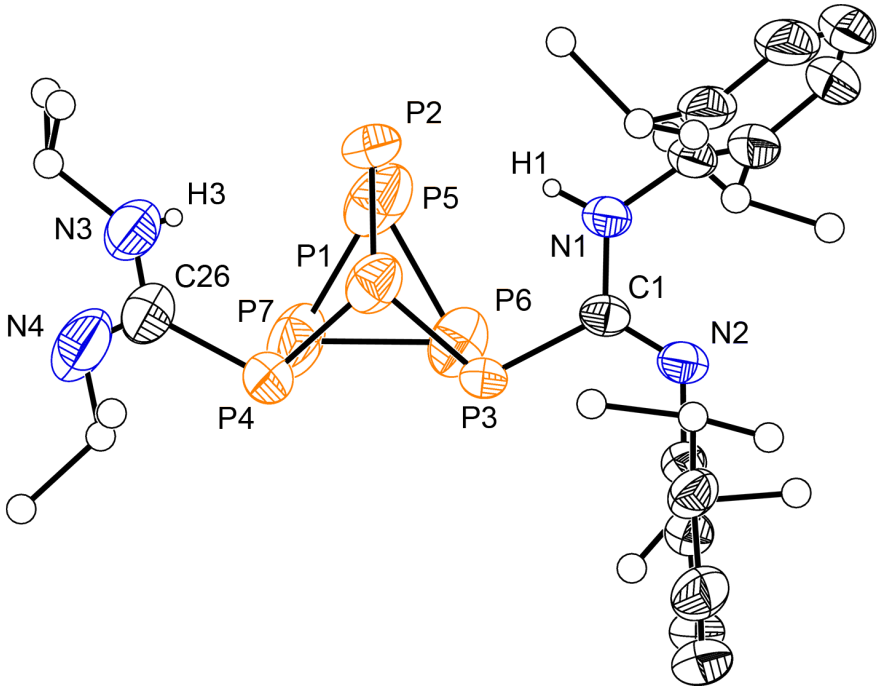

Figure 3.18: Thermal ellipsoid plot of **16**. Thermal ellipsoids are shown at the 50% probability level. Isopropyl groups are shown as spheres of arbitrary radius and all hydrogen atoms have been omitted for clarity with the exception of the amidine protons. Only the major component (78%) of the disorder is shown.

3.6.2 NMR Spectroscopic Studies on 14–16

The ^{31}P NMR spectrum of **14** reveals five multiplet resonances in the intensity ratio 2:1:1:1:2 (Figure 3.19 and Table 3.9). This suggests that the C_s symmetry of the heptaphosphide cage is retained in solution, since P3/P4 and P6/P7 are chemically equivalent. There is no evidence for the presence of any other phosphorus containing species, and as such the formation of other isomers during the hydrophosphination reaction can be conclusively disqualified. The spectrum was assigned with the assistance of a ^{31}P–^{31}P COSY experiment and the 1D ^{31}P spectrum simulated to extract the coupling constants (Appendix A).

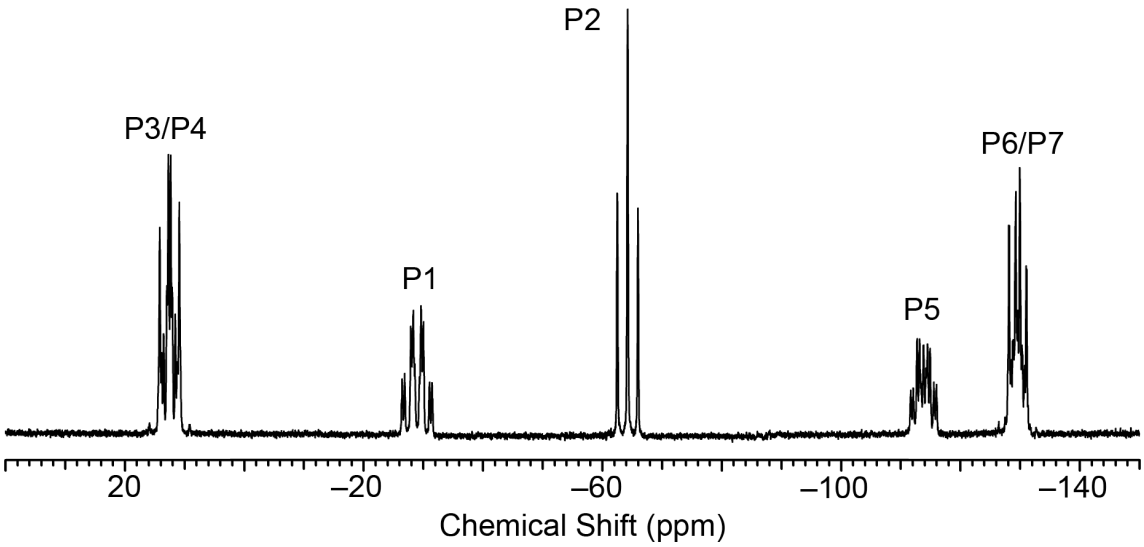

Figure 3.19: ^{31}P NMR spectrum of a d_5-pyridine solution of [K(2,2,2-crypt)][**14**]. Atom numbering is the same as that used in the crystal structure.

The ^{31}P NMR spectra of **15** and **16** superficially appear very similar to that obtained for **14**. Five apparent multiplet resonances are observed in the intensity ratio 2:1:1:1:2. On attempting to simulate the spectrum it becomes clear that the resonances for the substituted resonances P3 and P4 overlap extensively. The optimal model is obtained when the chemical shifts are allowed to freely refine and separate by around 3 ppm. This is also the case for P6 and P7, although the chemical shift difference is even smaller. It is not possible to discern which shift corresponds to the bis(Dipp) amidine substituted vertex, and which to the bis(alkyl) amidine substituted vertex. Based on chemical shift arguments, and by reference to the anions **5**–**7**, the more downfield shifted resonance was assigned to the bis(Dipp) amidine substituted vertex, P3. These observations are consistent with literature reports of disubstituted heptaphosphide anions.[10,11]

The ^{1}H NMR spectra of **14**–**16** are consistent with formation of a bis(amidine) functionalized cage. Only one amidine NH resonance is observed for **14** at 6.31 ppm due to the symmetry of the cage substitution. The NH of the bis(cyclohexyl)amidine in **15** was not

observed, likely because it overlaps with an intense 2,2,2-crypt resonance. The chemical shifts are in good agreement with those recorded for **5**–**7**.

Table 3.9: ^{31}P and ^{1}H chemical shifts for **14**–**16**.

Nucleus	14	15	16
P1	–29.0	–33.6	–34.1
P2	–64.2	–69.6	–69.6
P3	12.5	7.3	6.5
P4	12.5	4.9	3.2
P5	–113.8	–112.7	–112.2
P6	–129.5	–135.8	–134
P7	–129.5	–136.5	–136.3
H1	6.31	6.2	6.22
H3	6.31	Not observed	3.87

Owing to the high molecular weight and small quantities of the compounds synthesized, it was unfortunately not possible to observe the C1/C26 resonances in the ^{13}C{^{1}H} NMR spectrum, even using a spectrometer equipped with a highly sensitive dedicated ^{13}C cryoprobe. The ^{13}C{^{1}H} NMR spectra of **14**–**16** do, however, support their formulation as bis(amidine) functionalized cages as described above.

3.6.3 Computational Studies on 14–16

The geometries of **14**–**16** were optimized at the DFT level of theory. The calculated structures show an excellent agreement with those determined experimentally. As seen previously, computed bond lengths were elongated by approximately 0.05 Å compared to the experimental bond lengths (Table 3.12). The HOMO of the anions is mainly compromised of lone pair character on the phosphide (P2) vertices as would be expected.

Table 3.12: Tabulated bond metric data for the calculated structures of **14**–**16**.

Bond length (Å)	**14_{calc}**	**15_{calc}**	**16_{calc}**
P1–P2	2.183	2.178	2.180
P1–P3	2.264	2.265	2.266
P1–P4	2.261	2.258	2.252
P2–P5	2.183	2.181	2.180
P3–P6	2.250	2.248	2.248
P4–P7	2.256	2.248	2.248
P5–P6	2.272	2.277	2.276
P5–P7	2.271	2.275	2.276
P6–P7	2.267	2.262	2.267
P3–C1	1.918	1.919	1.919
C1–N1	1.368	1.369	1.368
C1–N2	1.290	1.291	1.292
N1–H1	1.034	1.035	1.036
P4–C26	1.92	1.924	1.924
C26–N3	1.367	1.380	1.376
C26–N4	1.292	1.288	1.289
N3–H3	1.035	1.030	1.029
Bond Angle (°)			
N1–C1–P3	116.5	116.4	116.4
N1–C1–N2	121.8	121.9	122.0
N2–C1–P3	121.7	121.6	121.5
N3–C26–P4	116.7	115.2	115.5
N3–C26–N4	121.8	121.7	121.6
N4–C26–P4	121.5	122.9	122.7

3.6.4 Mass Spectrometric Studies

Electrospray ionization mass spectrometry was performed on DMF solutions of the $[K(2,2,2\text{-crypt})]^+$ salts of **14**–**16**. The negative ion mode reveals mass envelopes at *m/z* ratios of 943.8, 788.4 and 707.4 corresponding to the molecular ions of **14**, **15** and **16**, respectively. The positive ion mode shows peaks at 1776.3, 1617.4 and 1538.1 Da, which result from the cation-paired species $\{[K(2,2,2\text{-crypt})]_2[\mathbf{14}]\}^+$, $\{[K(2,2,2\text{-crypt})]_2[\mathbf{15}]\}^+$ and $\{[K(2,2,2\text{-crypt})]_2[\mathbf{16}]\}^+$, respectively. This is further evidence for the composition and charge of the anions in solution.

3.7 FURTHER CHEMISTRY

Attempts were made to protonate or methylate **14** with Brookhart's acid and methyl iodide, respectively, to form neutral, trisubstituted cages. In both cases this resulted in the formation of an intractable mixture of products by ^{31}P NMR spectroscopy, and the reactions were not pursued further.

The isolobal analogy, which inspired the reactivity with carbodiimides and isocyanates, can be extended for carbon dioxide to give ketenes $R_2C{=}C{=}O$ and the parent allenes $R_2C{=}C{=}CR_2$. Preliminary reactivity studies show that both **1** and **3** react with ketenes and allenes, albeit only via a decomposition/cluster oxidation pathway.

3.8 CONCLUSION

This chapter has described the synthesis and characterization of twelve novel compounds of group 15 Zintl anions. A new method for the controlled synthesis of substituted clusters via a hydropnictination reaction of heteroallenes has been discovered and exploited to form a family of related heptapnictide clusters.

The reactivity of the heptaphosphide clusters $[P_7]^{3-}$ (**3**) and $[HP_7]^{2-}$ (**1**) towards carbon dioxide was investigated. Owing to the instability of the product of CO_2 addition to **3**, $[P_7{-}CO_2]^{2-}$ (**4**), it was only possible to observe **4** by ^{31}P NMR spectroscopy before cluster oxidation occurred.

The reaction of $[HE_7]^{2-}$ with carbodiimides or isocyanates as model compounds for carbon dioxide was explored. This resulted in the formation of a related family of monosubstituted anions $[E_7C(NHR)(NR)]^{2-}$ (E = P, R = Dipp (**5**), Cy (**6**), ^{i}Pr (**7**); E = As, R = Dipp (**9**), Cy (**10**), ^{i}Pr (**11**)) and $[E_7C(NHR)(O)]^{2-}$ (E = P, R = Ad (**8**); E = As, R = Ad (**12**)). These were

characterized by a combination of single crystal X-ray diffraction, multielement NMR spectroscopy and electrospray ionization mass spectrometry.

Protonation of the dianions **5**–**8** was attempted. While **6**–**8** showed cluster oxidation to $[P_{16}]^{2-}$ with elimination of the organic fragment, protonation of **5** was successful to form $[HP_7\{C(NHDipp)(NDipp)\}]^-$ (**13**). This was characterized by single crystal X-ray diffraction, multielement NMR spectroscopy and mass spectrometry. DFT calculations were performed to probe the inherent isomerism of the anion and suggest the likely isomers present.

Reaction of **13** with carbodiimides RN=C=NR (R = Dipp, Cy, ^{i}Pr) resulted in the formation of a series of disubstituted monoanionic cages $[P_7\{C(NHDipp)(NDipp)\}\{C(NHR)(NR)\}]^-$ (R = Dipp (**14**), Cy (**15**), ^{i}Pr (**16**)). These anions have been characterized by single crystal X-ray diffraction, multielement NMR spectroscopy and mass spectrometry.

Further protonation and methylation of **14** was attempted with no success.

3.9 REFERENCES

(1) Scharfe, S.; Kraus, F.; Stegmaier, S.; Schier, A.; Fässler, T. F. *Angew. Chem., Int. Ed.* **2011**, *50*, 3630–3670.

(2) Baudler, M.; Faber, W.; Hahn, J. *Z. Anorg. Allg. Chem.* **1980**, *469*, 15–21.

(3) Milyukov, V. A.; Kataev, A. V.; Hey-Hawkins, E.; Sinyashin, O. G. *Russ. Chem. Bull.* **2007**, *56*, 298–303.

(4) Fritz, G.; Schneider, H.-W. *Z. Anorg. Allg. Chem.* **1990**, *584*, 12–20.

(5) Fritz, G.; Hoppe, K. D.; Hönle, W.; Weber, D.; Mujica, C.; Manriquez, V.; von Schnering, H. G. *J. Organomet. Chem.* **1983**, *249*, 63–80.

(6) Von Schnering, H. G.; Fenske, D.; Hönle, W.; Binnewies, M.; Peters, K. *Angew. Chem. Int. Ed. Engl.* **1979**, *18*, 679–679.

(7) Fritz, G.; Layher, E.; Goesmann, H.; Hanke, D.; Persau, C. *Z. Anorg. Allg. Chem.* **1991**, *594*, 36–46.

(8) Ahlrichs, R.; Fenske, D.; Fromm, K.; Krautscheid, H.; Krautscheid, U.; Treutler, O. *Chem. Eur. J.* **1996**, *2*, 238–244.

(9) Fritz, G.; Harer, J.; Matern, E. *Z. Anorg. Allg. Chem.* **1983**, *504*, 38–46.

(10) Fritz, G.; Rothmann, H.; Matern, E. *Z. Anorg. Allg. Chem.* **1992**, *610*, 33–45.

(11) Charles, S.; Fettinger, J. C.; Eichhron, B. W. *J. Am. Chem. Soc.* **1995**, *117*, 5303–5311.

(12) Mattamana, S. P.; Promprai, K.; Fettinger, J. C.; Eichhorn, B. W. *Inorg. Chem.* **1998**, *37*, 6222–6228.

(13) Noblet, P.; Cappello, V.; Tekautz, G.; Baumgartner, J.; Hassler, K. *Eur. J. Inorg. Chem.* **2011**, *2011*, 101–109.

(14) Baudler, M.; Heumüller, R.; Langerbeins, K. *Z. Anorg. Allg. Chem.* **1984**, *514*, 7–17.

(15) In *IUPAC Compendium of Chemical Terminology*; Nič, M.; Jirát, J.; Košata, B.; Jenkins, A.; McNaught, A., Eds.; Blackwell Scientific Publications: Oxford, 1997.

(16) *Organic Chemistry*; 1st ed.; Oxford University Press: Oxford, 2001.

(17) Smith, M. *March's Advanced Organic Chemistry: Reactions, Mechanisms, and Structure*; 7th Edition.; Wiley: Hoboken, 2013.

(18) Turbervill, R. S. P.; Goicoechea, J. M. *Chem. Commun.* **2012**, *48*, 1470–1472.

(19) Turbervill, R. S. P.; Goicoechea, J. M. *Eur. J. Inorg. Chem.* **2014**, *2014*, 1660–1668.

(20) Turbervill, R. S. P.; Goicoechea, J. M. *Organometallics* **2012**, *31*, 2452–2462.

(21) Diemert, K.; Hahn, T.; Kuchen, W. *Phosphorus, Sulfur, and Silicon and the Related Elements* **1991**, *60*, 287–294.

(22) Buhro, W. E.; Chisholm, M. H.; Folting, K.; Huffman, J. C. *Inorg. Chem.* **1987**, *26*, 3087–3088.

(23) Mömming, C. M.; Otten, E.; Kehr, G.; Fröhlich, R.; Grimme, S.; Stephan, D. W.; Erker, G. *Angew. Chem., Int. Ed.* **2009**, *48*, 6643–6646.

(24) Baudler, M.; Heumüller, R.; Hahn, J. *Z. Anorg. Allg. Chem.* **1985**, *529*, 7–14.

(25) Baudler, M.; Düster, D.; Langerbeins, K.; Germeshausen, J. *Angew. Chem. Int. Ed. Engl.* **1984**, *23*, 317–318.

(26) Mansfield, N. E.; Grundy, J.; Coles, M. P.; Avent, A. G.; Hitchcock, P. B. *J. Am. Chem. Soc.* **2006**, *128*, 13879–13893.

(27) Mansfield, N. E.; Coles, M. P.; Avent, A. G.; Hitchcock, P. B. *Organometallics* **2006**, *25*, 2470–2474.

(28) Grundy, J.; Coles, M. P.; Hitchcock, P. B. *Dalton Trans.* **2003**, 2573–2577.

(29) Tzschach, A.; Schwarzer, R. *J. Organomet. Chem.* **1968**, *13*, 363–368.

(30) Tzschach, A.; Schwarzer, R. *Liebigs Ann.* **1967**, *709*, 248–256.

(31) Zhang, W.-X.; Nishiura, M.; Hou, Z. *Chem. Commun.* **2006**, 3812–3814.

(32) Crimmin, M. R.; Barrett, A. G. M.; Hill, M. S.; Hitchcock, P. B.; Procopiou, P. A. *Organometallics* **2008**, *27*, 497–499.

(33) Behrle, A. C.; Schmidt, J. A. R. *Organometallics* **2013**, *32*, 1141–1149.

(34) Sewald, N.; Jakubke, H.-D. In *Peptides: Chemistry and Biology*; Wiley-VCH: Weinheim, 2009; pp. 175–315.

(35) Kovacs, I.; Baum, G.; Fritz, G.; Fenske, D.; Wiberg, N.; Schuster, H.; Karaghiosoff, K. *Z. Anorg. Allg. Chem.* **1993**, *619*, 453–460.

(36) Coles, M. P.; Hitchcock, P. B. *Chem. Commun.* **2002**, 2794–2795.

(37) Jin, G.; Jones, C.; Junk, P. C.; Lippert, K.-A.; Rose, R. P.; Stasch, A. *New J. Chem.* **2009**, *33*, 64–75.

(38) Jin, G.; Jones, C.; Junk, P. C.; Stasch, A.; Woodul, W. D. *New J. Chem.* **2008**, *32*, 835–842.

(39) A survey of the Cambridge Structural Database (version 5.34, November 2012 update) for –C(O)NHR groups where the R functionality is acyclic yielded 9616 hits. Mean distances C=O: 1.230 Å (variance: 0.000, SD: 0.021); C−N: 1.340 Å (variance: 0.001, SD: 0.026); N−R: 1.451 Å (variance: 0.001, SD: 0.029).

(40) Boeré, R. T.; Klassen, V.; Wolmershäuser, G. *J. Chem. Soc., Dalton Trans.* **1998**, 4147–4154.

(41) Häfelinger, G.; Kuske, F. K. H. In *The Chemistry of Amidines and Imidates*; Patai, S.; Rappoport, Z., Eds.; The Chemistry of Functional Groups; Wiley: Chichester, 1991; Vol. 2.

(42) Kühl, O. *Phosphorus-31 NMR Spectroscopy: A Concise Introduction for the Synthetic Organic and Organometallic Chemist*; Springer: Berlin, 2008.

(43) Brookhart, M.; Grant, B.; Volpe, A. F. *Organometallics* **1992**, *11*, 3920–3922.

(44) Kesanli, B.; Mattamana, S. P.; Danis, J.; Eichhorn, B. *Inorg. Chim. Acta.* **2005**, *358*, 3145–3151.

(45) Charles, S.; Danis, J. A.; Fettinger, J. C.; Eichhorn, B. W. *Inorg. Chem.* **1997**, *36*, 3772–3778.

(46) Cahn, R. S.; Ingold, C.; Prelog, V. *Angew. Chem. Int. Ed. Engl.* **1966**, *5*, 385–415.

CHAPTER FOUR

Synthesis and Coordination Chemistry of Literature 1,2,3-Tripnictolide Anions

4.1 INTRODUCTION

1,3,4-Triphospholide isomers have a well-established chemistry, and numerous good yielding preparations for their synthesis exist (provided that the corresponding phosphaalkyne is synthetically accessible).[1–4] The related 1,2,3-triphospholide isomers, in contrast, are much less well known. Only scattered examples exist throughout the literature as either free anions or in the coordination sphere of a transition metal, and to date no general method for their synthesis has been reported.

The first mention of their existence was in 1987, when Baudler and co-workers reported the ^{31}P NMR spectroscopic observation of $[1,2,3\text{-}P_3C_2H_2]^-$ (although it was initially misassigned as $[P_3CH_2]^-$) in the reaction between sodium and white phosphorus in diglyme.[5,6] Multiple other phosphorus containing products are formed during the reaction, including $[P_5]^-$, $[P_4CH]^-$, $[P_{16}]^{2-}$ and $[P_{21}]^{3-}$ (Scheme 4.1). Presumably the C_2H_2 unit arises from solvent decomposition under the highly reductive reaction conditions.

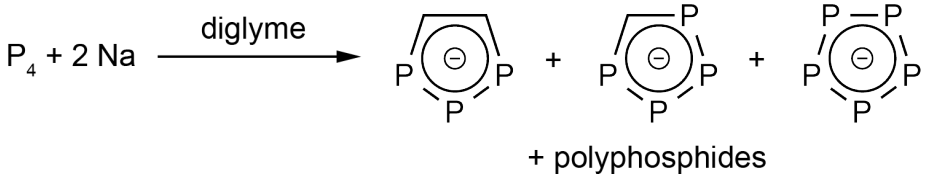

Scheme 4.1: The products observed by Baudler from the reaction of sodium and white phosphorus in diglyme.

A synthetic route was developed in 1994 by the group of Mathey (Scheme 4.2).[7] The overall yield is poor, purification laborious, and the reaction dependent on the carbon substituents. While they could isolate reasonable quantities of $[1,2,3\text{-}P_3C_2Ph_2]^-$, only small amounts of $[1,2,3\text{-}P_3C_2Ph^tBu]^-$ were detectable by ^{31}P NMR spectroscopy and the method fails completely when attempting to prepare $[1,2,3\text{-}P_3C_2PhEt]^-$.

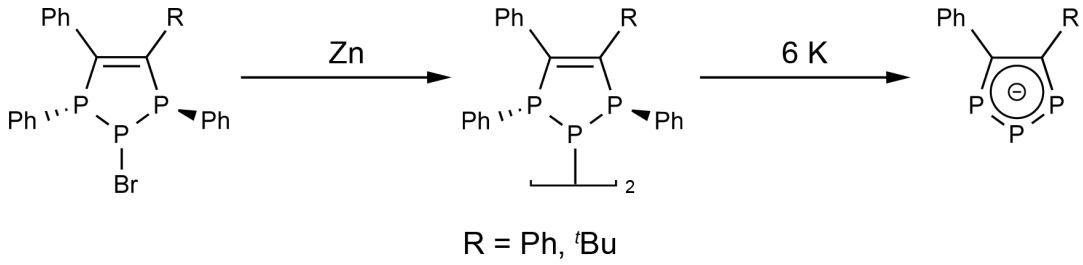

Scheme 4.2: Mathey's route to 1,2,3-triphospholide anions.

In 2008 two independent syntheses of the $[1,2,3\text{-}P_3C_6H_4]^-$ anion, a phosphorus containing analogue of the indenide anion, were reported.[8,9] Both syntheses started from the same synthon, 1,2-diphosphinobenzene, but used different synthetic methods. That of Russell and co-workers involves the deprotonation with ^{n}BuLi and subsequent reaction with PCl_3 to install the third phosphorus atom (Scheme 4.3). Use of $AsCl_3$ instead of PCl_3 gave the mixed 1,3-diphospha-2-arsa-indenide anion. During the reaction, a second, minor product could be crystallized and was found to have a P_8 skeleton reminiscent of that found in Hittorf's phosphorus. The authors tentatively suggest that it might arise from decomposition of the 1,2,3-triphospholide anion.

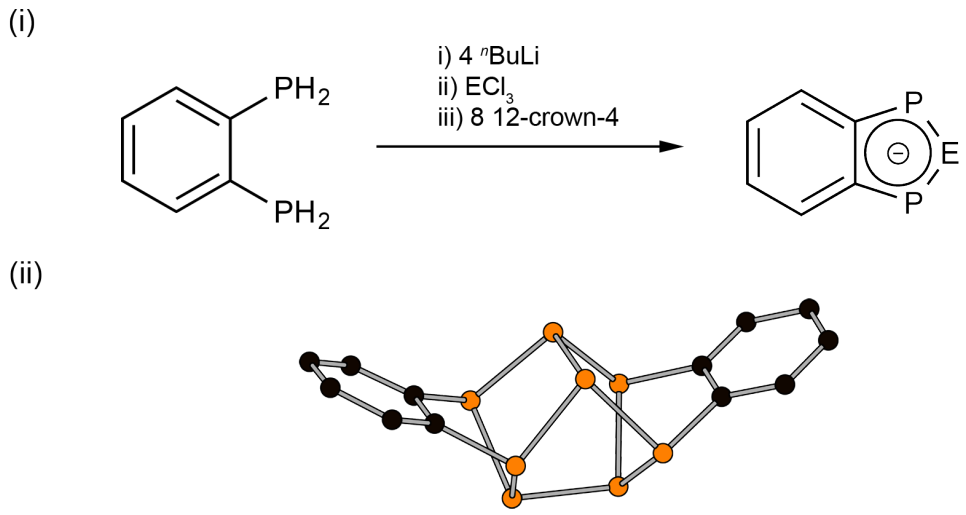

Scheme 4.3: The Russell synthesis (i) and a ball and stick representation of the minor product (ii). Hydrogen atoms have been omitted for clarity.

The second route, from the group of Wright, uses a mixed ^{n}BuLi/Sb(NMe$_2$)$_3$ base with 1,2,-diphosphinobenzene. Through a series of ^{31}P NMR and ESR spectroscopic investigations, and targeted synthesis of intermediates, they were able to propose a mechanism for the transformation (Scheme 4.4).[10]

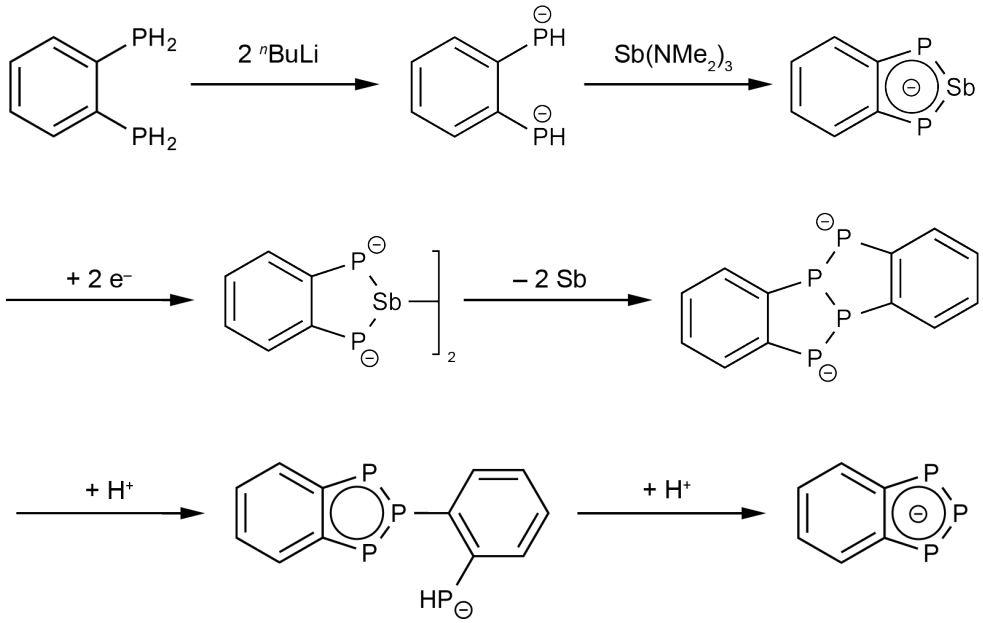

Scheme 4.4: The mechanism proposed by Wright and co-workers for the formation of [1,2,3-$P_3C_4H_6$]$^-$. Figure adapted from Edge et al.[10]

In both of these cases, the [Li(12-crown-4)$_2$]$^+$ salt of the anion was prepared and characterized. The ^{31}P NMR spectra shows multiplet resonances at 335.2 and 260.7 ppm, characteristic of an A_2B spin system with an extremely large $^1J_{P–P}$ value of 500 Hz. The P–P (2.093(av) and 2.090(av) Å) and P–C distances (1.778(av) and 1.775(av) Å) are intermediate between the respective double and single bonds, indicative of some degree of aromatic delocalization within the P_3C_2 ring system.

The only other examples of 1,2,3-triphospholides are coordinated to a transition metal centre, as triphosphaferrocenes. The reaction of phenyl- or diphenylacetylene with a transition metal phosphide derived from white phosphorus results in the formation of novel

triphosphaferrocenes in moderate yield (Scheme 4.5).[11,12] The secondary coordination of the phosphorus lone pairs in these compounds has also been investigated to give a series of coordination polymers and bimetallic systems.[12,13]

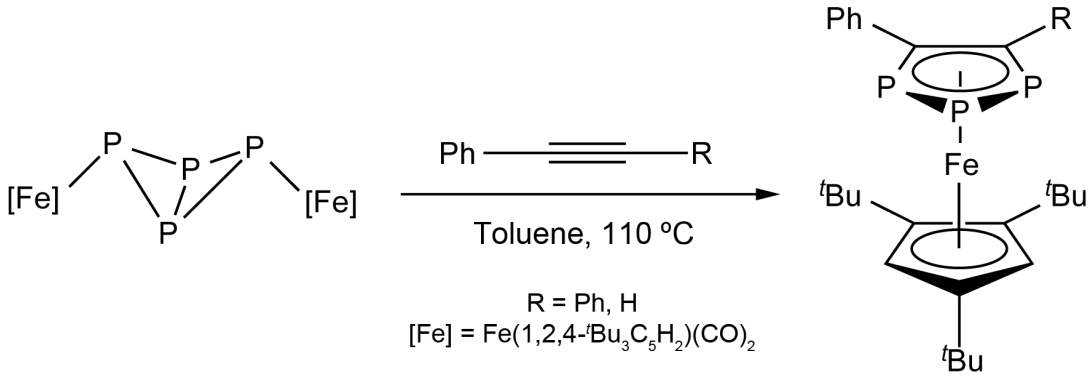

Scheme 4.5: Synthesis of 1,2,3-triphosphaferrocenes.

4.2 OBJECTIVES

When we initially started the work described in this chapter, we were looking to extend the hydrophosphination activity described in Chapter Three to other unsaturated substrates. This chapter will describe the reactivity of **1**, **2** and **3** towards acetylene, and then the extension to other substituted alkynes. A series of 1,2,3-tripnictolide anions could be obtained from these investigations.[14,15] All of the phosphorus anions reported have been previously observed, or in some cases isolated. The arsenic analogues reported are entirely novel compounds. Their syntheses and structures will be discussed, as will an initial study of their ligand properties towards diamagnetic ruthenium and molybdenum fragments.

4.3 REACTIVITY OF $[E_7]^{3-}$ TOWARDS ACETYLENE

Monitoring the addition of bis(trimethylsilyl)acetylene to a DMF solution of [K(2,2,2-crypt)]$_2$[**1**] by ^{31}P NMR spectroscopy revealed the disappearance of the resonances attributable to **1**, and appearance of resonances arising from the [1,2,3-$P_3C_2H_2$]$^-$ (**17**) anion.

The identity of **17** was confirmed by a single crystal X-ray diffraction experiment. Presumably the C–Si bonds in the starting material are reductively cleaved under the reaction conditions, with the protons originating from the solvent.

This reaction leading to the formation of **17** is both extremely low yielding and gives rise to many phosphorus-containing products. We reasoned that since the reaction involves the net linking of a P_3 unit and a C_2H_2 unit, a logical alkyne for the reaction would be acetylene, C_2H_2. Exposure of DMF solutions of **1** (as either the $[K(2,2,2\text{-crypt})]^+$ or $[K(18\text{-crown-6})]^+$ salt), or of K_3P_7 and three equivalents of 2,2,2-crypt or 18-crown-6, to acetylene results in a rapid darkening and thickening of the solution. Removal of solvent under reduced pressure, and repeated extraction of the dark residue with THF allowed the synthesis of **17** in approximately 20% yield as a pale yellow crystalline solid. The same methodology could also be used to produce the novel $[1,2,3\text{-}As_3C_2H_2]^-$ (**18**) anion from K_3As_7 in comparable yield as a green crystalline material (Scheme 4.6).

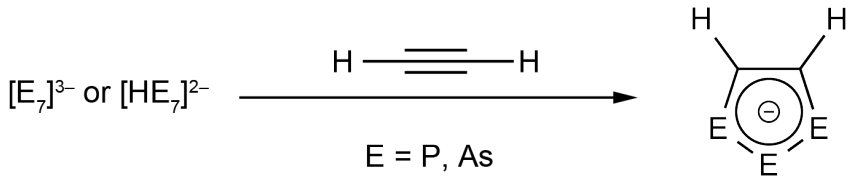

Scheme 4.6: Synthesis of $[1,2,3\text{-}E_3C_2H_2]^-$ anions from heptapnictide Zintl anions.

4.3.1 Structures of 17 and 18

Crystals suitable for analysis by single crystal X-ray diffraction of the $[K(2,2,2\text{-crypt})]^+$ and $[K(18\text{-crown-6})]^+$ salts of **17** and **18** could be grown by diffusion of hexane into a THF solution of the product. As might be expected for such similar anions, the structures are isostructural for a given cation, with only a small expansion of unit cell parameters for **18**. The $[K(18\text{-crown-6})]^+$ salts of **17** and **18** (which are also isostructural) display two distinct

anion environments, both of which are disordered so the structures will not be discussed. The $[K(2,2,2\text{-crypt})]^+$ salt of **17** is fully ordered, whereas the analogous structure of **18** shows rotational disorder of the anion. This makes a detailed comparison of the bond metric data inadvisable, although the composition and connectivity of the anion is unequivocal. The structures of the anions are shown in Figure 4.1.

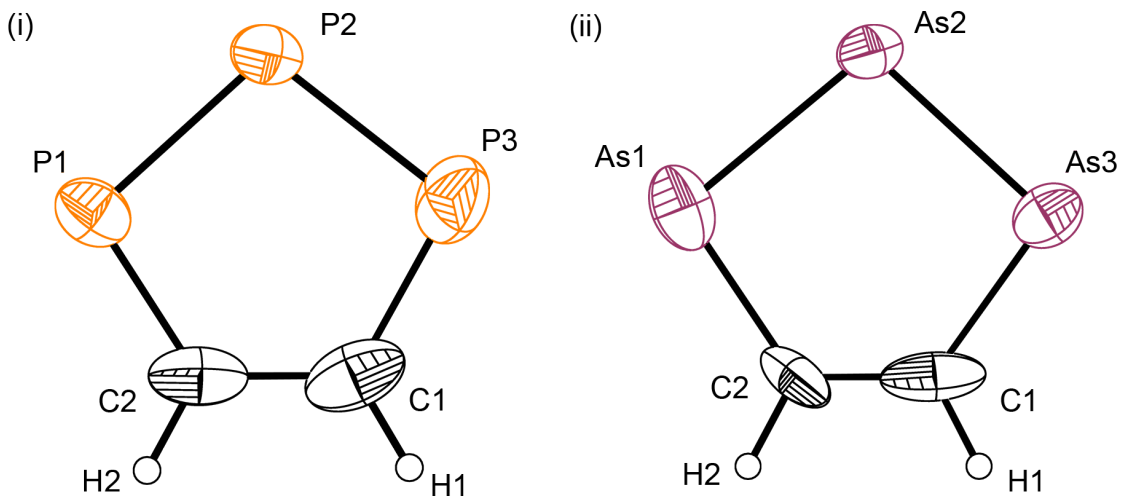

Figure 4.1: Thermal ellipsoid plots of **17** (i) and **18** (ii). Thermal ellipsoids are set at the 50% probability level. Hydrogen atoms are shown as spheres of arbitrary radius. Only the major component of the disordered anion in **18** is shown.

Bond metric data for both the experimentally observed and computed (at the DFT level of theory) geometries of **17** and **18** are shown in Table 4.1. In general, good agreement between the experimental and computed geometries is observed. A more detailed analysis of the computational results and electronic structure of **17** and **18** will be given in Section 4.3.3. The anions are essentially planar (deviation from planarity 0.002 and 0.012 Å, for **17** and **18**, respectively). The P–P and P–C bond distances are intermediate between single and double bonds in **17** (2.088(av) Å and 1.754(av) Å, respectively for **17**), and the C–C bond distance of 1.393(3) Å is characteristic of an aromatic bond. The carbon atoms are essentially sp^2 hybridized (angles of 119.21(15) and 122.56(16)º) while the angles at the P atoms are distinctly more acute (99.41(av)º). In all likelihood this is an effect of the longer

bonds involving the P atoms. These data are in excellent agreement with those reported previously.[8,9] A similar series of observations can made for **18**, although the inherent disorder of the anion makes a detailed analysis unwise.

Table 4.1: Bond metric data for **17** and **18**. Data shown for **18** correspond to the major component of the disordered anion.

Bond distance (Å)	**17_{exp}**	**18_{exp}**	**17_{calc}**	**18_{calc}**
E1–E2	2.081(1)	2.302(1)	2.128	2.346
E2–E3	2.094(1)	2.293(1)	2.128	2.345
E3–C1	1.781(3)	1.863(4)	1.759	1.895
C1–C2	1.393(3)	1.297(7)	1.392	1.381
E1–C2	1.727(2)	1.927(6)	1.759	1.894
C1–H1	fixed	fixed	1.095	1.096
C2–H2	fixed	fixed	1.095	1.096
Deviation from planarity	0.002	0.012	0.001	0.000
Bond angles (°)				
E1–E2–E3	99.78(3)	97.78(5)	99.04	97.19
E2–E3–C1	98.98(8)	96.84(13)	98.83	97.06
E3–C1–C2	119.21(15)	125.8(3)	121.65	124.33
C1–C2–E1	122.56(16)	123.8(3)	121.66	124.37
C2–E1–E2	99.46(8)	95.67(13)	98.83	97.05
E3–C1–H1	fixed	fixed	118.19	115.89
H1–C1–C2	fixed	fixed	120.16	119.78
C1–C2–H2	fixed	fixed	120.2	119.8
H2–C2–E1	fixed	fixed	118.14	115.83

4.3.2 NMR Spectroscopic Studies on 17 and 18

NMR studies were performed on d_8-THF solutions of [K(2,2,2-crypt)][**17**] and [K(2,2,2-crypt)][**18**]. The $^{31}P\{^{1}H\}$ spectrum of **17** shows a characteristic AA′B spectrum with resonances observed at 272.8 and 261.1 ppm in a 1:2 intensity ratio. On coupling the proton channel, a significantly more complex spectrum is observed, indicative of an AA′BXX′ spin system (Figure 4.2). The C*H* resonances of **17** are extremely downfield shifted, resonating as a multiplet at 9.03 ppm. This collapses to a singlet on broadband ^{31}P decoupling. The spectrum was simulated to extract the ^{31}P–^{31}P and ^{31}P–^{1}H coupling constants. Tabulated

values can be found in Appendix A, and were found to be in good agreement with those previously reported by Baudler and co-workers.[6] Of particular note is the very large $^{1}J_{P-P}$ value of 493 Hz, which is strongly suggestive of multiple bond character within the ring. The $^{13}C\{^{1}H\}$ NMR spectrum shows a multiplet resonance at 155.2 ppm. The NMR data obtained for **18** are consistent with that observed for **17**, exhibiting singlet resonances in the ^{1}H and $^{13}C\{^{1}H\}$ spectra at 10.68 and 172.4 ppm, respectively.

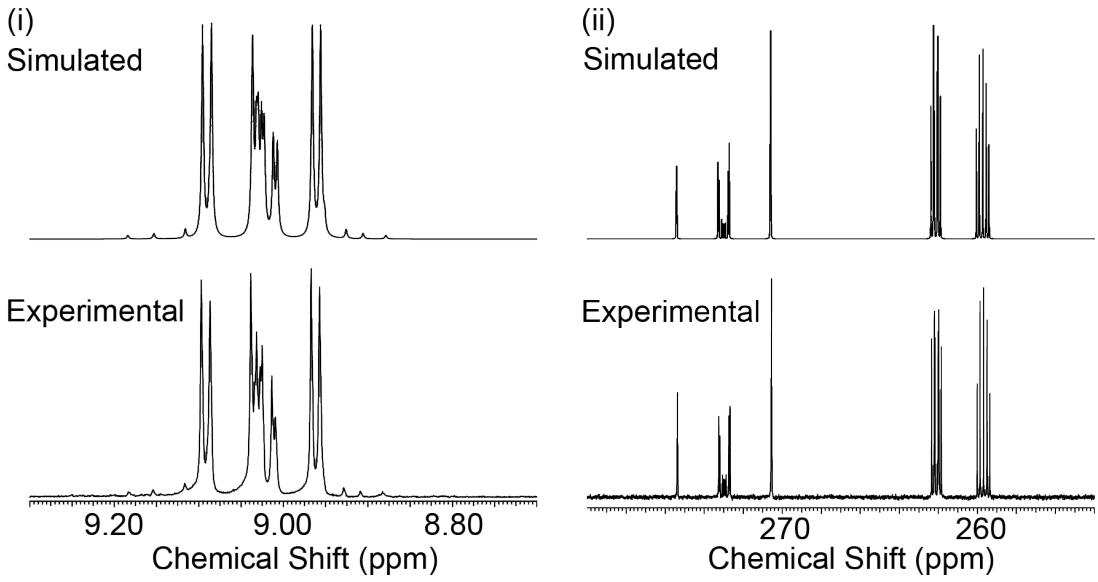

Figure 4.2: Expansion of the simulated and experimental ^{1}H (i) and ^{31}P (ii) NMR spectra of a d_8-THF solution of [K(2,2,2-crypt)][**17**].

4.3.3 Electronic Structure of 17 and 18

As mentioned in Section 4.3.1, the structures of **17** and **18** were computationally optimized at the DFT level of theory. The computed geometries show good agreement with those observed experimentally, with small variations likely due to the overly simplistic method used to simulate the presence of cations. A frontier orbital analysis of **17** and **18** shows a mixing of orbitals possessing pnictogen element lone pair character with the π-manifold orbitals (Figure 4.3). The overall form of the π orbitals is very similar to that of $[C_5H_5]^-$, and indeed what would be predicted using Hückel theory and the Frost mnemonic.[16–18] There is

some slight variance of the relative energies of the orbitals between **17** and **18**, which is attributable to energy differences in the parent atomic orbitals. Overall, compared to $[C_5H_5]^-$, there is an overall lowering of the energy of the ring π orbitals, particularly the unoccupied orbitals. A similar effect has been noted for the 1,3,4-triphospholide anion,[19] and suggest that the anions should act as enhanced π acceptor ligands compared to the cyclopentadienide anion.

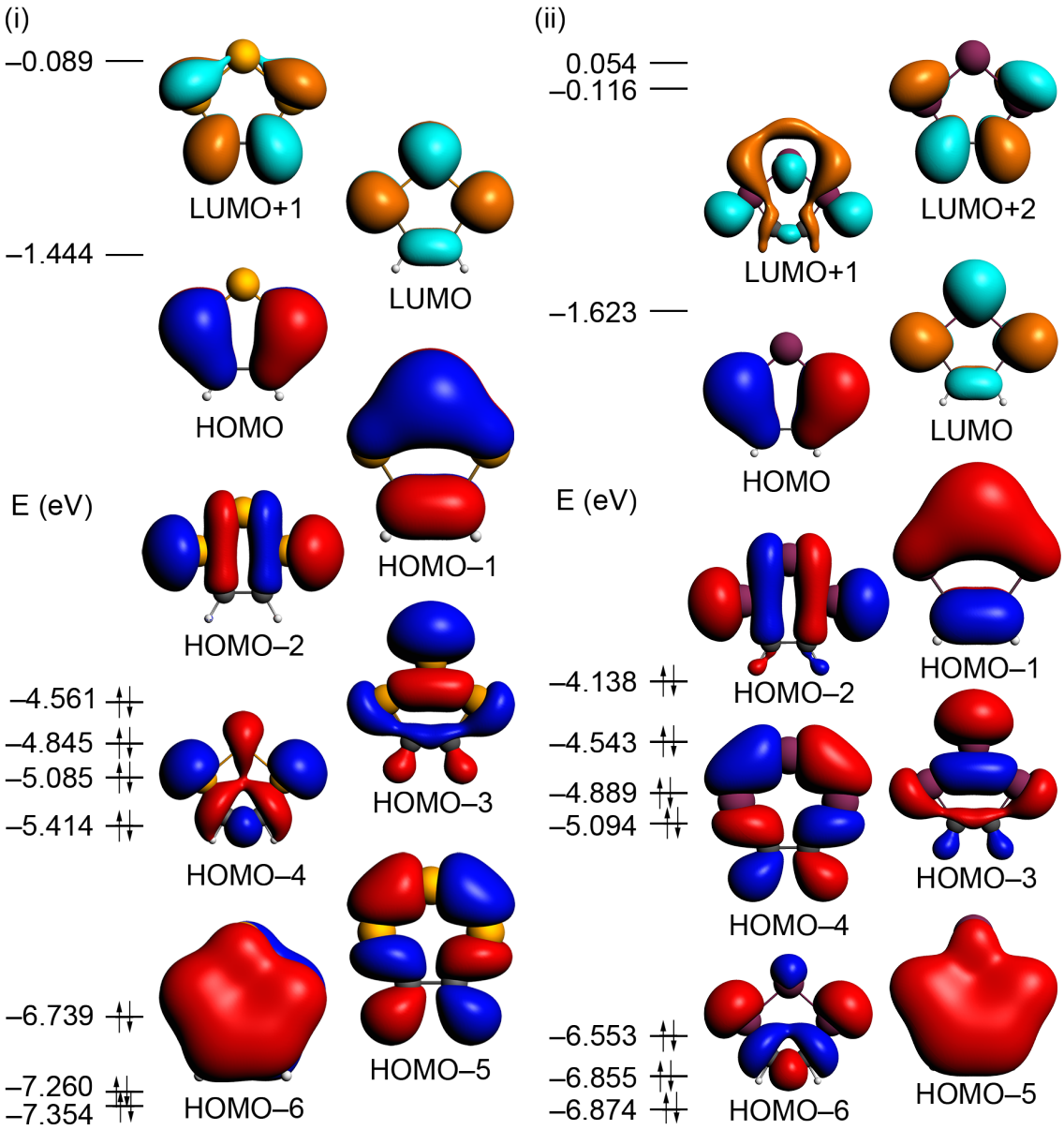

Figure 4.3: Kohn-Sham molecular orbital representations (contour values 0.03 au) and energies for selected frontier orbitals of **17** (i) and **18** (ii).

4.3.4 Mass Spectrometric Studies

Electrospray mass spectrometry of DMF solutions of [K(2,2,2-crypt)][**17**] and [K(2,2,2-crypt)][**18**] was performed in both negative and positive ion modes. The negative ion mode mass spectrum showed the unfragmented molecular ions at *m/z* values of 118.9 and 250.8 for **17** and **18**, respectively. The positive ion mode revealed the cation-paired species $\{[K(2,2,2\text{-crypt})]_2[E_3C_2H_2]\}^+$ at 949.6 (**17**) and 1081.3 (**18**) Da.

4.4 Further Synthesis of 1,2,3-Tripnictolides

To ascertain the synthetic scope of the transformation, a series of small-scale reactions were performed between **1** and a variety of alkynes and monitored by ^{31}P NMR spectroscopy. Rapid reaction was observed at room temperature for phenylacetylene and diphenylacetylene, with formation of the corresponding 1,2,3-triphospholide anion observed by NMR spectroscopy. Analogous reactions with the aliphatic internal alkynes RCCR′ (R = Me, R′ = Me, ^{n}Pr; R = R′ = Et) require extended reaction times at high temperatures for any reaction to occur. On heating, a singlet resonance at 470 ppm corresponding to the $[P_5]^-$ anion was seen, with concomitant loss of the characteristic resonances for **1**. Upon further heating, small quantities of alkyl-substituted 1,2,3-triphospholides could be detected, but the major product was $[P_5]^-$ alongside other unidentified polyphosphides. This chemistry will be further described in Chapter Six. Based on these preliminary results, we decided to target all of the already known 1,2,3-triphospholides as free anions, namely $[P_3C_2Ph_2]^-$, $[P_3C_2HPh]^-$ and $[P_3C_6H_4]^-$, and their unknown arsenic congeners.

Treatment of a stirring DMF solution of $[K(18\text{-crown-6})]_2$[**1**] with three equivalents of diphenylacetylene results in a rapid darkening of the reaction mixture. Subsequent workup involves the intentional introduction of air, which decomposes and precipitates the side-

products, while the air-stable $[1,2,3\text{-}P_3C_2Ph_2]^-$ anion remains in solution. This procedure allows the isolation of the $[K(18\text{-crown-}6)]^+$ salt of $[1,2,3\text{-}P_3C_2Ph_2]$ (**19**) as a pale brown solid in approximately 70% yield based on phosphorus. The same procedure can be used to prepare $[K(18\text{-crown-}6)][P_3C_2HPh]$ (**21**). The synthesis of the arsenic congeners can be achieved from K_3As_7 and an appropriate cation sequestering agent, however the oxidation step must be avoided as arsolides are air-sensitive. Accordingly, $[K(2,2,2\text{-crypt})][As_3C_2Ph_2]$ (**20**) and $[K(18\text{-crown-}6)][As_3C_2HPh]$ (**22**) were prepared as yellow-green solids (Scheme 4.7).

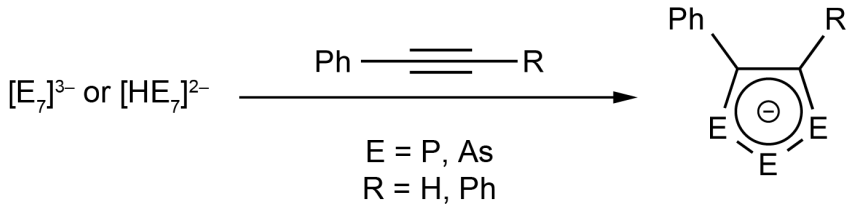

Scheme 4.7: Synthesis of $[1,2,3\text{-}E_3C_2PhR]^-$ anions from heptapnictide Zintl anions.

It seemed reasonable that the synthesis of the remaining known 1,2,3-triphospholide, the 1,2,3-triphosphaindenide anion reported by the groups of Russell and Wright, might be achieved from benzyne. Benzyne was generated in situ by addition of *o*-trimethylsilylphenyl triflate to a stirring solution of CsF and $[K(18\text{-crown-}6)]_2$[**1**] in pyridine/acetonitrile solvent mixtures (Scheme 4.8).[20] The mixture darkened overnight, and analysis by ^{31}P NMR spectroscopy displayed the characteristic resonances of the $[P_3C_6H_4]^-$ anion (**23**). Unfortunately it did not prove possible to obtain a compositionally pure sample of the compound. It was found that the use of acetonitrile as a solvent was necessary for the formation of benzyne from the precursors, however **1** (and **3**) both react with acetonitrile to form $[P_{16}]^{2-}$ and $[P_{21}]^{3-}$. In addition, the [Cs][OTf] by-product proved challenging to separate. Nevertheless, it was possible to obtain both ^{31}P NMR data and a single crystal X-ray structure to prove the formation of **23** using the "Zintl anion" synthetic protocol.

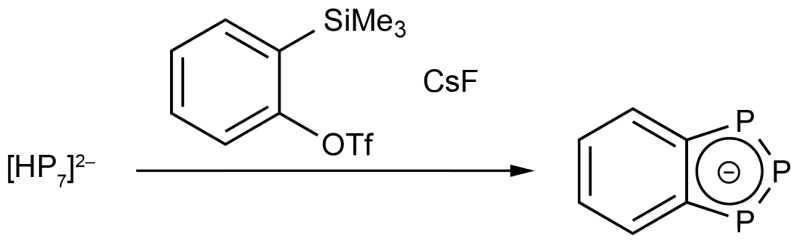

Scheme 4.8: Synthesis of $[1,2,3\text{-}P_3C_6H_4]^-$ from **1**.

4.4.1 Structures of 19–23

Crystals of the $[K(18\text{-crown-6})]^+$ salts of **19** and **22**, the $[K(2,2,2\text{-crypt})]^+$ salt of **20**, and the (unexpected) $[Cs(18\text{-crown-6})]^+$ salt of **23** suitable for single crystal X-ray diffraction could be grown by diffusion of hexane into THF solutions of the products. Two polymorphs of [K(2,2,2-crypt)][**20**] were crystallographically characterized (**20a** and **20b**), of which one (**20a**) was the dominant crystalline phase. Despite repeated attempts varying both the cation and solvent mixture, it did not prove possible to grow crystals of **21**. As expected, all the structures show the same gross structural features within the pnictolide ring. A general discussion of the features will be made, followed by a brief note on the specific details of a particular structure.

Selected bond metric data for **19**, **20**, **22** and **23** are presented in Table 4.2. The bond metric data for the phospholides (**19** and **23**) are in good agreement with that observed for the parent anion **17**, and to previous literature reports. A lack of crystallographic disorder allows the bond metric data within the previously unreported class of 1,2,3-tripnictolides to be analysed. The interatomic distances within the arsolides **20** and **22** are very similar. The As–As bond distances in both polymorphs of **20** are around 2.31 Å in length, approximately 0.20 Å longer than the equivalent bonds in **19**. This is consistent with the increased atomic radius of arsenic as compared to phosphorus (Δr_{cov} = 0.10 and 0.12 Å for single and double bonds, respectively).[21,22] The lengths are intermediate between single and double bonds.[23]

The As–C bonds in **20** are identical within experimental error, while in **22** the As1–C2 distance is slightly (but significantly) shorter than the As3–C1 distance (1.870(2) and 1.894(2) Å). In all of the phenyl-substituted anions the plane of the phenyl groups is twisted from the plane of the pnictolide ring (torsion angles (Φ) of 46.3 and 53.4º (**19**), 53.6 and 58.1º (**20a**) and 46.5º (**22**)). This is likely an effect of the steric demands of the system, and gives a propeller-like arrangement of the phenyl rings for the diphenyl-subsituted anions **19** and **20**. All of the anions possess planar tripnictolide cores, with only small deviations from planarity observed. The previously noted trend for significantly more acute angles at the pnictogen atoms compared to the carbon atoms is also observed for each of **19**, **20**, **22** and **23**.

Table 4.1: Bond metric data for **19, 20, 22** and **23.** Two polymorphs of **20** (**20a** and **20b**) were crystallographically characterized. Data are presented for both.

Bond distance (Å)	**19**	**23**	**20a**	**20b**	**22**
E1–E2	2.098(1)	2.082(2)	2.300(1)	2.309(av)	2.311(1)
E2–E3	2.091(1)	2.090(2)	2.306(1)	2.306(av)	2.303(1)
E3–C1	1.762(1)	1.777(5)	1.896(4)	1.894(av)	1.894(2)
C1–C2	1.402(2)	1.432(5)	1.377(5)	1.397(av)	1.375(3)
E1–C2	1.760(1)	1.783(4)	1.890(4)	1.894(av)	1.870(2)
C1–R1	1.490(2)	1.414(6)	1.495(6)	1.496(av)	1.485(3)
C2–R2	1.492(2)	1.413(6)	1.495(5)	1.498(av)	fixed
Deviation from planarity	0.004	0.002	0.014	0.010	0.005
Bond angles (º)					
E1–E2–E3	98.95(2)	101.11(7)	96.66(2)	96.20(av)	97.18(1)
E2–E3–C1	100.15(5)	99.08(13)	98.45(13)	99.21(av)	98.08(6)
E3–C1–C2	120.43(11)	120.6(3)	123.0(3)	122.7(av)	122.16(14)
C1–C2–E1	120.35(11)	119.8(3)	123.1(3)	122.8(av)	125.17(14)
C2–E1–E2	100.11(5)	99.44(14)	98.75(11)	99.11(av)	97.39(6)
E3–C1–R1	115.49(10)	121.2(3)	114.0(3)	144.08(av)	117.12(13)
R1–C1–C2	123.95(12)	118.2(4)	123.0(3)	123.25(av)	120.72(16)
C1–C2–R2	122.84(13)	118.6(4)	122.7(3)	123.10(av)	fixed
R2–C2–E1	116.76(10)	121.6(3)	114.2(3)	113.94(av)	fixed

The anion **19** was crystallographically characterized in [K(18-crown-6)$(THF)_2$][**19**]. The structure of the anion is shown in Figure 4.5. Two separate solvates of **20** were discovered,

[K(2,2,2-crypt)][**20**] (**20a**) and [K(2,2,2-crypt)][**20**]·0.5THF (**20b**). Comparison of a powder X-ray diffractogram of the crystalline material to the patterns calculated for the distinct polymorphs showed that the former is the predominant crystalline phase (Figure 4.4). The asymmetric unit of the first phase contains a single cation and anion, while the second phase contains two crystallographically unique cations and anions. As such, the bond metric data given for **20b** in Table 4.2 are averages of the two anions. The structure of the anion present in the solvent free polymorph (**20a**) is shown in Figure 4.5.

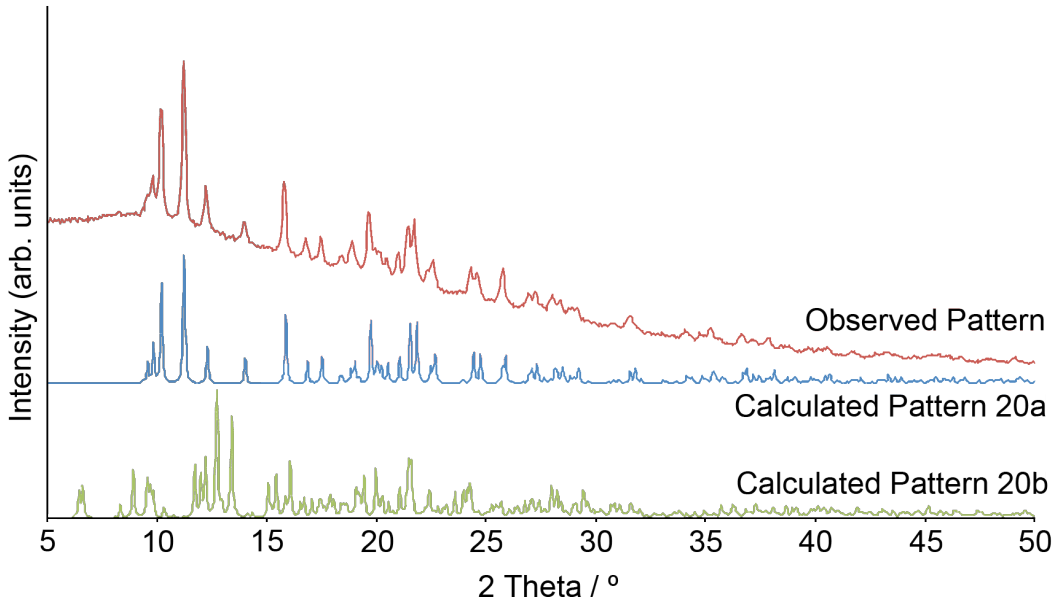

Figure 4.5: Comparison of experimental (red) and calculated (blue, **20a**; green, **20b**) powder X-ray diffraction patterns for [K(2,2,2-crypt)][**20**]. **20a** is the dominant bulk crystalline phase, as shown by the agreement between the experimentally observed pattern of the bulk sample and calculated pattern for **20a**. Experimental PXRD data were collected at room temperature.

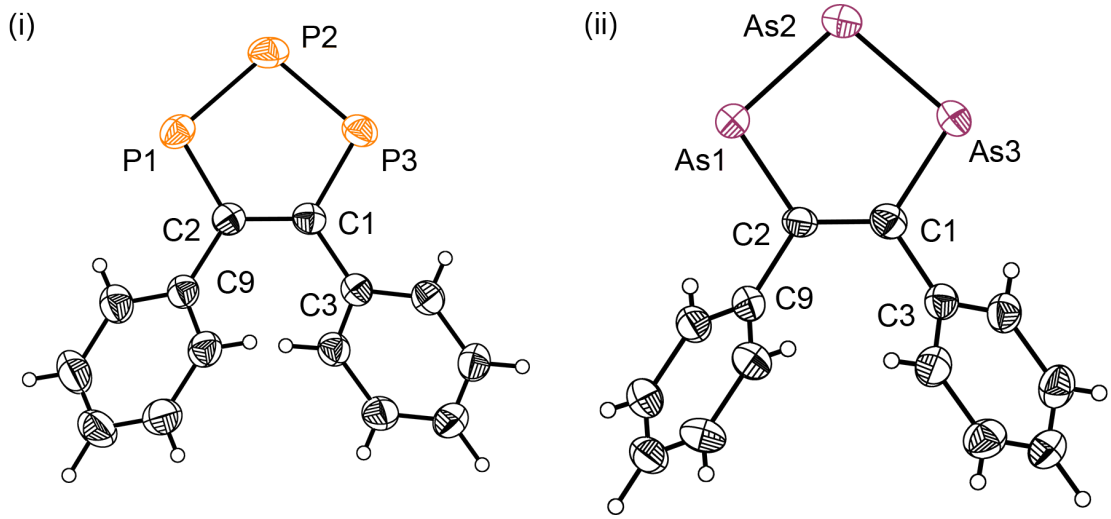

Figure 4.5: Thermal ellipsoid plots of **19** (i) and **20** (ii). Thermal ellipsoids are set at the 50% probability level. Hydrogen atoms are shown as spheres of arbitrary radius.

The disymmetrically substituted triarsolide anion **22** was crystallographically characterized in [K(18-crown-6)(THF)][**22**]. It crystallizes in *P*–1 with one anion in the asymmetric unit alongside two distinct half cation complexes. The structure of the anion is shown in Figure 4.6.

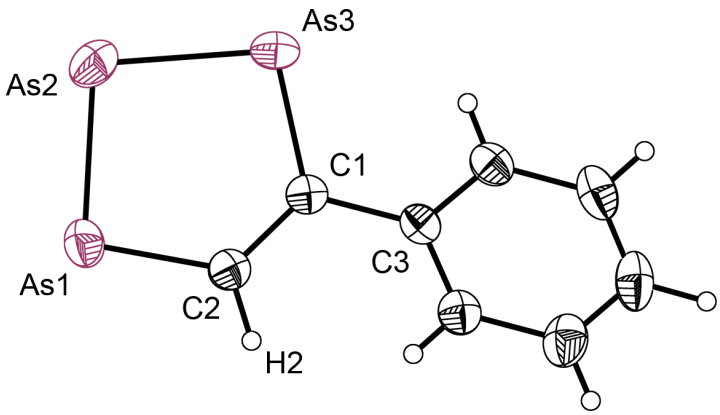

Figure 4.6: Thermal ellipsoid plots of **22**. Thermal ellipsoids are set at the 50% probability level. Hydrogen atoms are shown as spheres of arbitrary radius.

Finally, the triphosphaindenide analogue **23** was characterized in [Cs(18-crown-6)][**23**]. This species was previously isolated as a $[Li(12\text{-crown-4})_2]^+$ salt.[8,9] Cs^+ has replaced the K^+ cation within the crown ether molecule, possibly due to precipitation of KF from the reaction mixture. The structure of the anion is shown in Figure 4.7.

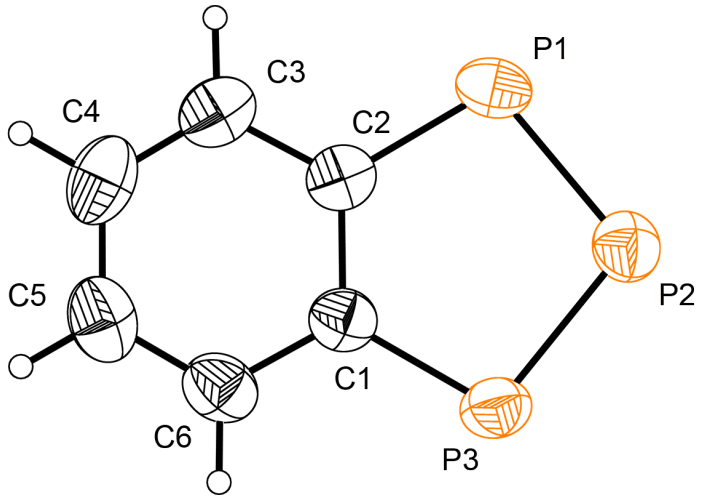

Figure 4.7: Thermal ellipsoid plot of **23**. Thermal ellipsoids are set at the 50% probability level. Hydrogen atoms are shown as spheres of arbitrary radius.

4.4.2 NMR Spectroscopic Studies on 19–23

The tripnictolides **19**–**22** were characterized by multielement NMR spectroscopy as the $[K(18\text{-crown-6})]^+$ or $[K(2,2,2\text{-crypt})]^+$ salts in d_8-THF (or d_5-pyridine in the case of **20**), while **23** was only characterized by ^{31}P NMR spectroscopy.

The ^{31}P NMR spectra of **19** and **21** display two and three multiplet resonances for an AB_2 and ABC spin system, respectively. This is as would be expected for symmetrically and disymmetrically substituted 1,2,3-triphospholide anions. The nuclei resonate at high chemical shift values due to the deshielding effect of the aromatic ring. Tabulated data of the ^{31}P, $^{13}C\{^1H\}$ and ^1H chemical shifts for all of the synthesized free tripnictolide anions in this chapter are given in Table 4.3. The spectra for the triphospholides **19**, **21** and **23** were

simulated to extract the internuclear *J* coupling constants (see Appendix A). These show remarkably large (ca. 500 Hz) $^{1}J_{P-P}$ values, which was also noted for **17** and is indicative of electron delocalization within the ring imparting multiple bond character.

Table 4.3: ^{31}P, ^{13}C and ^{1}H chemical shifts for **17**–**23**.

	Chemical Shift (ppm)						
	17	**18**	**19**	**20**	**21**	**22**	**23**
P1	272.8	–	297.9	–	275.5	–	261.3
P2	261.1	–	273.3	–	289.2	–	335.2
P3	272.8	–	297.9	–	269.0	–	261.3
C1	155.2	172.4	174.9	193.1	178.5	194.0	–
C2	155.2	172.4	174.9	193.1	157.7	172.0	–
H1/2	9.03	10.68	–	–	8.97	10.58	–

The ^{1}H and $^{13}C\{^{1}H\}$ NMR spectra of **19**–**22** support their formulation as aromatic 1,2,3-tripnictolide anions, but are otherwise unremarkable. The resonances arising from the carbon atoms of the tripnictolide ring appear to be the most sensitive to substitution pattern. Substituting H for Ph results in a downfield shift of approximately 20 ppm of the attached carbon atom, while replacing P with As shifts all pnictolide ring carbon atoms downfield by around 20 ppm. This is consistent with what would be expected since phenyl groups are inductively electron withdrawing compared to hydrogen. The ^{1}H spectra of **21** and **22** reveal a single resonance for the proton of the pnictolide backbone that appears as a ddd multiplet for **21** due to coupling to three inequivalent phosphorus atoms.

The ^{1}H and $^{13}C\{^{1}H\}$ NMR spectra of **19** and **20** display three and four resonances for the phenyl groups, respectively. This is indicative of the two phenyl substituents being equivalent, and that there is free rotation around the C1–C3 and C2–C9 bonds so that the propeller-like arrangement observed in the solid state is not retained in solution. A similar observation is seen in the ^{1}H and $^{13}C\{^{1}H\}$ spectra for the phenyl groups of **21** and **22**.

4.4.3 Electronic Structure of 19–22

Calculations at the DFT level of theory were performed on **19**–**22** to probe their electronic structure. In general, the optimized computed geometries are in good agreement with the geometries determined by single crystal X-ray diffraction. There is some slight lengthening of the bond distances, particularly the E–E and E–C bonds within the rings, which is likely attributable to the continuum dielectric model used to model the presence of the cations in the crystal lattice. Tabulated data are presented in Table 4.4.

Table 4.4: Computationally determined bond lengths and angles for the optimized computed geometries of **19**–**22**.

Bond distance (Å)	**19_{calc}**	**21_{calc}**	**20_{calc}**	**22_{calc}**
E1–E2	2.115	2.128	2.333	2.349
E2–E3	2.114	2.113	2.336	2.335
E3–C1	1.775	1.781	1.917	1.921
C1–C2	1.407	1.400	1.394	1.389
E1–C2	1.773	1.781	1.916	1.883
C1–R1	1.489	1.484	1.488	1.484
C2–R2	1.489	1.094	1.488	1.096
Bond angle (º)				
E1–E2–E3	98.42	98.93	96.34	97.04
E2–E3–C1	100.43	100.07	98.84	98.29
E3–C1–C2	120.29	118.93	122.93	121.17
C1–C2–E1	120.48	123.46	122.95	126.64
C2–E1–E2	100.37	98.71	98.93	96.86
E3–C1–R1	115.63	119.72	112.98	117.77
R1–C1–C2	123.90	121.44	123.85	121.03
C1–C2–R2	123.83	119.51	123.85	118.65
R2–C2–E1	115.51	117.00	112.97	114.68

The principal electronic structures for the anions are all very similar. A frontier orbital analysis shows that there is mixing of the pnictogen element lone pairs amongst the π manifold orbitals. Additionally, due to the small torsion angles between the pnictolide ring and the phenyl group in the optimized computed geometries (for example, Φ = 29.5º in **20**)

there is mixing of orbitals with both phenyl and pnictolide ring π character, which disrupts the simple analysis achievable for **17**.

In all cases the HOMO and HOMO–1 are part of the π manifold, possessing a single angular node. A lower π orbital, made up of the in phase combination of the ring p_z orbitals and with no angular nodes, is the HOMO–4 in **19**–**22** (raised from the HOMO–6 and HOMO–5 in **17** and **18**, respectively). This orbital appears the most sensitive to the nature of the carbon substituents. Hydrogen atoms lower the energy of the orbital, increasing the carbon p_z orbital contribution, whereas phenyl groups raise the orbital energy and decrease the participation of the carbon p_z orbital (Figure 4.8). The net result of this is that in **19** the orbital is mostly derived from the phosphorus p_z orbitals, and is localized on the phospholide atoms. Upon coordination to a metal centre, one therefore might expect more triphosphaallylic character observed for **19** compared to a more cyclopentadienyl-like coordination for **17**.

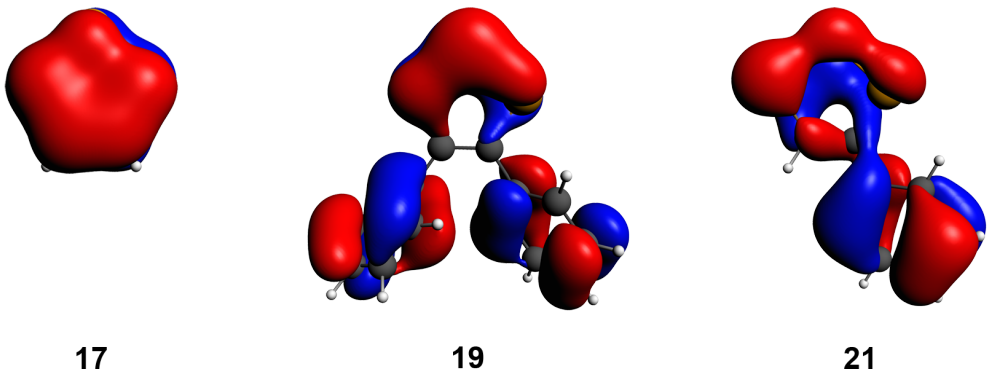

Figure 4.8: Comparison of the lowest energy π manifold Kohn-Sham molecular orbital representations (contour values 0.025 au) for **17**, **19** and **21**.

The substituent effect is also reflected in the non-bonding unoccupied orbitals. In the extreme case of **17**, the LUMO and LUMO+1 are both π antibonding orbitals, with two angular nodes. The other extreme, **19**, shows a LUMO that is essentially localized on the

phosphorus atoms while the LUMO+6 is C–C antibonding in nature. The disymmetrically substituted triphospholide **21** lies somewhere between the two described limits.

These effects are also observed for the arsolide anions **18**, **20** and **22**.

4.4.4 Mass Spectrometric Studies

Further characterization of **19**–**22** in solution was performed using electrospray mass spectrometry. The anions could be observed as the parent ion in the negative ion mode mass spectra, and the cation-paired species were seen in the positive ion mode. Tabulated data are given in Table 4.5.

Table 4.5: Electrospray mass spectrometry data for **19**–**22**.

Anion	Negative ion mode	Positive ion mode
19	270.7 $[M]^-$	877.8 $\{M+[K(18\text{-crown-6})]_2\}^+$
20	402.7 $[M]^-$	1233.5 $\{M+[K(2,2,2\text{-crypt})]_2\}^+$
21	195.1 $[M]^-$	801.4 $\{M+[K(18\text{-crown-6})]_2\}^+$
22	327.0 $[M]^-$	933.7 $\{M+[K(18\text{-crown-6})]_2\}^+$

4.5 Initial Studies on the Coordination Chemistry of 17 and 18

With an established protocol to make moderate quantities of the previously rare 1,2,3-tripnictolide anions, we set out to explore their coordination chemistry. For simplicity, the parent anions **17** and **18** were chosen for preliminary studies. Several diamagnetic transition metal fragments possessing a labile ligand were screened using small-scale reactions in an NMR tube. The most successful of these was with the ruthenium organometallic complex $[Ru(COD)(\eta^3\text{-}CH_3C(CH_2)_2)_2]$, which possesses a labile 1,5-cyclooctadiene ligand. Upon gentle heating (45 ºC) of equimolar quantities of [K(2,2,2-crypt)][**17**] and $[Ru(COD)(\eta^3\text{-}CH_3C(CH_2)_2)_2]$ in d_8-THF the characteristic resonances attributable to **17** in the ^{31}P NMR spectrum disappear and are gradually replaced by a new set of resonances that are

significantly shifted upfield. Concomitant appearance of free 1,5-cyclooctadiene is also observed in the ^{1}H NMR spectrum. After approximately three hours heating, quantitative formation of the novel complex [Ru(η^5-$P_3C_2H_2$){η^1-$CH_3C(CH_2)_2$}{η^3-$CH_3C(CH_2)_2$}]$^-$ (**24**) is seen. Repeating the reaction with [K(2,2,2-crypt)][**18**] yielded the novel arsolide-containing complex [Ru(η^5-$As_3C_2H_2$){η^1-$CH_3C(CH_2)_2$}{η^3-$CH_3C(CH_2)_2$}]$^-$ (**25**) (Scheme 4.9). The complexes **24** and **25** can be isolated as orange solids in moderate to good yields after workup to remove the 1,5-cyclooctadiene.

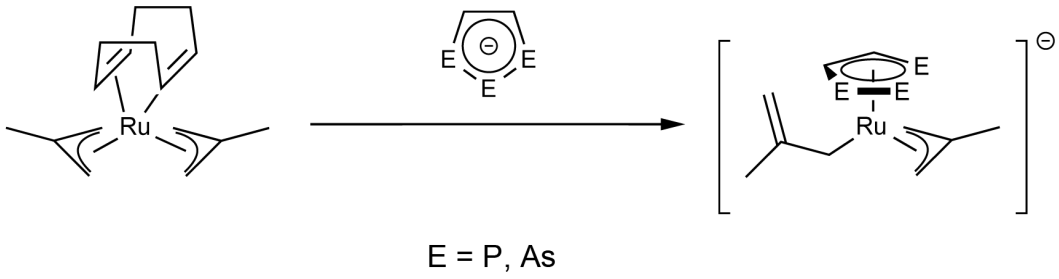

Scheme 4.9: Synthesis of **24** and **25**. E = P (**24**), As (**25**).

The reaction involves a net displacement of a four-electron donor ligand, 1,5-cyclooctadiene, with a six-electron donor ligand, the 1,2,3-tripnictolide. In order to maintain an eighteen valence electron count at the metal centre, one of the η^3-methylallyl ligands undergoes a haptotropic shift from η^3 coordination where it acts as a four-electron donor (using the ionic model for electron counting at a metal centre), to η^1 coordination where it acts as a two-electron donor.

4.5.1 Structure of 25

Orange, block-like crystals of [K(2,2,2-crypt)][**25**] suitable for single crystal X-ray diffraction were grown by diffusion of hexane into a THF solution of the product. Despite repeated attempts varying both cation and solvent system it did not prove possible to grow suitable crystals of the phosphorus congener **24**.

The molecular structure of **25** is shown in Figure 4.9. The structure shows an η^5-coordinated $[As_3C_2H_2]^-$ ligand and two inequivalent methylallyl groups, one coordinated to ruthenium in a η^1 fashion and the other in an η^3 manner. The transition metal complex is monoanionic, crystallizing alongside one $[K(2,2,2\text{-crypt})]^+$ cation in the asymmetric unit. There is a moderate lengthening of the intra-ring bonds within the pnictolide upon complexation, which suggests a degree of backbonding from the metal into unoccupied π anti-bonding orbitals. This is consistent with the pnictolide acting as a π acceptor ligand, an effect that has previously been noted for the 1,3,4-triphospholides.[19,24–26] Asymmetric coordination of **18** to the ruthenium centre is seen, with the Ru–C bonds being markedly shorter than the Ru–As bonds (average lengths Ru–C 2.259(av) Å, Ru–As 2.570(av) Å). This effect can be contributed to both the increased size of arsenic as compared to carbon, and to the asymmetric distribution of electron density within the π manifold of the arsolide.

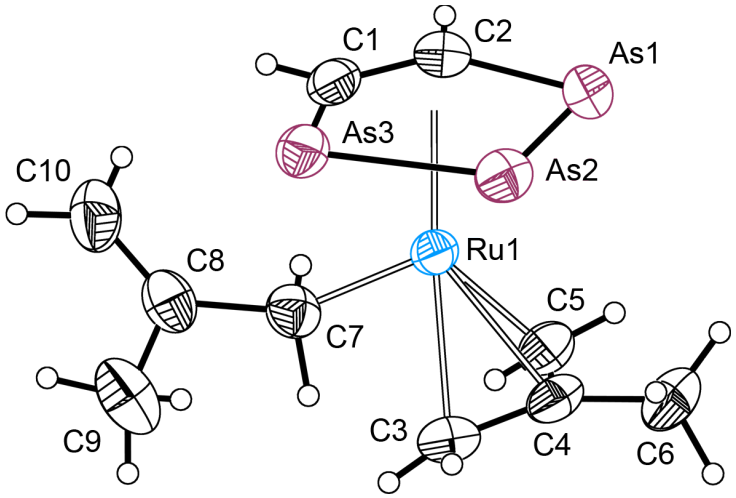

Figure 4.9: Thermal ellipsoid plot of **25**. Thermal ellipsoids are set at the 50% probability level. Hydrogen atoms are shown as spheres of arbitrary radius.

The two methylallyl groups are clearly inequivalent, and this is corroborated by the bond metric data. The η^3-coordinated ligand posseses C–C bond distances that are statistically identical (C3–C4 1.424(3) Å, C4–C5 1.424(2) Å) due to electron delocalization across the

allyl moiety. In contrast, the equivalent bonds in the η^1-coordinated methylallyl group (C7–C8 1.482(2) Å, C8–C10 1.332(3) Å) show distinct localized single and double bond character, respectively.

Table 4.6: Selected bond distances for **25**, $\mathbf{24_{calc}}$ and $\mathbf{25_{calc}}$.

Bond distance (Å)	25	$\mathbf{24_{calc}}$	$\mathbf{25_{calc}}$
Ru1–E1	2.5318(2)	2.443	2.549
Ru1–E2	2.5943(2)	2.529	2.652
Ru1–E3	2.5734(2)	2.512	2.618
Ru1–C1	2.232(2)	2.248	2.249
Ru1–C2	2.286(2)	2.298	2.296
E1–E2	2.3537(3)	2.184	2.394
E2–E3	2.3538(3)	2.182	2.388
E3–C1	1.900(2)	1.797	1.925
C1–C2	1.382(2)	1.410	1.400
C2–E1	1.904(2)	1.797	1.924
Ru1–C3	2.177(2)	2.195	2.193
Ru1–C4	2.141(2)	2.158	2.153
Ru1–C5	2.185(2)	2.217	2.206
Ru1–C7	2.202(2)	2.233	2.229
C3–C4	1.424(3)	1.438	1.436
C4–C5	1.424(2)	1.435	1.436
C4–C6	1.508(2)	1.512	1.510
C7–C8	1.482(2)	1.484	1.484
C8–C9	1.507(3)	1.515	1.515
C8–C10	1.332(3)	1.357	1.356

Selected bond metric data for both the experimentally determined structure of **25** and the computed optimized structures $\mathbf{24_{calc}}$ and $\mathbf{25_{calc}}$ are presented in Table 4.6. The computed structure of **25** shows good correlation with the structural parameters observed in the experimental structure. The computed structure of **24** is very similar to that of **25**. The largest deviations are the interatomic distances for the bonds involving phosphorus, which are predictably shorter due to the decreased covalent radius of phosphorus as compared to arsenic. The HOMOs of both **24** and **25** arise from the ruthenium d_{z^2} orbital, while the

LUMO is an anti-phase combination of the ruthenium $d_{x^2-y^2}$ orbital and the LUMO of the free pnictolide.

4.5.2 NMR Spectroscopic Studies on 24 and 25

Anions **24** and **25** were both characterized by multielement NMR spectroscopy as the $[K(2,2,2\text{-crypt})]^+$ salts in d_8-THF. The ^{31}P NMR spectrum of **24** displays two multiplet resonances at 25.9 and –29.8 ppm, integrating in the intensity ratio 2:1. These were assigned as arising from P1/P3 and P2, respectively. They are upfield shifted by approximately 200–250 ppm compared to the free phospholide **17**, with P2 experiencing the larger upfield shift (Figure 4.10). That P2 experiences a greater change in chemical shift is unsurprising when the fact that the electron density in the π manifold is highly anistropically distributed is considered. This large upfield shift, observed in the ^{31}P, ^{1}H and $^{13}C\{^{1}H\}$ spectra, turns out to be extremely diagnostic of η^5-coordination of the pnictolide.

The ^{31}P spectrum could be simulated in order to confirm the assignment and extract the internuclear *J* values (Appendix A). A general reduction in the size of the coupling constants within the ring was observed ($^{1}J_{P-P}$ = –415 Hz compared to –493 Hz in free **17**). This is consistent with loss of some electron density (in donation to the ruthenium centre) from the occupied orbitals of the π system, reducing the multiple bond character within the ring.

The characteristic proton resonance in the ^{1}H NMR spectrum of the pnictolide is also shifted upfield upon complexation, from 9.03 to 4.95 ppm in **24**, and from 10.68 to 6.41 ppm in **25**. The remainder of the ^{1}H NMR spectrum of **24** and **25** are very similar, showing six resonances arising from the methylallyl groups, alongside the three resonances attributable to the $[K(2,2,2\text{-crypt})]^+$ cation.

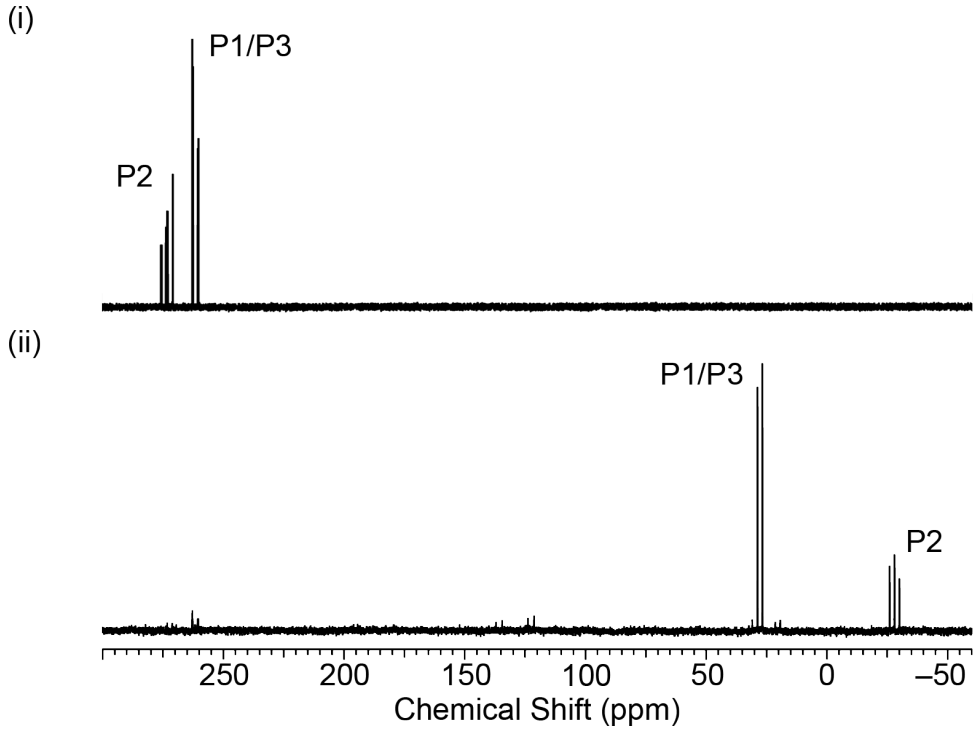

Figure 4.10: Comparison of the $^{31}P\{^{1}H\}$ NMR spectra of d_8-THF solutions of [K(2,2,2-crypt)]**[17]** (i) and [K(2,2,2-crypt)][**24**] (ii).

The $^{13}C\{^{1}H\}$ NMR spectra of **24** and **25** shows the expected number of resonances for the two distinct coordination modes of the methylallyl groups, and the pnictolide ring carbon atom resonates at 106.8 and 123.6 ppm for **24** and **25**, respectively.

4.5.3 Mass Spectrometric Studies

Further solution characterization of **24** and **25** was achieved by means of electrospray mass spectrometry. The negative ion mode revealed mass envelopes arising from the molecular ions at 331.0 and 426.7 Da for **24** and **25**, respectively. In the positive ion mode evidence for the cation-paired species $\{[K(2,2,2\text{-crypt})]_2[\mathbf{24}]\}^+$ and $\{[K(2,2,2\text{-crypt})]_2[\mathbf{25}]\}^+$ was seen at *m/z* values of 1161.4 and 1292.8, respectively.

4.6 Systematic Evaluation of the Ligand Properties of 17–22

As has been noted both previously, isolobal replacement of methine units in cyclopentadienide with phosphorus gives a series of phospholides. The presence of phosphorus atoms within the ring has the net effect of lowering the overall energy of the π manifold, making the phospholides increasing good π acceptor ligands. The coordination chemistry of the 1,3,4-triphospholides has been extensively probed, while the lack of a viable synthetic route to the 1,2,3-triphospholide isomer has resulted in no such reports dealing with the ligand properties of this isomer. With a feasible synthetic route for the preparation of all of the previously reported 1,2,3-triphospholide anions as their potassium salts, we set out to make a homologous series of compounds in order to systematically study their properties. Molybdenum piano stool complexes of the general form $[Mo(\eta^5\text{-}E_3C_2R_2)(CO)_3]^-$ were chosen for this purpose. This was due both to their facile synthesis and the presence of carbonyl groups that can be readily interrogated by IR spectroscopy to reveal the comparative electron richness of the metal centre.

Monitoring the reaction of [K(18-crown-6][**17**] with $Mo(CO)_6$ in d_8-THF at reflux revealed the gradual disappearance of the resonances arising from **17**, with concomitant growth of a new set of resonances corresponding to the piano-stool complex $[Mo(\eta^5\text{-}P_3C_2H_2)(CO)_3]^-$ (**26**). It was later found that the more labile acetonitrile ligands in $Mo(CO)_3(MeCN)_3$ are more readily displaced by **17**, with only gentle warming required for reaction. This methodology was extended to the anions **18**–**23** to give a homologous series of η^5-coordinated pnictolide-molybdenum tricarbonyl complexes $[Mo(\eta^5\text{-}E_3C_2RR')(CO)_3]^-$ (R = R′ = H; E = P (**26**), As (**27**); R = R′ = Ph; E = P (**28**), As (**29**); R = Ph, R′ = H; E = P (**30**), As (**31**)) as either the $[K(18\text{-crown-6})]^+$ (**26**–**28**, **30**, **31**) or $[K(2,2,2\text{-crypt})]^+$ (**29**) salts (Scheme 4.10).

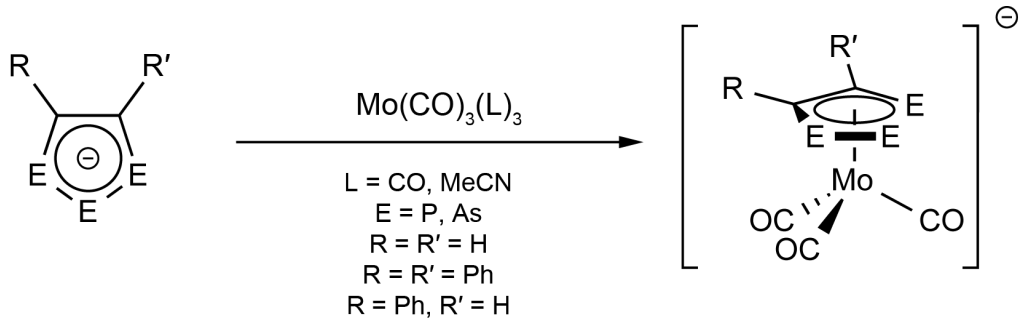

Scheme 4.10: Synthesis of **26**–**31**.

The formation of **26**–**31** is quantitative as assessed by multielement NMR spectroscopy, and the compounds are isolable in generally good yields as yellow (phospholides) or orange (arsolides) solids after workup.

4.6.1 Structures of 26 to 31

Crystals of **26**–**29** and **31** suitable for single crystal X-ray diffraction experiments could be grown by diffusion of hexane into THF solutions of either the $[K(18\text{-crown-6})]^+$ salts (**26**–**28**, **31**) or $[K(2,2,2\text{-crypt})]^+$ (**29**) salts of the anions. Despite repeated attempts, it did not prove possible to crystallographically characterize **30**. In each of the crystal structures, the anionic metal complex reveals η^5-coordination of the pnictolide ring to a molybdenum centre. In turn, this is supported by three carbonyl ligands in a piano-stool like geometry, with an overall eighteen valence electron count. Selected bond metric data for the complexes are presented in Table 4.7.

The pnictolide ring exhibits rotational disorder over two positions in both **26** and **27** and additionally in **31**, but the pnictolide ring is fully ordered in **28** and **29**, which allows a detailed discussion of the bond distances. The P–P, P–C and C–C bond lengths in **28** are 2.142(av), 1.780(av) and 1.419(2) Å, respectively, which are statistically longer than the equivalent bonds in the free phospholide **19** (2.095 (av), 1.761(av) and 1.402(2) Å). Upon

coordination to the electron rich molybdenum fragment there is a moderate lengthening of the phospholide ring P–P bonds (Δd = 0.05 Å), as would be expected for a π acceptor ligand. A similar effect is noted for **29**, with As–As, As–C and C–C bond lengths of 2.354(av), 1.912(av) and 1.403(3) Å (cf. 2.306(av), 1.895(av) and 1.384(av) in **20**). Positional disorder of the pnictolide ring in **26**, **27** and **31** prevents a similar examination of the changes in bond length upon coordination, but a tentative analysis suggests that the same trend is observed.

Table 4.7: Selected bond distances for **26**–**29** and **31**. There are two crystallographically unique anions in the asymmetric unit of [K(18-crown-6)][**29**]. Data for both are given. **26**, **27** and **31** display disorder of the pnictolide ring, only data for the major component are given.

Bond distance (Å)	**26**	**27**	**28**	**29a′**	**29b′′**	**31**
E1–E2	2.119(7)	2.325(5)	2.146(1)	2.365(1)	2.344(1)	2.351(2)
E2–E3	2.131(7)	2.329(7)	2.138(1)	2.343(4)	2.349(1)	2.346(1)
E3–C1	1.763(9)	1.996(1)	1.776(2)	1.910(2)	1.931(2)	1.936(3)
C1–C2	1.400(8)	1.375(8)	1.419(2)	1.403(3)	1.392(3)	1.384(6)
E1–C2	1.734(6)	1.822(8)	1.784(2)	1.914(2)	1.922(2)	1.876(8)
C1–R1	fixed	fixed	1.495(2)	1.498(3)	1.499(3)	1.488(5)
C2–R2	fixed	fixed	1.497(2)	1.502(3)	1.497(3)	fixed
Mo1–E1	2.576(5)	2.679(3)	2.594(1)	2.706(1)	2.680(1)	2.725(3)
Mo1–E2	2.694(9)	2.800(5)	2.699(1)	2.790(3)	2.719(1)	2.795(1)
Mo1–E3	2.551(5)	2.677(4)	2.579(1)	2.667(1)	2.720(1)	2.672(1)
Mo1–C1	2.311(1)	2.369(7)	2.413(2)	2.431(2)	2.437(2)	2.416(3)
Mo1–C2	2.386(7)	2.400(7)	2.389(2)	2.414(2)	2.435(2)	2.351(6)
Mo1–CO(1)	1.945(2)	1.950(3)	1.957(2)	1.938(3)	1.953(2)	1.957(4)
Mo1–CO(2)	1.953(2)	1.946(3)	1.945(2)	1.955(3)	1.972(2)	1.965(3)
Mo1–CO(3)	1.954(2)	1.956(3)	1.960(2)	1.937(3)	1.951(2)	1.953(4)
C–O CO(1)	1.168(3)	1.163(4)	1.158(2)	1.154(4)	1.159(3)	1.155(5)
C–O CO(2)	1.160(3)	1.164(3)	1.167(2)	1.155(3)	1.152(3)	1.150(4)
C–O CO(3)	1.165(3)	1.162(3)	1.162(2)	1.164(4)	1.165(3)	1.165(4)

The C–O distances of the carbonyl moieties are statistically identical throughout the anions, and do not warrant discussion beyond this. The Mo–C distances lie in a narrow range, and there is no discernible trend on changing the nature of the substituents on the ring, or moving from phosphorus to arsenic.

The average Mo–E and Mo–C pnictolide distances are perhaps more interesting, and reveal subtle differences between the coordination properties of the diprotic (**17**, **18**) and diphenyl (**19**, **20**) pnictolides. There is an increase in the average Mo–C bond length from 2.349(av) to 2.401(av) Å when comparing **26** to **28**. While it is conceivable that this results entirely from the increased steric demands of a phenyl group as compared to a hydrogen atom, it could also be the manifestation of an effect noted earlier. The in-phase π orbital has a decreased carbon p_z contribution in **19**, and it was observed that this could lead to a more phosphaallylic character on binding to a metal centre, increasing the metal–carbon bond distances. A similar effect is observed for the arsenic congeners **27** and **29** (Mo–C 2.385(av) and 2.423(av) Å, respectively). Unfortunately, this may simply be an artefact of the disorder inherent to the pnicolide moieties in **26** and **27**, distorting the true bond distances.

The anions **26** and **27** were crystallographically characterized in [K(18-crown-6)][**26**] and [K(18-crown-6)][**27**], respectively (Figure 4.11). They are isostructural, displaying a single crystallographically unique anion accompanied by a $[K(18\text{-crown-6})]^+$ cation, which displays a short contact to one of the carbonyl groups (K101–O1 3.015(2) (**26**) and 3.035(3) Å (**27**), K101–C3 3.225(2) (**26**) and 3.308(3) Å (**27**)). As noted above, this has no statistically significant effect on the M–C or C–O distances of this particular carbonyl moiety, and is likely just a crystal packing effect. In both cases, the pnictolide ring was modelled as disordered over two positions, with the occupancy of the major component refining to 65% and 58% in **26** and **27**, respectively.

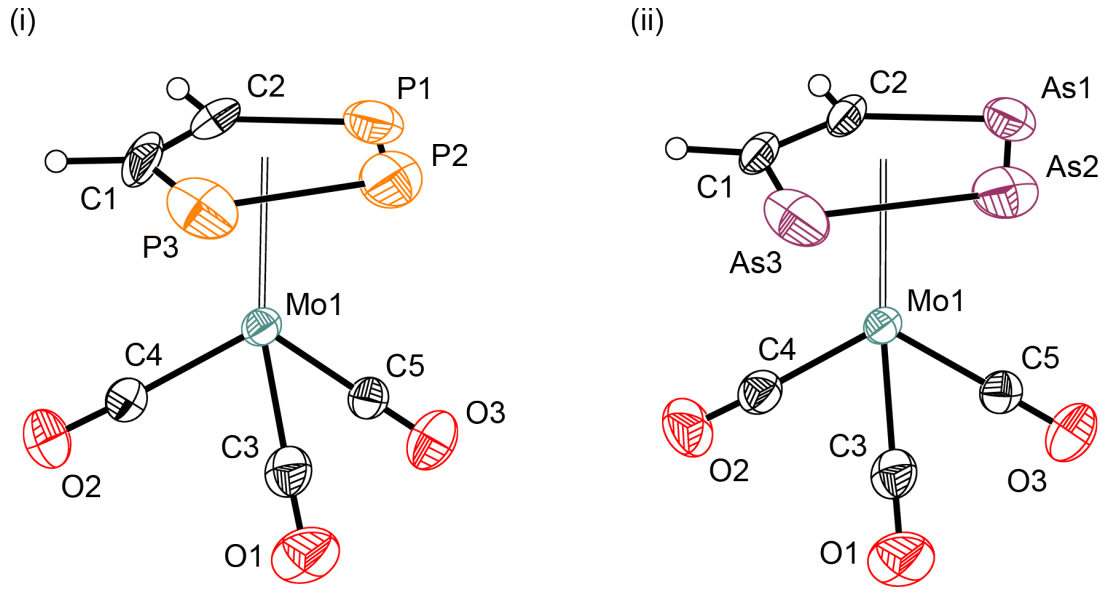

Figure 4.11: Thermal ellipsoid plot of **26** (i) and **27** (ii). Thermal ellipsoids are set at the 50% probability level. Hydrogen atoms are shown as spheres of arbitrary radius. Only the major component of the disordered pnictolide ring is shown.

The structures of the anions **28** and **29** were determined in [K(18-crown-6)(THF)][**28**] and [K(2,2,2-crypt)][**29**], respectively (Figure 4.12). There are two crystallographically unique anions in the asymmetric unit of [K(2,2,2-crypt)][**29**]. Unlike **26** and **27** the pnictolide ring is fully ordered in both structures, which is likely an effect of the (comparatively) large phenyl rings determining and locking the orientation within the crystal lattice.

The anion **31** was structurally characterized in [K(18-crown-6)(THF)][**31**] in the space group *P*–1 (Figure 4.13). There is discrete positional disorder of the arsolide moiety within the single anion in the asymmetric unit. This could be modelled as two components refining in a 68:32 ratio, with the $Mo(CO)_3$ unit and phenyl group fixed in the same position in both components. The disorder is effectively a result of both possible enantiomers (disymmetrically substituted pnictolides form complexes with planar chirality upon coordination to a metal centre) of the complex occupying the same site in the crystal lattice.

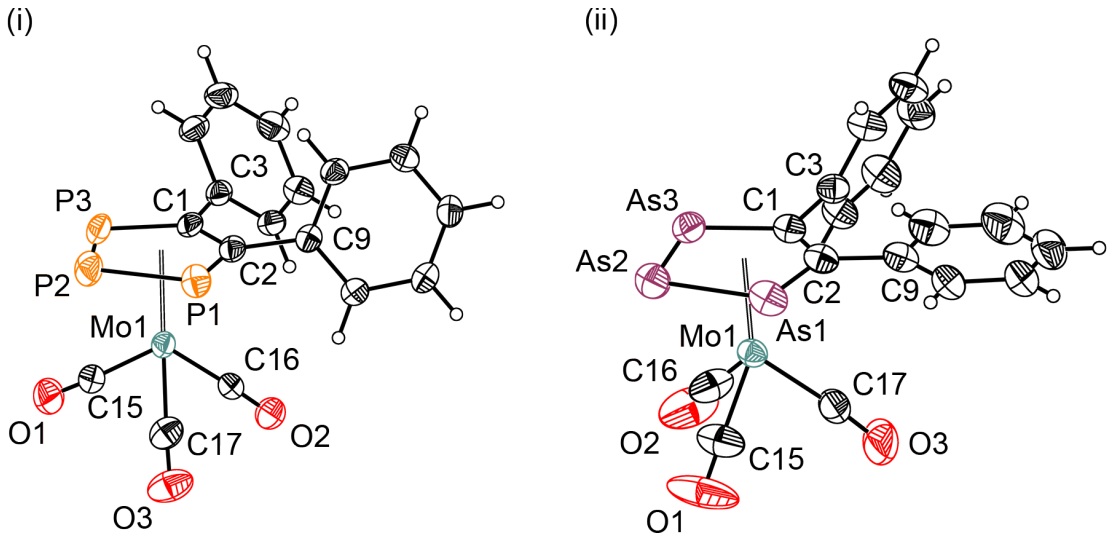

Figure 4.12: Thermal ellipsoid plot of **28** (i) and **29** (ii). Thermal ellipsoids are set at the 50% probability level. Hydrogen atoms are shown as spheres of arbitrary radius.

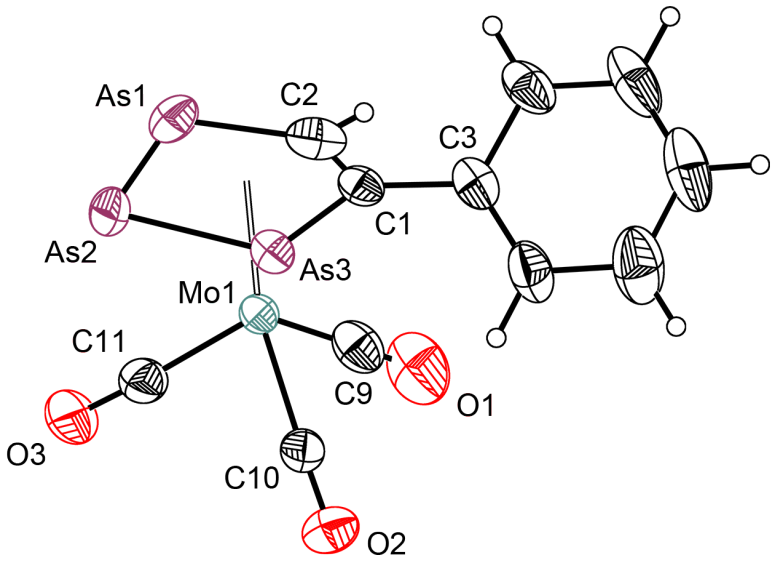

Figure 4.13: Thermal ellipsoid plot of **31**. Thermal ellipsoids are set at the 50% probability level. Hydrogen atoms are shown as spheres of arbitrary radius. Only the major component of the disordered arsolide ring is shown.

4.6.2 NMR Spectroscopic Studies on 26–31

Multielement NMR spectroscopy was used to characterize **26**–**31** in solution. Data were collected on d_8-THF or d_5-pyridine solutions, and were found to support their formulation as $[(\eta^5\text{-pnictolide})Mo(CO)_3]^-$ complexes.

The ^{31}P NMR spectra of **26** and **28** reveal two multiplets in a 2:1 intensity ratio, with chemical shifts typical of η^5 coordinated 1,2,3-triphospholides (67.3 and 34.5 ppm (**26**), 97.6 and 70.8 (**28**)). The disymmetrically substituted triphospholide complex, **30**, shows three equal intensity resonances at 77.0, 70.6 and 40.5 ppm. This large upfield shift upon complexation to an electron rich metal centre is consistent with that observed for the ruthenium complex **24**. As for the ruthenium complex, the largest upfield shift is seen for P2 ($\Delta\delta$ = –226.6, –252.5 and –248.7 ppm for **26**, **28** and **30**, respectively). The ^{31}P NMR spectra were simulated to extract the internuclear coupling constants (Appendix A). The *J* values obtained are generally reduced relative to the free phospholides. This effect was also observed for **24**, and is attributable to the reduced multiple bond character within the ring.

Table 4.8: ^{31}P, ^{13}C and ^{1}H chemical shifts for **26**–**31**.

	Chemical Shift (ppm)					
	26	**27**	**28**	**29**	**30**	**31**
P1	67.3	–	97.6	–	70.6	–
P2	34.5	–	20.8	–	40.5	–
P3	67.3	–	97.6	–	77.0	–
C1	111.5	124.1	140.5	142.3	139.9	145.6
C2	111.5	124.1	140.5	142.3	113.8	113.9
C(carbonyl)	227.8	228.1	228.5	229.8	228.9	229.2
H1/2	5.82	7.04	–	–	6.16	7.29

Tabulated data for the chemical shifts is presented in Table 4.8. The pnictolide ring proton in **26**, **27**, **30** and **31** resonates at significantly lower chemical shift compared to the free pnictolide upon complexation to the $Mo(CO)_3$ moiety. Only one carbonyl resonance is observed in all of the $^{13}C\{^1H\}$ NMR spectra. This implies a single carbon environment, and in turn free rotation of the $Mo(CO)_3$ unit around the Mo–ring centroid making all of the carbonyls equivalent on the NMR timescale. The chemical shift of this resonance, in the narrow range 227–230 ppm, is typical of terminal metal–carbonyl complexes.[27]

4.6.3 IR Spectroscopic Studies on 26–31

The carbonyl stretching frequency, ν_{CO}, of metal-carbonyl complexes is an extremely sensitive probe of the electron density at the metal centre. This has been exemplified in the Tolman electronic parameter, a measure of the electron donor/acceptor ability of a ligand as measured by the carbonyl stretching frequency of its $Ni(CO)_3$ complex.[28,29] To put the $[(\eta^5$-pnictolide$)Mo(CO)_3]^-$ complexes on a comparative donor-acceptor scale to their all carbon analogue, $[(\eta^5\text{-}C_5H_5)Mo(CO)_3]^-$, the IR spectra of all the compounds were recorded as solids in a Nujol mull. Tabulated values are shown in Table 4.9. The IR spectrum of $[(\eta^5\text{-}C_5H_5)Mo(CO)_3]^-$ has previously been reported.[30,31]

Table 4.9: Comparison of carbonyl stretching frequencies for **26**–**31** and $[(\eta^5\text{-}C_5H_5)Mo(CO)_3]^-$.

Complex	ν_{CO} (cm^{-1})
26	1916 (A′), 1834, 1814 (A′ + A″)
27	1910 (A′), 1830, 1817 (A′ + A″)
28	1921 (A′), 1842, 1821 (A′ + A″)
29	1910 (A′), 1836, 1818 (A′ + A″)
30	1925 (A′), 1842, 1828 (A′ + A″)
31	1911 (A′), 1828, 1818 (A′ + A″)
$[Mo(\eta^5\text{-}C_5H_5)(CO)_3]^-$	1884 (A_1), 1760 (E)

The values recorded show that any significant differences in the π-acceptor properties of the synthesized pnictolides, should there be any, are not manifested in the electronic properties of the $Mo(CO)_3$ unit upon complexation. In general, the phospholides gives a marginally higher stretching frequency than the equivalent arsolides. However, they are markedly different to the all carbon analogue $[(\eta^5\text{-}C_5H_5)Mo(CO)_3]^-$. The carbonyl stretching frequencies for the $Mo(CO)_3$ unit are significantly higher for the pnictolide complexes. This is caused by weaker M–CO backbond, which in turn is due to the increased π acceptor properties of the pnictolide ligands. The addition of three pnictogen atoms into the ring lifts the degeneracy of the E vibrational mode to give two bands (Figure 4.14).

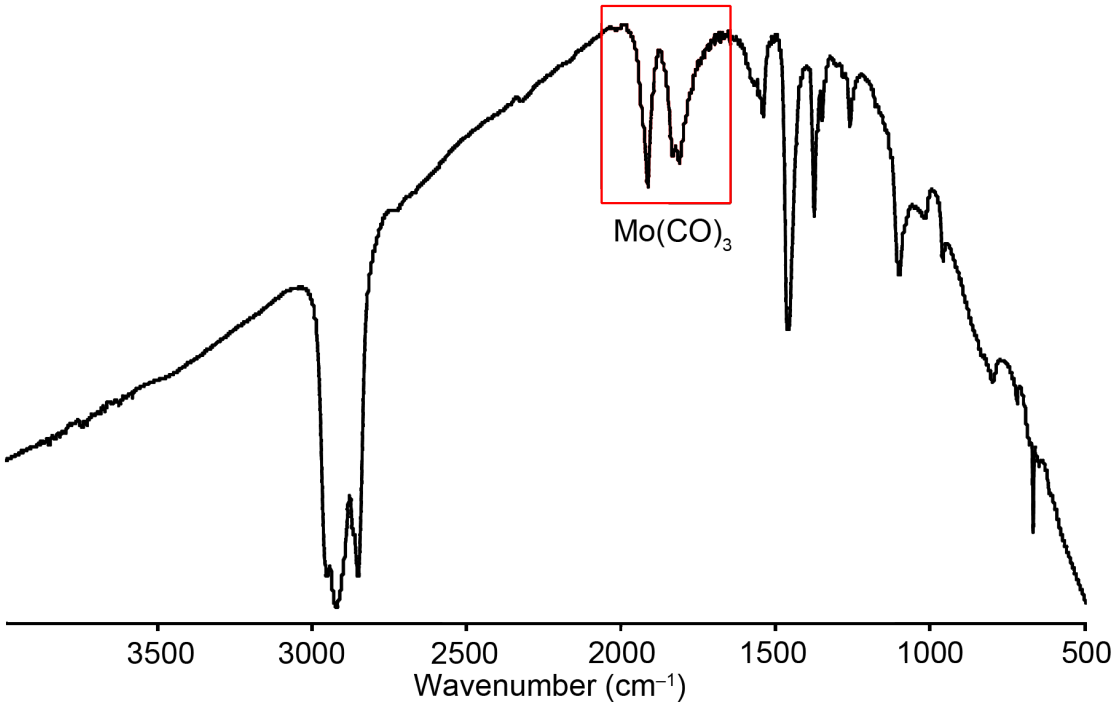

Figure 4.14: The IR spectrum of [K(18-crown-6)][**26**], highlighting the carbonyl stretching region.

4.6.4 Computational Studies on 26–31

The electronic structures of **26–31** were investigated using density functional theory. Generally good agreement was found between the computationally optimized geometries and the geometry observed experimentally. Tabulated bond metric data for the computed geometries are presented in Table 4.10.

The electronic structures of **26–31** are all similar, and comparable to the all carbon analogue, $[(\eta^5\text{-}C_5H_5)Mo(CO)_3]^-$. Within the series, the energies and ordering of the important frontier orbitals is similar. There are two key differences between the frontier orbitals of **26–31** and $[(\eta^5\text{-}C_5H_5)Mo(CO)_3]^-$. The first is the mixing of pnictogen lone pair character into metal-ligand bonding orbitals. A second, and more interesting observation, is the increased δ bonding present in **26–31**. The HOMO and HOMO–2 are of Mo d_{xy} and $d_{x^2-y^2}$ parentage, and are capable of participating in δ bonding to the pnictolide ring.

Table 4.10: Selected bond distances for $\mathbf{26_{calc}}$–$\mathbf{31_{calc}}$.

Bond distance (Å)	$\mathbf{26_{calc}}$	$\mathbf{27_{calc}}$	$\mathbf{28_{calc}}$	$\mathbf{29_{calc}}$	$\mathbf{30_{calc}}$	$\mathbf{31_{calc}}$
E1–E2	2.161	2.374	2.161	2.386	2.174	2.397
E2–E3	2.176	2.395	2.157	2.381	2.152	2.375
E3–C1	1.776	1.922	1.793	1.94	1.8	1.939
C1–C2	1.412	1.396	1.427	1.412	1.417	1.407
E1–C2	1.775	1.917	1.797	1.935	1.775	1.916
C1–R1	1.093	1.094	1.496	1.494	1.487	1.094
C2–R2	1.092	1.094	1.495	1.497	1.092	1.489
Mo1–E1	2.605	2.733	2.592	2.730	2.647	2.746
Mo1–E2	2.721	2.812	2.731	2.876	2.699	2.839
Mo1–E3	2.644	2.778	2.615	2.692	2.596	2.710
Mo1–C1	2.389	2.406	2.465	2.447	2.462	2.515
Mo1–C2	2.426	2.461	2.41	2.486	2.381	2.383
Mo1–CO(1)	1.963	1.956	1.966	1.962	1.958	1.957
Mo1–CO(2)	1.953	1.957	1.951	1.953	1.959	1.956
Mo1–CO(3)	1.96	1.951	1.958	1.945	1.960	1.954
C–O CO(1)	1.177	1.181	1.176	1.177	1.177	1.181
C–O CO(2)	1.182	1.180	1.182	1.179	1.179	1.179
C–O CO(3)	1.179	1.184	1.177	1.184	1.179	1.181

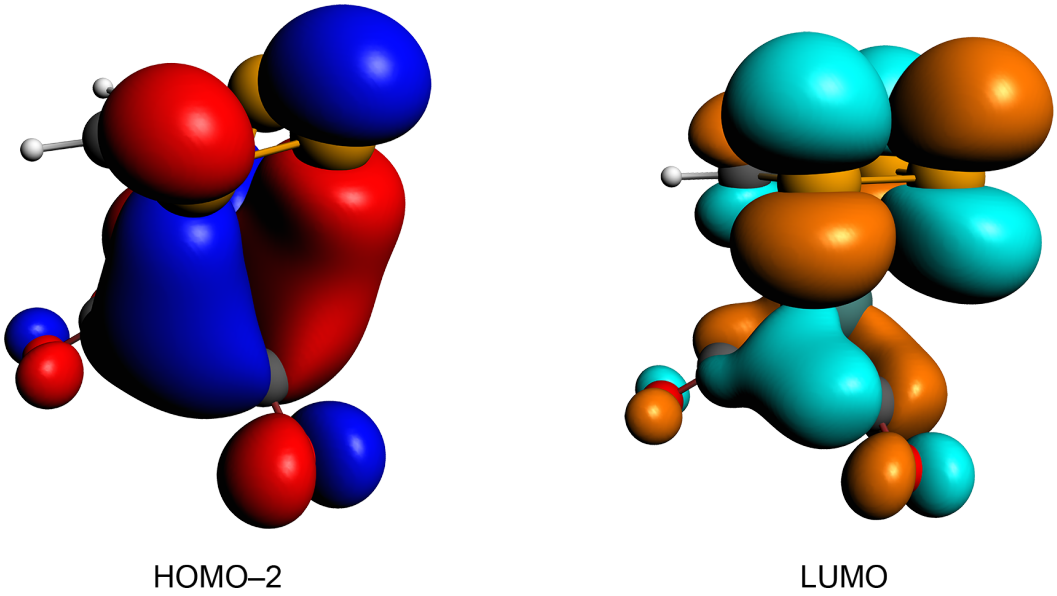

Figure 4.15: Kohn-Sham molecular orbital representations (contour values 0.025 au) for the HOMO–2 and LUMO in **26**.

In **26**–**31** the HOMO–2 is lowered in energy (it is the HOMO–1 in $[(\eta^5\text{-}C_5H_5)Mo(CO)_3]^-$), and forms a prominent δ bonding interaction with a pnictolide π orbital that possesses a single angular node (Figure 4.15). In all cases the LUMO is an antibonding ligand π orbital with two angular nodes.

4.6.5 Mass Spectrometric Studies

Further corroboration of the composition of **26**–**31** was obtained from electrospray mass spectrometry of DMF solutions of the complexes. Table 4.11 presents the observed data. In the negative ion mode the complexes were observed as the molecular parent ion, while in the positive ion mode the cation-paired complexes could generally be seen.

Anion	Negative ion mode	Positive ion mode
26	300.8 $[M]^-$	Not observed
27	432.7 $[M]^-$	1039.1 $\{M+[K(18\text{-crown-}6)]_2\}^+$
28	452.2 $[M]^-$	1058.1 $\{M+[K(18\text{-crown-}6)]_2\}^+$
29	584.8 $[M]^-$	1415.5 $\{M+[K(2,2,2\text{-crypt})]_2\}^+$
30	376.9 $[M]^-$	Not observed
31	508.8 $[M]^-$	1115.1 $\{M+[K(18\text{-crown-}6)]_2\}^+$

4.7 Conclusion

This chapter has described the synthesis and characterization of a series of anions of the form $[1,2,3\text{-}E_3C_2RR']^-$ (R = R′ = H, E = P (**17**), As (**18**); R = R′ = Ph, E = P (**19**), As (**20**); R = H, R′ = Ph, E = P (**21**), As (**22**)) from heptapnictide Zintl anion precursors. All of the phosphorus species had been observed previously, either by ^{31}P NMR spectroscopy or in the coordination sphere of a transition metal but never isolated as free anions. The analogous arsenic compounds are entirely novel anions. **17**–**22** were characterized by single crystal X-ray diffraction, multielement NMR spectroscopy and mass spectrometry. DFT calculations were performed to probe the electronic structure of the anions.

The utility of this "Zintl anion" methodology was demonstrated for the synthesis of the remaining known 1,2,3-triphospholide, the $[1,2,3\text{-}P_3C_6H_4]^-$ anion (**23**), which was observed by ^{31}P NMR spectroscopy and crystallographically characterized as the $[Cs(18\text{-crown-}6)]^+$ salt.

Preliminary studies on the coordination chemistry of the parent anions **17** and **18** with a ruthenium organometallic resulted in the formation and characterization of $[Ru(\eta^5\text{-}E_3C_2H_2)\{\eta^1\text{-}CH_3C(CH_2)_2\}\{\eta^3\text{-}CH_3C(CH_2)_2\}]^-$ (E = P (**24**), As (**25**)). These anions have been characterized by a combination of single crystal X-ray diffraction, multielement NMR spectroscopy and mass spectrometry.

A homologous series of monoanionic $[(\eta^5\text{-}E_3C_2RR')Mo(CO)_3]^-$ (R = R′ = H; E = P (**26**), As (**27**); R = R′ = Ph; E = P (**28**), As (**29**); R = Ph, R′ = H; E = P (**30**), As (**31**)) piano stool geometry complexes were formed by derivatization of the free anions **17**–**22** with $Mo(CO)_3(L)_3$ (L = CO, MeCN). These anions were characterized by a combination of single crystal X-ray diffraction, multielement NMR spectroscopy, electrospray mass spectrometry and DFT level calculations. IR spectroscopy was used to probe the carbonyl stretching frequencies of the $Mo(CO)_3$ unit, and comparison of the obtained frequencies with those for the all carbon analogue $[(\eta^5\text{-}C_5H_5)Mo(CO)_3]^-$ showed the 1,2,3-tripnictolides to be significantly enhanced π acceptor ligands relative to the cyclopentadienide anion.

4.8 REFERENCES

(1) Bartsch, R.; Nixon, J. F. *Polyhedron* **1989**, *8*, 2407.

(2) Bartsch, R.; Nixon, J. F. *J. Organomet. Chem.* **1991**, *415*, C15–C18.

(3) Lynam, J. M.; Copsey, M. C.; Green, M.; Jeffery, J. C.; McGrady, J. E.; Russell, C. A.; Slattery, J. M.; Swain, A. C. *Angew. Chem., Int. Ed.* **2003**, *42*, 2778–2782.

(4) Fish, C.; Green, M.; Jeffery, J. C.; Kilby, R. J.; Lynam, J. M.; Russell, C. A.; Willans, C. E. *Organometallics* **2005**, *24*, 5789–5791.

(5) Baudler, M.; Düster, D.; Ouzounis, D. *Z. Anorg. Allg. Chem.* **1987**, *544*, 87–94.

(6) Hahn, J.; Baudler, M. *Z. Naturforsch. B* **1990**, *45*, 1139–42.

(7) Maigrot, N.; Sierra, M.; Charrier, C.; Mathey, F. *Bull. Soc. Chim. Fr.* **1994**, *131*, 397–399.

(8) Butts, C. P.; Green, M.; Hooper, T. N.; Kilby, R. J.; McGrady, J. E.; Pantazis, D. A.; Russell, C. A. *Chem. Commun.* **2008**, 856–858.

(9) García, F.; Less, R. J.; Naseri, V.; McPartlin, M.; Rawson, J. M.; Tomas, M. S.; Wright, D. S. *Chem. Commun.* **2008**, 859–861.

(10) Edge, R.; Less, R. J.; Naseri, V.; McInnes, E. J. L.; Mulvey, R. E.; Wright, D. S. *Dalton Trans.* **2008**, 6454–6460.

(11) Scherer, O. J.; Hilt, T.; Wolmershäuser, G. *Angew. Chem., Int. Ed.* **2000**, *39*, 1425–1427.

(12) Deng, S.; Schwarzmaier, C.; Eichhorn, C.; Scherer, O.; Wolmershäuser, G.; Zabel, M.; Scheer, M. *Chem. Commun.* **2008**, 4064–4066.

(13) Deng, S.; Schwarzmaier, C.; Zabel, M.; Nixon, J. F.; Timoshkin, A. Y.; Scheer, M. *Organometallics* **2009**, *28*, 1075–1081.

(14) Turbervill, R. S. P.; Goicoechea, J. M. *Chem. Commun.* **2012**, *48*, 6100–6102.

(15) Turbervill, R. S. P.; Jupp, A. R.; McCullough, P. S. B.; Ergöçmen, D.; Goicoechea, J. M. *Organometallics* **2013**, *32*, 2234–2244.

(16) Hückel, E. *Z. Physik* **1931**, *70*, 204–286.

(17) Hückel, E. *Z. Physik* **1931**, *72*, 310–337.

(18) Frost, A. A.; Musulin, B. *J. Chem. Phys.* **1953**, *21*, 572–573.

(19) Cloke, F. G. N.; Green, J. C.; Hanks, J. R.; Nixon, J. F.; Suter, J. L. *J. Chem. Soc., Dalton Trans.* **2000**, 3534–3536.

(20) Himeshima, Y.; Sonoda, T.; Kobayashi, H. *Chem. Lett.* **1983**, *12*, 1211–1214.

(21) Pyykkö, P.; Atsumi, M. *Chem. Eur. J.* **2009**, *15*, 186–197.

(22) Pyykkö, P.; Atsumi, M. *Chem. Eur. J.* **2009**, *15*, 12770–12779.

(23) Allen, F. H.; Kennard, O.; Watson, D. G.; Brammer, L.; Orpen, A. G.; Taylor, R. *J. Chem. Soc., Perkin Trans. 2* **1987**, S1–S19.

(24) Cloke, F. G. N.; Hanks, J. R.; Hitchcock, P. B.; Nixon, J. F. *Chem. Commun.* **1999**, 1731–1732.

(25) Clark, T.; Elvers, A.; Heinemann, F. W.; Hennemann, M.; Zeller, M.; Zenneck, U. *Angew. Chem., Int. Ed.* **2000**, *39*, 2087–2091.

(26) Black, S. J.; Francis, M. D.; Jones, C. *J. Chem. Soc., Dalton Trans.* **1997**, 2183–2190.

(27) Elschenbroich, C. *Organometallics*; 3rd ed.; Wiley-VCH: Weinheim, 2006.

(28) Tolman, C. A. *Chem. Rev.* **1977**, *77*, 313–348.

(29) Crabtree, R. H. In *The Organometallic Chemistry of the Transition Metals*; John Wiley & Sons, Inc., 2005; pp. 87–124.

(30) Brown, T. L.; Darensbourg, D. J. *Inorg. Chem.* **1967**, *6*, 971–977.

(31) Haines, R. J.; Nolte, C. R. *J. Organomet. Chem.* **1970**, *24*, 725–736.

CHAPTER FIVE

Synthesis and Coordination Chemistry of Novel 1,2,3-Tripnictolide Anions

5.1 INTRODUCTION

Beyond their enhanced π acceptor ability relative to the cyclopentadienide anion, phospholides (and by extension, arsolides) possess a lone pair on every phosphorus atom. This makes such ligands capable of interactions with metal fragments beyond the ubiquitous η^5 coordination mode that would be predicted by analogy with carbon chemistry. The fundamental chemistry behind this concept was discussed in Chapter One, and some applications briefly mentioned. This section will expand on the ways in which unique properties of the phospholides have been exploited, focusing on their application in catalysis.

Scherer and co-workers have extensively studied and reviewed the chemistry of P_n and As_n ligands.[1] A variety of homo- and hetero- multimetallic complexes have been characterized containing a wide number of pnictogen atoms. A particularly intensively studied molecule is the pentaphospholide-containing species $[Fe(\eta^5\text{-}C_5Me_5)(\eta^5\text{-}P_5)]$. The secondary coordination available has resulted in the isolation of molecules exhibiting a wide range of coordination modes, from triple decker complexes to bridging η^1 and η^2 systems.[2–5]

More recently, the group of Scheer has used the reaction of $[Fe(\eta^5\text{-}C_5Me_5)(\eta^5\text{-}P_5)]$ with copper halides to form both coordination polymers and supramolecular assemblies, the first of which was pictured in Chapter One.[6,7] More practical applications of the secondary coordinating abilities of phospholides are found in asymmetric catalysis, which has notably been exploited by Fu and co-workers in a host of metal catalysed organic transformations.

Planar chirality is induced upon η^5-coordination of disymmetrically substituted cyclopentadienides to a metal centre (i.e. the cyclopentadienides are prochiral).[8] This similarly applies to phospholide ligands. However, the resulting metal complexes possess

the ability for secondary coordination through the lone pair on phosphorus. Phosphametallocenes, particularly ferrocenes are popular for their thermodynamic stability and inertness towards ligand substitution. Inclusion of an additional chelating tether confers conformational stability upon the complexes that can be formed between the phosphametallocene and a catalytically active metal. Monophosphametallocenes with a variety of chelating arms have been prepared and their properties as ligands for a wide range of catalytic applications studied.[9]

The most notable class of ligand possess a chelating oxazoline moiety (Figure 5.1). These have been used as ligands in copper catalysed enantioselective cycloadditions and conjugate addition reactions.[10–13] Additionally, they are excellent supporting ligands for palladium catalyzed alkylations.[14]

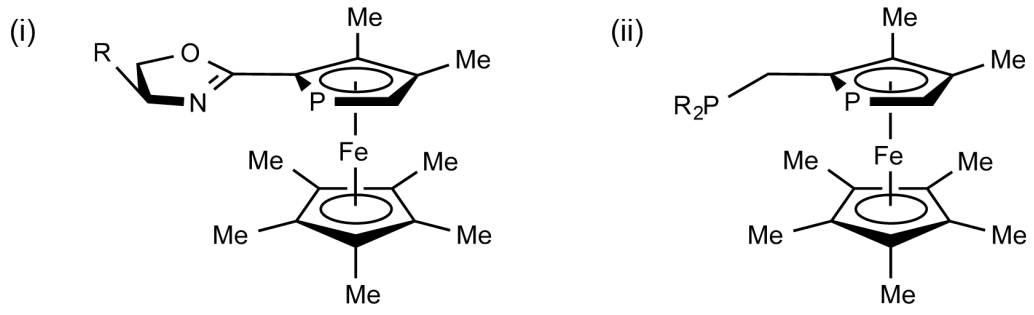

Figure 5.1: Planar chiral chelating phosphaferrocene ligands bearing oxazoline (i) and phosphine (ii) donors.

A second type of monophosphaferrocene, bearing a phosphine donor, have been used as ligands for rhodium catalysed isomerizations and hydrogenations.[15–19]

5.2 OBJECTIVES

The chemistry detailed in Chapter Four allowed the synthesis of a related series of 1,2,3-tripnictolides, all of which had some literature precedent either as free anions or in transition metal complexes. We sought to extend our Zintl anion methodology to the synthesis of entirely novel 1,2,3-tripnictolide anions. With the chemistry described in Section 5.1 in mind, we decided to focus synthetic efforts towards molecules that would be capable of exhibiting multiple coordination modes or possessing groups that might allow for further chemical transformations. This chapter will describe the results of these investigations.

The synthesis and coordination chemistry of the 4-(2′-pyridyl)-1,2,3-triphospholide anion towards molybdenum carbonyl fragments will be discussed.[20] Additionally, the synthesis of two further novel 1,2,3-tripnictolides bearing pendant amine and ferrocenyl groups will be reported. The drawbacks of this new synthetic methodology will be highlighted using these examples.

5.3 SYNTHESIS OF THE 4-(2′-PYRIDYL)-1,2,3-TRIPHOSPHOLIDE ANION

We decided to target a 1,2,3-triphospholide anion bearing a pendant 2-pyridyl donor group. The logical synthon for this anion is 2-ethynylpyridine. Upon dropwise addition of a slight excess (based on phosphorus) of 2-ethynylpyridine to a solution of [K(2,2,2-crypt)][**1**] in pyridine a deep purple colour instantly develops. Analysis of the resulting mixture by ^{31}P NMR spectroscopy revealed the multiplet resonances characteristic of the expected 1,2,3-triphospholide (Scheme 5.1). We postulate that the intense purple colouration of the reaction mixture is likely due to formation of pyridyl and bipyridyl radical anions.[21] This effect was previously described in Chapter Two.

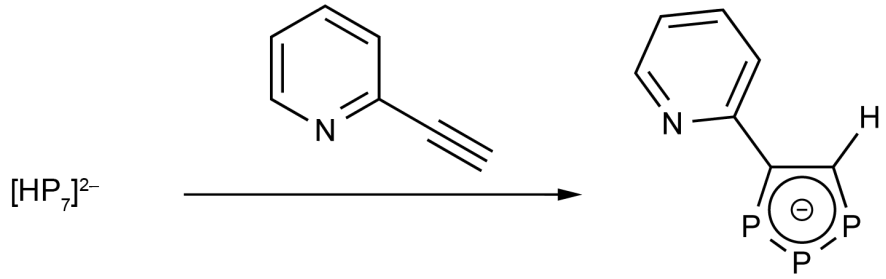

Scheme 5.1: Synthesis of the $[P_3C_2H(2\text{-pyridyl})]^-$ anion (**32**).

Following aerobic workup, which decomposes and precipitates the undesired radical sideproducts, the $[P_3C_2H(2\text{-pyridyl})]^-$ (**32**) anion can be isolated in approximately 20% yield as a pale orange crystalline solid. The species is isolobal to the 2-pyridylcyclopentadienide anion, the coordination chemistry of which has been particularly studied as a ferrocene derivative.[22–25] Of the related isolobal phospholides, only the 2-(2′-pyridyl)monophospholide has been synthesized.[26] Its ferrocene derivative has been shown to act as a κ^2-*P*,*N* chelating ligand towards $W(CO)_4$.[27]

5.3.1 Structure of 32

Single crystals of [K(2,2,2-crypt)][**32**] of suitable quality for single crystal X-ray diffraction were obtained by diffusion of hexane into a THF solution of the product. The asymmetric unit contains one anion of **32**, which possesses a *trans*-planar configuration, accompanied by a single charge-balancing $[K(2,2,2\text{-crypt})]^+$ cation. The structure of **32** is shown in Figure 5.2. In addition to the experimental study, the geometries of the *cis* and *trans* isomers (which refers to the relative orientations of P3 and N1, Figure 5.3) of **32** were optimized at the DFT level of theory, and show good agreement with the experimentally determined structure. The *cis* isomer is slightly higher in energy than the *trans* isomer by 1.59 kJ mol^{-1}, which is insignificant.

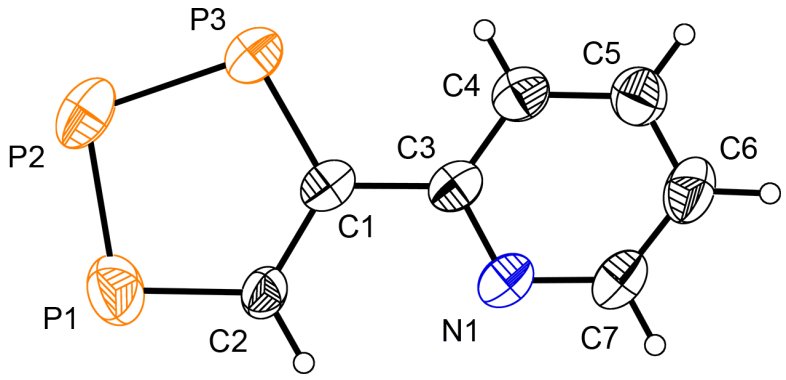

Figure 5.2: Thermal ellipsoid plot of **32**.Thermal ellipsoids are set at the 50% probability level. Hydrogen atoms are shown as spheres of arbitrary radius.

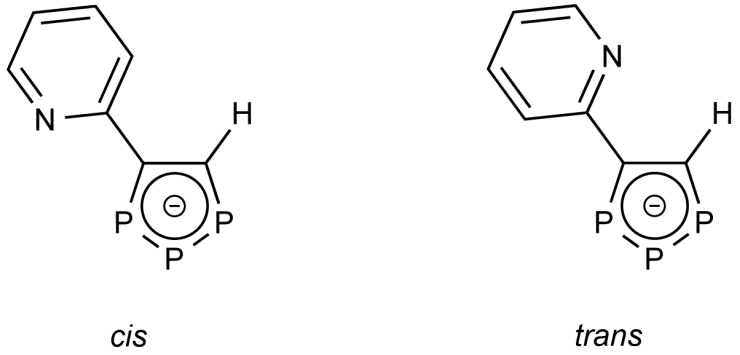

Figure 5.3: The *cis* and *trans* isomers of **32**.

Selected bond metric data for **32** are shown in Table 5.2, along with the distances for the two computed isomers of **32** (*cis* and *trans*). The internuclear distances generally agree well with those previously reported for other 1,2,3-triphospholides.[28,29] The notable exception is C1–C2, which is significantly elongated (1.460(4) Å) when compared to related species (for example in **19** C1–C2: 1.402(2) Å). While this might arise from an increased degree of π-bonding between the two aromatic phospholide and pyridyl ring systems, both the inter-ring bond length of 1.488(4) Å and torsion angle (33.1º) would seem to preclude such an interpretation. This is additionally supported by the computational studies, which show a C1–C2 distance of 1.402 and 1.401 Å for the *cis* and *trans* isomers of **32**, respectively. The most reasonable explanation for the elongated C1–C2 distance would therefore seem to be

unresolved discrete positional crystallographic disorder due to the presence of both the *cis* and *trans* isomers occupying the same site in the lattice. If such disorder is present it could not be resolved crystallographically.

Table 5.1: Bond metric data for the both the experimentally determined structure of **32** and the two computed isomers of **32**.

Bond distance (Å)	**32**	***cis*-32$_{calc}$**	***trans*-32$_{calc}$**
P1–P2	2.102(1)	2.130	2.136
P2–P3	2.072(1)	2.112	2.110
P3–C1	1.757(3)	1.784	1.782
C1–C2	1.460(4)	1.402	1.401
C2–P1	1.737(3)	1.745	1.745
C1–C3	1.488(4)	1.477	1.480
C3–C4	1.392(4)	1.413	1.412
C4–C5	1.385(4)	1.390	1.389
C5–C6	1.379(5)	1.398	1.400
C6–C7	1.376(5)	1.395	1.395
C7–N1	1.335(4)	1.340	1.343
N1–C3	1.361(3)	1.358	1.358
Total bonding energy (kJ mol^{-1})	-	–10,244.85	–10,246.44

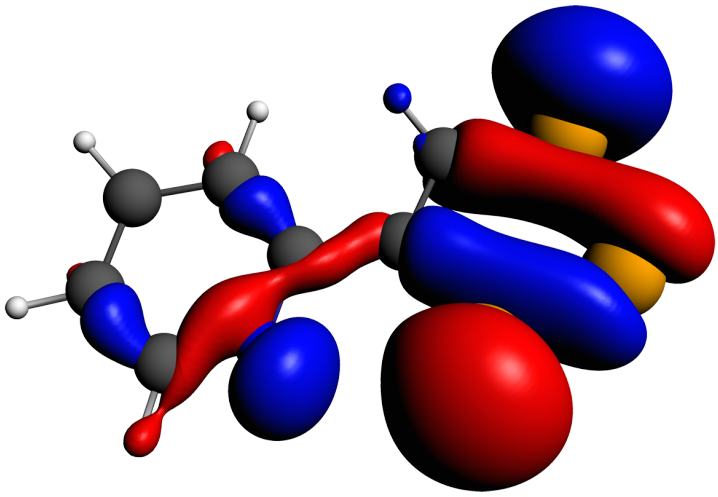

Figure 5.4: Kohn-Sham molecular orbital representation (contour values 0.03 au) of the HOMO–2 in for the *cis* isomer of **32**.

The HOMO and HOMO–1 of ***trans*-32$_{calc}$** exhibit pnictolide ring π-bonding character, each possessing a single angular node. Significant mixing of both the phosphorus lone pairs and

pyridyl π system into the frontier orbitals is seen. This is additionally observed in the unoccupied π-antibonding LUMO, LUMO+1 and LUMO+2. A molecular orbital with significant nitrogen lone pair character is found as the HOMO–3 in ***trans*-32$_{calc}$**, and as the HOMO–2 in ***cis*-32$_{calc}$**, hinting at the ability of **32** to form a κ^2-*P*,*N* chelate (Figure 5.4).

5.3.2 NMR Spectroscopic Studies on 32

[K(2,2,2-crypt)][**32**] was characterized in a d_8-THF solution using multielement NMR spectroscopy. The ^{31}P NMR spectrum displays three equal intensity multiple resonances at 293.1, 278.3 and 274.3 ppm corresponding to P2, P3 and P1, respectively (using the numbering scheme in Figure 5.2). This spectrum was simulated to extract the internuclear coupling constants (Appendix A). The chemical shifts and coupling constants measured are comparable to those observed previously for related systems, and agree with the anions formulation as an aromatic 1,2,3-triphospholide anion. The phospholide proton resonates as a ddd multiplet at 9.88 ppm in the ^{1}H NMR spectrum, collapsing to a singlet on ^{31}P decoupling. The two phospholide carbon resonances are observed at 162.3 (C2) and 161.3 (C1).

5.3.3 Mass Spectrometric Studies

Negative ion mode electrospray ionization mass spectrometry of DMF solutions of [K(2,2,2-crypt)][**32**] revealed a peak with an *m/z* ratio of 195.6. The positive ion mode mass spectrum showed a mass envelope corresponding to the cation-paired species $\{[K(2,2,2\text{-crypt})]_2[\mathbf{32}]\}^+$ at 1026.8 Da.

5.4 Reactivity of the 4-(2′-Pyridyl)-1,2,3-triphospholide Anion

We were prompted to explore the coordination chemistry of **32**, and particularly intrigued by the additional coordination modes available. Similarly, and inspired by the work of Fu (amongst others), we wanted to probe the possibility of synthesizing a proof of concept bimetallic system. We decided to use molybdenum carbonyl fragments for a variety of reasons. They are readily available, diamagnetic species that carry several spectroscopic handles allowing the properties of a coordinated ligand to be probed using a variety of techniques. The reactivity observed for **32** is summarized in Scheme 5.2.

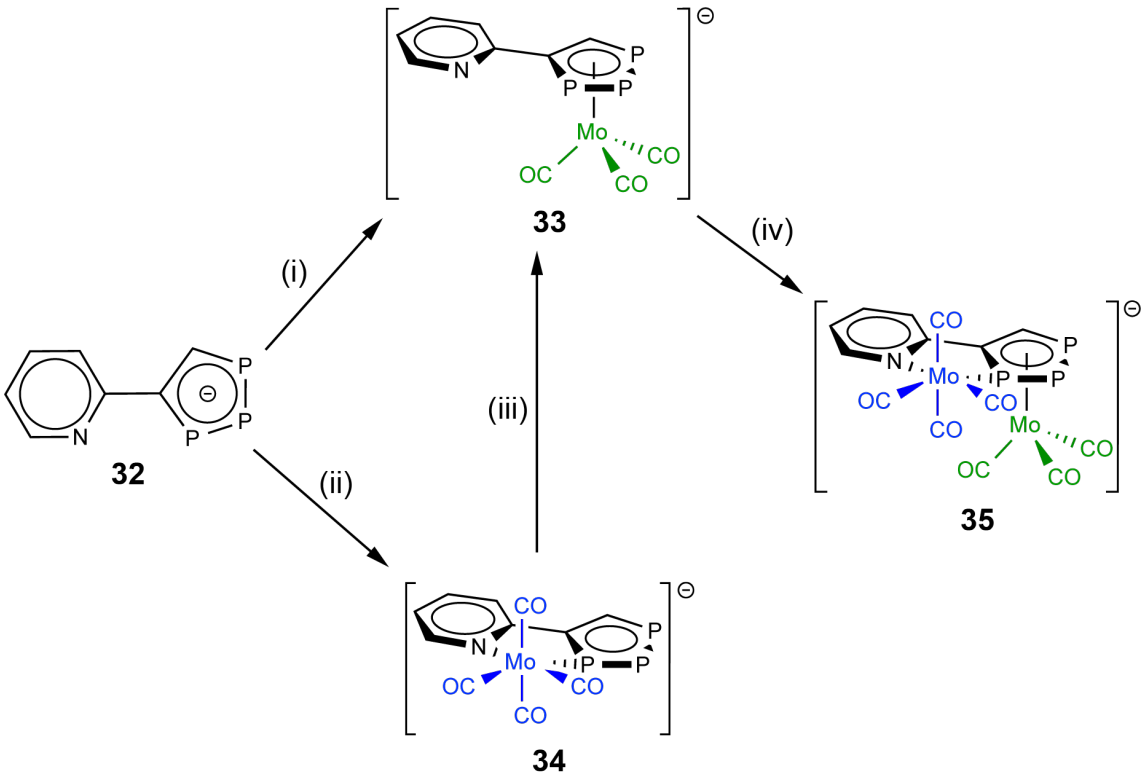

Scheme 5.2: Summary of the coordination chemistry of **32**.

5.4.1 Synthesis of 33

Reaction of [K(2,2,2-crypt)][**32**] with $Mo(CO)_6$ or $Mo(py)_3(CO)_3$ in THF resulted in the formation of the expected η^5-coordinated complex $[(\eta^5\text{-}\mathbf{32})Mo(CO)_3]^-$ (**33**). The reaction is quantitative by ^1H and ^{31}P NMR spectroscopy, and the complex can be isolated in high yield as an orange-yellow solid after a simple workup.

5.4.1.1 Structure of 33

Crystals of [K(2,2,2-crypt)][**33**] were grown by diffusion of hexane into a THF solution of the product at 5 ºC. The structure crystallizes in the highly symmetric *Cmca* space group, with several of the atoms of the anionic complex lying on crystallographic special positions. In addition, the triphospholide moiety exhibits positional disorder over two discrete positions such that both the *cis*- and *trans*-planar isomers of the triphospholide are present. These complications mean that a detailed analysis of the bond metric data in the complex is inadvisable, however the data are of sufficient quality to confirm the composition and connectivity of the anion. The structure of **33** is shown in Figure 5.5.

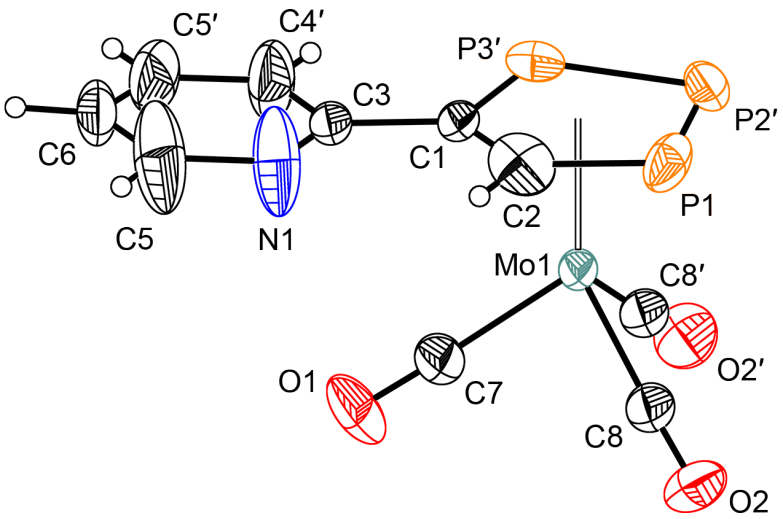

Figure 5.5: Thermal ellipsoid plot of **33**. Thermal ellipsoids are shown at the 50% probability level. Hydrogen atoms are shown as spheres of arbitrary radius. Symmetry operation ′: 1 – x, +y, +z.

The geometries of the *cis*- and *trans*-planar conformations of the complex were computationally optimized using DFT methods. The results show that the *trans*-isomer is modestly lower in energy by 2.69 kJ mol^{-1}, although as for **32** it is not significant. Table 5.2 presents selected bond distances for the experimental and computational geometries. The bond distances are similar to those in the free phospholide and related complexes. The Mo–P bonds to the phospholide ring are longer than the Mo–C bonds, in accordance with the increased atomic radius of phosphorus as compared to carbon.

Table 5.2: Bond metric data for **33**.

Bond distance (Å)	**33**	***cis*-33$_{calc}$**	***trans*-33$_{calc}$**
P1–P2	2.097(3)	2.153	2.157
P2–P3	2.153(5)	2.168	2.164
P3–C1	1.772(4)	1.808	1.806
C1–C2	1.429(11)	1.415	1.414
C2–P1	1.702(17)	1.771	1.768
C1–C3	1.489(3)	1.491	1.495
C3–C4	1.340(3)	1.406	1.406
C4–C5	1.364(4)	1.394	1.391
C5–C6	1.357(5)	1.395	1.398
C6–C7	1.357(5)	1.397	1.395
C7–N1	1.364(4)	1.340	1.343
N1–C3	1.340(3)	1.351	1.351
Mo1–P1	2.610(1)	2.607	2.607
Mo1–P2	2.616(1)	2.696	2.700
Mo1–P3	2.536(4)	2.660	2.651
Mo1–C1	2.361(2)	2.425	2.416
Mo1–C2	2.372(17)	2.432	2.436
Mo1–C8	1.964(3)	1.963	1.963
Mo1–C9	1.962(2)	1.954	1.955
Mo1–C10	1.962(2)	1.958	1.958
C8–O1	1.157(4)	1.179	1.179
C9–O2	1.155(3)	1.180	1.179
C10–O3	1.155(3)	1.177	1.177
Total bonding energy (kJ mol^{-1})	-	–15,892.21	–15,894.9

The increased π acceptor properties of the phospholides as compared to the all carbon analogues was documented in Chapter Four. This is due to the lowering of the π manifold,

which facilitates δ interactions between the ligand and metal centre. Such an interaction is clearly observed as the HOMO–2 Kohn-Sham molecular orbital of **33**$_{calc}$ (Figure 5.6).

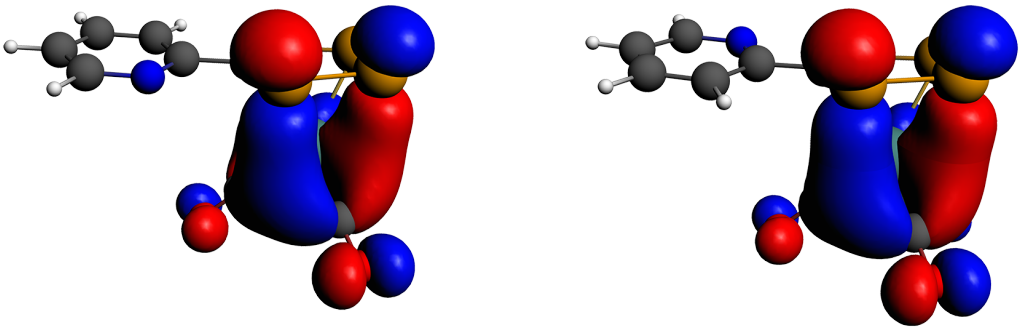

***cis*-33**$_{calc}$ HOMO–2 ***trans*-33**$_{calc}$ HOMO–2

Figure 5.6: Kohn-Sham molecular orbital representations (contour values 0.03 au) of the δ bonding HOMO–2 of **33**.

5.4.1.2 NMR Spectroscopic Studies on 33

The ^{31}P NMR spectrum of **33** exhibits three multiplet resonances at 77.6, 70.8 and 42.4 ppm corresponding to P3, P1 and P2, respectively (Figure 5.5). These are shifted significantly upfield from their values in **32**. P2 experiences a greater change in chemical shift (Δδ = –250.7 ppm) compared to P1 and P3 (approximately –200 ppm). A similar effect was observed for the η^5-1,2,3-tripnictolide complexes discussed in Chapter Four. The spectrum was simulated to extract the *J* values, which were in agreement with the previously documented values, and show a slight decrease upon coordination to the metal centre.

The ^{1}H and ^{13}C{^{1}H} NMR spectra are both consistent with the described formulation of the complex. The phospholide proton appears as a ddd multiplet at 6.84 ppm, and the two phospholide carbon atoms C1 and C2 resonate as multiplets due to phosphorus coupling at 134.3 and 114.9 ppm, respectively. A singlet resonance arising from the carbonyl groups is observed at 228.2 ppm, implying rapid rotation around the Mo–ring centroid on the NMR timescale.

5.4.1.3 IR Spectroscopic Studies on 33

The IR spectrum of **33** was recorded in a Nujol mull. Carbonyl stretching bands were observed at 1924, 1828 and 1812 cm^{-1}, which are comparable to those recorded for **26**–**31**. This is evidence for the enhanced π acceptor ability of the triphospholides relative to their isolobal all carbon analogues (c.f. $[(\eta^5\text{-}C_5H_5)Mo(CO)_3]^-$ 1884 and 1760 cm^{-1}).

5.4.1.4 Mass Spectrometric Studies

The negative ion mode electrospray ionization mass spectrum of a DMF solution of [K(2,2,2-crypt)][**33**] showed a mass envelope for the molecular ion at 378.5 Da. Evidence for the cation-paired species $\{[K(2,2,2\text{-crypt})]_2[\mathbf{33}]\}^+$ was seen in the positive ion mode at *m/z* 1210.0.

5.4.2 Synthesis of 34

Having synthesized the η^5-coordinated complex, **33**, we turned our attention to attempting to access alternative coordination modes of **32**. The *cis*-conformation of the ligand brings the lone pairs of P3 and the pyridyl nitrogen into an arrangement that is reminiscent of bidentate chelating ligands such as 2,2′-bipyridine. We therefore wondered whether, by judicious choice of metal reagent, we could access a κ^2-*P*,*N* chelating mode for **32**.

Monitoring the reaction of [K(2,2,2-crypt)][**32**] with $Mo(COD)(CO)_4$ in CD_2Cl_2 by NMR spectroscopy revealed the gradual disappearance of the resonances corresponding to **32** with concomitant growth of a new set of resonances. These were assigned to the $[(\kappa^2\text{-}P,N\text{-}\mathbf{32})Mo(CO)_4]^-$ (**34**) anion. Upon leaving the reaction mixture for extended periods, this complex slowly decomposes in solution with loss of CO to form **33**. Quantitative conversion from **34** to **33** can be achieved simply by heating solutions at reflux in THF.

Attempts were made to convert from **33** to **34** using various pressures of CO gas, but no conversion was observed. The tungsten analogue of **33**, $\mathbf{33_W}$, (synthesized in situ from [K(2,2,2-crypt)][**32**] and $W(py)_3(CO)_3$) appears to show a very limited conversion to $\mathbf{34_W}$ (less than one percent by integration of the ^{31}P NMR spectrum) under approximately two atmospheres of CO, reverting to $\mathbf{33_W}$ when the pressure is released. This chemistry was not explored further due to the requirement for specialized equipment to safely handle higher (and known) pressures of CO.

Taken together, these data suggest that **32** has a very strong preference for η^5 coordination to molybdenum (and tungsten) carbonyl fragments. Despite the thermodynamic instability of **34** with respect to loss of carbon monoxide, it was possible to isolate and characterize it as an orange solid by crystallization from DCM/pentane mixtures at –35 ºC.

5.4.2.1 Structure of 34

The complex was crystallographically characterized in [K(2,2,2-crypt)][**34**]·$0.5CH_2Cl_2$. The structure shows a pseudo-octahedral metal centre coordinated by **32** in a κ^2-*P*,*N* chelating fashion (Figure 5.7). Four carbonyl groups (two axial and two equatorial) make up the coordination sphere of the molybdenum(0) centre. The anion has overall approximate C_s symmetry.

In addition to the experimental studies, the geometry of **34** was optimized at the DFT level of theory. The computationally determined structure shows very good agreement with the experimental structure, with a slight lengthening of most bonds as is typically observed as a due to the simplistic continuum dielectic model used to simulate the presence of cations in the lattice. Bond metric data for both **34** and $\mathbf{34_{calc}}$ are shown in Table 5.3.

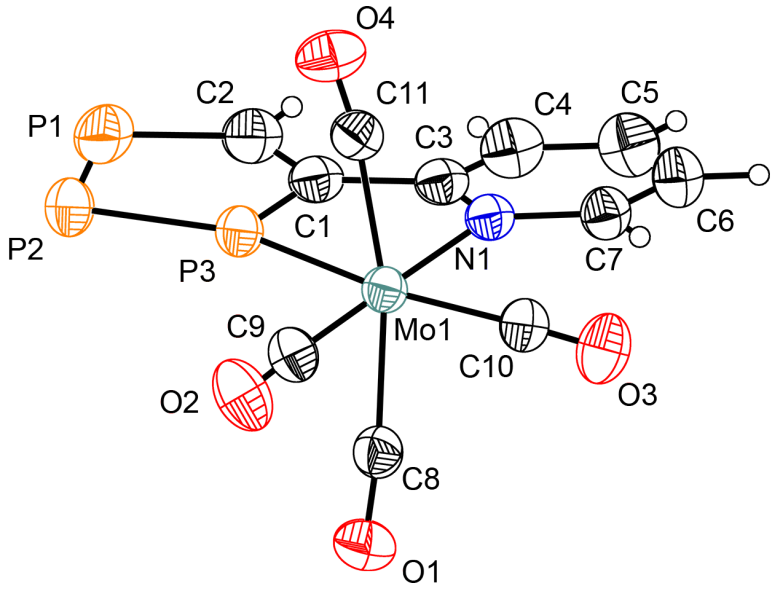

Figure 5.7: Thermal ellipsoid plot of **34**. Thermal ellipsoids are set at the 50% probability level. Hydrogen atoms are shown as spheres of arbitrary radius.

Table 5.3: Bond metric data for **34**.

Bond distance (Å)	34	34_{calc}
P1–P2	2.118(1)	2.147
P2–P3	2.064(1)	2.091
P3–C1	1.736(2)	1.757
C1–C2	1.403(3)	1.402
C2–P1	1.726(2)	1.741
C1–C3	1.462(3)	1.460
C3–C4	1.400(3)	1.411
C4–C5	1.367(3)	1.386
C5–C6	1.383(3)	1.399
C6–C7	1.378(3)	1.388
C7–N1	1.352(2)	1.355
N1–C3	1.369(2)	1.376
Mo1–P3	2.483(1)	2.511
Mo1–N1	2.323(2)	2.353
Mo1–C8	2.032(2)	2.043
Mo1–C9	1.956(2)	1.959
Mo1–C10	1.982(2)	1.976
Mo1–C11	2.047(2)	2.042
C8–O1	1.137(3)	1.164
C9–O4	1.156(3)	1.175
C10–O2	1.144(2)	1.176
C11–O3	1.138(2)	1.164

The bond distances within the triphospholide moiety are comparable to those of the free ligand, **32**. The Mo1–P3 and Mo1–N1 bond distances are 2.483(1) and 2.323(2) Å, respectively. These are much closer than would be expected simply by comparing the single bond covalent radii of phosphorus and nitrogen (Δr_{cov} = 0.30 Å).[30] The Mo1–P3 bond is of comparable length to a typical Mo–P bond, but the Mo1–N1 bond is significantly longer than a normal Mo–N bond.[31] A comparable chelating pyridyl donor, such as in Mo(2,2′-bipyridine)$(CO)_4$ has Mo–N distances of 2.249(3) and 2.240(3) Å.[32] A possible explanation for this is the wide bite angle of the ligand (the P–Mo–N bond angle in the resulting five-membered chelate ring is 74.69(4)º). Another explanation for this observation is an increased degree of π backbonding between Mo1 and the phospholide ring. More evidence for this backbonding is found in the Mo–carbonyl bond lengths. The Mo–C bond for the carbonyl *trans* to P3 is significantly longer than the Mo–C bond for the carbonyl *trans* to N1 (1.982(2) and 1.956(2) Å, respectively). The increased bond length implies weaker backbonding between the metal centre and the carbonyl ligand, which can result from a π acceptor ligand (the triphospholide) competing for electron density from the same metal d orbital. Corroborative evidence for such an interaction can be found by performing a frontier orbital analysis of the computational results. The HOMO–4 strongly resembles such a π backbonding interaction between the metal centre and the phospholide π manifold (Figure 5.8).

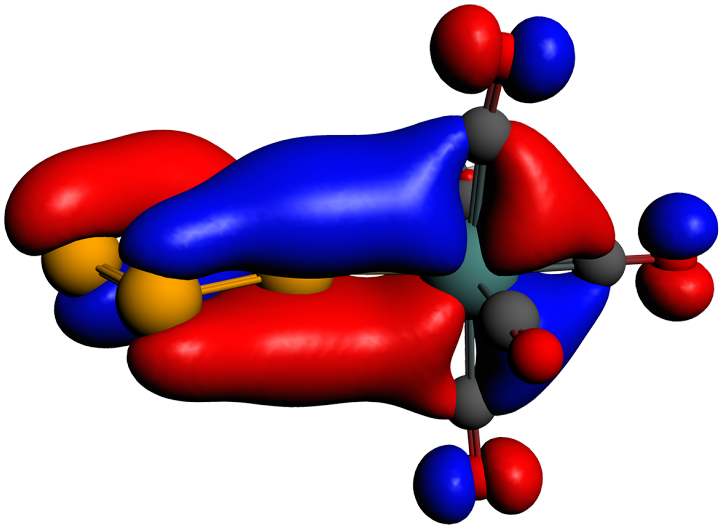

Figure 5.8: Kohn-Sham molecular orbital representation (contour values 0.03 au) of the HOMO–4 of **34**.

5.4.2.2 NMR Spectroscopic Studies on 34

CD_2Cl_2 solutions of [K(2,2,2-crypt)][**34**] were characterized by multielement NMR spectroscopy. In a typical experiment, an NMR tube equipped with a gas-tight valve was charged with [K(2,2,2-crypt)][**32**] and $Mo(COD)(CO)_4$. CD_2Cl_2 (0.5 mL) was added to the mixture, and the reaction monitored by ^{1}H and ^{31}P NMR spectroscopy. The optimal spectra were obtained after approximately 48 hours at 20 ºC, when the mixture contained approximately 85% of **34**, 10% of **32** and 5% of **33** by integration. A typical $^{31}P\{^{1}H\}$ NMR spectrum at this time is shown in Figure 5.9.

The ^{31}P NMR spectrum of **34** shows three multiplet resonances that are only slightly shifted upfield from free **32**, at 266.6, 262.5 and 240.2 ppm for P1, P3 and P2, respectively. This is in contrast to the large upfield shifts observed for **33**. The resonance for P3 is barely shifted ($\Delta\delta$ = –15.8 ppm) while that for P2 is shifted rather substantially ($\Delta\delta$ = –52.9 ppm), which seems somewhat unexpected. This may arise due to the existence of two competing effects at P3, which effectively cancel each other out. The loss of the lone pair on coordination to

Mo would be expected to induce a downfield shift, but significant π backbonding from Mo into the phospholide ring disrupts the aromaticity and results in an upfield shift. The net effect of these two phenomena is a small upfield shift for P3 but a much greater upfield shift for P2, which only experiences the π backbonding effect. P1 is more remote, and relatively less affected.

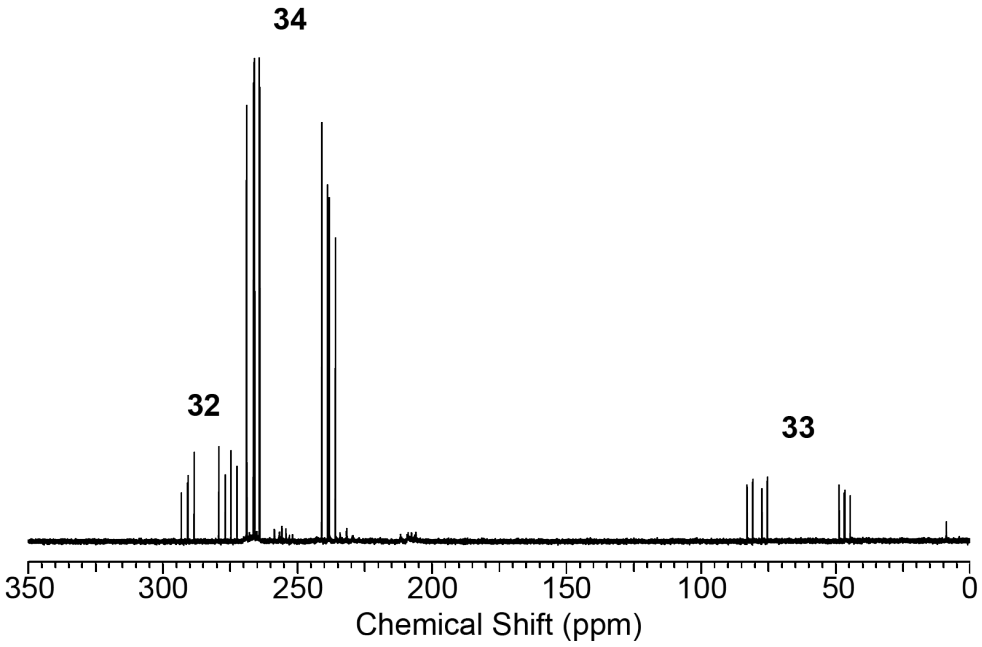

Figure 5.9: $^{31}P\{^{1}H\}$ NMR spectrum of a mixture of [K(2,2,2-crypt)][**32**] and $Mo(COD)(CO)_4$ in CD_2Cl_2 after 48 hours at 20 ºC. **34** is the predominant product, but there are small amounts of **32** and **33** (labelled).

A similarly small change in chemical shift is seen for the phospholide ring proton, which shifts from 9.88 ppm in **32** to 9.51 in **34**. The most telling area of the $^{13}C\{^{1}H\}$ NMR spectrum is found in the carbonyl region (Figure 5.10). The two axial carbonyl ligands (C8 and C11 in Figure 5.6) resonate as a doublet at 207.4 ppm ($^{2}J_{P-C}$ = 11 Hz). The two equatorial carbonyl ligands can be distinguished by their multiplet structure. C10, which lies *trans* to P3, appears as a doublet of doublets ($^{2}J_{P-C}$ = 34 Hz, $^{3}J_{P-C}$ = 3 Hz) at 221.1 ppm due to coupling to both P3 and P2 whereas C9, which lies trans to N1, resonates as a doublet ($^{2}J_{P-C}$ = 6 Hz) since coupling is only resolved to P3.

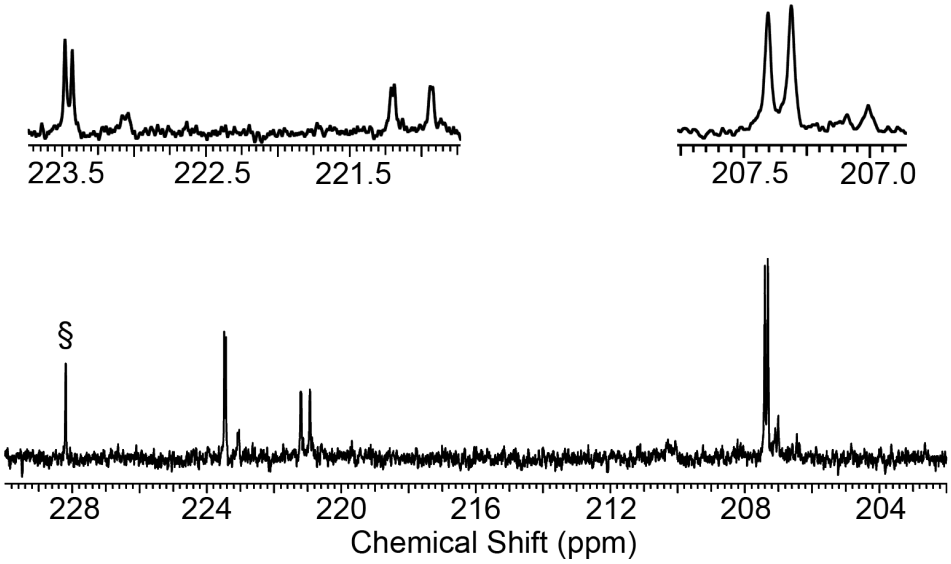

Figure 5.10: Expansion of the carbonyl region of the $^{13}C\{^{1}H\}$ NMR spectrum of a CD_2Cl_2 solution of [K(2,2,2-crypt)][**34**]. The resonance marked with § arises from **33**.

5.4.2.3 IR Spectroscopic Studies on 34

The IR spectrum of **34** recorded in a Nujol mull showed bands at 2004, 1895, 1879 and 1828 cm^{-1} for the carbonyl stretching modes. This is consistent with the C_s symmetry of the complex.

5.4.2.4 Mass Spectrometric Studies

The negative ion mode electrospray mass spectrum of a DMF solution of [K(2,2,2-crypt)][**34**] showed the molecular ion peak corresponding to the η^5 complex, **33**. This is unsurprising, given the desolvation temperature required in the experiment (150 ºC) and the previous observation of CO loss from **34** in solution at 70 ºC. Upon closer inspection, however, a minor mass envelope arising from **34** was visible at 406.0 Da. No evidence of **34** was observed in the positive ion mode mass spectrum.

5.4.3 Synthesis of 35

Disymmetrically substituted 1,2,3-triphospholide anions are prochiral. Upon coordination to a metal centre, a complex with planar chirality results. As discussed earlier, related enantiopure monophosphaferrocene systems have been used as supporting ligands in asymmetric catalysis to achieve a wide variety of synthetic transformations. We were intrigued at the possibility of using the η^5-coordinated, **33**, as a chelating κ^2-*P*,*N* ligand for a further $Mo(CO)_4$ fragment to give a bimetallic system.

The reaction of [K(2,2,2-crypt)][**33**] with $Mo(COD)(CO)_4$ results in the formation of the bimetallic $[\{\mu{:}\eta^5,\kappa^2\text{-}P,N\text{-}\mathbf{32}\}\{Mo(CO)_3\}\{Mo(CO)_4\}]^-$ (**35**) anion after gentle heating. The complex was isolated as an orange-yellow oil following characterization by multielement NMR spectroscopy.

5.4.3.1 Structure of 35

Despite repeated attempts, it did not prove possible to grow a crystal containing **35** suitable for single crystal X-ray diffraction. The combined NMR, IR and mass spectrometric data suggest the formulation of **35** as containing a bridging $\mu{:}\eta^5,\kappa^2$-*P*,*N* ligand, and it was possible to obtain an accurate elemental microanalysis to support the composition. The structure of **35** was optimized at the DFT level of theory using the coordinates from ***cis*-33$_{calc}$** as a starting point. The geometry thus obtained is shown in Figure 5.11. Selected bond metric data for the optimized geometry are presented in Table 5.4. The internuclear distances are very similar to those measured experimentally for **33** and **34**, including the elongated Mo2–N1 distance (2.358 Å in **35$_{calc}$** compared to 2.323(2) and 2.353 Å for **34** and **34$_{calc}$**, respectively).

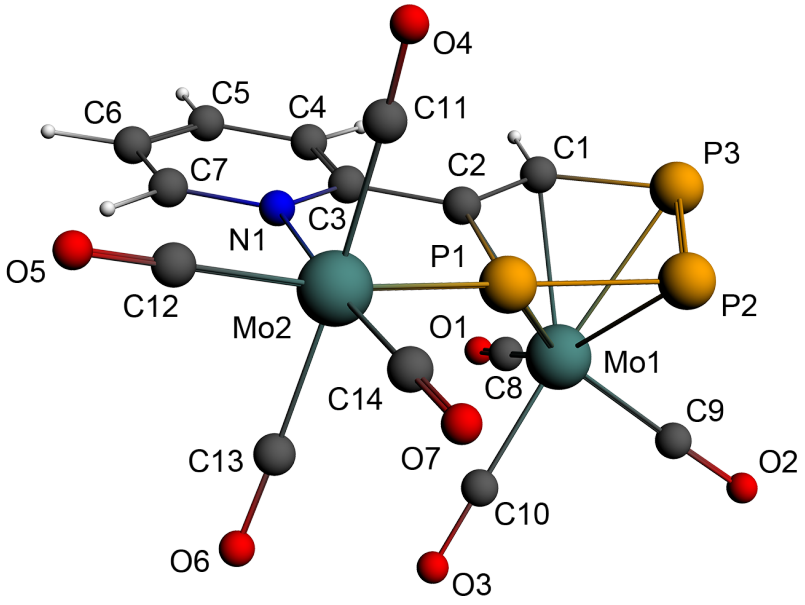

Figure 5.11: Optimized computed geometry of **35**.

Table 5.4: Selected bond metric data for $\mathbf{35}_{calc}$.

Bond distance (Å)	$\mathbf{35}_{calc}$	Bond distance (Å)	$\mathbf{35}_{calc}$
P1–P2	2.184	Mo1–C8	1.963
P2–P3	2.134	Mo1–C9	1.958
P3–C1	1.780	Mo1–C10	1.970
C1–C2	1.417	C8–O1	1.176
C2–P1	1.778	C9–O2	1.175
C1–C3	1.468	C10–O3	1.175
C3–C4	1.408	Mo2–P3	2.515
C4–C5	1.386	Mo2–N1	2.358
C5–C6	1.398	Mo2–C11	2.039
C6–C7	1.388	Mo2–C12	1.975
C7–N1	1.355	Mo2–C13	2.046
N1–C3	1.373	Mo2–C14	1.961
Mo1–P1	2.637	C11–O4	1.163
Mo1–P2	2.716	C12–O5	1.173
Mo1–P3	2.593	C13–O6	1.162
Mo1–C1	2.471	C14–O7	1.174
Mo1–C2	2.363		

5.4.3.2 NMR Spectroscopic Studies on 35

The ^{31}P NMR spectrum of **35** is effectively a superposition of the combined electronic effects observed for the spectra of **33** and **34** (*vide supra*). Three multiplet resonances are observed at 119.4, 63.5 and –21.7 ppm corresponding to P1, P3 and P2, respectively (Figure 5.12).

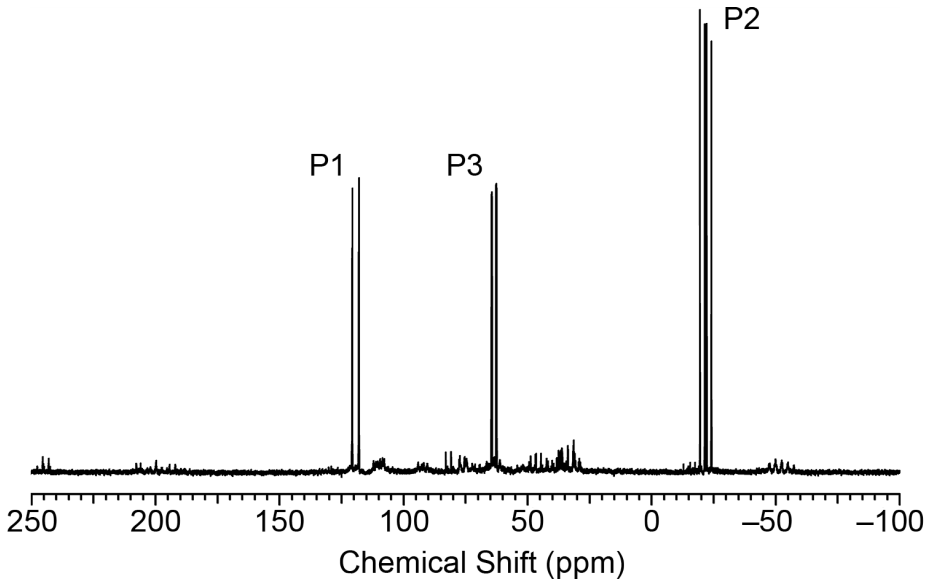

Figure 5.12: $^{31}P\{^{1}H\}$ NMR spectrum of a CD_2Cl_2 solution of [K(2,2,2-crypt)][**35**].

The phospholide proton resonates at 6.68 ppm, symbolic of coordination to a $Mo(CO)_3$ fragment. The most striking evidence for the structure of **35** is found in the $^{13}C\{^{1}H\}$ NMR spectrum, where five carbonyl resonances are observed (Figure 5.13). A singlet at 226.2 ppm arises for the three equivalent carbonyl groups of the $Mo(CO)_3$ fragment, and the remaining four result from the $Mo(CO)_4$ group. As a result of the reduced symmetry relative to **34**, induced by the addition of the η^5-$Mo(CO)_3$ moiety, the two axial carbonyls are no longer equivalent and appear as separate doublets at 206.2 and 205.2 ppm. Two equatorial carbonyls can be distinguished at 222.3 and 217.7 corresponding to the carbonyls *trans* to N1 and P3, respectively.

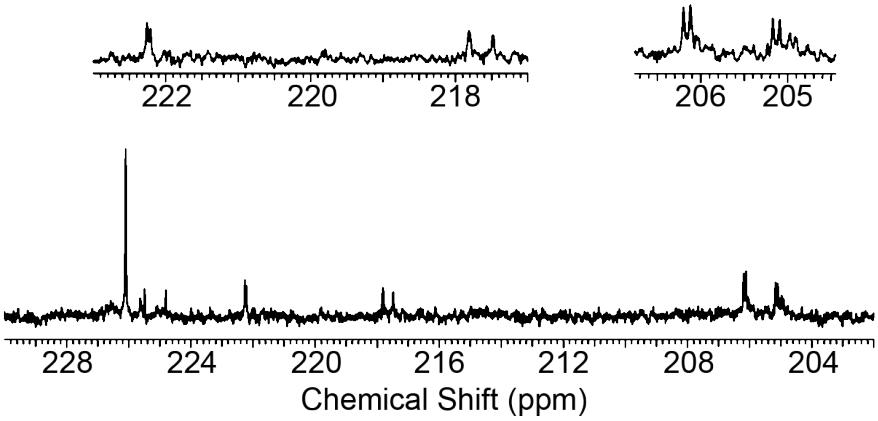

Figure 5.13: Expansion of the carbonyl region of the $^{13}C\{^{1}H\}$ NMR spectrum of a CD_2Cl_2 solution of [K(2,2,2-crypt)][**35**].

5.4.3.3 IR Spectroscopic and Mass Spectrometric studies on 35

The carbonyl region of the IR spectrum of a Nujol mull of [K(2,2,2-crypt)][**35**] shows bands at 2020, 1940, 1912, 1884 and 1847 cm^{-1}. More bands would be expected based on the structure of **35**, and the appearance of the spectrum is likely due to overlap between bands lying at similar energies.

Evidence for CO loss (analogous to **34**) is observed in the negative ion mode electrospray mass spectrum, where the molecular ion is $[\mathbf{35}–CO]^-$, observed at 556.2 Da. There is a much less intense peak corresponding to $[\mathbf{35}]^-$ at 584.3 Da.

5.5 Further Novel 1,2,3-Tripnictolide Anions

Further investigations on the synthesis of novel 1,2,3-tripnictolide anions have been performed. Four of the anions thus obtained, bearing amine and ferrocenyl substituents, will be described in this section. Their synthesis serves to illustrate the major drawback of the Zintl anion methodology for the preparation of 1,2,3-tripnictolide anions. In some cases, isolation and purification is relatively straightforward (**17**–**20**), whereas in other cases

analytically pure material is more challenging to obtain (**32**) or has not proved possible (**21**, **22**, and the following anions).

The reaction between ethynylferrocene and [K(18-crown-6)]$_2$[**1**] was monitored by ^{31}P NMR spectroscopy. This revealed that the expected 1,2,3-triphospholide anion $[P_3C_2H\{Fe(C_5H_4)(C_5H_5)\}]^-$ (**36**) was formed as the major phosphorus containing product, but full consumption of **1** required six equivalents of the alkyne (full incorporation of every phosphorus atom from the cage into a 1,2,3-triphospholide product would require 7/3 = 2.333… equivalents of alkyne). Additionally, the reaction proceeded much more slowly, requiring 48 hours to reach completion. It proved possible to isolate the compound as an impure yellow powder, which exhibited, in addition to the expected resonances, broad features in the ^{1}H NMR spectrum. Despite exhaustive attempts, it did not prove possible to isolate a compositionally pure sample of **36**. The chemistry could be extended to the K_3As_7 phase to give $[As_3C_2H\{Fe(C_5H_4)(C_5H_5)\}]^-$ (**37**).

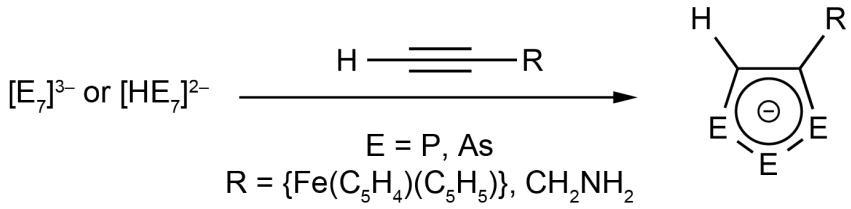

Scheme 5.3: Synthesis of **36**–**39**.

Very similar behaviour was observed in the reactivity between propargylamine and either [K(18-crown-6)]$_2$[**1**] or K_3As_7, to form the $[E_3C_2H(CH_2NH_2)]^-$ (E = P (**38**), As (**39**)) anions. Owing to the formation of unidentified side-products, it did not prove possible to isolate a compositionally pure sample of either anion, although it was possible to characterize them by a combination of single crystal X-ray diffraction, multielement NMR spectroscopy and electrospray mass spectrometry.

5.5.1 Structures of 37 and 39

Crystals of the $[K(2,2,2\text{-crypt})]^+$ salts of **37** and **39** (in very low yield) could be grown by diffusion of hexane into THF solutions of the products. Despite repeated attempts varying the conditions and cations, it did not prove possible to crystallize **36** or **38**. This may be due to the relatively poor purity attained for these compounds. The structures of the anions are shown in Figures 5.14 and 5.15.

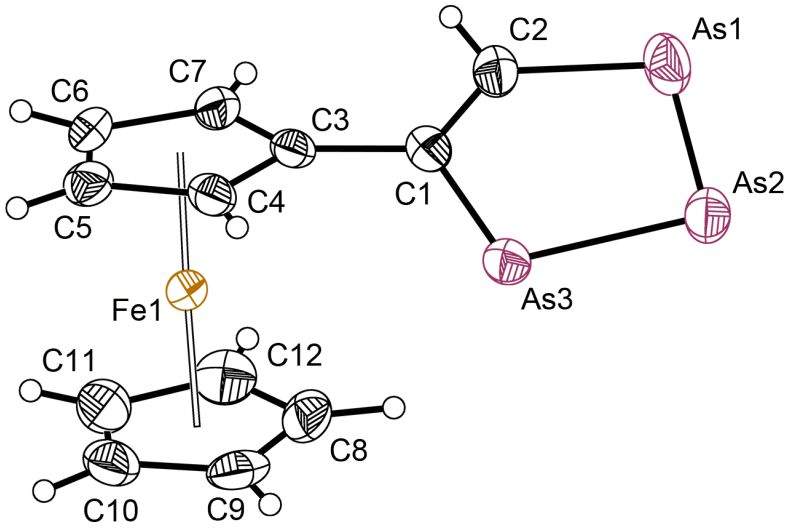

Figure 5.14: Thermal ellipsoid plot of **37**. Thermal ellipsoids are set at the 50% probability level. Hydrogen atoms are shown as spheres of arbitrary radius.

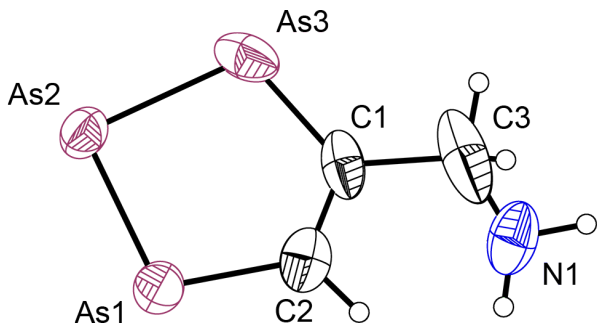

Figure 5.15: Thermal ellipsoid plot of **39**. Thermal ellipsoids are set at the 50% probability level. Hydrogen atoms are shown as spheres of arbitrary radius.

Bond metric data for the anions are consistent with those previously observed for 1,2,3-triarsolide anions. Data for the 1,2,3-triarsolide moiety of **37** are presented in Table 5.5. The bond lengths within the two cyclopentadienyl rings lie within the expected range (1.411(6) to 1.444(5) Å), and there are no significant differences between the distances within the two distinct rings. The arsolide moiety also has no measurable effect on the Fe–C distances, which lie in the range 2.035(3) to 2.057(3) Å for the arsolide substituted ring and 2.031(4) to 2.054(4) Å for the unsubstituted cyclopentadienyl ligand. The torsion angle between the arsolide ring and the directly bonded cyclopentadienyl ring is 23.3º.

Table 5.5: Selected bond metric data for **37**.

Bond distance (Å)	**37**
As1–As2	2.308(1)
As2–As3	2.302(1)
As3–C1	1.904(4)
C1–C2	1.377(5)
C2–As1	1.871(4)
C1–C3	1.478(5)

Inherent issues with the structure of **39** results in elevated R-indices and low levels of precision on the internuclear distances, although the structure is of sufficient quality to confirm composition and connectivity. As a result, it is not possible to perform a detailed analysis of the bond metric data, although they are broadly consistent with that previously observed for related anions.

5.5.2 NMR Spectroscopic Studies on 36–39

The anions **36**–**39** were characterized in solution by multielement NMR spectroscopy. Chemical shift data are presented in Table 5.6, and are in good agreement with prior reported 1,2,3-tripnictolide anions. In the case of **36**, it was not possible to obtain a $^{13}C\{^{1}H\}$ NMR spectrum that unequivocally allowed the assignment of the C1 and C2 resonances.

Table 5.6: NMR data for **36**–**39**.

	Chemical Shift (ppm)			
	36	**37**	**38**	**39**
P1	268.4	–	276.5	–
P2	276.4	–	279.7	–
P3	265.4	–	263.7	–
C1	–	193.8	158.6	203.8
C2	–	174.9	144.6	174.7
H2	9.93	11.54	9.71	11.24

5.5.3 Mass Spectrometric Studies

Further corroboration of the existence of **36**–**39** was provided by means of electrospray mass spectrometry upon DMF solutions of their $[K(18\text{-crown-6})]^+$ or $[K(2,2,2\text{-crypt})]^+$ salts. In the negative ion mode the anions could be observed as the molecular ion, while in the positive ion mode evidence for the cation-paired species could be seen for **36** and **38** (Table 5.7).

Table 5.7: Electrospray mass spectrometry data for **36**–**39**.

Anion	Negative ion mode	Positive ion mode
36	303.0 $[M]^-$	909.5 $\{M+[K(18\text{-crown-6})]_2\}^+$
37	434.8 $[M]^-$	Nothing observed
38	148.1 $[M]^-$	755.1 $\{M+[K(18\text{-crown-6})]_2\}^+$
39	280.3 $[M]^-$	Nothing observed

5.6 Chemistry of 36–39

Initial investigations on the reactivity of **36**–**39** have shown that they are, predictably, capable of forming η^5 coordinated $Mo(CO)_3$ complexes. The crystal structure of one such complex, **39–Mo(CO)$_3$**, is shown in Figure 5.16. Likely due to the low purity of **39**, we have not obtained sufficient material to allow additional characterization of this complex.

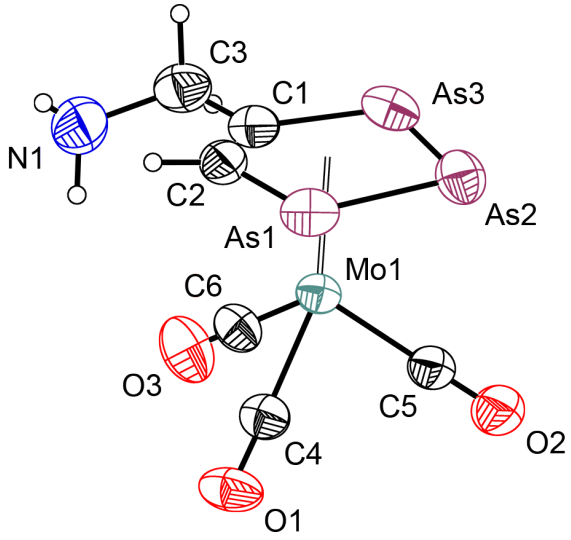

Figure 5.16: Thermal ellipsoid plot of **39–Mo(CO)$_3$**. Thermal ellipsoids are set at the 50% probability level. Hydrogen atoms are shown as spheres of arbitrary radius. Only the major component of the disordered arsolide ring is shown.

Of more interest is the reactivity of the amine functionality in **36** and **37**. We envisioned using an aldehyde condensation reaction to append organic groups on to the tripnictolide anions. Preliminary reactions with benzaldehyde show that **36** is indeed capable of forming a Schiff base adduct, but the water sensitivity of both **36** and the resulting product have precluded isolation and further characterization.

5.7 Conclusion

This chapter has described the extension of the synthetic methodology detailed in Chapter Four for the synthesis of 1,2,3-tripnictolide anions. Five novel anions have been synthesized and characterized.

The reaction of $[HP_7]^{2-}$ with 2-ethynylpyridine resulted in the formation of the $[P_3C_2H(2\text{-pyridyl})]^-$ anion (**32**). This has been thoroughly characterized, and its coordination chemistry towards molybdenum carbonyl fragments explored. This resulted in the formation of three anionic complexes (**33**–**35**) displaying three distinct coordination modes.

Reaction of $[HP_7]^{2-}$ or $[As_7]^{3-}$ with ethynylferrocene or propargylamine yielded the $[E_3C_2HR]^-$ anions (R = $\{Fe(C_5H_4)(C_5H_5)\}$, E = P (**36**), As (**37**); R = CH_2NH_2, E = P (**38**), As (**39**)). These anions have been characterized by a combination of X-ray diffraction, NMR spectroscopic and mass spectrometric techniques. Purification of these anions proved extremely challenging, and illustrates that while the Zintl anion methodology for the synthesis of 1,2,3-tripnictolides encompasses a range of previously inaccessible substrates, it has significant drawbacks.

5.8 REFERENCES

(1) Scherer, O. J. *Acc. Chem. Res.* **1999**, *32*, 751–762.

(2) Scherer, O. J.; Brück, T.; Wolmershäuser, G. *Chem. Ber.* **1989**, *122*, 2049–2054.

(3) Detzel, M.; Mohr, T.; Scherer, O. J.; Wolmershäuser, G. *Angew. Chem. Int. Ed. Engl.* **1994**, *33*, 1110–1112.

(4) Detzel, M.; Friedrich, G.; Scherer, O. J.; Wolmershäuser, G. *Angew. Chem. Int. Ed. Engl.* **1995**, *34*, 1321–1323.

(5) Scherer, O. J.; Weigel, S.; Wolmershäuser, G. *Chem. Eur. J.* **1998**, *4*, 1910–1916.

(6) Bai, J.; Virovets, A. V.; Scheer, M. *Angew. Chem., Int. Ed.* **2002**, *41*, 1737–1740.

(7) Bai, J.; Virovets, A. V.; Scheer, M. *Science* **2003**, *300*, 781–783.

(8) Halterman, R. L. *Chem. Rev.* **1992**, *92*, 965–994.

(9) Fu, G. C. *Acc. Chem. Res.* **2006**, *39*, 853–860.

(10) Shintani, R.; Fu, G. C. *Org. Lett.* **2002**, *4*, 3699–3702.

(11) Shintani, R.; Fu, G. C. *J. Am. Chem. Soc.* **2003**, *125*, 10778–10779.

(12) Shintani, R.; Fu, G. C. *Angew. Chem., Int. Ed.* **2003**, *42*, 4082–4085.

(13) Suárez, A.; Downey, C. W.; Fu, G. C. *J. Am. Chem. Soc.* **2005**, *127*, 11244–11245.

(14) Shintani, R.; Lo, M. M.-C.; Fu, G. C. *Org. Lett.* **2000**, *2*, 3695–3697.

(15) Qiao, S.; Fu, G. C. *J. Org. Chem.* **1998**, *63*, 4168–4169.

(16) Tanaka, K.; Qiao, S.; Tobisu, M.; Lo, M. M.-C.; Fu, G. C. *J. Am. Chem. Soc.* **2000**, *122*, 9870–9871.

(17) Tanaka, K.; Fu, G. C. *J. Org. Chem.* **2001**, *66*, 8177–8186.

(18) Carmichael, D.; Goldet, G.; Klankermayer, J.; Ricard, L.; Seeboth, N.; Stankevič, M. *Chem. Eur. J.* **2007**, *13*, 5492–5502.

(19) Carmichael, D.; Klankermayer, J.; Muller, E.; Pietrusiewicz, K. M.; Ricard, L.; Seeboth, N.; Sowa, S.; Stankevič, M. *Organometallics* **2011**, *30*, 1804–1811.

(20) Turbervill, R. S. P.; Goicoechea, J. M. *Inorg. Chem.* **2013**, *52*, 5527–5534.

(21) Carrington, A.; dos Santos-Veiga, J. *Mol. Phys.* **1962**, *5*, 21–29.

(22) Schlögl, K.; Fried, M. *Monatsh. Chem.* **1963**, *94*, 537–543.

(23) Yoshida, T.; Tani, K.; Yamagata, T.; Tatsuno, Y.; Saito, T. *J. Chem. Soc., Chem. Commun.* **1990**, 292–294.

(24) Hijazi, A.; Djukic, J.-P.; Pfeffer, M.; Ricard, L.; Kyritsakas-Gruber, N.; Raya, J.; Bertani, P.; de Cian, A. *Inorg. Chem.* **2006**, *45*, 4589–4591.

(25) Štěpnička, P.; Schulz, J.; Klemann, T.; Siemeling, U.; Císařová, I. *Organometallics* **2010**, *29*, 3187–3200.

(26) Holand, S.; Jeanjean, M.; Mathey, F. *Angew. Chem. Int. Ed. Engl.* **1997**, *36*, 98–100.

(27) Deschamps, B.; Ricard, L.; Mathey, F. *J. Organomet. Chem.* **1997**, *548*, 17–22.

(28) Butts, C. P.; Green, M.; Hooper, T. N.; Kilby, R. J.; McGrady, J. E.; Pantazis, D. A.; Russell, C. A. *Chem. Commun.* **2008**, 856–858.

(29) García, F.; Less, R. J.; Naseri, V.; McPartlin, M.; Rawson, J. M.; Tomas, M. S.; Wright, D. S. *Chem. Commun.* **2008**, 859–861.

(30) Pyykkö, P.; Atsumi, M. *Chem. Eur. J.* **2009**, *15*, 186–197.

(31) A survey of the Cambridge Structural Database (CSD; version 5.34, November 2012 update) shows 2613 reported complexes containing a Mo−P bond (2.496 Å; mean SE 0.001; sample SD 0.068) and 4432 entries containing an Mo−N bond (2.172 Å; mean SE 0.001; sample SD 0.148).

(32) Braga, S. S.; Coelho, A. C.; Gonçalves, I. S.; Almeida Paz, F. A. *Acta. Cryst. E* **2007**, *63*, m780–m782.

CHAPTER SIX

Synthesis and Protonation Chemistry of the Pentaphospholide Anion

6.1 INTRODUCTION

The first report of the free pentaphosphacyclopentadienide (or pentaphospholide) anion was in 1987 by the group of Baudler, who reported its formation amongst other polyphosphides and phospholides on the reaction of P_4 with sodium in diglyme.[1] This synthesis was further refined to give pure (by ^{31}P NMR spectroscopy) solutions of [Na(18-crown-6)][P_5] in THF.[2] These solutions were reported to be extremely air- and moisture-sensitive, and decompose to $[P_{16}]^{2-}$ and $[P_{21}]^{3-}$ on attempts to isolate a solid. Characterization and structural assignment was performed using mass spectrometry (which suggested the $[P_5]^-$ formula) and ^{31}P NMR spectroscopy. The anion displays a singlet resonance at around 470 ppm, suggesting a single phosphorus environment in a highly deshielded system.

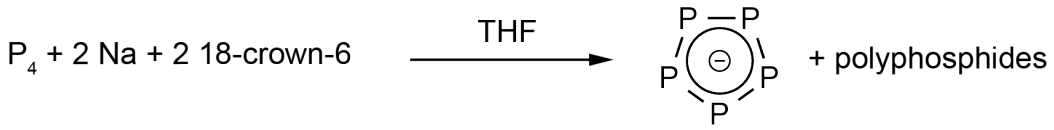

Scheme 6.1: Synthesis of NaP_5 solutions by Baudler and co-workers. The yield of $[P_5]^-$ is around 15% based on phosphorus.

The proposed structure is isolobal with cyclopentadienide, and was captured in a low-yielding synthesis of [Fe(η^5-P_5)(η^5-C_5Me_5)] by reaction of $FeCl_2$ with a mixture of [Na][C_5Me_5] and a solution of [Na][P_5].[2] An independent synthesis of this compound was reported by the group of Scherer by reaction of $[Cp^*Fe(CO)_2]_2$ with P_4 at high temperature.[3] The activation of white phosphorus at transition metal centres has resulted in a limited number of structurally authenticated compounds containing an [η^5-P_5] moiety. These include the previously discussed homoleptic $[Ti(\eta^5\text{-}P_5)_2]^{2-4}$ and a host of triple-decker complexes, for example [{(η^5-C_5Me_5)Cr}$_2$(μ^2,η^5-P_5)], amongst others.[5–9]

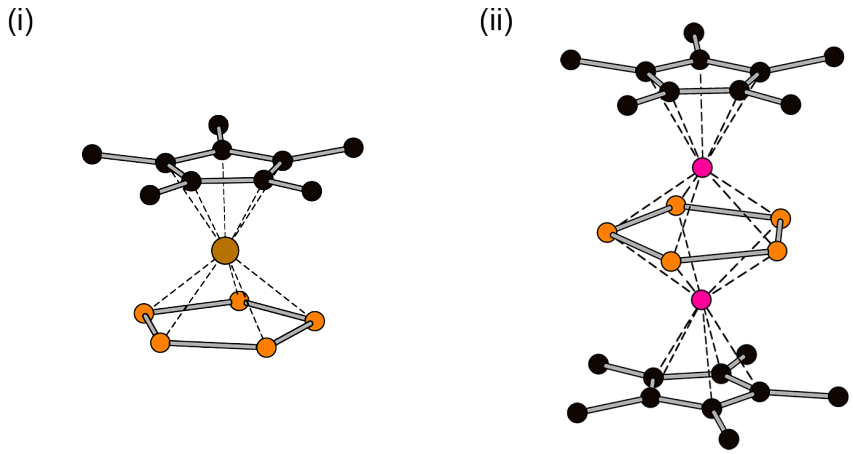

Figure 6.2: Ball and stick representations of $[Fe(\eta^5\text{-}P_5)(\eta^5\text{-}C_5Me_5)]$ (i) and $[\{(\eta^5\text{-}C_5Me_5)Cr\}_2(\mu^2,\eta^5\text{-}P_5)]$ (ii).

The remarkable π-acceptor properties of $[\eta^5\text{-}P_5]^-$ make it an intriguing supporting ligand for transition metals. Current synthetic procedures to access these systems are limited, however, since the solutions are non-trivial to prepare and handle, and activation of P_4 to form $[\eta^5\text{-}P_5]$ ligands is by no means general.

6.2 OBJECTIVES

Formation of the $[P_5]^-$ anion was observed when heating solutions of **1** or **3** in the presence of an alkyne in Chapter Four. We sought to optimize the formation of $[P_5]^-$, and were successful in obtaining compositionally pure, solid samples of the anion as its $[K(18\text{-crown-}6)]^+$ salt.

Following on from this, the protonation chemistry of $[P_5]^-$ was explored. This resulted in the formation and preliminary characterization of two novel "phospha-organic" compounds containing an intact P_5 ring: a neutral polyphosphane and its conjugate base.

6.3 SYNTHESIS OF $[P_5]^-$

6.3.1 Synthesis of $[P_5]^-$ from K_3P_7

During the course of the research described in Chapter Four we observed that on heating DMF or pyridine reaction mixtures of $[P_7]^{3-}$ (**3**) with alkyl-substituted alkynes, $[P_5]^-$ (**40**) was formed alongside other products. Control experiments showed that the alkyne plays no role in the formation of $[P_5]^-$. DMF solutions containing exclusively **40** could be obtained by heating K_3P_7 and 18-crown-6 under reflux for 36 hours. Overall, the reaction can be considered a mild oxidation of the $[P_7]^{3-}$ cage. The average charge per phosphorus atom is decreased from –0.429 in $[P_7]^{3-}$ to –0.200 in $[P_5]^-$. We propose that the oxidant arises from solvent decomposition to Me_2NH and CO (which is lost under the flow of dinitrogen used during reaction), a noted effect for DMF. The Me_2NH oxidizes the cluster and in doing so is reduced to the corresponding amide (Scheme 6.2). It is important to note that this is purely conjecture, and no experiments have been conducted to verify this.

$$K_3P_7 + 3\ \text{18-crown-6} + Me_2NH \xrightarrow{\text{DMF, 160 °C}} [K(\text{18-crown-6})][P_5] + [Me_2N]^- + H_2$$

Scheme 6.2: Possible mechanism for the formation of **40**. Me_2NH is formed by decomposition of DMF at high temperature.

It proved possible to isolate compositionally pure, samples of the $[K(18\text{-crown-6})]^+$ salt of **40** as an orange-yellow solid from these solution by precipitation from THF with diethyl ether. This procedure is not especially reproducible, likely due to the high air- and moisture-sensitivity of **40**, and frequently furnished dark oils which were heavily contaminated by the polyphosphides $[P_{21}]^{3-}$ and $[P_{16}]^{2-}$, only occasionally allowing the isolation of compositionally pure [K(18-crown-6)][**40**].

6.3.2 Synthesis of $[P_5]^-$ from $[K(18\text{-crown-6})]_3[P_7]$

At a later date, we became interested in investigating the activation of $[P_7]^{3-}$ with nucleophilic carbenes, by analogy with the work performed on P_4 described in Chapter One. No reactivity is observed for pyridine solutions of the N-heterocyclic carbene IPr and $[K(18\text{-crown-6})]_3$[**3**] at room temperature, but upon heating at reflux, a bright yellow solid immediately precipitated from solution. Analysis by ^{31}P NMR showed that only **3** was present in solution, but as heating continued it was gradually consumed and replaced by a resonance arising from **40**. In light of the work described in Section 6.3.1 this is perhaps unsurprising. However, workup of the resulting product is straightforward, yielding bright yellow and free-flowing solids of [K(18-crown-6)][**40**] in 90% yield based on phosphorus. Careful inspection of the ^{1}H NMR spectrum reveals small quantities (around one percent based on integration relative to the 18-crown-6 resonance) of an unidentified carbene derived compound. A host of C–H, C–C and C–N activation processes are known for this class of carbene, especially under reductive conditions.[10–15]

While it might be tempting to suggest that the carbene acts as the oxidant, control experiments showed that formation of **40** was quantitative under the same conditions but in the absence of IPr. The formation of **40** is thus likely a solvent activation process analogous to that described in Section 6.3.1. The carbene does, however, play an important role. Attempts to isolate [K(18-crown-6)][**40**] formed by this method in the absence of IPr were plagued by the formation of dark oils containing $[P_{21}]^{3-}$ and $[P_{16}]^{2-}$ alongside **40**. In the presence of IPr, free flowing yellow solids uncontaminated by other polyphosphides are obtained. The reasons for these observations remain unclear.

6.3.3 Characterization of 40

Solutions of **40** have previously been characterized by ^{31}P NMR spectroscopy, showing a singlet resonance at approximately 470 ppm, with the exact shift varying depending on solvent.[1,2] The ^{31}P NMR spectrum of [K(18-crown-6)][**40**] in d_5-pyridine are in good agreement with these prior observations, displaying a singlet resonance at 471.1 ppm (Figure 6.2). Further evidence for the synthesis of **40** is found in the electrospray ionization mass spectrum of DMF solutions of [K(18-crown-6)[**40**]. The negative ion mode show the molecular ion at 155.7 Da, and the positive ion mode displays a mass envelope corresponding to the cation-paired species $\{[K(18\text{-crown-6}]_2[P_5]\}^+$ at an *m/z* ratio of 761.7. An accurate (to within 0.1% for C and H) elemental microanalysis confirms the compositional purity of the sample.

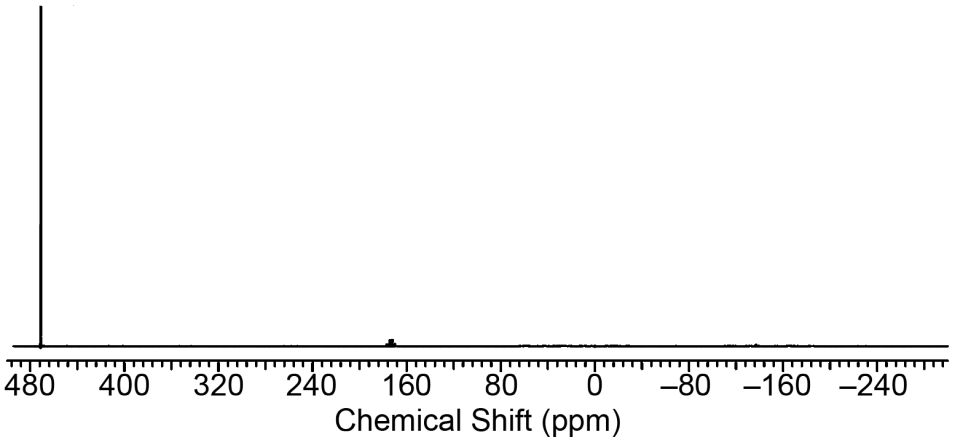

Figure 6.2: ^{31}P NMR spectrum of a d_5-pyridine solution of [K(18-crown-6)][**40**].

It proved possible to grow crystals of [K(18-crown-6)][**40**] suitable for single crystal X-ray diffraction by diffusion of diethyl ether into THF solutions of the product. Despite the good quality of the obtained data, inherent issues with the sample make a solution clearly displaying the $[P_5]^-$ ring impossible to obtain. The compound crystallizes with hexagonal metric symmetry in the trigonal crystal system, clearly driven by the six-fold symmetric

[K(18-crown-6)]$^{+}$ cation. A partial solution can be reached in the rhombohedral space group *R*–3, which shows that the $[P_5]^-$ anion sits on a six-fold rotation axis and is thus necessarily highly disordered. Unfortunately this leads to a structure that is essentially useless for determining bond metric data, or indeed even composition and connectivity of the anion. Nevertheless, the other obtained data strongly support the first successful isolation of **40** as a solid, "bottle-able" compound.

6.4 Protonation Chemistry of 40

Protonation of **40** would be expected to occur at a phosphorus lone pair. This would dearomatize the ring, yielding an extremely reactive bis(diphosphene) (Scheme 6.3). We postulated that this might be able to be trapped by a diene such as 2,3-dimethyl-1,3-butadiene as has been used previously to trap reactive diphosphene moieties.[16] Accordingly, a solution of pyridinium triflate in pyridine was added dropwise to a stirring solution of [K(18-crown-6)][**40**] and twenty molar equivalents of 2,3-dimethyl-1,3-butadiene. This resulted in the formation of a pale solution and copious amounts of brown precipitate. A colourless oil could be obtained in low yield from the mixture by extraction with hexane. Analysis by multielement NMR spectroscopy in d_8-THF showed the formation of a polyphosphorus compound containing five distinct phosphorus environments and a P–H bond. We were unable to structurally characterize this compound, but instead were able to obtain a crystal structure of its conjugate base. This suggested that the compound obtained from protonation is $[HP_5C_6H_{12}]$ (**41**).

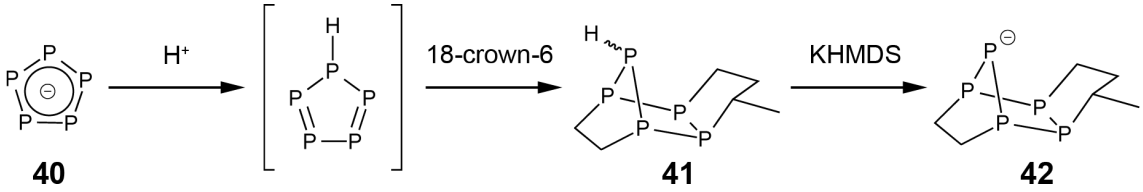

Scheme 6.3: Formation of **41** and **42** from **40**.

Addition of KHMDS and 2,2,2-crypt to THF solutions of **41** results in an instant colour change to a bright yellow, consistent with the formation of a phosphide anion. Analysis by ^{1}H and ^{31}P NMR spectroscopy show retention of the polyphosphorus skeleton and loss of the P–H bond. Crystals suitable for single crystal X-ray diffraction were grown by diffusion of hexane into the THF solution, and showed the formation of the $[P_5C_6H_{12}]^-$ (**42**) anion.

The structure of **42** (and **41**) suggests that 2,3-dimethyl-1,3-butadiene is not involved in their formation. To confirm this the protonation was performed in the absence of the diene, which showed the formation of **41** from **40**. The source of the "C_6H_{12}" unit is less obvious. Reactions were performed in pyridine or THF using pyridinium triflate or triflic acid, and extracted into either hexane or toluene. All of the reactions showed the formation of **41**. The only constant carbon source was the 18-crown-6 moiety of the $[K(18\text{-crown-6})]^+$ cation. We therefore propose that the anion arises from the degradation of 18-crown-6 by the putative bis(diphosphene) formed on protonation of **40**. Cleavage of the C–O bonds in 18-crown-6 and other crown ethers is known under highly reactive conditions.[17,18]

6.4.1 Structure of 42

42 was crystallographically characterized in [K(2,2,2-crypt)][**42**]. The structure consists of a single crystallographically unique anion accompanied by a $[K(2,2,2\text{-crypt})]^+$ cation. The structure of the anion is shown in Figure 6.3. It displays a bicyclic structure with an intact P_5 ring. The hydrogen atoms of the anion could be located in the difference map and their

positions refined following anisotropic refinement of all non-hydrogen atoms and geometric placement of the hydrogen atoms of the 2,2,2-crypt unit.

Since the current primary evidence for the elemental composition of **42** results from this single crystal X-ray structure, we wanted to confirm this to the best of our ability. Replacement of any of C1 to C6 with neighbouring atoms in the periodic table (N or O) resulted in a significant rise in the crystallographic R-indices. This suggests that the atom assignments as carbon are likely correct. Further corroborative evidence can be found in the interatomic bond distances (Table 6.1). The C–C, C–P and P–P bonds all lie in the typical ranges for single bonds. The P–P bonds involving the phosphide vertex (P1) are significantly shorter.

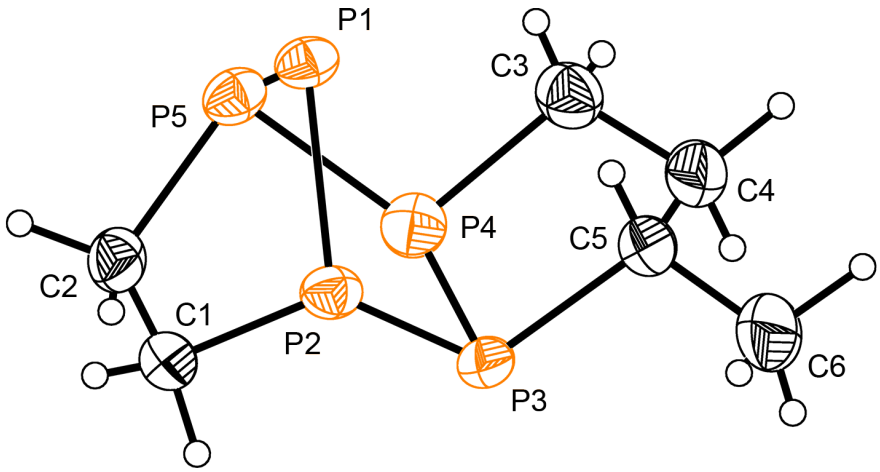

Figure 6.3: Thermal ellipsoid plot of **42**. Thermal ellipsoids are set at the 50% probability level. Hydrogen atoms are shown as spheres of arbitrary radius.

It seems likely that **41** possesses a very similar structure to **42**, differing only in being protonated at P1.

Table 6.1: Bond metric data for **42**.

Bond distance (Å)	42
P1–P2	2.151(1)
P2–P3	2.232(1)
P3–P4	2.217(1)
P4–P5	2.246(1)
P5–P1	2.143(1)
P2–C1	1.876(2)
C1–C2	1.544(3)
C2–P5	1.875(2)
P3–C5	1.879(2)
P4–C3	1.873(2)
C3–C4	1.525(3)
C4–C5	1.515(3)
C5–C6	1.531(3)

6.4.2 NMR Spectroscopy

6.4.2.1 NMR Spectroscopic Studies on 41

The $^{31}P\{^{1}H\}$ NMR spectrum of **41** displays five equal intensity multiplet resonances at –6.8, –8.4, –13.4, –23.1 and –76.5 ppm assigned to P2, P5, P3, P4 and P1, respectively. These were assigned with the assistance of a ^{31}P–^{31}P COSY experiment and simulation of the ^{31}P and $^{31}P\{^{1}H\}$ spectra. A comparison of the simulated and experimental spectra is shown in Figure 6.4. Upon coupling the proton channel, the resonance attributed to P1 (numbering as per Figure 6.3) displays an additional $^{1}J_{H–P}$ coupling constant of 182 Hz. The ^{1}H NMR spectrum shows a doublet at 2.67 ppm with the same coupling constant, which collapses to a singlet on broadband ^{31}P decoupling.

It is possible to distinguish several lower intensity resonances in the baseline. This is possibly a second isomer of **41**, differing in the orientation of the P–H bond (two isomers are possible). This was reproducibly observed in the synthesis of **41**. At this juncture is not

possible to definitively state which of the two isomers is present in solution, or indeed if there is interconversion between the two.

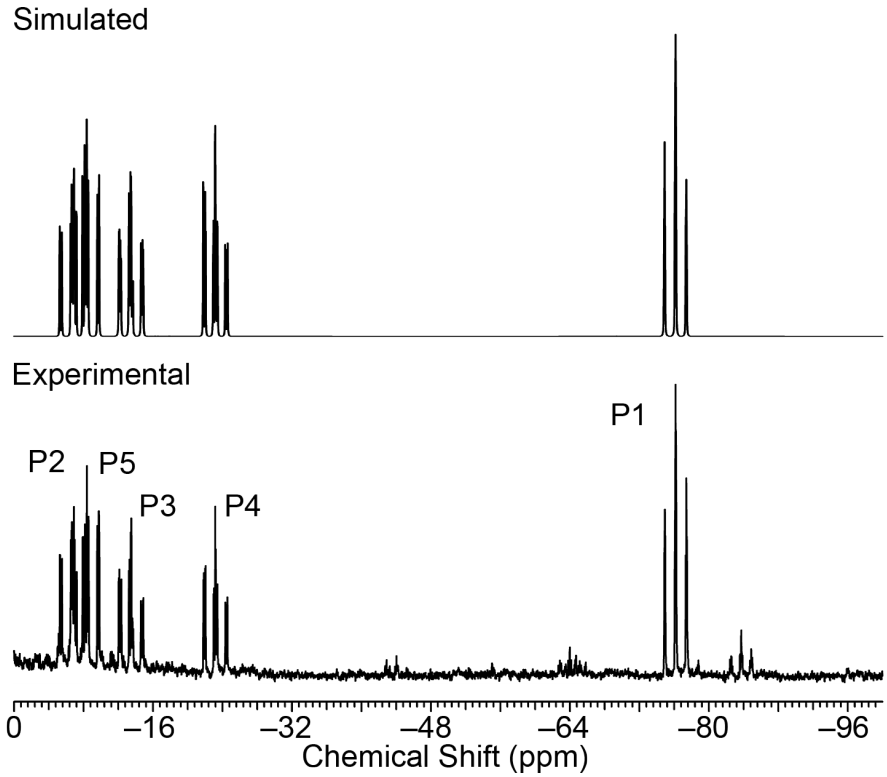

Figure 6.4: Comparison of the simulated and experimental $^{31}P\{^{1}H\}$ NMR spectrum of a d_8-THF solution of **41**.

6.4.2.2 NMR Spectroscopic Studies on 42

The ^{31}P NMR spectrum of **42** is broadly similar to the ^{31}P NMR spectrum of **41**, displaying five equal intensity resonances (Figure 6.5). These occur at 29.6, 27.5, –18.0, –29.6 and –156.3 ppm, corresponding to P2, P5, P3, P4 and P1, respectively. As would be expected, P1 is most affected on deprotonation, shifting downfield by approximately 80 ppm. This upfield shift is consistent with the formation of a phosphide from a phosphane. The ^{31}P and $^{31}P\{^{1}H\}$ NMR spectra are identical, suggesting the absence of a direct P–H bond. Further

corroboration of this is found in the ^{1}H spectrum, which lacks the characteristic P*H* resonance at 2.67 ppm observed for **41**.

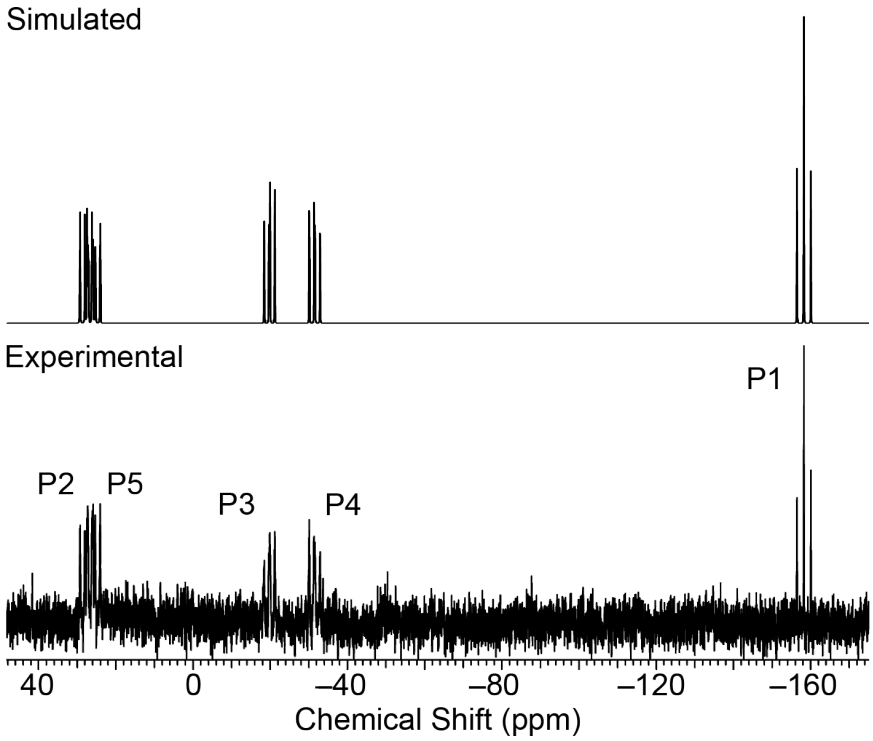

Figure 6.4: Comparison of the simulated and experimental $^{31}P\{^{1}H\}$ NMR spectrum of a d_8-THF solution of [K(2,2,2-crypt)][**42**].

6.5 CONCLUSION

This short chapter has described the first successful synthesis and isolation of $[P_5]^-$ (**40**) as a compositionally pure solid. Preliminary studies into the protonation chemistry of **40** have yielded two novel phospha-organic compounds (**41** and **42**) by an unusual degradation of an 18-crown-6 unit. Studies into the formation and characterization of **41** and **42** are currently ongoing.

6.6 REFERENCES

(1) Baudler, M.; Düster, D.; Ouzounis, D. *Z. Anorg. Allg. Chem.* **1987**, *544*, 87–94.

(2) Baudler, M.; Akpapoglou, S.; Ouzounis, D.; Wasgestian, F.; Meinigke, B.; Budzikiewicz, H.; Münster, H. *Angew. Chem., Int. Ed.* **1988**, *27*, 280–281.

(3) Scherer, O. J.; Brück, T. *Angew. Chem. Int. Ed. Engl.* **1987**, *26*, 59–59.

(4) Urnėžius, E.; Brennessel, W. W.; Cramer, C. J.; Ellis, J. E.; Schleyer, P. von R. *Science* **2002**, *295*, 832–834.

(5) Scherer, O. J.; Schwalb, J.; Wolmershäuser, G.; Kaim, W.; Gross, R. *Angew. Chem. Int. Ed. Engl.* **1986**, *25*, 363–364.

(6) Goh, L. Y.; Wong, R. C. S.; Chu, C. K.; Hambley, T. W. *J. Chem. Soc., Dalton Trans.* **1990**, 977–982.

(7) Hughes, A. K.; Murphy, V. J.; O'Hare, D. *J. Chem. Soc., Chem. Commun.* **1994**, 163–164.

(8) Kudinov, A. R.; Loginov, D. A.; Starikova, Z. A.; Petrovskii, P. V.; Corsini, M.; Zanello, P. *Eur. J. Inorg. Chem.* **2002**, *2002*, 3018–3027.

(9) Li, T.; Wiecko, J.; Pushkarevsky, N. A.; Gamer, M. T.; Köppe, R.; Konchenko, S. N.; Scheer, M.; Roesky, P. W. *Angew. Chem., Int. Ed.* **2011**, *50*, 9491–9495.

(10) Huang, J.; Stevens, E. D.; Nolan, S. P. *Organometallics* **2000**, *19*, 1194–1197.

(11) Galan, B. R.; Gembicky, M.; Dominiak, P. M.; Keister, J. B.; Diver, S. T. *J. Am. Chem. Soc.* **2005**, *127*, 15702–15703.

(12) Caddick, S.; Cloke, F. G. N.; Hitchcock, P. B.; de K. Lewis, A. K. *Angew. Chem., Int. Ed.* **2004**, *43*, 5824–5827.

(13) Ellul, C. E.; Mahon, M. F.; Saker, O.; Whittlesey, M. K. *Angew. Chem., Int. Ed.* **2007**, *46*, 6343–6345.

(14) Arnold, P. L.; Liddle, S. T. *Organometallics* **2006**, *25*, 1485–1491.

(15) Wang, Y.; Xie, Y.; Abraham, M. Y.; Wei, P.; Schaefer, H. F.; Schleyer, P. v. R.; Robinson, G. H. *J. Am. Chem. Soc.* **2010**, *132*, 14370–14372.

(16) Masuda, J. D.; Schoeller, W. W.; Donnadieu, B.; Bertrand, G. *Angew. Chem., Int. Ed.* **2007**, *46*, 7052–7055.

(17) Ugrinov, A.; Sevov, S. C. *C. R. Chim.* **2005**, *8*, 1878–1882.

(18) Musgrave, R. A.; Turbervill, R. S. P.; Irwin, M.; Herchel, R.; Goicoechea, J. M. *Dalton Trans.* **2014**, *43*, 4335–4344.

CHAPTER SEVEN

Concluding Remarks and Future Work

7.1 CONCLUSION

This thesis has described the synthesis and characterization of forty-two compounds, almost all exclusively anionic, derived from the K_3E_7 (E = P, As) Zintl phases. These range from new syntheses of known compounds ($[HP_7]^{2-}$, $[P_7]^{3-}$, $[1,2,3\text{-}P_3C_2Ph_2]^-$, $[1,2,3\text{-}P_3C_6H_4]^-$), through the isolation of previously observed compounds ($[1,2,3\text{-}P_3C_2H_2]^-$, $[P_5]^-$) and finally to the synthesis and isolation of entirely novel compounds (all other reported species).

The $[E_7]^{3-}$ cages display a diverse and unpredictable reactivity towards unsaturated organic molecules. Reactions have been described in which the original nortricyclane-like geometry of the cage is retained (Chapters Two and Three), but additionally where cage fragmentation is observed (Chapters Four to Six). In light of both these results and other work from the group, perhaps the best way to describe the $[E_7]^{3-}$ cages is as anionic sources of E atoms and synthons for unusual "pnicta-organic" molecules.

The majority of the compounds reported contain a direct E–C bond that was absent in the starting materials. The chemistry described within this work is therefore a new route for the chemical activation of elemental phosphorus and arsenic. In contrast to previous group 15 element activation, which has focused almost exclusively on the E_4 cages, the initial group 15 element sources for this work are the relatively innocuous red phosphorus and grey arsenic. Although both circuitous and bearing their own drawbacks (the requirement for both elemental potassium and specialized equipment for the preparation of the K_3E_7 phases), the chemistry of heptapnictide trianions with organic molecules possesses great potential for future development.

7.2 FUTURE WORK

The work described in this thesis is by no means complete. Given more time, there is much more chemistry that I would like to investigate. Some potential future avenues of investigation are listed below.

A rather obvious line of research is the synthesis of metallocene derivatives of the 1,2,3-tripnictolides (or pentaphospholide). This is an area that a fair amount of both time and 1,2,3-$[P_3C_2H_2]^-$/$[P_5]^-$ has been dedicated to! Reactions have been performed with a host of transition metal and post transition metal salts, both halides and hexafluorophosphate salts, with and without additional coordinating ligands (generally PPh_3 or MeCN). In all cases reaction appeared to occur immediately upon mixing of reagents, precipitating insoluble brown solids that defied characterization. There seem to be two possible explanations for this. The first involves the lone pairs of the phospholide creating extended coordination polymers and the second invokes redox chemistry, driven by the π-acceptor ability of the phospholides. This is the primary reason why all of the coordination chemistry described in this work dealt with simple ligand displacements of low oxidation state, early transition metal compounds.

The redox chemistry of the 1,2,3-triphospholides is another potentially fascinating area. Reaction of $[P_3C_2Ph_2]^-$ or $[P_3C_2H(2\text{-pyridyl})]^-$ with $[CPh_3]^+$ results in the formation of bright yellow solutions. Analysis by ^1H NMR spectroscopy reveals that the $[CPh_3]^+$ is reduced to the $[CPh_3]^\cdot$ radical, observed as the diamagnetic dimer. The solutions are silent in the ^{31}P NMR spectrum between +1000 and –1000 ppm. This suggests the oxidation of the triphospholide to a neutral radical. Work is currently ongoing to isolate and characterize these compounds.

I would also like to spend more time investigating the basic protonation and alkylation chemistry of the 1,2,3-triphospholides. Some preliminary research in this area has been fruitful, giving rather convoluted ^{31}P NMR spectra that hint at the formation of a complex polyphosphorus skeleton. By analogy with the 1,3,4-isomers, it seems likely that a series of cycloadditions of P=C and P=P bonds may be occurring. Trapping experiments with dienes and dienophiles may prove useful (and can also be extended to the chemistry described in Chapter Six).

Besides the unsaturated molecules mentioned in this thesis, several other functional groups have had their reactivity towards both $[HP_7]^{2-}$ and $[P_7]^{3-}$ screened by myself unsuccessfully. These resulted in either no reaction or a rapid cluster oxidation to $[P_{16}]^{2-}$ and $[P_{21}]^{3-}$, as was observed for CO_2. Given the success that can be achieved with some organic groups, it seems possible that there are exciting new classes of molecules achievable by reaction of $[E_7]^{3-}$ anions with unsaturated *inorganic* groups. Some progress was made towards this with ^{t}BuCP (generously donated by Nell Townsend of the Russell Group at the University of Bristol), which showed the formation of the known $[1,3,4\text{-}P_3C_2{}^{t}Bu_2]^{-}$ (amongst other phosphorus containing species) on reaction with $[P_7]^{3-}$.

CHAPTER EIGHT

Experimental

8.1 General Synthetic Considerations

All reactions and product manipulations were performed under an inert atmosphere of argon or dinitrogen using standard Schlenk or glovebox techniques (MBraun UNILab glovebox maintained at < 0.1 ppm O_2 and < 0.1 ppm H_2O) unless otherwise noted.

Tetrahydrofuran (THF; Fisher, HPLC grade) and pyridine (py; Alfa-Aesar, 99+%) were distilled from a sodium/benzophenone mixture and CaH_2, respectively. N,N-dimethylformamide (DMF; Rathburn, peptide synthesis grade), acetonitrile (MeCN; Sigma Aldrich, HPLC grade), dichloromethane (DCM; Sigma Aldrich, HPLC grade), diethyl ether (Et_2O; Fisher, pesticide residue grade), hexane (hex; Sigma Aldrich, HPLC grade), pentane (pent; Sigma Aldrich, HPLC grade) and toluene (tol; Sigma Aldrich, HPLC grade) were purified using an MBraun SPS-800 solvent system. d_7-DMF (Apollo Scientific, >99.50%), d_5-pyridine (Eurisotop, >99.5%), d_8-THF (Eurisotop, >99.5%) and CD_2Cl_2 (Eurisotop, >99.5%) were dried over CaH_2, vacuum distilled, and degassed before use. All dry solvents were stored under argon in gas-tight ampoules. Additionally dichloromethane, diethyl ether, hexane, pentane, THF and toluene were stored over activated 3 Å molecular sieves. Deionized water was obtained from a Millipore Milli-Q machine.

The intermetallic precursors, K_3E_7 (E = P, As), were synthesized according to a previously reported synthetic procedure from stoichiometric mixtures of the elements heated to 600 °C (E = P) or 550 ºC (E = As) for 72 hours in sealed niobium tubes.[1,2] The niobium vessels were jacketed in silica ampoules under vacuum prior to heating in order to avoid oxidation of the vessels at the high reaction temperatures.

The source and purification procedures for commercially available compounds are detailed in Table 8.1.

Table 8.1: Supplier and purification procedures for commercially available chemicals.

Compound	Purity	Supplier	Purification
Potassium	99.95%	Strem	Used as received
Phosphorus	99.99%	Sigma Aldrich	Dried under vacuum
Arsenic	99.99%	Alfa-Aesar	Dried under vacuum
2,2,2-crypt	99%	VWR	Dried under vacuum
18-crown-6	99%	Alfa-Aesar	Dried under vacuum with heating
2,6-diisopropyl aniline	90%	Sigma Aldrich	Used as received
Carbon disulfide	anhydrous, ≥99%	Sigma Aldrich	Used as received
Triethylamine	99%	Rathburn	Dried over CaH_2, vacuum distilled and degassed
Bis(cyclohexyl) carbodiimide	99%	Sigma Aldrich	Dried under vacuum
Bis(isopropyl) carbodiimide	99%	Sigma Aldrich	Used as received
1-Adamantyl isocyanate	97%	Sigma Aldrich	Dried under vacuum
HCl in diethyl ether	2.0M	Sigma Aldrich	Used as received
Glyoxal in water	40 wt. %	Sigma Aldrich	Used as received
Paraformaldehyde	95%	Sigma Aldrich	Used as received
Potassium *tert*-butoxide	95%	Sigma Aldrich	Dried under vacuum
Trimethylsilyl chloride	98%	Sigma Aldrich	Used as received
KHMDS	95%	Sigma Aldrich	Used as received
Carbon dioxide	99.995%	Argo International	Used as received
Ruthenium (III) chloride hydrate	99.9%	Alfa-Aesar	Used as received
Calcium carbide	Technical grade	Sigma Aldrich	Used as received
1,5-Cyclooctadiene	99%	Sigma Aldrich	Dried over 3Å molecular sieves
3-chloro-2-methylpropene	98%	Alfa-Aesar	Used as received
Magnesium metal	Turnings	Fisher	Used as received
Diphenylacetylene	98%	Sigma Aldrich	Dried under vacuum
Phenylacetylene	98%	Sigma Aldrich	Used as received
2-Ethynylpyridine	98%	Alfa-Aesar	Used as received
Molybdenum hexacarbonyl	98%	Acros Organics	Sublimed under vacuum
Ethynylferrocene	97%	Sigma Aldrich	Used as received
Propargyl amine	98%	Alfa-Aesar	Used as received
Pyridinium triflate	97%	Sigma Aldrich	Dried under vacuum

Bis(2,6-diisopropyl)carbodiimide,[3] $Mo(CO)_3(py)_3$,[4] $Mo(CO)_3(MeCN)_3$,[5] $Mo(COD)(CO)_4$,[6] and 1,3-bis(2,6-diisopropylphenyl)-imidazol-2-ylidene (IPr)[7,8] were prepared according to literature procedures and stored at ambient temperature in an inert atmosphere glovebox. Brookhart's acid, $[H(OEt_2)_2][BAr^F_4]$,[9] and $[Ru(COD)(\eta^3\text{-}CH_3C(CH_2)_2)_2]$[10,11] were prepared according to literature procedures and stored at –25 ºC in an inert atmosphere glovebox. Acetylene was generated by the reaction of CaC_2 with water, dried over magnesium sulfate, and stored over 3 Å molecular sieves for one week before use.

8.2 Characterization Techniques

8.2.1 Single Crystal X-ray Structure Determination

Single-crystal X-ray diffraction data were collected using either an Oxford Diffraction Supernova dual-source diffractometer equipped with a 135 mm Atlas CCD area detector or an Enraf-Nonius kappa-CCD diffractometer equipped with a 95 mm CCD area detector. Crystals were selected under Paratone-N oil, mounted on micromount loops, and quench-cooled using an Oxford Cryosystems open flow N_2 cooling device.[12] Data were collected at 150 K using mirror monochromated Cu Kα radiation (λ = 1.5418 Å; Oxford Diffraction Supernova) or graphite-monochromated Mo Kα radiation (λ = 0.71073 Å; Enraf-Nonius kappa-CCD). Data collected on the Oxford Diffraction Supernova diffractometer were processed using the CrysAlisPro package, including unit cell parameter refinement and interframe scaling (which was carried out using SCALE3 ABSPACK within CrysAlisPro).[13] Equivalent reflections were merged and diffraction patterns processed with the CrysAlisPro suite. For data collected on the Enraf-Nonius kappa-CCD diffractometer equivalent reflections were merged and the diffraction patterns processed with the DENZO and SCALEPACK programs.[14] Structures were subsequently solved using direct methods,

and refined on F^2 using the SHELXL 97-2 package.[15–17] Tables of selected data collection and refinement parameters are provided in Appendix B.

8.2.2 NMR Spectroscopy

^{1}H, ^{13}C, and ^{31}P NMR spectra were acquired at 500, 125.8, and 202.4 MHz, respectively, on a Bruker AVIII 500 MHz NMR spectrometer, a Bruker AVII 500 MHz NMR spectrometer (equipped with a dedicated ^{13}C cryoprobe), or a Varian Unity 500 MHz NMR spectrometer. ^{1}H and ^{13}C spectra are reported relative to $SiMe_4$ (δ_H 0 ppm, δ_C 0 ppm) and were referenced to the most downfield residual solvent resonance (d_5-pyridine: δ_H 8.74 ppm, δ_C 150.2 ppm; d_7-DMF: δ_H 8.04 ppm, δ_C 163.2 ppm; d_8-THF: δ_H 3.58 ppm, δ_C 67.2 ppm; CD_2Cl_2: δ_H 5.32 ppm, δ_C 53.8 ppm). ^{31}P spectra were externally referenced to 85% H_3PO_4 (δ_P 0 ppm). Spectra were obtained at 25 ºC unless otherwise specified. Spectral simulations were carried out using the program gNMR.[18] All coupling constant data provided are for the fitted simulated spectra starting from experimentally and computationally determined J values. Tables summarizing the results of the spectral simulations are provided in Appendix A. When provided, numbering of nuclei is identical to that in the crystal structure.

8.2.3 Mass Spectrometry

Positive and negative ion mode electrospray mass spectra were recorded on DMF solutions of the compounds (10−20 μM) on a Waters LCT time of flight mass spectrometer with a Z-spray source (150 °C source temperature, 200 °C desolvation temperature, 2.4 kV capillary voltage, and 25 V cone voltage). The samples were made up inside a glovebox under an inert atmosphere and rapidly transferred to the spectrometer in an airtight syringe. Samples were introduced directly with a 1 mL SGE syringe and a syringe pump at 0.6 mL hour^{-1}.

8.2.4 IR Spectroscopy

IR data were recorded on solid samples in Nujol mulls. The mulls were made up inside an inert-atmosphere glovebox and the KBr plates placed in an airtight sample holder prior to data collection. Spectra were recorded on a Thermo Scientific Nicolet iS5 FT-IR spectrometer in absorbance mode.

8.2.5 Powder X-ray Diffraction

Transmission powder X-ray patterns were recorded using a Siemens D5000 diffractometer in modified Debye−Scherrer geometry equipped with an MBraun position sensitive detector. The instrument produced Cu $K\alpha_1$ radiation (λ = 1.54056 Å) using a germanium monochromator and a standard Cu source. Data were recorded on samples in flame-sealed capillaries under dinitrogen. The capillaries were mounted on a goniometer head and aligned so that rotation occurred along the long central axis of the capillary. During a measurement the capillary was rotated at 60 rpm to minimize any preferred orientation effects that might occur.

8.2.6 Elemental Analysis

CHN elemental microanalyses were carried out by Stephen Boyer of the London Metropolitan University or Elemental Microanalysis Ltd., Devon. Samples were submitted in Pyrex ampoules sealed under vacuum.

8.2.7 Computational Details

All calculations were performed by Dr. Jose Goicoechea. Geometry optimizations were performed using the Amsterdam Density Functional package.[19–21] A triple-ζ Slater-type basis set, extended with a double polarization function (TZ2P), was used to describe all atoms. The local density approximation was employed for the optimizations,[22] along with

the local exchange-correlation potential of Vosko, Wilk, and Nusair,[23] and the gradient corrections to exchange and correlation proposed by Becke and Perdew (BP86).[24,25] Relativistic effects were incorporated using the zeroth order relativistic approximation (ZORA).[26–28] The presence of cations in the crystal lattice was modeled by surrounding the anion with a continuum dielectric using COSMO.[29] The chosen dielectric constants of ε = 7.58 or ε = 16.9 correspond to those of tetrahydrofuran (**17**–**35, 40, 42**) and ammonia (**1**–**16**), respectively, although structural parameters were not strongly dependent on this choice. All structures were optimized using the gradient algorithm of Versluis and Ziegler.[30]

The signs and approximate magnitudes associated with the spin−spin coupling constants (*J*) for all complexes were determined by computing Fermi contact values using the Gaussian09 program package revision A02.[31] The B3PW91 functional[32,33] was employed along with the 6-311++G (2d, 2p) basis set for all of the light atoms (H, C, N, O, P).[34–36] The 3-21G basis set was used to describe the molybdenum atoms in anions **26-31** and **33-35** (the nature of the basis set used to describe molybdenum had no effect on the computed signs of the spin−spin coupling constants).[37] Initial atomic coordinates were taken from single-crystal X-ray diffraction experiments when available, or the optimized computed geometry when not.

8.3 Specific Syntheses

8.3.1 Synthesis of Heptapnictide Precursors

8.3.1.1 $[K(18\text{-crown-6})]_2[1]$ (1: $[HP_7]^{2-}$)

To a vigorously stirred slurry of K_3P_7 (8.00 g, 23.9 mmol) in pyridine (80 mL), deionised water (0.96 mL, 47.8 mmol) was added dropwise. This resulted in a colour change to a dark orange-brown. The mixture was stirred for 5 minutes before 18-crown-6 (12.62 g, 47.8

mmol) was added under a flow of argon. The mixture was stirred for a further 15 minutes then filtered through a short plug of Celite® to give a bright orange solution. The solution was concentrated under vacuum to approximately one third of its original volume, and toluene (300 mL) was added to precipitate the product as a microcrystalline yellow powder. The solid was isolated by filtration and dried under dynamic vacuum for 2 hours. Yield 17.60 g (89%). Crystals suitable for single crystal X-ray diffraction were grown by diffusion of toluene into a pyridine solution of the product. ^{1}H NMR (500 MHz, d_7-DMF): δ (ppm) 3.49 (s, 48H, 18-crown-6), 0.47 (s, br, 1H, *H*P$_7$). ^{1}H NMR (500 MHz, d_7-DMF, –50 ºC): δ (ppm) 3.49 (s, 48H, 18-crown-6), 0.47 (d, $^{1}J_{H–P}$ = 160 Hz, 1H, *H*P$_7$). ^{1}H{^{31}P} NMR (500 MHz, d_7-DMF, –50 ºC): δ (ppm) 0.47 (s, 1H, *H*P$_7$), the rest of the resonances observed are as detailed above. ^{31}P{^{1}H} NMR (202.4 MHz, d_7-DMF): δ (ppm) –18.4 (br, m), –112.4 (br, s). ^{31}P{^{1}H} NMR (202.4 MHz, d_7-DMF, –50 ºC): δ (ppm) –22.7 (m, $^{1}J_{P–P}$ = –298 Hz, $^{1}J_{P–P}$ = –363 Hz, $^{2}J_{P–P}$ = –19 Hz, $^{2}J_{P–P}$ = 9 Hz, $^{2}J_{P–P}$ = –5 Hz, ^{2}J$_{P–P}$ = 3 Hz, 1P, P3), –48.8 (m, $^{1}J_{P–P}$ = –349 Hz, $^{2}J_{P–P}$ = –368 Hz, $^{2}J_{P–P}$ = 69 Hz, $^{2}J_{P–P}$ = 46 Hz, $^{2}J_{P–P}$ = 10 Hz, 1P, P1), –76.8 (m, $^{1}J_{P–P}$ = –454 Hz, $^{2}J_{P–P}$ = –13 Hz, $^{2}J_{P–P}$ = 8 Hz, $^{2}J_{P–P}$ = –8 Hz, 1P, P4), –110.0 (m, overlapping resonance, $^{1}J_{P–P}$ = –425 Hz, $^{2}J_{P–P}$ = 9 Hz, $^{2}J_{P–P}$ = 9 Hz, 1P, P2), –111.3 (m, overlapping resonance, $^{1}J_{P–P}$ = –235 Hz, $^{1}J_{P–P}$ = –185 Hz, 1P, P5), –123.5 (m, $^{1}J_{P–P}$ = –177 Hz, 1P, P7), –235.9 (m, 1P, P6). ESI–MS (DMF): *m/z* 216.0 $[HP_7]^-$ (there is extensive decomposition of the $[HP_7]^{2-}$ dianion during the ionization process, resulting in complex spectra that show evidence of higher nuclearity polyphosphides). ESI+MS (DMF): *m/z* 1129.1 $\{[K(18\text{-crown-6})]_3[HP_7]\}^+$. Anal. Calcd for: $C_{24}H_{49}K_2O_{12}P_7$: C 34.94, H 5.99. Found: C 34.49, H 5.43.

8.3.1.2 [K(2,2,2-crypt)]$_2$[1]

A procedure analogous to that detailed above in section 8.3.1.1 was used to prepare the $[K(2,2,2\text{-crypt})]^+$ salt of $[HP_7]^{2-}$ using 2,2,2-crypt in place of 18-crown-6. Spectroscopic

data are very similar to those detailed in section 8.3.1.1. Upon prolonged exposure to vacuum (12 hours) or standing in an inert atmosphere glovebox (weeks) the product changes colour from orange to a bright yellow. This is attributed to loss of pyridine from the crystal lattice and does not affect further reactivity. ^{1}H NMR (500 MHz, d_7-DMF): δ (ppm) 3.77 (s, 24H, 2,2,2-crypt), 3.74 (t, $^{3}J_{H–H}$ = 5 Hz, 24H, 2,2,2-crypt), 2.73 (t, 24H, 2,2,2-crypt), 0.46 (br s, 1H, *H*P$_7$). ^{1}H NMR (500 MHz, d_7-DMF, −50 °C): δ (ppm) 3.77 (s, 24H, 2,2,2-crypt), 3.74 (t, $^{3}J_{H–H}$ = 5 Hz 24H, 2,2,2-crypt), 2.73 (t, 24H, 2,2,2-crypt), 0.49 (d, $^{1}J_{P–H}$ = 159 Hz, 1H, *H*P$_7$). ^{31}P{^{1}H} NMR (202.4 MHz, d_7-DMF): δ (ppm) −23.7 (br m), −111.4 (br m). ^{31}P{^{1}H} NMR (202.4 MHz, d_7-DMF, −50 °C): δ (ppm) −22.7 (m, 1P), −48.8 (m, 1P), −76.8 (m, 1P), −110.8 (m, 1P, overlapping resonance), −111.6 (m, 1P, overlapping resonance), −123.6 (m, 1P), −235.8 (m, 1P). ESI−MS (DMF): *m/z* 216.0 $[HP_7]^-$ (there is extensive decomposition of the $[HP_7]^{2-}$ anion during the ionization process, resulting in a complex spectrum that shows evidence of higher nuclearity oxidized polyphosphides). No evidence of **1** was observed in the positive ion mode mass spectrum. Anal. Calcd for $C_{41}H_{78}K_2N_5O_{12}P_7$: C, 43.65; H, 6.97; N, 6.21. Found: C, 43.39; H, 6.60; N, 5.99.

8.3.1.3 [K(18-crown-6)]$_2$[1–D] (1–D: [DP$_7$]$^{2–}$)

An isotopically labelled version of **1**, incorporating deuterium into the cage was made using D_2O in place of H_2O in the procedure above. All other experimental considerations remained the same. ^{1}H NMR (500 MHz, DMF): δ 3.60 (s, 18-crown-6). ^{2}H NMR (76.7 MHz, DMF): δ 0.33 (br, DP$_7$). ^{2}H NMR (76.7 MHz, DMF, –50 °C): δ 0.35 (d, $^{1}J_{D–P}$ = 22 Hz, *D*P$_7$). Judging by the NMR spectra of this sample there is less than 10% of the protic species, $[HP_7]^{2–}$, present in solution (presumably arising due to adventitious moisture from the solvent or 18-crown-6).

8.3.1.4 $[K(18\text{-crown-6})]_2[2]$ (2: $[HAs_7]^{2-}$)

A procedure analogous to that detailed in section 1.2.1.1 using K_3As_7 (500 mg, 0.78 mmol), 18-crown-6 (412 mg, 1.56 mmol) and H_2O (28 μL, 1.56 mmol) was used to prepare the title compound as an orange powder. Yield 697 mg (79%). Crystals suitable for single crystal X-ray diffraction were grown by diffusion of hexane into a 1:1 THF/pyridine solution of the product. ^{1}H NMR (500 MHz, d_7-DMF): δ 3.62 (s, 48H, 18-crown-6), 1.17 (s, 1H, *H*As_7). ESI−MS (DMF): *m/z* 526.7 $[HAs_7]^-$. ESI+MS (DMF): 1170.4 $\{K[K(18\text{-crown-6})]_2[HAs_7]\}^+$. Anal. Calcd for $C_{24}H_{49}K_2O_{12}As_7$: C, 25.44; H, 4.36. Found: C, 26.15; H, 4.45.

8.3.1.5 $[K(18\text{-crown-6})]_2[2\text{–D}]$ (2–D: $[DAs_7]^{2-}$)

An isotopically labelled version of **2**, incorporating deuterium into the cage was made using D_2O in place of H_2O in the procedure above. All other experimental considerations remained the same. ^{1}H NMR (500 MHz, DMF): δ 3.62 (s, 18-crown-6). ^{2}H NMR (76.7 MHz, DMF): δ 1.21 (s, *D*As_7). Judging by the NMR spectra of this sample there is less than 5% of the protic species, $[HAs_7]^{2-}$, present in solution (presumably arising due to adventitious moisture from the solvent or 18-crown-6).

8.3.1.6 $[K(18\text{-crown-6})]_3[3]$ (3: $[P_7]^{3-}$)

$[K(18\text{-crown-6})]_2$[**1**] (4.00 g, 4.85 mmol), KHMDS (1.07 g, 5.36 mmol) and 18-crown-6 (1.42 g, 5.36 mmol) were weighed into a Schlenk tube and slurried in THF (40 mL). Pyridine was added with stirring until a homogeneous dark red-brown solution was obtained (approximately 80 mL), and the mixture left to stir for 12 hours. The solvent was then removed under vacuum and the dark orange residue washed with THF (3 × 40 mL) and Et_2O (3 × 40 mL) to remove amine byproducts and excess base. The bright yellow solid obtained was dried under vacuum for 1 hour. Yield 5.02g (92%). ^{1}H NMR (500 MHz, d_5-

pyridine): δ 3.52 (s, 72H). $^{31}P\{^{1}H\}$ NMR (202.4 MHz, d_5-pyridine): δ (ppm) –120 (br s). $^{31}P\{^{1}H\}$ NMR (202.4 MHz, 1:1 THF/pyridine, –85 ºC, unlocked) δ (ppm) –30 (br m, 1P), –115 (br m, 3P), –170 (br m, 3P). ESI−MS (DMF): 217.5 $[P_7]^{3-}$. ESI+MS (DMF): 1129.1 $\{[K(18\text{-crown-6})]_3[P_7]\}^{+}$.

8.3.2 NMR Studies on CO_2

8.3.2.1 $[K(18\text{-crown-6})]_3[4]$ (4: $[P_7–CO_2]^{3-}$)

$[K(18\text{-crown-6})]_3[P_7]$ (50 mg, 44 μmol) was weighed into an NMR tube equipped with a gas-tight valve, and dissolved in a 1:1 mixture of THF and pyridine (0.6 mL) to give an orange solution. The tube was degassed three times by the freeze-pump-thaw method, and placed under CO_2 (1 atmosphere), resulting in an immediate colour change to yellow. The reaction was immediately analyzed by ^{31}P NMR spectroscopy at both 25 ºC and –65 ºC. $^{31}P\{^{1}H\}$ NMR (202.4 MHz, 1:1 THF/pyridine, unlocked): δ (ppm) –10 (br s), –68 (br s). $^{31}P\{^{1}H\}$ NMR (202.4 MHz, 1:1 THF/pyridine, –65 ºC, unlocked) δ (ppm) 117 (br m, 1P), 63 (br m, 1P), 30 (br m, 1P), –94 (br m, 1P), –140 (br m, 2P), –194 (br m, 1P).

8.3.3 General Procedure for Hydropnictination Reactions

The protonated heptapnictide cage, $[K(18\text{-crown-6})]_2[HE_7]$ (E = P (**1**), As (**2**)), and one equivalent of carbodiimide or isocyanate were weighed into an NMR tube equipped with a gas-tight valve. Solvent (d_7-DMF or d_5-pyridine, 0.5 mL) was added and the tube agitated to mix the contents. The resulting solution was immediately analyzed by NMR spectroscopy, revealing quantitative conversion to the product. Following analysis, the contents of the NMR tube were transferred to a Schlenk tube. The solvent was removed under dynamic

vacuum and the oily solid resulting washed with diethyl ether (3 × 2 mL) to precipitate the product as a powder that was isolated by filtration and dried under vacuum.

8.3.3.1 $[K(18\text{-crown-6})]_2[5]$ (5: $[P_7C(NHDipp)(NDipp)]^{2-}$)

$[K(18\text{-crown-6})]_2$[**1**] (50 mg, 61 μmol) and bis(2,6-diisopropylphenyl)carbodiimide (22 mg, 61 μmol) were used, giving the product as a yellow powder. Yield 43 mg (60 %). Crystals suitable for single crystal X-ray diffraction were grown by diffusion of hexane into a THF solution of the product. ^{1}H NMR (500 MHz, d_7-DMF): δ (ppm) 6.93 (overlapping m, 3H, Ar*H*), 6.81 (d, $^{3}J_{H–H}$ = 5 Hz, 2H, Ar*H*), 6.64 (t, $^{3}J_{H–H}$ = 5 Hz, 1H, Ar*H*), 6.29 (br s, 1H, N*H*), 3.58 (s, 48H, 18-crown-6), 3.38 (sept, $^{3}J_{H–H}$ = 5 Hz, 2H, C*H*$(CH_3)_2$), 3.21 (sept, $^{3}J_{H–H}$ = 5 Hz, 2H, C*H*$(CH_3)_2$), 1.42 (d, 6H, CH_3), 1.18 (d, 6H, CH_3), 1.14 (d, 6H, CH_3), 0.86 (d, 6H, CH_3). ^{31}P{^{1}H} NMR (202.4 MHz, d_7-DMF): δ (ppm) –6.4 (m, P3), – 83.2 (br), –111.9 (br). ^{31}P NMR (202.4 MHz, d_7-DMF, –50 ºC): δ (ppm) –6.3 (m, $^{1}J_{P–P}$ = –392 Hz, $^{1}J_{P–P}$ = –339 Hz, $^{2}J_{P–P}$ = –29 Hz, $^{2}J_{P–P}$ = –12 Hz, $^{2}J_{P–P}$ = 7 Hz, 1P, P3), –28.3 (m, $^{1}J_{P–P}$ = –381 Hz, $^{1}J_{P–P}$ = –354 Hz, $^{2}J_{P–P}$ = 64 Hz, $^{2}J_{P–P}$ = 44 Hz, $^{2}J_{P–P}$ = –10 Hz, 1P, P1), –68.7 (m, $^{1}J_{P–P}$ = –419 Hz, $^{1}J_{P–P}$ = –184 Hz, $^{1}J_{P–P}$ = –225 Hz, $^{2}J_{P–P}$ = –12 Hz, 1P, P5), –91.6 (m, $^{1}J_{P–P}$ = –425 Hz, $^{2}J_{P–P}$ = –15 Hz, $^{2}J_{P–P}$ = –12 Hz, 1P, P4), –100.0 (m, $^{2}J_{P–P}$ = –9 Hz, $^{2}J_{P–P}$ = 8 Hz, $^{2}J_{P–P}$ = –8 Hz, 1P, P2), –134.1 (m, $^{1}J_{P–P}$ = –184 Hz, 1P, P7), –211.7 (m, 1P, P6). ^{13}C{^{1}H} NMR (500 MHz, d_7-DMF): 165.7 ($^{1}J_{C–P}$ = 82 Hz, P*C*N_2), 149.1 (Ar*C*), 148.2 (Ar*C*), 139.5 (Ar*C*), 139.1 (Ar*C*), 125.7 (Ar*C*), 122.3 (Ar*C*), 121.6 (Ar*C*), 120.6 (Ar*C*), 28.7 (*C*H$(CH_3)_2$), 27.7 (*C*H$(CH_3)_2$), 27.4(*C*H_3), 24.9(*C*H_3), 24.3(*C*H_3), 22.6 (*C*H_3). ESI–MS (DMF): *m/z* 581.3 $\{P_7C(NHDipp)(NDipp)]+H\}^{-}$. No evidence of **5** was observed in the positive ion mode ESI+MS spectrum. Elemental analyses were found to reproducibly give low values of C, H, and N, presumably due to the formation of non-volatile products on heating. Anal. Calcd for $C_{49}H_{83}K_2N_2O_{12}P_7$: C, 49.77; H, 7.05; N, 2.36. Found: C, 43.52; H, 5.46; N, 2.07.

8.3.3.2 $[K(18\text{-crown-6})]_2[5\text{-D}]$ (5-D: $[P_7C(NDDipp)(NDipp)]^{2-}$)

Bis(2,6-diisopropylphenyl)carbodiimide (18 mg, 49 μmol) and $[K(18\text{-crown-6})]_2[\mathbf{1–D}]$ (40 mg, 49 μmol) were used in DMF (0.5 mL). ^{2}H NMR (76.7 MHz, DMF): δ 6.23 (br s). ^{2}H NMR (76.7 MHz, DMF, –50 °C): δ 6.92 (very broad). $^{31}P\{^1H\}$ NMR (202.4 MHz, DMF): δ –6.5 (m), –82.4 (br), –111.2 (br). ^{31}P NMR (202.4 MHz, DMF, –50 °C): δ –8.7 (m, 1P), –29.4 (m, 1P), –69.4 (m, 1P), – 91.6 (m, 1P), –99.7 (m, 1P), –132.7 (m, 1P), –208.9 (m, 1P). The spectrum was not simulated to extract the coupling constants since it was extremely similar to that observed for **5**.

8.3.3.3 $[K(2,2,2\text{-crypt})]_2[6]$ (6: $[P_7C(NHCy)(NCy)]^{2-}$)

$[K(2,2,2\text{-crypt})]_2[\mathbf{1}]$ (50 mg, 48 μmol) and bis(cyclohexyl)carbodiimide (10 mg, 48 μmol) were used, giving the product as a yellow powder. Yield 32 mg (55%). ^{1}H NMR (500 MHz, d_7-DMF): δ (ppm) 4.11 (overlapping m, 2H, C*H* of Cy), 3.60 (s, 24H, 2,2,2-crypt), 3.57 (t, $^3J_{H–H}$ = 5 Hz, 24H, 2,2,2-crypt), 3.14 (s, 1H, N*H*), 2.56 (t, 24H, 2,2,2-crypt), 1.84–0.94 (m, 20H, Cy). $^{31}P\{^1H\}$ NMR (202.4 MHz, d_7-DMF): δ (ppm) −18.5 (m, P3), −87.5 (br), −111.7 (br). $^{31}P\{^1H\}$ NMR (202.4 MHz, d_7-DMF, −50 °C): δ (ppm) −18.7 (m, $^1J_{P–P}$ = –338 Hz, $^1J_{P–P}$ = –401 Hz, $^2J_{P–P}$ = –21 Hz, $^2J_{P–P}$ = –12 Hz, $^2J_{P–P}$ = 7 Hz, 1P, P3), −28.2 (m, $^1J_{P–P}$ = –378 Hz, $^1J_{P–P}$ = –378 Hz, $^2J_{P–P}$ = 63 Hz, $^2J_{P–P}$ = 46 Hz, $^2J_{P–P}$ = –10 Hz, 1P, P1), −73.5 (m, $^1J_{P–P}$ = –423 Hz, $^1J_{P–P}$ = –227 Hz, $^1J_{P–P}$ = –176 Hz, $^2J_{P–P}$ = 63 Hz, 1P, P5), −95.7 (m, $^1J_{P–P}$ = –438 Hz, $^2J_{P–P}$ = –15 Hz, $^2J_{P–P}$ = –8 Hz, 1P, P4), −103.8 (m, $^2J_{P–P}$ = –9 Hz, $^2J_{P–P}$ = 8 Hz, $^2J_{P–P}$ = –8 Hz, 1P, P2), −130.3 (m, $^1J_{P–P}$ = –181 Hz, 1P, P7), −222.4 (m, 1P, P6). $^{13}C\{^1H\}$ NMR (125.8 MHz, d_7-DMF): δ (ppm) 161.3 (d obscured by solvent, P*C*N_2), 57.3 (d, $^3J_{C–P}$ = 32 Hz, N*C*H), 48.5 (NH*C*H), 36.3 (Cy), 32.0 (Cy), 26.7 (Cy), 26.6 (Cy), 25.4 (Cy), 24.8 (Cy). ESI−MS (DMF): *m/z* 424.9 $\{[P_7C(NHCy)(NCy)]+H\}^-$. ESI+MS (DMF): *m/z* 1668.7

{[K(2,2,2-crypt)]$_3$[P_7C(NHCy)(NCy)]}$^+$. Anal. Calcd for $C_{49}H_{95}K_2N_6O_{12}P_7$: C, 46.88; H, 7.63; N, 6.69. Found: C, 46.66; H, 7.91; N, 6.62.

8.3.3.4 [K(2,2,2-crypt)]$_2$[7] (7: [P_7C(NH^{i}Pr)(N^{i}Pr)]$^{2-}$)

[K(2,2,2-crypt)]$_2$[**1**] (50 mg, 48 μmol) and bis(isopropyl)carbodiimide (8 μL, 48 μmol) were used, giving the product as a yellow powder. Yield 30 mg (52%). Single-crystal X-ray diffraction quality crystals of [K(2,2,2-crypt)]$_2$[**7**] were unattainable; however the use of [K(18-crown-6)]$_2$[**1**] in place of [K(2,2,2-crypt)]$_2$[**1**] allowed crystals of [K(18-crown-6)]$_2$[**7**] to be grown by diffusion of hexane into a 1:1 THF/pyridine solution of the product. ^{1}H NMR (500 MHz, d_7-DMF): δ (ppm) 4.50 (sept, $^3J_{H–H}$ = 6 Hz, 1H, C*H*(CH$_3$)$_2$), 4.05 (s, 1H, N*H*), 3.60 (s, 24H, 2,2,2-crypt), 3.57 (t, 24H, $^3J_{H–H}$ = 5 Hz, 2,2,2-crypt), 3.32 (d sept, $^3J_{H–H}$ = 6 Hz, 1H, C*H*(CH$_3$)$_2$), 2.55 (t, 24H, 2,2,2-crypt), 0.92 (d, 6H, C*H*$_3$), 0.72 (d, 6H, C*H*$_3$). ^{31}P{^{1}H} NMR (202.4 MHz, d_7-DMF): δ (ppm) −18.3 (m, P3), −87.6 (br), −111.8 (br). ^{31}P{^{1}H} NMR (202.4 MHz, d_7-DMF, −50 °C): δ (ppm) −17.7 (m, $^1J_{P–P}$ = –401 Hz, $^1J_{P–P}$ = –355 Hz, $^2J_{P–P}$ = –21 Hz, $^2J_{P–P}$ = –12 Hz, $^2J_{P–P}$ = –8 Hz, 1P, P3), −28.9 (m, $^1J_{P–P}$ = –381 Hz, $^1J_{P–P}$ = –366 Hz, $^2J_{P–P}$ = 63 Hz, $^2J_{P–P}$ = 46 Hz, $^2J_{P–P}$ = –10 Hz, 1P, P1), −73.0 (m, $^1J_{P–P}$ = –423 Hz, $^1J_{P–P}$ = –184 Hz, $^1J_{P–P}$ = –229 Hz, 1P, P5), −96.2 (m, $^1J_{P–P}$ = –437 Hz, $^2J_{P–P}$ = –15 Hz, $^2J_{P–P}$ = –8 Hz, 1P, P4), –105.0 (m, $^2J_{P–P}$ = –9 Hz, $^2J_{P–P}$ = 8 Hz, 1P, P2), –130.3 (m, $^1J_{P–P}$ = 184 Hz, 1P, P7), –224.9 (m, 1P, P6). ^{13}C{^{1}H} NMR (125.8 MHz, d_7-DMF): δ (ppm) 161.8 (d obscured by solvent, P*C*N$_2$), 48.9 (d, $^3J_{C–P}$ = 31 Hz, N*C*H), 41.9 (NH*C*H), 25.8 (*C*H$_3$), 22.1 (C*H*$_3$). ESI−MS (DMF): *m/z* 344.7 {[P_7C(NH^{i}Pr)(N^{i}Pr)]+H}$^-$. ESI+MS (DMF): *m/z* 1588.3 {[K(2,2,2-crypt)]$_3$[P_7C(NH^{i}Pr)(N^{i}Pr)]}$^+$. Anal. Calcd for $C_{43}H_{87}K_2N_6O_{12}P_7$: C, 43.95; H, 7.46; N, 7.15. Found: C, 43.82; H, 7.53; N, 6.83.

8.3.3.5 [K(18-crown-6)]$_2$[8] (8: [$P_7C(O)(NHAd)]^{2-}$)

[K(18-crown-6)]$_2$[**1**] (60 mg, 73 μmol) and 1-adamantyl isocyanate (13 mg, 73 μmol) were used, giving the product as a yellow powder. Yield 33 mg, (45%). Crystals suitable for single crystal X-ray diffraction were grown by diffusion of hexane into a 1:1 THF/pyridine solution of the product. ^{1}H NMR (500 MHz, d_7-DMF): δ (ppm) 5.88 (s, 1H, N*H*), 3.66 (s, 48H, 18-crown-6), 1.83 (s, 3H, Ad), 1.72 (s, 6H, Ad), 1.52 (s, 6H, Ad). ^{31}P{^{1}H} NMR (202.4 MHz, d_7-DMF): δ (ppm) 10.9 (m, P3), –85.2 (br), –119.2 (br). ^{31}P{^{1}H} NMR (202.4 MHz, d_7-DMF, –50 ºC): δ (ppm) 7.4 (m, $^1J_{P–P}$ = –320 Hz, $^2J_{P–P}$ = –10 Hz, $^2J_{P–P}$ = –23 Hz, $^2J_{P–P}$ = 14 Hz, $^1J_{P–P}$ = –381 Hz, $^2J_{P–P}$ = –15 Hz, 1P, P3), –33.8 (m, $^1J_{P–P}$ = –362 Hz, $^1J_{P–P}$ = –348 Hz, $^1J_{P–P}$ = –320 Hz, $^2J_{P–P}$ = 61 Hz, $^2J_{P–P}$ = –13 Hz, $^2J_{P–P}$ = 47 Hz, 1P, P1), –71.3 (m, $^1J_{P–P}$ = –419 Hz, $^2J_{P–P}$ = –7 Hz, $^1J_{P–P}$ = –422 Hz, $^1J_{P–P}$ = –184 Hz, $^1J_{P–P}$ = –225 Hz, 1P, P5), –102.7 (m, $^2J_{P–P}$ = –16 Hz, 1P, P4), –105.6 (m, $^2J_{P–P}$ = –8 Hz, $^2J_{P–P}$ = –10 Hz, 1P, P2), –134.2 (m, $^1J_{P–P}$ = –182 Hz, 1P, P7), –206.6 (m, 1P, P6). ^{13}C{^{1}H} NMR (500 MHz, d_7-DMF): 182.8 (d, $^1J_{C–P}$ = 82 Hz, P*C*ON), 70.3 (18-crown-6), 51.7 (Ad), 45.0 (Ad), 41.6 (Ad), 36.8 (Ad). ESI–MS (DMF): *m/z* 396.1 {[$P_7C(O)(NHAd)$]+H}$^-$. ESI+MS (DMF): *m/z* 1306.2 {[K(18-crown-6)]$_3$[$P_7C(O)(NHAd)$]}$^+$. Anal. Calcd for $C_{40}H_{69}K_2N_2O_{13}P_7$: C, 44.44; H, 6.43; N, 2.59. Found: C, 44.24; H, 6.36; N, 2.66.

8.3.3.6 [K(18-crown-6)]$_2$[9] (9: [$As_7C(NHDipp)(NDipp)]^{2-}$)

[K(18-crown-6)]$_2$[**2**] (100 mg, 88 μmol) and bis(2,6-diisopropylphenyl)carbodiimide (32 mg, 88 μmol) were used, giving the product as an orange powder. Yield 81 mg (61%). Crystals suitable for single crystal X-ray diffraction were grown by diffusion of hexane into a THF solution of the product. ^{1}H NMR (500 MHz, d_5-pyridine): δ (ppm) 7.24 (d, $^3J_{H–H}$ = 7 Hz, 2H, Ar*H*), 7.21 (t, 1H, Ar*H*), 7.19 (d, $^3J_{H–H}$ = 7 Hz, 2H, Ar*H*), 7.06 (t, 1H, Ar*H*), 6.60 (s, 1H, N*H*), 4.07 (sept, $^3J_{H–H}$ = 6 Hz, 2H, C*H*(CH_3)$_2$), 3.89 (sept, $^3J_{H–H}$ = 6 Hz, 2H,

C*H*(CH_3)$_2$), 3.50 (s, 48H, 18-crown-6), 1.88 (d, 6H, C*H*$_3$), 1.69 (d, 6H, C*H*$_3$), 1.45 (d, 6H, C*H*$_3$), 1.16 (d, 6H, C*H*$_3$). ^{13}C{^{1}H} NMR (125.8 MHz, d_5-pyridine): δ (ppm) 168.9 (As*C*N$_2$), 150.0 (Ar*C*), 149.4 (Ar*C*), 140.9 (Ar*C*), 139.9 (Ar*C*), 127.0 (Ar*C*), 123.2 (Ar*C*), 123.0 (Ar*C*), 122.0 (Ar*C*), 71.0 (18-crown-6), 29.6 (*C*H(CH_3)$_2$), 28.9 (*C*H(CH_3)$_2$), 28.6 (*C*H$_3$), 26.3 (*C*H$_3$), 25.2 (*C*H$_3$), 23.6 (*C*H$_3$). ESI–MS (DMF): *m/z* 889.1 {[As_7C(NHDipp)(NDipp)]+H}$^-$. No evidence of **9** was observed in the positive ion mode ESI+MS spectrum. Anal. Calcd for $C_{49}H_{83}As_7K_2N_2O_{12}$: C, 39.35; H, 5.60; N, 1.87. Found: C, 40.30; H, 5.82; N, 1.76.

8.3.3.7 [K(18-crown-6)]$_2$[10] (10: [As_7C(NHCy)(NCy)]$^{2-}$)

[K(18-crown-6)]$_2$[**2**] (50 mg, 44 μmol) and bis(cyclohexyl)carbodiimide (9 mg, 44 μmol) were used. Crystals suitable for single crystal X-ray diffraction were grown by diffusion of hexane into a THF solution of the product. The product was isolated as crystals (9 mg, 15%). ^{1}H NMR (500 MHz, d_5-pyridine): δ (ppm) 4.62 (m, 1H, C*H* of Cy), 4.38 (s, 1H, N*H*), 3.90 (m, 1H, C*H* of Cy), 3.52 (s, 48H, 18-crown-6), 2.33–1.09 (overlapping m, 20H, Cy). ^{13}C{^{1}H} NMR (125.8 MHz, d_5-pyridine): δ (ppm) 163.9 (As*C*N$_2$), 71.1 (18-crown-6), 60.5 (Cy), 50.0 (Cy), 36.6 (Cy), 35.0 (Cy), 32.6 (Cy), 26.6 (Cy), 26.5 (Cy), 25.8 (Cy), 25.4 (Cy), 24.6 (Cy), 23.3 (Cy), 21.1 (Cy). ESI–MS (DMF): *m/z* 732.7 {[As_7C(NHCy)(NCy)]+H}$^-$. ESI+MS (DMF): *m/z* 1643.1 {[K(18-crown-6)]$_3$[As_7C(NHCy)(NCy)]}$^+$. Anal. Calcd for $C_{37}H_{71}As_7K_2N_2O_{12}$: C, 33.18; H, 5.35.; N, 2.09. Found: C, 34.94; H, 5.22; N, 2.79.

8.3.3.8 [K(18-crown-6)]$_2$[11] (11: [As_7C(NH^{i}Pr)(N^{i}Pr)]$^{2-}$)

[K(18-crown-6)][**2**] (50 mg, 44 μmol) and bis(isopropyl)carbodiimide (7 μL, 44 μmol) were used, giving the product as an orange powder. Yield 35 mg (62%). Crystals suitable for single crystal X-ray diffraction were grown by diffusion of hexane into a 1:1 THF/pyridine solution of the product. ^{1}H NMR (500 MHz, d_5-pyridine): δ (ppm) 4.98 (sept, 1H, $^3J_{H–H}$ = 7

Hz, C*H*(CH_3)$_2$), 4.39 (d, 1H, $^3J_{H–H}$ = 7 Hz, N*H*), 4.13 (d sept, $^3J_{H–H}$ = 7 Hz, 1H, C*H*(CH_3)$_2$), 3.53 (s, 48H, 18-crown-6), 1.43 (d, 6H, CH_3), 1.28 (d, 6H, CH_3). ^{13}C{^{1}H} NMR (125.8 MHz, d_5-pyridine): δ (ppm) 165.9 (As*C*N_2), 71.8 (18-crown-6), 53.6 (*C*H(CH_3)$_2$), 44.5 (*C*H(CH_3)$_2$), 27.7 (*C*H_3), 24.3 (*C*H_3). ESI–MS (DMF): *m/z* 652.2 {[$As_7C(NH^iPr)(N^iPr)$]+H}$^+$. ESI+MS (DMF): *m/z* 1562.9 {[K(18-crown-6)]$_3$[$As_7C(NH^iPr)(N^iPr)$]}$^+$. Anal. Calcd for $C_{31}H_{63}As_7K_2N_2O_1$: C, 29.57; H, 5.05; N, 2.23. Found: C, 29.32; H, 4.91; N, 2.32.

8.3.3.9 [K(18-crown-6)]$_2$[12] (12: [$As_7C(O)(NHAd)]^{2–}$)

[K(18-crown-6)]$_2$[**2**] (50 mg, 44 μmol) and 1-adamantyl isocyanate (8 mg, 44 μmol) were used. Crystals suitable for single crystal X-ray diffraction were grown by diffusion of hexane into a 1:1 THF/pyridine solution of the product. The product was isolated as crystals (16 mg, 28%). ^{1}H NMR (500 MHz, d_5-pyridine): δ (ppm) 6.18 (s, 1H, N*H*), 3.51 (s, 48H, 18-crown-6), 2.26 (s, 6H, Ad), 1.82 (s, 3H, Ad), 1.49 (m, 3H, Ad), 1.42 (m, 3H, Ad). ^{13}C{^{1}H} NMR (125.8 MHz, d_5-pyridine): δ (ppm) 186.0 (As*C*ON), 71.6 (18-crown-6), 54.6 (Ad), 43.6 (Ad), 38.2 (Ad), 31.3 (Ad). ESI–MS (DMF): *m/z* 704.5 {[$As_7C(O)(NHAd)$]+H}$^-$. No evidence of **12** was observed in the positive ion mode ESI+MS spectrum. Anal. Calcd for $C_{40}H_{69}As_7K_2N_2O_{13}$: C, 34.58; H, 5.01.; N, 2.02. Found: C, 32.91; H, 4.49; N, 2.34.

8.3.4 Protonation of Amidine Functionalized Cages

8.3.4.1 [K(2,2,2-crypt)][13] (13: [$HP_7C(NHDipp)(NDipp)]^-$)

In a inert atmosphere glovebox, [K(2,2,2-crypt)]$_2$[**1**] (60 mg, 57 μmol) and bis(2,6-diisopropylphenyl)carbodiimide (21 mg, 57 μmol) were weighed into a glass vial and dissolved in DMF (2 mL) to give an orange solution of the hydrophosphination product [K(2,2,2-crypt)][**5**]. To this solution, [H(OEt_2)$_2$][$BAr^F{}_4$] (58 mg, 57 μmol) was added in

small aliquots over approximately 2 minutes, and the resulting solution was stirred for 1 hour. The reaction mixture was filtered through Celite® and the solvent removed under dynamic vacuum to afford a yellow-brown oil. This was washed with Et_2O (5 × 2 mL) to remove the [K(2,2,2-crypt)][BAr^F_4] byproduct, and dried under dynamic vacuum to yield the product as a pale yellow powder. Yield 32 mg (57%). Crystals suitable for single crystal X-ray diffraction were obtained by diffusion of hexane into a THF solution of the product at 5 ºC. An approximate 1:1 mixture of two isomers was observed in the NMR spectra. $^1H\{^{31}P\}$ NMR (500 MHz, d_5-pyridine): δ (ppm) 7.30–7.10 (overlapping multiplets, 12H, Ar*H*), 6.57 (s, 1H, N*H*), 6.27 (s, 1H, N*H*), 3.82–3.49 (overlapping sept, 8H, $^3J_{H–H}$ = 7 Hz, C*H*$(CH_3)_2$), 3.36 (s, 24H, 2,2,2-crypt), 3.31 (t, 24H, $^3J_{H–H}$ = 4 Hz, 2,2,2-crypt), 2.31 (t, 24H, 2,2,2-crypt), 1.86 (d, 3H, CH_3), 1.81 (d, 3H, CH_3), 1.73 (d, 3H, CH_3), 1.65 (d, 3H, CH_3), 1.61 (d, 3H, CH_3), 1.52 (d, 3H, CH_3), 1.38 (overlapping d, 6H, CH_3), 1.36 (d, 3H, CH_3), 1.34 (d, 3H, CH_3), 1.32 (overlapping d, 6H, CH_3), 1.15 (d, 3H, CH_3), 1.11 (d, CH_3), 1.08 (d, 3H, CH_3), 1.03 (d, 3H, CH_3), 0.95 (s, 2H, P*H*). $^1H\{^{31}P\}$–^{31}P 1D-HMQC NMR (500 MHz, d_5-pyridine) δ (ppm) 0.95 (s, P*H*). ^1H–^{31}P 1D-HMQC NMR (500 MHz, d_5-pyridine) δ (ppm) 0.95 (d, $^1J_{H–P}$ = 254 Hz, P*H*), 0.95 (d, $^1J_{H–P}$ = 117 Hz, P*H*). $^{31}P\{^1H\}$ NMR (202.4 MHz, d_5-pyridine): δ (ppm) Isomer 1: 34.8 (m, 1P, P3), –32.4 (m, 1P, P2), –75.6 (m, 1P, P1), –92.7 and –95.0 (overlapping multiplets, 2P, P4 and P5), –165.3 (m, 1P, P7), –191.7 (m, 1P, P6); Isomer 2: 14.6 (m, 1P, P3), 0.0 (m, 1P, P2), –50.8 and –54.0 (overlapping multiplets, 2P, P1 and P4), –112.2 (m, 1P, P5), –152.9 (m, 1P, P7), –170.6 (m, 1P, P6). Due to the presence of two isomers, both of which possess multiple overlapping resonances, it was not possible to simulate the spectrum. $^{13}C\{^1H\}$ NMR (125.8 MHz, d_5-pyridine): δ (ppm) 156.2 (d, $^1J_{C–P}$ = 63 Hz, P*C*N_2, other resonance not observed), 150.7 (Ar*C*), 148.7 (Ar*C*), 148.6 (Ar*C*), 148.2 (Ar*C*), 140.9 (Ar*C*), 140.6 (Ar*C*), 140.0 (Ar*C*), 139.9 (Ar*C*), 129.9 (Ar*C*), 129.2 (Ar*C*), 128.0 (Ar*C*), 126.3 (Ar*C*), 123.7 (Ar*C*), 123.6 (Ar*C*), 123.4

(Ar*C*), 123.2 (Ar*C*), 71.0 (2,2,2-crypt), 68.2 (2,2,2-crypt), 54.4 (2,2,2-crypt), 29.9 (*C*H(CH$_3$)$_2$), 29.7 (*C*H(CH$_3$)$_2$), 29.6 (*C*H(CH$_3$)$_2$), 29.5 (*C*H(CH$_3$)$_2$), 29.0 (*C*H$_3$), 28.9 (*C*H$_3$), 28.8 (*C*H$_3$), 28.5 (*C*H$_3$), 27.8 (*C*H$_3$), 27.7 (*C*H$_3$), 27.6 (*C*H$_3$), 24.9 (*C*H$_3$), 24.9 (*C*H$_3$), 24.8 (*C*H$_3$), 24.7 (*C*H$_3$), 23.5 (*C*H$_3$), 23.4 (*C*H$_3$), 22.6 (*C*H$_3$), 22.5 (*C*H$_3$). ESI–MS (DMF): *m/z* 581.3 [HP$_7$C(NHDipp)(NDipp)]$^-$. ESI+MS (DMF): *m/z* 1414.0 {[K(2,2,2-crypt)]$_2$[HP$_7$C(NHDipp)(NDipp)]}$^+$. Anal. Calcd for $C_{43}H_{72}KN_4O_6P_7$: C, 51.80; H, 7.28; N, 5.62 Found: C, 51.58; H, 7.15; N, 5.50.

8.3.5 Formation of Bis(amidine) Functionalized Cages

In a glovebox, [K(2,2,2-crypt)]$_2$[**1**] (60 mg, 57 μmol) and bis(2,6-diisopropylphenyl)carbodiimide (21 mg, 57 μmol) were weighed into a glass vial and dissolved in DMF (2 mL) to give an orange solution of the hydrophosphination product [K(2,2,2-crypt)]$_2$[**5**]. To this stirring solution, [H(OEt$_2$)$_2$][BAr$^F_4$] (58 mg, 57 μmol) was added portionwise over approximately 2 minutes. The solution was stirred for 1 hour, after which one equivalent of the appropriate carbodiimide was added and the mixture stirred for 20 hours. The solution was then filtered through Celite, and the solvent removed under dynamic vacuum to give a yellow oil, which was washed with Et$_2$O (5 × 2 mL) and dried *in vacuo* to yield a pale yellow powder.

8.3.5.1 [K(2,2,2-crypt)][14] (14: [P$_7${C(NHDipp)(NDipp)}$_2$]$^-$)

Bis(2,6-diisopropylphenyl)carbodiimide (21 mg, 57 μmol) was used as the second carbodiimide. Yield 53 mg (67%). Crystals suitable for single crystal X-ray diffraction were grown by diffusion of hexane into a THF solution of the product at 5 ºC. ^{1}H NMR (500 MHz, d_5-pyridine): δ (ppm) 7.26 (m, 2H, Ar*H*), 7.19 (overlapping multiplets, 8H, Ar*H*), 7.11 (m, 2H, Ar*H*), 6.31 (br s, 2H, N*H*), 3.72 (sept, $^3J_{H–H}$ = 7 Hz, 2H, C*H*(CH$_3$)$_2$), 3.66 (sept, $^3J_{H–H}$ = 7 Hz, 2H, C*H*(CH$_3$)$_2$), 3.41 (sept, partially obscured by 2,2,2-crypt, $^3J_{H–H}$ = 7

Hz, C*H*$(CH_3)_2$), remaining C*H*$(CH_3)_2$ resonance obscured by 2,2,2-crypt, 3.40 (s, 12H, 2,2,2-crypt), 3.35 (t, $^3J_{H-H}$ = 5 Hz, 12H, 2,2,2-crypt), 2.34 (t, 12H, 2,2,2-crypt), 1.81 (d, 6H, C*H*$_3$), 1.57 (d, 6H, C*H*$_3$), 1.55 (d, 6H, C*H*$_3$), 1.35 (d, 6H, C*H*$_3$), 1.27 (d, 6H, C*H*$_3$), 1.26 (d, 6H, C*H*$_3$), 1.11 (d, 6H, C*H*$_3$), 0.97 (d, 6H, C*H*$_3$). $^{31}P\{^1H\}$ NMR (202.4 MHz, d_5-pyridine): δ (ppm) 12.5 (m, $^1J_{P-P}$ = –292 Hz, $^1J_{P-P}$ = –347 Hz, $^2J_{P-P}$ = 270 Hz, $^2J_{P-P}$ = –30 Hz, $^2J_{P-P}$ = 20 Hz, $^2J_{P-P}$ = 13 Hz, 2P, P3/P4), −29.0 (m, $^1J_{P-P}$ = –345 Hz, $^2J_{P-P}$ = 87 Hz, $^2J_{P-P}$ = 21 Hz, 1P, P1), −64.2 (m, $^1J_{P-P}$ = –357 Hz, $^2J_{P-P}$ = –4 Hz, 1P, P2), −113.8 (m, $^1J_{P-P}$ = –216 Hz, 1P, P5), −129.5 (m, $^1J_{P-P}$ = –194 Hz, 2P, P6/P7). $^{13}C\{^1H\}$ NMR (125.8 MHz, d_5-pyridine): δ (ppm) P*C*N_2 not observed, 149.4 (Ar*C*), 149.3 (Ar*C*), 148.3 (Ar*C*), 147.8 (Ar*C*), 143.0 (Ar*C*), 141.6 (Ar*C*), 140.7 (Ar*C*), 139.6 (Ar*C*), 131.0 (Ar*C*), 130.3 (Ar*C*), 129.2 (Ar*C*), 127.4 (Ar*C*), 124.9 (Ar*C*), 124.5 (Ar*C*), 124.4 (Ar*C*), 124.2 (Ar*C*), 72.1 (2,2,2-crypt), 69.3 (2,2,2-crypt), 55.6 (2,2,2-crypt), 30.9 (*C*H$(CH_3)_2$), 30.7 (*C*H$(CH_3)_2$), 29.9 (*C*H$(CH_3)_2$), 29.0 (*C*H$(CH_3)_2$), 28.7 (C*H*$_3$), 26.5 (C*H*$_3$), 26.4 (C*H*$_3$), 26.3 (C*H*$_3$), 25.6 (C*H*$_3$), 24.7 (C*H*$_3$), 23.5 (C*H*$_3$), 23.0 (C*H*$_3$). ESI−MS (DMF): *m/z* 943.8 $[P_7\{C(NHDipp)(NDipp)\}_2]^-$. ESI+MS (DMF): *m/z* 1776.3 $\{[K(2,2,2\text{-crypt})]_2[P_7\{C(NHDipp)(NDipp)\}_2]\}^+$. Anal. Calcd for $C_{68}H_{106}KN_6O_6P_7$: C, 60.06; H, 7.86; N, 6.18. Found: C, 60.12; H, 8.76; N, 5.57.

8.3.5.2 [K(2,2,2-crypt)][15] (15: $[P_7\{C(NHDipp)(NDipp)\}\{C(NHCy)(NCy)\}]^-$)

Bis(cyclohexyl)carbodiimide (12 mg, 57 μmol) was used as the second carbodiimide. Yield 47 mg (68%). Crystals suitable for single crystal X-ray diffraction were grown by diffusion of hexane into a THF solution of the product at 5 ºC. ^1H NMR (500 MHz, d_5-pyridine): δ (ppm) 7.28−7.10 (overlapping m, 6H, Ar*H*), 6.20 (s, 1H, N*H*Dipp), 4.41 (br m, 1H, C*H* of Cy), 4.00 (br m, 1H, C*H* of Cy), 3.71 (sept, $^3J_{H-H}$ = 7 Hz, 2H, C*H*$(CH_3)_2$), 3.64 (sept, $^3J_{H-H}$ = 7 Hz, 2H, C*H*$(CH_3)_2$), N*H* of N*H*Cy is obscured by 2,2,2-crypt, 3.37 (s, 12H, 2,2,2-crypt),

3.32 (t, $^{3}J_{H–H}$ = 5 Hz, 12H, 2,2,2-crypt), 2.32 (t, 12H, 2,2,2-crypt), 2.03–1.04 (overlapping m, 20H, Cy), 1.83 (d, 3H, CH_3), 1.61 (d, 3H, CH_3), 1.59 (d, 3H, CH_3), 1.38 (d, 3H, CH_3), 1.30 (overlapping d, 6H, CH_3), 1.10 (d, 3H, CH_3), 1.02 (d, 3H, CH_3). $^{31}P\{^{1}H\}$ NMR (202.4 MHz, d_5-pyridine): δ (ppm) 7.3 (overlapping m, $^{1}J_{P–P}$ = –350 Hz, $^{1}J_{P–P}$ = –287 Hz, $^{2}J_{P–P}$ = 294 Hz, $^{2}J_{P–P}$ = –30 Hz, $^{2}J_{P–P}$ = 20 Hz, $^{2}J_{P–P}$ = 13 Hz, 1P, P3), 4.9 (overlapping m, $^{1}J_{P–P}$ = –305 Hz, $^{1}J_{P–P}$ = –355 Hz, $^{2}J_{P–P}$ = –30 Hz, $^{2}J_{P–P}$ = 23 Hz, $^{2}J_{P–P}$ = 13 Hz, 1P, P4), −33.6 (m, $^{1}J_{P–P}$ = –353 Hz, $^{2}J_{P–P}$ = 87 Hz, $^{2}J_{P–P}$ = 21 Hz, 1P, P1), −69.6 (m, $^{1}J_{P–P}$ = –368 Hz, $^{2}J_{P–P}$ = 4 Hz, 1P, P2), −112.7 (m, $^{1}J_{P–P}$ = –216 Hz, $^{1}J_{P–P}$ = –216 Hz, 1P, P5), −135.8 (overlapping m, $^{1}J_{P–P}$ = –194 Hz, 1P, P6), −136.5 (overlapping m, 1P, P7). $^{13}C\{^{1}H\}$ NMR (125.8 MHz, d_5-pyridine): δ (ppm) P*C*N_2 not observed, 149.6 (Ar*C*), 149.2 (Ar*C*), 141.7 (Ar*C*), 141.0 (Ar*C*), 129.1 (Ar*C*), 124.5 (Ar*C*), 124.4 (Ar*C*), 124.2 (Ar*C*), 61.7 (d, $^{3}J_{C–P}$ = 37 Hz, *C*H of Cy), 51.6 (*C*H of Cy), 38.03, 37.7, 34.3, 34.0, 30.9, 30.7, 30.0, 29.9, 28.9, 28.0, 27.5, 26.9, 26.8, 26.45, 26.4, 26.1, 25.8, 24.7, 23.6 (Cy and ^{i}Pr of Dipp). ESI−MS (DMF): *m/z* 788.4 $[P_7\{C(NHDipp)(NDipp)\}\{C(NHCy)(NCy)\}]^-$. ESI+MS (DMF): *m/z* 1617.4 $\{[K(2,2,2\text{-crypt})]_2[P_7\{C(NHDipp)(NDipp)\}\{C(NHCy)(NCy)\}]\}^+$. Despite repeated attempts, it did not prove possible to obtain a satisfactory elemental microanalysis of this compound.

8.3.5.3 [K(2,2,2-crypt)][16] (16: $[P_7\{C(NHDipp)(NDipp)\}\{C(NH^{i}Pr)(N^{i}Pr)\}]^-$)

Bis(isopropyl)carbodiimide (9 μL, 57 μmol) was used as the second carbodiimide. Yield 36 mg (57%). Crystals suitable for single crystal X-ray diffraction were grown by diffusion of hexane into a THF solution of the product at 5 ºC. ^{1}H NMR (500 MHz, d_5-pyridine): δ (ppm) 7.30−7.10 (overlapping multiplets, 6H, Ar*H*), 6.22 (s, 1H, N*H*Dipp), 4.75 (sept, $^{3}J_{H–H}$ = 6 Hz, 1H, C*H*$(CH_3)_2$ of ^{i}Pr), 3.87 (s, 1H, N*H*^{i}Pr) 3.72 (sept, $^{3}J_{H–H}$ = 6 Hz, 1H, C*H*$(CH_3)_2$ of ^{i}Pr), 3.60 (overlapping sept, $^{3}J_{H–H}$ = 7 Hz, 2H, 2 × C*H*$(CH_3)_2$ of Dipp), 3.56

(overlapping sept, $^{3}J_{H-H}$ = 7 Hz, 2H, 2 × C*H*$(CH_3)_2$ of Dipp), 3.40 (s, 12H, 2,2,2-crypt), 3.35 (t, $^{3}J_{H-H}$ = 4 Hz, 12H, 2,2,2-crypt), 2.34 (t, 12H, 2,2,2-crypt), 1.82 (d, 3H, C*H*$_3$ of Dipp), 1.63 (d, 3H, C*H*$_3$ of Dipp), 1.58 (d, 3H, C*H*$_3$ of Dipp), 1.38 (d, 3H, C*H*$_3$ of Dipp), 1.30−1.25 (overlapping d, 12H, C*H*$_3$ of ^{i}Pr), 1.08–1.07 (overlapping d, 6H, C*H*$_3$ of Dipp), 1.02 (d, 3H, C*H*$_3$ of Dipp), 0.92 (d, 3H, C*H*$_3$ of Dipp). $^{31}P\{^{1}H\}$ NMR (202.4 MHz, d_5-pyridine): δ (ppm) 6.5 (overlapping m, $^{1}J_{P-P}$ = –348 Hz, $^{1}J_{P-P}$ = –295 Hz, $^{2}J_{P-P}$ = 295 Hz, $^{2}J_{P-P}$ = –30 Hz, $^{2}J_{P-P}$ = 20 Hz, $^{2}J_{P-P}$ = 13 Hz, 1P, P3), 3.2 (overlapping m, $^{1}J_{P-P}$ = –295 Hz, $^{1}J_{P-P}$ = –356 Hz, $^{2}J_{P-P}$ = –30 Hz, $^{2}J_{P-P}$ = 23 Hz, $^{2}J_{P-P}$ = 13 Hz, 1P, P4), −34.1 (m, $^{1}J_{P-P}$ = –351 Hz, $^{2}J_{P-P}$ = 87 Hz, $^{2}J_{P-P}$ = 21 Hz, $^{2}J_{P-P}$ = 21 Hz, 1P, P1), −69.6 (m, $^{1}J_{P-P}$ = –368 Hz, $^{2}J_{P-P}$ = 4 Hz, $^{2}J_{P-P}$ = 4 Hz, 1P, P2), −112.2 (m, $^{1}J_{P-P}$ = –216 Hz, $^{1}J_{P-P}$ = –216 Hz, 1P, P5), −134.0 (m, $^{1}J_{P-P}$ = –194 Hz, 1P, P6), −136.3 (m, 1P, P7). $^{13}C\{^{1}H\}$ NMR (125.8 MHz, d_5-pyridine): δ (ppm) P*C*N_2 not observed, 149.6 (Ar*C*), 149.2 (Ar*C*), 141.7 (Ar*C*), 141.0 (Ar*C*), 124.7 (Ar*C*), 124.5 (Ar*C*), 124.4 (Ar*C*), 124.3 (Ar*C*), 53.6 (d, $^{3}J_{C-P}$ = 37 Hz, N*C*H), 45.0 (NH*C*H), 30.9, 30.7, 30.1, 28.9, 27.6, 27.4, 26.8, 26.0, 25.9, 24.6, 24.3, 24.1, 23.6. ESI−MS (DMF): *m/z* 707.4 $[P_7\{C(NHDipp)(NDipp)\}\{C(NH^{i}Pr)(N^{i}Pr)]\}^{-}$. ESI+MS (DMF): *m/z* 1538.1 $\{[K(2,2,2\text{-crypt})]_2[P_7\{C(NHDipp)(NDipp)\}\{C(NH^{i}Pr)(N^{i}Pr)\}]\}^{+}$. Despite repeated attempts, it did not prove possible to obtain a satisfactory elemental microanalysis of this compound.

8.3.6 Synthesis of Literature 1,2,3-Tripnictolide Anions

8.3.6.1 [K(2,2,2-crypt)][17] (17: $[P_3C_2H_2]^{-}$)

In a glovebox K_3P_7 (127 mg, 0.38 mmol) and 2,2,2-crypt (358 mg, 0.95 mmol) were dissolved in DMF (3.5 mL) and transferred into an ampoule equipped with a gas-tight tap. The ampoule was degassed via the freeze-pump-thaw method, and the atmosphere replaced with acetylene (approximately 1.2 bar, corresponding to 1.14 mmol based on the residual

volume of the ampoule). The ampoule was then sealed and stirred overnight, resulting in a very dark brown solution. The solvent was removed under dynamic vacuum and the dark brown solid extracted with THF (4 × 5 mL) with sonication on each extraction to break up the solid residue. The combined THF fractions were split and filtered into two crystallization ampoules, then layered with hexane and left to diffuse at 5 ºC. After 1 week yellow-brown crystals of the product suitable for single crystal X-ray diffraction were isolated by filtration and dried under dynamic vacuum for 1 hour. Combined crystalline yield 82 mg (17% based on P). ^{1}H NMR (500 MHz, d_8-THF): δ (ppm) 9.03 (m, $^{3}J_{H–H}$ = –8Hz, $^{2}J_{H–P}$ = –47Hz, $^{3}J_{H–P}$ = –18Hz, $^{3}J_{H–P}$ = 6Hz, 2H, C*H*), 3.53 (s, 12H, 2,2,2-crypt), 3.49 (t, $^{3}J_{H–H}$ = 5 Hz, 12H, 2,2,2-crypt), 2.49 (t, 12H, 2,2,2-crypt). ^{1}H{^{31}P} NMR (500 MHz, d_8-THF): δ (ppm) 9.03 (s, 2H, C*H*), the rest of the resonances observed are as detailed above. ^{31}P NMR (202.4 MHz, d_8-THF): δ (ppm) 272.8 (m, $^{1}J_{P–P}$ = –493 Hz, 1P, P2), 261.1 (m, $^{2}J_{P–P}$ = 10Hz, 2P, P1/P3). ^{13}C{^{1}H} NMR (125.8 MHz, d_8-THF): δ (ppm) 155.2 (m, P_3C_2), 68.5 (2,2,2-crypt), 65.7 (2,2,2-crypt), 52.0 (2,2,2-crypt). ESI–MS (DMF): *m/z* 118.9 $[P_3C_2H_2]^-$. ESI+MS (DMF): *m/z* 949.6 $\{[K(2,2,2\text{-crypt})]_2[P_3C_2H_2]\}^+$. Anal. Calcd for $C_{20}H_{38}KN_2O_6P_3$: C, 44.94; H, 7.17; N, 5.24. Found: C, 45.49; H, 7.19; N, 5.20.

An identical method can be used to synthesize [K(18-crown-6)][**17**] using 18-crown-6 in place of 2,2,2-crypt. Yield 72 mg by precipitation from a THF solution with hexane (19% based on P). Crystals suitable for single crystal X-ray diffraction were grown by diffusion of hexane into a THF solution of the product at 5 ºC. The NMR spectroscopic data for the anion are identical. Anal. Calcd for $C_{14}H_{26}KO_6P_3$: C, 39.79; H, 6.21. Found: C, 39.88; H, 6.27.

8.3.6.2 [K(2,2,2-crypt)][18] (18: $[As_3C_2H_2]^-$)

In a glovebox K_3As_7 (244 mg, 0.38 mmol) and 2,2,2-crypt (358 mg, 0.95 mmol) were dissolved in DMF (3.5 mL) and transferred into an ampoule equipped with a gas-tight tap. The ampoule was degassed via the freeze-pump-thaw method, and the atmosphere replaced with acetylene (approximately 1.2 bar, corresponding to 1.14 mmol based on the residual volume of the ampoule). The ampoule was then sealed and stirred overnight, resulting in a very dark green-black solution. The solvent was removed under dynamic vacuum and the dark green-black solid extracted with THF (4 × 5 mL) with sonication on each extraction to break up the solid residue. The combined THF fractions were split and filtered into two crystallization ampoules, then layered with hexane and left to diffuse at 5 ºC. After 1 week yellow-green crystals of the product suitable for single crystal X-ray diffraction were isolated by filtration and dried under dynamic vacuum for 1 hour. A powder X-ray diffractogram was collected and found to match the pattern calculated from the single crystal X-ray structure. Combined crystalline yield 110 mg (19% based on As). ^{1}H NMR (500 MHz, d_8-THF): δ (ppm) 10.68 (s, 2H, C*H*), 3.52 (s, 12H, 2,2,2-crypt), 3.48 (t, $^3J_{H–H}$ = 5 Hz, 12H, 2,2,2-crypt), 2.48 (t, 12H, 2,2,2-crypt). ^{13}C{^{1}H} NMR (125.8 MHz, d_8-THF): δ (ppm) 172.4 (m, As_3C_2), 68.5 (2,2,2-crypt), 65.7 (2,2,2-crypt), 52.0 (2,2,2-crypt). ESI–MS (DMF): *m/z* 250.8 $[As_3C_2H_2]^-$. ESI+MS (DMF): *m/z* 1081.3 $\{[K(2,2,2\text{-crypt})]_2[As_3C_2H_2]\}^+$. Anal. Calcd for $C_{20}H_{38}KN_2O_6As_3$: C, 36.05; H, 5.75; N, 4.20. Found: C, 37.20; H, 5.76; N, 4.21.

8.3.6.3 [K(18-crown-6)][19] (19: $[P_3C_2Ph_2]^-$)

$[K(18\text{-crown-6})]_2$[**1**] (400 mg, 0.49 mmol) and diphenylacetylene (258 mg, 1.45 mmol) were stirred overnight in DMF (10 mL), yielding a deep maroon solution. The solvent was then removed under dynamic vacuum and the resulting dark residue extracted with THF (20

mL). Air was bubbled through the solution for 5 minutes, and the dark red-brown solution was filtered. Volatiles were removed from the filtrate under reduced pressure, and the dark residue was washed with diethyl ether (2 × 10 mL) to yield the product as a pale red-brown powder (463 mg, 70% yield based on P). Crystals suitable for single-crystal X-ray diffraction were grown by slow diffusion of hexane (20 mL) into a THF solution (5 mL) of the product. ^{1}H NMR (500 MHz, d_8- THF): δ (ppm) 7.20 (m, 4H, Ph), 6.92 (m, 4H, Ph), 6.83 (m, 2H, Ph), 3.49 (s, 24H, 18-crown-6). ^{31}P{^{1}H} NMR (202.4 MHz, d_8-THF): δ (ppm) 297.9 (m, $^{1}J_{P-P}$ = −492 Hz, 2P, P1/P3), 273.3 (m, 1P, P2). ^{13}C{^{1}H} NMR (125.8 MHz, d_8-THF): δ (ppm) 174.9 (P_3C_2), 146.7 (Ph), 131.5 (Ph), 127.2 (Ph), 123.9 (Ph), 71.3 (18-crown-6). ESI–MS (DMF): *m/z* 270.7 $[P_3C_2(C_6H_5)_2]^-$. ESI+MS (DMF): *m/z* 877.8 $\{[K(18\text{-crown-6})]_2[P_3C_2(C_6H_5)_2]\}^+$. Anal. Calcd for $C_{28}H_{45}KO_8P_3$: C, 56.80; H, 7.01. Found: C, 56.66; H, 6.81.

8.3.6.4 [K(2,2,2-crypt)][20] (20: $[As_3C_2Ph_2]^-$)

K_3As_7 (970 mg, 1.51 mmol), diphenylacetylene (672 mg, 4.53 mmol), and 2,2,2-crypt (1.705 g, 3.71 mmol) were dissolved in DMF (20 mL) and stirred overnight under argon. The solvent was then removed under dynamic vacuum and the resulting dark residue extracted with THF (50 mL). The filtrate was reduced to half its original volume, and hexane (100 mL) was added to precipitate the product as a yellow-green solid. This was isolated by filtration and washed with hexane (3 × 15 mL) and then dried under dynamic vacuum for 3 hours. Yield: 1.161 g (39% based on As). Crystals suitable for single-crystal X-ray diffraction were grown by diffusion of hexane into a THF solution of the compound. ^{1}H NMR (500 MHz, d_5-pyridine): δ (ppm) 7.90 (m, 4H, Ph), 7.20 (m, 4H, Ph), 7.08 (m, 2H, Ph), 3.40 (s, 12H, 2,2,2-crypt), 3.35 (t, $^{3}J_{H-H}$ = 5 Hz, 12H, 2,2,2-crypt), 2.35 (t, 12H, 2,2,2-crypt). ^{13}C{^{1}H} NMR (125.8 MHz, d_5-pyridine): δ (ppm) 193.1 (As_3C_2), 148.4 (Ph), 131.2 (Ph), 127.7 (Ph), 124.5 (Ph), 70.8 (2,2,2-crypt), 68.1 (2,2,2-crypt), 54.3 (2,2,2-crypt). ESI–

MS (DMF): *m/z* 402.7 $[As_3C_2(C_6H_5)_2]^-$. ESI+MS (DMF): *m/z* 1233.5 {[K(2,2,2-crypt)]$_2$[$As_3C_2(C_6H_5)_2$]}$^+$. Anal. Calcd for $C_{32}H_{46}N_2O_6KAs_3$: C, 46.93; H, 5.67; N, 3.42. Found: C, 47.18; H, 5.72; N, 3.52.

8.3.6.5 [K(18-crown-6)][21] (21: $[P_3C_2HPh]^-$)

[K(18-crown-6)]$_2$[**1**] (0.200 g, 0.242 mmol) was dissolved in DMF (5 mL) and phenylacetylene (79 μL, 0.715 mmol) was added, giving rise to a dark purple solution which was stirred overnight under argon. The solvent was removed under dynamic vacuum, yielding a dark purple oil, which was redissolved in THF (5 mL). The solution was stirred under air for 15 minutes, resulting in an orange-brown solution, which was filtered. The product was precipitated by addition of hexane (20 mL), isolated by filtration and dried under dynamic vacuum. Yield 173 mg (61% based on P). ^{1}H NMR (500 MHz, d_8-THF): δ (ppm) 8.97 (ddd, $^2J_{H-P}$ = 45Hz, $^3J_{H-P}$ = 9Hz, $^3J_{H-P}$ = 6Hz, 1H, C*H*), 7.75 (m, 2H, Ph), 7.05 (m, 2H, Ph), 6.85 (m, 1H, Ph), 3.45 (s, 24H, 18-crown-6). ^{31}P{^{1}H} NMR (202.4 MHz, d_8-THF): δ (ppm) 289.2 (dd, $^1J_{P-P}$ = −499Hz, $^1J_{P-P}$ = −467 Hz, 1P, P2), 275.5 (dd, $^2J_{P-P}$ = 14 Hz, 1P, P1), 269.0 (dd, 1P, P3). ^{13}C{^{1}H} NMR (125.8 MHz, d_8-THF): δ (ppm) 178.5 (P_3C_{Ph}), 157.7 (P_3C_H) 146.3 (Ph), 132.4 (Ph), 128.2 (Ph), 124.1 (Ph), 71.3 (18-crown-6). ESI–MS (DMF): *m/z* 195.1 $[P_3C_2H(C_6H_5)]^-$. ESI+MS (DMF): *m/z* 801.4 {[K(18-crown-6)]$_2$[$P_3C_2H(C_6H_5)$]}$^+$. It did not prove possible to obtain a sample of the compound sufficiently pure for elemental microanalysis.

8.3.6.6 [K(18-crown-6)][22] (22: $[As_3C_2HPh]^-$)

The same procedure used for the synthesis of [K(18-crown-6)][**21**] was employed, using K_3As_7 (100 mg, 0.156 mmol), 18-crown-6 (123 mg, 0.468 mmol), and phenylacetylene (51 μL, 0.390 mmol). It was not necessary to stir the THF solution in air. Yield 152 mg (66% based on As). Crystals suitable for single crystal X-ray diffraction were grown by diffusion

of hexane into a THF solution of the product. ^{1}H NMR (500 MHz, d_8-THF): δ (ppm) 10.58 (s, 1H, C*H*), 7.80 (m, 2H, Ph), 7.14 (m, 2H, Ph), 6.97 (m, 1H, Ph), 3.52 (s, 24H, 18-crown-6). ^{13}C{^{1}H} NMR (125.8 MHz, d_8-THF): δ (ppm) 194.0 (As_3C_{Ph}), 172.0 (As_3C_H), 146.4 (Ph), 139.8 (Ph), 126.0 (Ph), 121.1 (Ph), 68.3 (18-crown-6). ESI–MS (DMF): *m/z* 327.0 $[P_3C_2H(C_6H_5)]^-$. ESI+MS (DMF): *m/z* 933.7 $\{[K(18\text{-crown-6})]_2[P_3C_2H(C_6H_5)]\}^+$. It did not prove possible to obtain a sample of the compound sufficiently pure for elemental microanalysis.

8.3.6.7 [Cs(18-crown-6)][23] (23: $[P_3C_6H_4]^-$)

2-(Trimethylsilyl)phenyl trifluoromethanesulfonate (74 μL, 0.153 mmol) was added to a stirring solution of $[K(18\text{-crown-6})]_2$[**1**] (100 mg, 0.061 mmol) and CsF (46 mg, 0.153 mmol) in a mixture of pyridine (2 mL) and acetonitrile (3 mL). The mixture was left to stir for 12 hours, over which time it gradually changed colour from orange to brown. The solvent was removed under reduced pressure and washed with benzene (5 mL). The residue was extracted into THF (5 mL), filtered, and layered with hexane. Small yellow needles of the product form together with colourless crystals, which were assumed to be [K/Cs(18-crown-6)][OTf]. ^{31}P NMR analysis of the reaction mixture reveals the characteristic 1,2,3-triphospholide resonances, alongside the known polyphosphide $[P_{16}]^{2-}$ which arise due to reaction of [**1**] with the acetonitrile used as solvent. ^{31}P NMR (202.4 MHz, THF): δ (ppm) 335.2 (m, $^{1}J_{P-P}$ = –501 Hz, 1P, P2), 261.3 (m, 2P, P1/P3).

8.3.7 Coordination Compounds of 1,2,3-Tripnictolides

8.3.7.1 [K(2,2,2-crypt)][24] (24: $[Ru(\eta^5\text{-}P_3C_2H_2)\{\eta^1\text{-}CH_3C(CH_2)_2\}\{\eta^3\text{-}CH_3C(CH_2)_2\}]^-$)

In a glovebox, [K(2,2,2-crypt)][**17**] (50 mg, 94 μmol) and [Ru(COD)(η^3- $CH_3C(CH_2)_2)_2$] (30 mg, 94 μmol) were weighed into a Schlenk tube. The solids were dissolved in THF (3 mL), and stirred at 45 ºC under argon for 3 hours to give a slightly cloudy yellow solution. The solution was filtered, and the solvent removed under dynamic vacuum to give an oily orange solid that was washed with pentane (3 × 2 mL) and dried under dynamic vacuum to give the product as an orange powder. Yield 55 mg (78%). ^{1}H NMR (500 MHz, d_8-THF): δ (ppm) 4.96 (m, $^3J_{H–H}$ = –4 Hz, $^2J_{H–P}$ = –41 Hz, $^3J_{H–P}$ = –16 Hz, 2H, C*H*), 3.92 (m, 2H), 3.60 (s, 12H, 2,2,2-crypt), 3.56 (t, $^3J_{H–H}$ = 5 Hz, 12H, 2,2,2-crypt), 2.94 (s, 2H), 2.56 (t, 12H, 2,2,2-crypt), 1.75 (s, 3H), 1.58 (s, 3H), 0.75 (s, 2H), 0.65 (s, 2H). ^{1}H{^{31}P} NMR (500 MHz, d_8-THF): δ (ppm) 4.96 (s, 1H, C*H*), the rest of the resonances observed are as detailed above. ^{31}P NMR (202.4 MHz, d_8-THF): δ (ppm) 25.8 (m, $^1J_{P–P}$ = –415 Hz, $^2J_{P–P}$ = 10 Hz, 2P, P1/P3), –29.8 (m, 1P, P2). ^{13}C{^{1}H} NMR (125.8 MHz, d_8-THF): δ (ppm) 157.1, 108.2, 106.8 (m, P_3C_2), 94.5, 89.4, 68.6 (2,2,2-crypt), 65.7 (2,2,2-crypt), 52.1 (2,2,2-crypt), 44.8, 27.9, 21.4. ESI–MS (DMF): *m/z* 331.0 $[Ru(P_3C_2H_2)\{CH_3C(CH_2)_2\}_2]^-$, 276.0 $[Ru(P_3C_2H_2)\{CH_3C(CH_2)_2\}]^-$. ESI+MS (DMF): *m/z* 1161.4 $\{[K(2,2,2\text{-crypt})]_2[Ru(P_3C_2H_2)\{CH_3C(CH_2)_2\}_2]\}^+$. Anal. Calcd for $C_{28}H_{52}KN_2O_6P_3Ru$: C, 45.07; H, 7.03; N, 3.76. Found: C, 46.17; H, 7.04; N, 3.74.

8.3.7.2 [K(2,2,2-crypt)][25] (25: [Ru(η^5-As$_3$C$_2$H$_2$){η^1-CH$_3$C(CH$_2$)$_2$}{η^3-CH$_3$C(CH$_2$)$_2$}]$^-$)

K(2,2,2-crypt)][**18**] (21 mg, 63 μmol) and [Ru(COD)(η^3-CH$_3$C(CH$_2$)$_2$)$_2$] (13 mg, 79 μmol) were weighed into an NMR tube equipped with a gas-tight valve. d_8-THF (0.5 mL) was added, and the tube was heated to 45 ºC. The reaction was monitored by ^{1}H NMR spectroscopy, which showed quantitative conversion to a single product after 3 hours. The reaction was filtered into a crystallization ampoule and diluted with THF to 3 mL then layered with hexane. After a few days of storage at 5 ºC small orange crystals of the product formed. Isolated crystalline yield 6 mg (10%). A powder X-ray diffractogram was collected and found to match the pattern calculated from the single crystal X-ray structure. ^{1}H NMR (500 MHz, d_8-THF): δ (ppm) 6.41 (s, 2H, C*H*), 3.93 (m, 2H) 3.61 (s, 12H, 2,2,2-crypt), 3.56 (t, $^3J_{H–H}$ = 5 Hz, 12H, 2,2,2-crypt), 2.89 (s, 2H), 2.56 (t, 12H, 2,2,2-crypt), 1.79 (s, 3H), 1.58 (s, 3H), 0.68 (s, 2H), 0.56 (s, 2H). ^{13}C{^{1}H} NMR (125.8 MHz, d_8-THF): δ (ppm) 158.9, 123.6, 110.0, 97.0, 89.0, 70.4 (2,2,2-crypt), 67.6 (2,2,2-crypt), 53.9 (2,2,2-crypt), 45.4, 31.4, 23.7. ESI–MS (DMF): *m/z* 462.7 [Ru(As$_3$C$_2$H$_2$){CH$_3$C(CH$_2$)$_2$}$_2$]$^-$, 406.7 [Ru(As$_3$C$_2$H$_2$){CH$_3$C(CH$_2$)$_2$}]$^-$. ESI+MS (DMF): *m/z* 1292.8 {[K(2,2,2-crypt)]$_2$[Ru(As$_3$C$_2$H$_2$){CH$_3$C(CH$_2$)$_2$}$_2$]}$^+$. Anal. Calcd for $C_{28}H_{52}KN_2O_6As_3Ru$: C, 38.30; H, 5.97; N, 3.19. Found: C, 38.22; H, 5.86; N, 2.86.

8.3.7.3 [K(18-crown-6)][26] (26: [(η^5-P$_3$C$_2$H$_2$)Mo(CO)$_3$]$^-$)

Mo(CO)$_3$(MeCN)$_3$ (72 mg, 0.238 mmol) and [K(18-crown-6)][**17**] (100 mg, 0.238 mmol) were dissolved in THF (5 mL) and stirred overnight under argon to give a dark red solution. The solution was filtered into an ampoule and layered with hexane (20 mL). After several days yellow crystals suitable for single-crystal X-ray diffraction had formed. Monitoring the reaction by NMR spectroscopy shows that the reaction is quantitative. Isolated crystalline

yield: 18 mg (13%). ^{1}H NMR (500 MHz, d_8-THF): δ (ppm) 5.82 (m, $^{3}J_{H–H}$ = 6 Hz, $^{2}J_{H–P}$ = 44 Hz, $^{3}J_{H–P}$ = 13 Hz, $^{3}J_{H–P}$ = 4 Hz, 2H, C*H*), 3.64 (s, 24H, 18-crown-6). ^{1}H{^{31}P} NMR (500 MHz, d_8-THF): δ (ppm) 5.83 (s, 2H, C*H*), the rest of the resonances observed are as detailed above. ^{31}P NMR (202.4 MHz, d_8-THF): δ (ppm) 67.3 (m, $^{1}J_{P–P}$ = −422 Hz, $^{2}J_{P–P}$ = 8 Hz, 2P, P1/P3), 34.5 (m, 1P, P2). ^{13}C{^{1}H} NMR (125.8 MHz, d_8-THF): δ (ppm) 227.8 (*C*O), 111.5 (m, *C*H), 70.3 (18-crown-6). ESI–MS (DMF): *m/z* 300.8 $[Mo(CO)_3(P_3C_2H_2)]^-$. No evidence of **26** was observed in the positive ion mode ESI+MS spectrum. IR (ν_{CO}, cm^{-1}): 1916, 1834, 1814. Anal. Calcd for $MoC_{17}H_{26}O_9KP_3$: C, 33.90; H, 4.35. Found: C, 32.76; H, 4.28.

8.3.7.4 [K(18-crown-6)][27] (27: $[(\eta^5\text{-}As_3C_2H_2)Mo(CO)_3]^-$)

The reaction was carried out as for [K(18-crown-6)][**26**], using $Mo(CO)_3(MeCN)_3$ (72 mg, 0.238 mmol) and [K(18-crown-6)][**18**] (132 mg, 0.238 mmol). Monitoring the reaction by NMR spectroscopy shows that the reaction is quantitative. Isolated crystalline yield: 26 mg (15%). ^{1}H NMR (500 MHz, d_8-THF): δ (ppm) 7.04 (s, 2H, C*H*), 3.67 (s, 24H, 18-crown-6). ^{13}C{^{1}H} NMR (125.8 MHz, d_8-THF): δ (ppm) 228.1 (*C*O), 124.1 (*C*H), 70.2 (18-crown-6). ESI–MS (DMF): *m/z* 432.7 $[Mo(CO)_3(As_3C_2H_2)]^-$. ESI+MS (DMF): 1039.1 $\{[K(18\text{-crown-}6)]_2[Mo(CO)_3(As_3C_2H_2)]\}^+$. IR ($\nu_{CO}$, cm^{-1}): 1910, 1830, 1817. Anal. Calcd for $MoC_{17}H_{26}O_9KAs_3$: C, 27.81; H, 3.57. Found: C, 28.79; H, 3.72.

8.3.7.5 [K(18-crown-6)][28] (28: $[(\eta^5\text{-}P_3C_2Ph_2)Mo(CO)_3]^-$)

[K(18-crown-6)][**19**] (100 mg, 0.174 mmol) and $Mo(CO)_6$ (46 mg, 0.174 mmol) were dissolved in THF (5 mL) and heated at 50 °C for 36 hours. The reaction mixture was filtered into a clean Schlenk tube, and hexane (20 mL) was added to precipitate out an orange solid. This solid was isolated by filtration and dried under vacuum for one hour. Yield 61 mg (46%). Crystals of [K(18-crown-6)THF][**27**] could be grown from slow

diffusion of hexane into a THF solution of the product. ^{1}H NMR (500 MHz, d_8-THF): δ (ppm) 7.13 (m, 2H, Ph), 6.89 (m, 2H, Ph), 6.86 (m, 1H, Ph), 3.62 (s, 24H, 18-crown-6). ^{31}P NMR (202.4 MHz, d_8-THF): δ (ppm) 100.8 (m, $^{1}J_{P-P}$ = −415 Hz, 2P, P1/P3), 24.2 (m, 1P, P2). ^{13}C{^{1}H} NMR (125.8 MHz, d_8-THF): δ (ppm) 228.5 (*C*O), 140.6 (m, P_3C_2), 132.5 (Ph), 126.7 (Ph), 125.8 (Ph), *ipso* Ph not observed, 70.1 (18-crown-6). ESI–MS (DMF): *m/z* 452.5 $[Mo(CO)_3\{P_3C_2(C_6H_5)_2\}]^-$. ESI+MS (DMF): *m/z* 1058.1 $\{[K(18\text{-crown-}6)]_2[Mo(CO)_3\{P_3C_2(C_6H_5)_2\}]\}^+$. IR ($\nu_{CO}$, cm^{-1}): 1921, 1842, 1821. It did not prove possible to obtain a sample of the compound sufficiently pure for elemental microanalysis.

8.3.7.6 [K(2,2,2-crypt)][29] (29: $[(\eta^5\text{-}As_3C_2Ph_2)Mo(CO)_3]^-$)

[K(2,2,2-crypt)][**20**] (50 mg, 61 μmol) and $Mo(CO)_3(MeCN)_3$ (19 mg, 61 μmol) were dissolved in THF (5 mL) and stirred at 60 °C overnight to give a dark red solution. The reaction mixture was filtered into a gas-tight ampoule and layered with hexane. Orange crystals suitable for single-crystal X-ray diffraction were obtained after several days. Yield 30 mg (49%). ^{1}H NMR (500 MHz, d_5-pyridine): δ (ppm) 7.69 (m, 2H, Ph), 7.05 (m, 2H, Ph) 7.00 (m, 1H, Ph), 3.42 (s, 12H, 2,2,2-crypt), 3.37 (t, $^{3}J_{H-H}$ = 5 Hz, 12H, 2,2,2-crypt), 2.37 (t, 12H, 2,2,2-crypt). ^{13}C{^{1}H} NMR (125.8 MHz, d_5-pyridine): δ (ppm) 229.8 (*C*O), 156.4 (Ph), 142.3 (m, As_3C_2), 132.4 (Ph), 127.1 (Ph), 126.0 (Ph), 71.0 (2,2,2-crypt), 68.1 (2,2,2-crypt), 54.2 (2,2,2-crypt). ESI–MS (DMF): *m/z* 584.8 $[Mo(CO)_3\{As_3C_2(C_6H_5)_2\}]^-$. ESI+MS (DMF): *m/z* 1415.5 $\{[K(2,2,2\text{-crypt})]_2[Mo(CO)_3\{As_3C_2(C_6H_5)_2\}]\}^+$. IR ($\nu_{CO}$, cm^{-1}): 1910, 1836, 1818. Anal. Calcd for $C_{35}H_{46}KMoN_2O_9As_3$: C, 42.08; H, 4.64; N, 2.81. Found: C, 42.95; H, 4.58; N, 2.88.

8.3.7.7 [K(18-crown-6)][30] (30: $[(\eta^5\text{-}P_3C_2HPh)Mo(CO)_3]^-$)

The reaction was carried out as for [K(18-crown-6)][**28**], using [K(18-crown-6)][**21**] (100mg, 0.200 mmol) and $Mo(CO)_6$ (53 mg, 0.200 mmol). The product was isolated as an

orange powder. Yield 99 mg (74%). ^{1}H NMR (500 MHz, d_5-pyridine): δ (ppm) 7.49 (m, 2H, Ph), 7.08 (m, 2H, Ph), 7.01 (m, 1H, Ph), 6.16 (ddd, $^{2}J_{H–P}$ = 42Hz, $^{3}J_{H–P}$ = 10Hz, $^{3}J_{H–P}$ = 4Hz, 1H, C*H*), 3.55 (s, 24H, 18-crown-6). ^{1}H{^{31}P} NMR (500 MHz, d_5-pyridine): δ (ppm) 6.16 (s, 1H, C*H* of phospholide), the rest of the resonances observed are as detailed above. ^{31}P{^{1}H} NMR (202.4 MHz, d_5-pyridine): δ (ppm) 77.0 (dd, $^{1}J_{P–P}$ = −435 Hz, $^{2}J_{P–P}$ = 42 Hz, 1P, P3), 70.7 (dd, $^{1}J_{P–P}$ = −404 Hz, 1P, P1), 40.6 (dd, 1P, P2). ^{13}C{^{1}H} NMR (125.8 MHz, d_5-pyridine): δ (ppm) 228.9 (*C*O), 142.8 (C_{Ph}), 129.7 (Ph), 128.3 (Ph), 126.4 (Ph), 115.0 (C_H), 71.2 (18-crown-6), *ipso* Ph not observed. ESI–MS (DMF): *m/z* 376.9 $[Mo(CO)_3\{P_3C_2H(C_6H_5)\}]^-$. No evidence of **30** was observed in the positive ion mode ESI+MS spectrum. IR (ν_{CO}, cm^{-1}): 1925, 1842, 1828. It did not prove possible to obtain a sample of the compound sufficiently pure for elemental microanalysis.

8.3.7.8 [K(18-crown-6)][31] (31: $[(\eta^5\text{-}As_3C_2HPh)Mo(CO)_3]^-$)

The reactions was carried out as for [K(18-crown-6)][**28**], using [K(18-crown-6)][**22**] (100 mg, 0.159 mmol) and $Mo(CO)_6$ (42 mg, 0.159 mmol). The product was isolated as a bright orange solid. Yield 26 mg (20%). Crystals suitable for single crystal X-ray diffraction were grown by diffusion of hexane into a THF solution of the product. ^{1}H NMR (500 MHz, d_5-pyridine): δ (ppm) 7.48 (m, 2H, Ph), 7.29 (s, 1H, C*H* of arsolide) 7.09 (m, 2H, Ph), 7.04 (m, 1H, Ph), 3.61 (s, 24H, 18-crown-6). ^{13}C{^{1}H} NMR (125.8 MHz, d_5-pyridine): δ (ppm) 229.2 (*C*O), 153.6 (Ph), 145.6 (*C*Ph of arsolide), 130.6 (Ph), 128.2 (Ph), 126.4 (Ph), 113.9 (*C*H of arsolide), 71.4 (18-crown-6). ESI–MS (DMF): *m/z* 508.8 $[Mo(CO)_3\{As_3C_2H(C_6H_5)\}]^-$. ESI+MS (DMF): *m/z* 1115.1 $\{[K(18\text{-crown-}6)]_2[Mo(CO)_3\{As_3C_2H(C_6H_5)\}]\}^+$. IR ($\nu_{CO}$, cm^{-1}): 1911, 1828, 1818. Anal. Calcd for $C_{23}H_{30}KMoO_9As_3$: C, 34.09; H, 3.73. Found: C, 34.07; H, 3.60.

8.3.8 Chemistry of the $[P_3C_2H(2\text{-py})]^-$ Anion

8.3.8.1 [K(2,2,2-crypt)][32] (32: $[P_3C_2H(2\text{-pyridyl})]^-$)

2-Ethynylpyridine (58 μL, 0.57 mmol) was added dropwise to a stirring solution of $[K(2,2,2\text{-crypt})]_2$[**1**] (200 mg, 0.19 mmol) in DMF (3 mL), resulting in an instant color change of the reaction mixture to a deep purple. The solution was stirred overnight. The solvent was removed under dynamic vacuum to yield a deep purple oily solid, which was partially redissolved in THF (10 mL). Air was then bubbled through the solution for 2 minutes (in order to oxidize undesired radical side-products), which resulted in an instant colour change to orange-brown, and the formation of a pale precipitate. The solution was then filtered, and the THF removed under dynamic vacuum to give a brown-orange oil. The solid sample was washed with diethyl ether (10 mL) yielding a peach solid (81 mg, 30%). Crystals suitable for single crystal X-ray diffraction were grown by diffusion of hexane into a THF (5 mL) solution of the product. ^{1}H NMR (500 MHz, d_8-THF): δ (ppm) 9.88 (ddd, $^2J_{H-P}$ = 47 Hz, $^3J_{H-P}$ = 13 Hz, $^3J_{H-P}$ = 7 Hz, 1H, C*H* of phospholide), 8.39 (m, 1H, C*H* of pyridyl), 8.20 (m, 1H, C*H* of pyridyl), 7.42 (m, 1H, C*H* of pyridyl), 6.79 (m, 1H, C*H* of pyridyl), 3.48 (s, 12H, 2,2,2-crypt), 3.45 (t, $^3J_{H-H}$ = 5 Hz, 12H, 2,2,2-crypt), 2.45 (t, 12H, 2,2,2-crypt). ^{1}H{^{31}P} NMR (500 MHz, d_8-THF): δ (ppm) 9.88 (s, 1H, C*H* of phospholide), the rest of the resonances observed are as detailed above. ^{31}P NMR (202.4 MHz, d_8-THF): δ (ppm) 293.1 (m, $^1J_{P-P}$ = −462 Hz, $^1J_{P-P}$ = −505 Hz, 1P, P2), 278.3 (m, $^2J_{P-P}$ = 13 Hz, 1P, P3), 274.3 (m, 1P, P1). ^{13}C{^{1}H} NMR (125.8 MHz, d_8-THF): δ (ppm) 177.3 (m, *ipso C* of py), 162.3 (m, *C*pyridyl of phospholide), 161.3 (m, *C*H of phospholide), 149.5 (s, pyridyl), 135.5 (s, pyridyl), 123.6 (s, pyridyl), 118.7 (s, pyridyl), 71.5 (2,2,2-crypt), 68.7 (2,2,2-crypt), 55.0 (2,2,2-crypt). ESI–MS (DMF): *m/z* 195.9 $[P_3C_2H(C_5H_4N)]^-$. ESI+MS (DMF):

m/z 1025.8 $\{[K(2,2,2\text{-crypt})]_2[P_3C_2H(C_5H_4N)]\}^+$. Anal. Calcd for $C_{25}H_{41}KN_3O_6P_3$: C, 49.09; H, 6.76; N, 6.87. Found: C, 49.62; H, 6.54; N, 6.82.

8.3.8.2 [K(2,2,2-crypt)][33] (33: $[\{\eta^5\text{-}P_3C_2H(2\text{-pyridyl})\}Mo(CO)_3]^-$)

A mixture of [K(2,2,2-crypt)][**32**] (20 mg, 33 μmol) and $Mo(py)_3(CO)_3$ (9 mg, 33 μmol) were weighed into an NMR tube equipped with a gas-tight valve. d_8-THF (0.5 mL) was added and the tube sealed and agitated to mix the contents. It was then heated to 70 °C for 2 hours, after which ^{1}H and ^{31}P NMR spectroscopy indicated quantitative conversion to the product. The orange solution was transferred into a Schlenk tube under argon and solvent removed under vacuum yielding an orange oil which was washed with diethyl ether (3 × 2 mL) and dried under vacuum yielding the product, [K(2,2,2-crypt)][**32**], as an orange-yellow powder. Yield 24 mg (92%). Crystals suitable for single crystal X-ray diffraction were grown by diffusion of hexane into a THF solution of the product. ^{1}H NMR (500 MHz, d_8-THF): δ (ppm) 8.24 (m, 1H, C*H* of pyridyl), 7.61 (m, 1H, C*H* of pyridyl), 7.42 (m, 1H, C*H* of pyridyl), 6.88 (overlapping m, 1H, C*H* of pyridyl), 6.84 (ddd, $^2J_{H-P}$ = 43 Hz, $^3J_{H-P}$ = 11 Hz, $^3J_{H-P}$ = 4 Hz, 1H, C*H* of phospholide), 3.58 (12H, s, 2,2,2-crypt), 3.54 (t, $^3J_{H-H}$ = 5 Hz, 12H, 2,2,2-crypt), 2.56 (t, 12H, 2,2,2-crypt). ^{1}H{^{31}P} NMR (500 MHz, d_8-THF): δ (ppm) 6.84 (s, 1H, C*H* of phospholide), the rest of the resonances observed are as detailed above. ^{31}P NMR (202.4 MHz, d_8-THF): δ (ppm) 77.6 (m, $^1J_{P-P}$ = −438 Hz, $^2J_{P-P}$ = 13 Hz, 1P, P3), 70.8 (m, $^1J_{P-P}$ = −400 Hz, 1P, P1), 42.4 (m, 1P, P2). ^{13}C{^{1}H} NMR (125.8 MHz, d_8-THF): δ (ppm) 228.2 (s, *C*O), 160.6 (dd, $^2J_{C-P}$ = 22 Hz, $^3J_{C-P}$ = 4 Hz, *ipso C* of pyridyl), 148.7 (s, pyridyl), 135.7 (s, pyridyl), 134.3 (ddd, $^1J_{C-P}$ = −83 Hz, $^2J_{C-P}$ = −11 Hz, $^2J_{C-P}$ = −6 Hz, *C*py of phospholide), 123.6 (d, $^3J_{C-P}$ = 12 Hz, pyridyl), 120.8 (s, pyridyl), 114.9 (ddd, $^1J_{C-P}$ = −83 Hz, $^2J_{C-P}$ = −8 Hz, $^2J_{C-P}$ = −3.5 Hz, *C*H of phospholide), 71.2 (2,2,2-crypt), 68.4 (2,2,2-crypt), 54.7 (2,2,2-crypt). ESI–MS (DMF): *m/z* 378.5 $[\{P_3C_2H(C_5H_4N)\}Mo(CO)_3]^-$. ESI+MS (DMF): *m/z* 1210.0 {[K(2,2,2-

crypt)]$_2$[{$P_3C_2H(C_5H_4N)$}$Mo(CO)_3$]}$^+$. IR (ν_{CO}, cm^{-1}): 1924, 1828, 1812. Anal. Calcd for $MoC_{28}H_{41}KN_3O_9P_3$: C, 42.48; H, 5.22; N, 5.31. Found: C, 43.10; H, 5.37; N, 5.15.

8.3.8.3 [K(2,2,2-crypt)][34] (34: [{κ^2-P,N-P_3C_2H(2-pyridyl)}$Mo(CO)_4$]$^-$)

A mixture of [K(2,2,2-crypt)][**32**] (20 mg, 33 μmol) and Mo(COD)$(CO)_4$ (10 mg, 33 μmol) were weighed into an NMR tube equipped with a gas-tight valve. CD_2Cl_2 (0.5 mL) was added and the tube sealed and agitated to mix the contents. The reaction was then left at room temperature, and regularly monitored by NMR spectroscopy, showing the disappearance of resonances arising due to **32** with concomitant growth of resonances assigned to **34**. After 48 hours there was approximately 85% of **34**, alongside approximately 10% (by integration) of the η^5 complex (**33**) and 5% of **32**. After characterization by multielement NMR spectroscopy, the red-brown solution was layered with pentane and placed in a freezer at −35 °C. Crystals suitable for single crystal X-ray diffraction grew after a few days. This reaction may also be performed in d_8-THF; however, conversion to the η^5 complex (**33**) occurs much more rapidly in this solvent and all attempts to grow crystals were unsuccessful. ^{1}H NMR (500 MHz, d_8-THF): δ (ppm) 9.51 (ddd, $^2J_{H–P}$ = 44 Hz, $^3J_{H–P}$ = 28 Hz, $^3J_{H–P}$ = 4 Hz, 1H, C*H* of phospholide), 9.02 (m, 1H, C*H* of pyridyl), 8.00 (m, 1H, C*H* of pyridyl), 7.69 (m, 1H, C*H* of pyridyl), 6.82 (m, 1H, C*H* of pyridyl), 3.52 (s, 12H, 2,2,2-crypt), 3.46 (t, $^3J_{H–H}$ = 5 Hz, 12H, 2,2,2-crypt), 2.47 (t, 12H, 2,2,2-crypt). ^{1}H{^{31}P} NMR (500 MHz, d_8-THF): δ (ppm) 9.51 (s, 1H, C*H* of phospholide), the rest of the resonances observed are as detailed above. ^{31}P NMR (202.4 MHz, d_8-THF): δ (ppm) 266.6 (m, $^1J_{P–P}$ = −453 Hz, $^2J_{P–P}$ = 25 Hz, 1P, P1), 262.5 (m, $^1J_{P–P}$ = −585 Hz, 1P, P3), 240.2 (m, 1P, P2). ^{13}C{^{1}H} NMR (125.8 MHz, d_8-THF): δ (ppm) 223.5 (d, $^2J_{C–P}$ = −6 Hz, *C*O trans to N), 221.1 (dd, $^2J_{C–P}$ = 34 Hz, $^3J_{C–P}$ = 3 Hz, *C*O trans to P), 207.4 (d, $^2J_{C–P}$ = −11 Hz, axial *C*O), 168.8 (m, *C*py of phospholide), 156.9 (m, *C*H of phospholide), 156.3 (s, pyridyl), 149.5 (m, *ipso C*), 137.6 (s, pyridyl), 120.9 (d, $^2J_{C–P}$ = 9 Hz, pyridyl), 118.9 (s, pyridyl),

71.1 (2,2,2-crypt), 68.3 (2,2,2-crypt), 54.6 (2,2,2-crypt). ESI–MS (DMF): *m/z* 406.0 $[\{P_3C_2H(C_5H_4N)\}Mo(CO)_4]^-$. No evidence of **34** was observed in the positive ion mode ESI+MS spectrum. IR (ν_{CO}, cm^{-1}): 2004, 1895, 1879, 1828. Anal. Calcd for $MoC_{29}H_{41}KN_3O_{10}P_3$: C, 42.50; H, 5.04; N, 5.13. Found: C, 42.72; H, 5.03; N, 5.08.

8.3.8.4 [K(2,2,2-crypt)][35] (35: [{μ:η^{5}κ^2-P,N-P_3C_2H(2-pyridyl)}-{$Mo(CO)_3$}{$Mo(CO)_4$}]$^-$)

A mixture of [K(2,2,2-crypt)][**32**] (20 mg, 33 μmol) and $Mo(py)_3(CO)_3$ (9 mg, 33 μmol) were weighed into a Schlenk tube, dissolved in THF (1 mL) and heated at 70 °C under argon for 2 hours. The bright orange solution was then filtered, and the solvent removed under dynamic vacuum to yield an orange solid. The solid was redissolved in CD_2Cl_2 (0.5 mL); ^1H and ^{31}P NMR spectroscopy indicated quantitative conversion to [K(2,2,2-crypt)][**33**]. To this solution $Mo(COD)(CO)_4$ (10 mg, 33 μmol) was added, and the NMR tube was heated to 40 °C for 1 hour, at which point ^1H and ^{31}P NMR spectroscopy showed the formation of a new complex. After characterization by multielement NMR spectroscopy the intensely coloured orange solution was filtered into a Schlenk tube and layered with pentane yielding a yellow oil. ^1H NMR (500 MHz, CD_2Cl_2): δ (ppm) 8.86 (m, 1H, C*H* of pyridyl), 7.61 (m, 1H, C*H* of pyridyl), 7.43 (m, 1H, C*H* of pyridyl), 6.89 (m, 1H, C*H* of pyridyl), 6.68 (ddd, $^2J_{H-P}$ = 40 Hz, $^3J_{H-P}$ = 16 Hz, $^3J_{H-P}$ = 3 Hz, 1H, C*H* of phospholide), 3.57 (s, 1H, 2,2,2-crypt), 3.51 (t, 1H, $^3J_{H-H}$ = 5 Hz, 2,2,2-crypt), 2.52 (t, 1H, 2,2,2-crypt). $^1H\{^{31}P\}$ NMR (500 MHz, CD_2Cl_2): δ (ppm) 6.68 (s, 1H, C*H* of phospholide), the rest of the resonances observed are as detailed above. ^{31}P NMR (202.4 MHz, CD_2Cl_2): δ (ppm) 119.4 (m, $^1J_{P-P}$ = −546 Hz, $^2J_{P-P}$ = 21 Hz, 1P, P3), 63.5 (m, $^1J_{P-P}$ = −384 Hz, 1P, P1), −21.7 (m, 1P, P2). $^{13}C\{^1H\}$ NMR (125.8 MHz, CD_2Cl_2): δ (ppm) 226.2 (s, *C*O of $Mo(CO)_3$), 222.3 (d, $^2J_{C-P}$ = 7Hz, *C*O trans to N), 217.7 (dd, $^2J_{C-P}$ = 41Hz, $^3J_{C-P}$ = 2Hz, *C*O trans to P), 206.2 (d,

$^2J_{C–P}$ = 10 Hz, axial *C*O), 205.2 (d, $^2J_{C–P}$ = 11 Hz, axial *C*O), 160.7 (d, $^2J_{C–P}$ = 22 Hz, *ipso C* of pyridyl), 155.8 (m, *C*py of phospholide), 148.6 (s, pyridyl), 137.7 (s, pyridyl), 121.6 (d, $^3J_{C–P}$ = 8 Hz, pyridyl), 121.0 (s, pyridyl), 109.8 (dd, $^1J_{C–P}$ = 89 Hz, $^2J_{C–P}$ = 9 Hz, *C*H of phospholide), 70.9 (2,2,2-crypt), 68.0 (2,2,2-crypt), 58.4 (2,2,2-crypt). ESI–MS (DMF): *m/z* 584.3 ($[\{P_3C_2H(C_5H_4N)\}Mo_2(CO)_7\}]^-$), 556.2 ($[\{P_3C_2H(C_5H_4N)\}Mo_2(CO)_6\}]^-$). No evidence of **35** was observed in the positive ion mode ESI+MS spectrum. IR (ν_{CO}, cm^{-1}): 2020, 1940, 1912, 1884, 1847. Anal. Calcd for $Mo_2C_{32}H_{41}KN_3O_{13}P_3$: C, 38.45; H, 4.13; N, 4.20. Found: C, 38.89; H, 4.07; N, 4.24.

8.3.9 Further 1,2,3-Tripnictolide Synthesis

The syntheses given here are unoptimized, and in most cases yield material that is not spectroscopically pure. Nevertheless, the data obtained support the synthesis of the following anions.

8.3.9.1 [K(18-crown-6)][36] (36: $[P_3C_2H\{Fe(C_5H_4)(C_5H_5)\}]^-$)

$[K(18\text{-crown-6})]_2$[**1**] (302 mg, 0.268 mmol) and ethynylferrocene (393 mg, 1.87 mmol) were dissolved in pyridine (5 mL) and stirred for 48 hours under an argon atmosphere. The solvent was removed under dynamic vacuum to give a dark oil, which was extracted into THF (5 mL), filtered, and the product precipitated by addition of hexane (20 mL). The orange-red powder was washed with hexane (2 × 20 mL) and dried under vacuum. ^{1}H NMR (500 MHz, d_5-pyridine): δ (ppm) 9.93 (ddd, $^1J_{H–P}$ = 45 Hz, $^3J_{H–P}$ = 14 Hz, $^3J_{H–P}$ = 6 Hz, 1H, C*H* of phospholide), 5.19 (m, 2H, C_5H_4), 4.29 (m, 2H, C_5H_4), 4.21 (s, 5H, C_5H_5), 3.47 (s, 24H, 18-crown-6). ^{31}P NMR (202.4 MHz, d_5-pyridine): δ (ppm) 276.4 (m, $^1J_{P–P}$ = –470 Hz, $^1J_{P–P}$ = –493 Hz, 1P, P2), 268.4 (m, $^2J_{P–P}$ = 17 Hz, 1P, P1), 265.4 (m, 1P, P3). ESI–MS (DMF): *m/z* 303.0 $[P_3C_2H\{Fe(C_5H_4)(C_5H_5)\}]^-$. ESI+MS (DMF): *m/z* 909.5 {[K(18-crown-

6)]$_2$[P_3C_2H{$Fe(C_5H_4)(C_5H_5)$}]}$^+$. It did not prove possible to obtain a sample of the compound sufficiently pure for elemental microanalysis.

8.3.9.2 [K(2,2,2-crypt)][37] (37: [As_3C_2H{$Fe(C_5H_4)(C_5H_5)$}]$^-$)

K_3As_7 (152 mg, 0.237 mmol) and 18-crown-6 (188 mg, 0.713 mmol) were dissolved in pyridine (5 mL) and stirred for 10 minutes to ensure complete dissolution of the Zintl phase. Ethynylferrocene (291 mg, 1.39 mmol) was added in one portion, and the resulting mixture stirred overnight, resulting in a deep red-brown solution. The solvent was removed under dynamic vacuum and the residue dried to a dark oily solid. 2,2,2-crypt (200 mg, 0.530 mmol) in THF (5 mL) was added and the solution was filtered and layered with hexane. Slow diffusion yielded a small amount of the product as orange-yellow blocks suitable for single crystal X-ray diffraction. ^{1}H NMR (500 MHz, d_5-pyridine): δ (ppm) 11.54 (s, 1H, C*H*), 5.21 (m, 2H, C_5H_4), 4.33 (m, 2H, C_5H_4), 4.26 (s, 5H, C_5H_5), 3.41 (s, 12H, 2,2,2-crypt), 3.36 (t, $^3J_{H–H}$ = 4 Hz, 12H, 2,2,2-crypt), 2.34 (t, 12H, 2,2,2-crypt). It did not prove possible to obtain a bulk sample sufficiently pure to record a ^{13}C{^{1}H} NMR spectrum. ESI–MS (DMF): *m/z* 434.8 [As_3C_2H{$Fe(C_5H_4)(C_5H_5)$}]$^-$. No evidence of **37** was observed in the positive ion mode ESI+MS spectrum. It did not prove possible to obtain a sample of the compound sufficiently pure for elemental microanalysis.

8.3.9.3 [K(18-crown-6)][38] (38: [$P_3C_2H(CH_2NH_2)$]$^-$)

Propargylamine (0.24 mL, 3.64 mmol) was added to a solution of [K(18-crown-6)]$_2$[**1**] (498 mg, 0.604 mmol) in pyridine (5 mL). The mixture was stirred for 48 hours under argon, then all volatiles were removed under dynamic vacuum. The dark brown oil was extracted with THF (5 mL) and filtered. The impure product was precipitated as a yellow powder by addition of diethyl ether (40 mL) and washed with hexane (2 × 20 mL). ^{1}H NMR (500 MHz, d_5-pyridine): δ (ppm) 9.71 (ddd, $^2J_{H–P}$ = 47 Hz, $^2J_{H–P}$ = 14 Hz, $^3J_{H–P}$ = 4 Hz, 1H, C*H*),

4.97 (dt, $^{3}J_{H–P}$ = –10 Hz, $^{3}J_{H–H}$ = 7 Hz, 2H, CH_2), 3.49 (s, 24H, 18-crown-6), 2.11 (br d, 2H, NH_2). $^{1}H\{^{31}P\}$ NMR (500 MHz, d_5-pyridine): δ (ppm) 9.71 (s, 1H, C*H*), 4.97 (t, 2H, CH_2), the rest of the resonances observed are as detailed above. ^{31}P NMR (202.4 MHz, d_5-pyridine): δ (ppm) 279.7 (m, $^{1}J_{P–P}$ = –473 Hz, $^{1}J_{P–P}$ = –494 Hz, 1P, P2), 276.5 (m, $^{2}J_{P–P}$ = 14 Hz, 1P, P1), 263.7 (m, 1P, P3). $^{13}C\{^{1}H\}$ NMR (125.8 MHz, d_5-pyridine): δ (ppm) 158.6 (m, *C*(CH_2NH_2)), 144.6 (m, *C*H), 70.2 (18-crown-6), 48.6 (*C*H_2). ESI–MS (DMF): *m/z* 148.1 $[P_3C_2H(CH_2NH_2)]^-$. ESI+MS (DMF): *m/z* 755.1 $\{[K(18\text{-crown-6})]_2[P_3C_2H(CH_2NH_2)]\}^+$. It did not prove possible to obtain a sample of the compound sufficiently pure for elemental microanalysis.

8.3.9.4 [K(2,2,2-crypt)][39] (39: $[As_3C_2H(CH_2NH_2)]^-$)

Propargylamine (32 μL, 177 μmol) was added to a solution of [K(2,2,2-crypt)][**2**] (40 mg, 30 μmol) in pyridine (1 mL) and stirred overnight. The solvent was removed under dynamic vacuum and the dark residue extracted into THF (3 mL). The solution was filtered and layered with diethyl ether (10 mL). Small yellow crystals of the product suitable for single crystal X-ray diffraction grew after a few days. ^{1}H NMR (500 MHz, d_5-pyridine): δ (ppm) 11.24 (s, 1H, C*H*), 5.15 (t, $^{3}J_{H–H}$ = 7 Hz, 2H, CH_2), 3.42 (s, 12H, 2,2,2-crypt), 3.37 (t, $^{3}J_{H–H}$ = 5 Hz, 12H, 2,2,2-crypt), 2.22 (br d, 2H, NH_2). $^{13}C\{^{1}H\}$ NMR (125.8 MHz, d_5-pyridine): δ (ppm) 203.8 (*C*(CH_2NH_2)), 174.7 (*C*H), 70.9 (2,2,2-crypt), 68.2 (2,2,2-crypt), 54.4 (2,2,2-crypt), 51.8 (*C*H_2). ESI–MS (DMF): *m/z* 280.3 $[As_3C_2H(CH_2NH_2)]^-$. No evidence of **39** was observed in the positive ion mode ESI+MS spectrum. It did not prove possible to obtain a sample of the compound sufficiently pure for elemental microanalysis.

8.3.10 Synthesis and Chemistry of $[P_5]^-$

8.3.10.1 [K(18-crown-6)][40] (40: $[P_5]^-$) from the Zintl Phase

K_3P_7 (500 mg, 1.49 mmol) and 18-crown-6 (1.18 g, 4.47 mmol) were weighed into a 250 mL Schlenk flask and heated in DMF (100 mL) at reflux under a flow of dinitrogen for 36 hours. An aliquot of the reaction mixture was taken and analysed by ^{31}P NMR spectroscopy which showed quantitative conversion to the $[P_5]^-$ anion. The dark brown solution was cooled to room temperature and filtered, then the volatiles removed from the filtrate under reduced pressure to yield a brown oil. The oil was extracted with THF (100 mL), filtered, and the filtrate concentrated to approximately 20 mL. Et_2O (150 mL) was added to precipitate the product as a light brown solid that was isolated by filtration and dried under dynamic vacuum. Yield 545 mg (56% based on P). Crystals suitable for single crystal X-ray diffraction were grown by diffusion of Et_2O into a THF solution of the product at 5 ºC. ^{1}H NMR (500 MHz, d_5-pyridine): δ (ppm) 3.62 (s, 24H, 18-crown-6). ^{31}P{^{1}H} NMR (202.4 MHz, d_5-pyridine): δ (ppm) 471.1 (s). ^{13}C{^{1}H} NMR (125.8 MHz, d_5-pyridine): δ (ppm) 71.2 (18-crown-6). ESI–MS (DMF): *m/z* 155.68 $[P_5]^-$. ESI+MS (DMF): *m/z* 761.73 {[K(18-crown-6]$_2$[P_5]}$^+$. Anal. Calcd for $C_{12}H_{24}KO_6P_5$: C, 31.45; H, 5.28. Found: C, 31.48; H, 5.22.

8.3.10.2 [K(18-crown-6)][40] (40: $[P_5]^-$) from $[K(18\text{-crown-6})]_3[3]$

$[K(18\text{-crown-6})]_3$[**3**] (1.184 g, 1.05 mmol) and IPr (408 mg, 1.05 mmol) were dissolved in pyridine (20 mL) in an ampoule equipped with a gas-tight tap to give a dark orange-brown solution. The ampoule was sealed and heated to 120 ºC under argon until a clear orange solution was obtained. This typically took approximately 60 hours. The solution was filtered through a fritted glass filter and the solvent removed under reduced pressure to give a sticky orange-yellow residue. This was washed with Et_2O (3 × 20 mL) to give the product as a bright yellow solid, which was isolated by filtration and dried under dynamic vacuum.

Yield 606 mg (90% based on P). The product is spectroscopically identical to that detailed in section 8.3.10.1.

8.3.10.3 [41] (41: [$HP_5C_6H_{12}$])

In an inert atmosphere glovebox, a solution of pyridinium triflate (100 mg, 0.439 mmol) in pyridine (2 mL) was added dropwise over 5 minutes to a vigorously stirring solution of [K(18-crown-6)][**40**] (200 mg, 0.439 mmol) in pyridine (2 mL). The resulting mixture was stirred for 30 minutes, then transferred into a Schlenk tube and all volatiles were removed under dynamic vacuum. The brown residue was extracted with hexane (2 × 5 mL). The hexane extracts were combined and the solvent removed under reduced pressure to leave a colourless oily residue coating the walls of the Schlenk tube. This was dissolved in d_8-THF (0.5 mL) and analysed by ^{1}H and ^{31}P NMR spectroscopy. ^{1}H NMR (500 MHz, d_8-THF): δ (ppm) 2.67 (dm, $^1J_{H–P}$ = 182 Hz, 1H, P*H*). ^{1}H{^{31}P} NMR (500 MHz, d_8-THF): δ (ppm) 2.67 (s, 1H, P*H*). ^{31}P NMR (202.4 MHz, d_8-THF): δ (ppm) –6.8 (m, $^1J_{P–P}$ = –281 Hz, $^1J_{P–P}$ = –257 Hz, $^2J_{P–P}$ = 54 Hz, $^2J_{P–P}$ = –8 Hz, 1P, P2), –8.4 (m, $^1J_{P–P}$ = –277 Hz, $^1J_{P–P}$ = –249 Hz, $^2J_{P–P}$ = 41 Hz, 1P, P5), –13.4 (m, $^1J_{P–P}$ = –240 Hz, $^2J_{P–P}$ = 19 Hz, 1P, P3), –23.1 (m, $^2J_{P–P}$ = 11 Hz, 1P, P4), –76.2 (m, 1P, P1).

8.3.10.4 [K(2,2,2-crypt)][42] (42: $[P_5C_6H_{12}]^-$)

KHMDS (5 mg, 25 μmol) and 2,2,2-crypt (9 mg, 25 μmol) were added to the same NMR tube as detailed in Section 8.3.10.3, resulting in an immediate colour change to yellow-orange. The contents of the tube were analysed by ^{1}H and ^{31}P NMR spectroscopy, then layered with hexane. Small yellow crystals of the product formed suitable for single crystal X-ray diffraction. ^{31}P NMR (202.4 MHz, d_8-THF): δ (ppm) 29.6 (m, $^1J_{P–P}$ = –367 Hz, $^1J_{P–P}$ = –256 Hz, $^2J_{P–P}$ = 25 Hz, $^2J_{P–P}$ = 22 Hz, 1P, P2), 27.5 (m, $^1J_{P–P}$ = –368 Hz, $^1J_{P–P}$ = –252 Hz,

$^2J_{P-P}$ = 21 Hz, 1P, P5), –18.0 (m, $^1J_{P-P}$ = –310 Hz, $^2J_{P-P}$ = 10 Hz, 1P, P3), –29.6 (m, $^2J_{P-P}$ = 22 Hz, $^2J_{P-P}$ = 11 Hz, 1P, P4), –156.3 (m, 1P, P1).

8.4 REFERENCES

(1) Santandrea, R. P.; Mensing, C.; von Schnering, H. G. *Thermochim. Acta* **1986**, *98*, 301–311.

(2) Emmerling, F.; Rohr, C. *Z. Naturforsch., B: J. Chem. Sci.* **2002**, *57*, 963–975.

(3) Findlater, M.; Hill, N. J.; Cowley, A. H. *Dalton Trans.* **2008**, 4419–4423.

(4) Pearson, A. J.; Schoffers, E. *Organometallics* **1997**, *16*, 5365–5367.

(5) Tate, D. P.; Knipple, W. R.; Augl, J. M. *Inorg. Chem.* **1962**, *1*, 433–434.

(6) Tekkaya, A.; Kayran, C.; Ozkar, S.; Kreiter, C. G. *Inorg. Chem.* **1994**, *33*, 2439–2443.

(7) Hintermann, L. *Beilstein J. Org. Chem.* **2007**, *3*, 22.

(8) Jafarpour, L.; Stevens, E. D.; Nolan, S. P. *J. Organomet. Chem.* **2000**, *606*, 49–54.

(9) Brookhart, M.; Grant, B.; Volpe, A. F. *Organometallics* **1992**, *11*, 3920–3922.

(10) MacFarlane, K. S.; Rettig, S. J.; Liu, Z.; James, B. R. *J. Organomet. Chem.* **1998**, *557*, 213–219.

(11) Genêt, J. P.; Pinel, C.; Ratovelomanana-Vidal, V.; Mallart, S.; Pfister, X.; De Andrade, M. C. C.; Laffitte, J. A. *Tet. Asymm.* **1994**, *5*, 665–674.

(12) Cosier, J.; Glazer, A. M. *J. Appl. Cryst.* **1986**, *19*, 105–107.

(13) *CrysAlisPro*; Agilent Technologies.

(14) Otwinowski, Z.; Minor, W. *Macromol. Crystallogr. Part A* **1997**, *Volume 276*, 307–326.

(15) Sheldrick, G. M. *Acta. Cryst. A* **2008**, *64*, 112–122.

(16) Sheldrick, G. *Acta. Cryst. A* **1990**, *A46*, 467–473.

(17) Sheldrick, G. M. *SHELX97, Programs for Crystal Structure Analysis (Release 97−2)*; University of Göttingen: Göttingen, Germany, 1998.

(18) Budzelaar, P. H. M. *gNMR v5.0*; Ivorysoft, 1995.

(19) Te Velde, G.; Bickelhaupt, F. M.; Baerends, E. J.; Fonseca Guerra, C.; van Gisbergen, S. J. A.; Snijders, J. G.; Ziegler, T. *J. Comput. Chem.* **2001**, *22*, 931–967.

(20) Guerra, C. F.; Snijders, J. G.; Velde, G. te; Baerends, E. J. *Theor. Chem. Acc.* **1998**, *99*, 391–403.

(21) *ADF 2012.01*; SCM, Theoretical Chemistry, Vrije Universiteit: Amsterdam, The Netherlands.

(22) Parr, R. G.; Yang, W. *Density-Functional Theory of Atoms and Molecules*; Oxford University Press ; Clarendon Press: Oxford, 1989.

(23) Vosko, S. H.; Wilk, L.; Nusair, M. *Can. J. Phys. 58*, 1200–1211.

(24) Becke, A. D. *Phys. Rev. A* **1988**, *38*, 3098–3100.

(25) Perdew, J. P. *Phys. Rev. B* **1986**, *33*, 8822–8824.

(26) Lenthe, E. van; Baerends, E. J.; Snijders, J. G. *J. Chem. Phys.* **1993**, *99*, 4597–4610.

(27) Van Lenthe, E.; Baerends, E. J.; Snijders, J. G. *J. Chem. Phys.* **1994**, *101*, 9783–9792.

(28) Van Lenthe, E.; Ehlers, A.; Baerends, E.-J. *J. Chem. Phys.* **1999**, *110*, 8943–8953.

(29) Klamt, A.; Schüürmann, G. *J. Chem. Soc., Perkin Trans. 2* **1993**, 799–805.

(30) Versluis, L.; Ziegler, T. *J. Chem. Phys.* **1988**, *88*, 322–328.

(31) Frisch, M. J.; et al. *Gaussian 09, Revision A.02*; Gaussian, Inc.: Wallingford, CT, 2009.

(32) Becke, A. D. *J. Chem. Phys.* **1993**, *98*, 5648–5652.

(33) Perdew, J. P. In *Electronic Structure of Solids '91*; Ziesche, P.; Eschrig, H., Eds.; Akademie Verlag: Berlin, 1991; p. 11.

(34) Krishnan, R.; Binkley, J. S.; Seeger, R.; Pople, J. A. *J. Chem. Phys.* **1980**, *72*, 650–654.

(35) Blaudeau, J.-P.; McGrath, M. P.; Curtiss, L. A.; Radom, L. *J. Chem. Phys.* **1997**, *107*, 5016–5021.

(36) Clark, T.; Chandrasekhar, J.; Spitznagel, G. W.; Schleyer, P. V. R. *J. Comput. Chem.* **1983**, *4*, 294–301.

(37) Dobbs, K. D.; Hehre, W. J. *J. Comput. Chem.* **1987**, *8*, 880–893.

APPENDIX A

NMR Simulation Parameters

All chemical shifts and coupling constants reported are directly obtained from the spectral simulations of the ^{31}P and ^{1}H NMR spectra. The sign and magnitude of the starting *J* values for each simulation were determined computationally as detailed in Chapter Eight. Internuclear coupling constants (Hz) are reported to the nearest Hz, and chemical shifts (ppm) are reported to one decimal place. Simulation line-width parameters are not included. The absence of a coupling constant where one might be expected likely indicates that its magnitude is too small to be accounted for in the spectral simulation.

Table A.1: NMR parameters for **1**.

δ (ppm)		–48.8	–110.1	–22.7	–76.8	–111.3	–235.9	–123.5
		P1	**P2**	**P3**	**P4**	**P5**	**P6**	**P7**
–48.8	**P1**		–349	–298	–368	69	10	46
–110.1	**P2**	–349		–19	–8	–425	4	9
–22.7	**P3**	–298	–19		3	–5	–363	9
–76.8	**P4**	–368	–8	3		8	–13	–454
–111.3	**P5**	69	–425	–5	8		–185	–235
–235.9	**P6**	10	4	–363	–13	–185		–177
–123.5	**P7**	46	9	9	–454	–235	–177	

Table A.2: NMR parameters for **5**.

δ (ppm)		–28.3	–100.0	–6.3	–91.6	–68.7	–211.7	–134.1
		P1	**P2**	**P3**	**P4**	**P5**	**P6**	**P7**
–28.3	**P1**		–381	–339	–354	64	–10	44
–100.0	**P2**	–381		7	–8	–419	–9	8
–6.3	**P3**	–339	7		–29	–12	–392	-
–91.6	**P4**	–354	–8	–29		-	–15	–425
–68.7	**P5**	64	–419	–12	-		–184	–225
–211.7	**P6**	–10	–9	–392	–15	–184		–184
–134.1	**P7**	44	8	-	–425	–225	–184	

Table A.3: NMR parameters for **6**.

δ (ppm)		–28.2	–103.8	–18.7	–95.7	–73.5	–222.4	–130.3
		P1	**P2**	**P3**	**P4**	**P5**	**P6**	**P7**
–28.2	**P1**		–378	–338	–278	63	–10	46
–103.8	**P2**	–378		7	–8	–423	–9	8
–18.7	**P3**	–338	7		–21	–12	–401	-
–95.7	**P4**	–278	–8	–21		-	–15	–438
–73.5	**P5**	63	–423	–12	-		–176	–227
–222.4	**P6**	–10	–9	–401	–15	–176		–181
–130.3	**P7**	46	8	-	–438	–227	–181	

Table A.4: NMR parameters for **7**.

δ (ppm)		–28.9	–105.0	–17.7	–96.2	–73.0	–224.9	–130.3
		P1	**P2**	**P3**	**P4**	**P5**	**P6**	**P7**
–28.9	**P1**		–381	–355	–366	63	–10	46
–105.0	**P2**	–381		7	–8	–423	–9	8
–17.7	**P3**	–355	7		–21	–12	–401	-
–96.2	**P4**	–366	–8	–21		-	–15	–437
–73.0	**P5**	63	–423	–12	-		–184	–229
–224.9	**P6**	–10	–9	–401	–15	–184		–184
–130.3	**P7**	46	8	-	–437	–229	–184	

Table A.5: NMR parameters for **8**.

δ (ppm)		–33.0	–105.6	7.4	–103.7	–71.3	–206.6	–134.2
		P1	**P2**	**P3**	**P4**	**P5**	**P6**	**P7**
–33.0	**P1**		–362	–320	–347	61	–13	47
–105.6	**P2**	–362		–10	–16	–419	–8	–10
7.4	**P3**	–320	–10		–23	14	–381	–15
–103.7	**P4**	–347	–16	–23		-	–7	–422
–71.3	**P5**	61	–419	14	-		–184	–225
–206.6	**P6**	–13	–8	–381	–7	–184		–182
–134.2	**P7**	47	–10	–15	–422	–225	–182	

Table A.6: NMR parameters for **14**.

δ (ppm)		–30.0	–64.2	12.5	12.5	–113.8	–129.5	–129.5
		P1	**P2**	**P3**	**P4**	**P5**	**P6**	**P7**
–30.0	**P1**		–345	–292	–292	87	21	21
–64.2	**P2**	–345		13	13	–357	–4	–4
12.5	**P3**	–292	13		270	20	–347	–30
12.5	**P4**	–292	13	270		23	–30	–347
–113.8	**P5**	87	–357	20	23		–216	–216
–129.5	**P6**	21	–4	–347	–30	–216		–194
–129.5	**P7**	21	–4	–30	–347	–216	–194	

Table A.7: NMR parameters for **15**.

δ (ppm)		–33.6	–69.6	7.3	4.9	–112.7	–135.8	–136.5
		P1	**P2**	**P3**	**P4**	**P5**	**P6**	**P7**
–33.6	**P1**		–353	–287	–305	87	21	21
–69.6	**P2**	–353		13	13	–368	–4	–4
7.3	**P3**	–287	13		–294	20	–350	–30
4.9	**P4**	–305	13	294		23	–30	–355
–112.7	**P5**	87	–368	20	23		–216	–216
–135.8	**P6**	21	–4	–350	–30	–216		–194
–136.5	**P7**	21	–4	–30	–355	–216	–194	

Table A.8: NMR parameters for **16**.

δ (ppm)		–34.1	–69.6	6.5	3.2	–112.2	–134.0	–136.3
		P1	**P2**	**P3**	**P4**	**P5**	**P6**	**P7**
–34.1	**P1**		–351	–295	–295	87	21	21
–69.6	**P2**	–351		13	13	–368	–4	–4
6.5	**P3**	–295	13		295	20	–348	–30
3.2	**P4**	–295	13	295		23	–30	–356
–112.2	**P5**	87	–368	20	23		–216	–216
–134.0	**P6**	21	–4	–348	–30	–216		–194
–136.3	**P7**	21	–4	–30	–356	–216	–194	

Table A.9: NMR parameters for **17**.

δ (ppm)		261.1	272.8	261.1	9.03	9.03
		P1	**P2**	**P3**	**H1**	**H2**
261.1	**P1**		–493	10	18	48
272.8	**P2**	–493		–493	5	5
261.1	**P3**	10	–493		48	18
9.03	**H1**	18	5	48		8
9.03	**H2**	48	5	18	8	

Table A.10: NMR parameters for **19**.

δ (ppm)		297.9	273.3	297.9
		P1	**P2**	**P3**
297.9	**P1**		undefined	–492
273.3	**P2**	undefined		undefined
297.9	**P3**	–492	undefined	

Table A.11: NMR parameters for **21**.

δ (ppm)		275.5	289.2	269.0	8.97
		P1	**P2**	**P3**	**H2**
275.5	**P1**		–466	–4	45
289.2	**P2**	–466		–499	6
269.0	**P3**	–4	–499		13
8.97	**H2**	45	6	13	

Table A.12: NMR parameters for **23**.

δ (ppm)		261.3	335.2	261.3
		P1	**P2**	**P3**
261.3	**P1**		undefined	–501
335.2	**P2**	undefined		undefined
261.3	**P3**	–501	undefined	

Table A.13: NMR parameters for **24**.

δ (ppm)		25.9	–29.8	25.9	4.96	4.96
		P1	**P2**	**P3**	**H1**	**H2**
25.9	**P1**		–415	10	41	16
–29.8	**P2**	–415		–415	4	4
25.9	**P3**	10	–415		16	41
4.96	**H1**	41	4	16		4
4.96	**H2**	16	4	41	4	

Table A.14: NMR parameters for **26**.

δ (ppm)		67.2	34.6	67.2	5.82	5.82
		P1	**P2**	**P3**	**H1**	**H2**
67.2	**P1**		–422	–8	11	46
34.6	**P2**	–422		–422	4	4
67.2	**P3**	–8	–422		46	11
5.82	**H1**	11	4	46		6
5.82	**H2**	46	4	11	6	

Table A.15: NMR parameters for **28**.

δ (ppm)		100.8	24.2	100.8
		P1	**P2**	**P3**
100.8	**P1**		undefined	–415
24.2	**P2**	undefined		undefined
100.8	**P3**	–415	undefined	

Table A.16: NMR parameters for **30**.

δ (ppm)		70.7	40.6	77.0	6.16
		P1	**P2**	**P3**	**H2**
70.7	**P1**		–435	13	42
40.6	**P2**	–435		–404	4
77.0	**P3**	13	–404		10
6.16	**H2**	42	4	10	

Table A.17: NMR parameters for **32**.

δ (ppm)		274.3	293.1	278.3	9.88
		P1	**P2**	**P3**	**H2**
274.3	**P1**		–462	13	47
293.1	**P2**	–462		–505	7
278.3	**P3**	13	–505		13
9.88	**H2**	47	7	13	

Table A.18: NMR parameters for **33**.

δ (ppm)		70.8	42.4	77.6	6.84
		P1	**P2**	**P3**	**H2**
70.8	**P1**		–400	13	43
42.4	**P2**	–400		–438	4
77.6	**P3**	13	–438		11
6.84	**H2**	43	4	11	

Table A.19: NMR parameters for **34**.

δ (ppm)		266.6	240.2	262.5	9.51
		P1	**P2**	**P3**	**H2**
266.6	**P1**		–453	25	44
240.2	**P2**	–453		–585	4
262.5	**P3**	25	–585		28
9.51	**H2**	44	4	28	

Table A.20: NMR parameters for **35**.

δ (ppm)		63.5	–21.7	119.4	6.68
		P1	**P2**	**P3**	**H2**
63.5	**P1**		–344	21	40
–21.7	**P2**	–344		–546	3
119.4	**P3**	21	–546		16
6.68	**H2**	40	3	16	

Table A.21: NMR parameters for **36**.

δ (ppm)		268.4	276.4	265.4	9.93
		P1	**P2**	**P3**	**H2**
268.4	**P1**		–470	17	45
276.4	**P2**	–470		–493	6
265.4	**P3**	17	–493		14
9.93	**H2**	45	6	14	

Table A.22: NMR parameters for **38**.

δ (ppm)		276.5	279.6	263.7	9.71	4.97
		P1	**P2**	**P3**	**H2**	**CH_2**
276.5	**P1**		–473	14	47	–2
279.6	**P2**	–473		–494	4	2
263.7	**P3**	14	–494		14	–11
9.71	**H2**	47	4	14		7
4.97	**CH_2**	–2	2	–11	7	

Table A.23: NMR parameters for **41**.

δ (ppm)		–76.2	–6.8	–13.4	–23.1	–8.4	2.67
		P1	**P2**	**P3**	**P4**	**P5**	**H1**
–76.2	**P1**		–257	19	11	–249	–182
–6.8	**P2**	–257		–281	54	–8	-
–13.4	**P3**	19	–281		–240	41	-
–23.1	**P4**	11	54	–240		–277	-
–8.4	**P5**	–249	–8	41	–277		-
2.67	**H1**	–182	-	-	-	-	

Table A.24: NMR parameters for **42**.

δ (ppm)		–156.3	29.6	–18.0	–29.6	27.5
		P1	**P2**	**P3**	**P4**	**P5**
–156.3	**P1**		–367	10	11	–368
29.6	**P2**	–367		–256	22	25
–18.0	**P3**	10	–256		–310	21
–29.6	**P4**	11	22	–310		–252
27.5	**P5**	–368	25	21	–252	

APPENDIX B

X-Ray Data Collection and Refinement Parameters

compound	[K(crown)]$_2$[**1**]	[K(crown)]$_2$[**2**]	[K(crown)]$_3$[**3**]·2py	[K(crown)]$_2$[**5**]	[K(crown)]$_2$[**7**]
formula	$C_{24}H_{49}K_2O_{12}P_7$	$C_{24}H_{49}K_2O_{12}As_7$	$C_{46}H_{82}K_3O_{18}N_2P_7$	$C_{49}H_{83}K_2N_2O_{12}P_7$	$C_{49}H_{83}K_2N_2O_{12}P_7$
Fw (g mol^{-1})	824.62	1132.27	1285.27	1187.16	950.82
crystal system	monoclinic	monoclinic	hexagonal	monoclinic	monoclinic
space group	$P2_1/c$	$P2_1/c$	$P\bar{6}$	$P2_1/c$	$C2/c$
a (Å)	20.2357(2)	20.6915(2)	23.4939(1)	14.1477(1)	49.646(1)
b (Å)	10.0668(1)	10.2436(1)	23.4939(1)	19.1536(2)	9.7578(2)
c (Å)	19.7067(2)	19.9016(2)	23.8096(2)	69.3584(8)	20.2349(6)
α (°)					
β (°)	98.597(1)	102.524(1)		92.246(1)	105.114(3)
γ (°)					
V (Å^3)	3969.32(7)	4117.88(7)	11381.32(12)	18780.3(3)	9463.4(4)
Z	4	4	6	12	8
radiation, λ (Å)	Mo K$_\alpha$, 0.71073	Cu K$_\alpha$, 1.54178			
T (K)	150(2)				
ρ_{calc} (g cm^{-3})	1.380	1.826	1.584	1.260	1.335
μ (mm^{-1})	0.571	8.710	5.120	3.477	4.462
reflns collected	12093	23553	79308	168980	24236
independent reflns	6871	8526	15788	33114	9773
parameters	573	561	592	2392	549
R(int)	0.0234	0.0235	0.0384	0.0427	0.0388
R1/wR2, $I \geq 2\sigma_I$ (%)	3.49/8.74	2.75/7.06	11.62/37.21	6.47/14.43	4.45/11.41
R1/wR2, all data (%)	4.18/9.13	3.03/7.23	14.39/42.08	6.81/14.59	5.27/12.29
GOF	1.036	1.104	1.628	1.131	1.035
A	0.0415	0.0302	0.2000	0.0383	0.0686
B	1.8462	4.1308	0	44.3741	6.9064

[a] $R1 = [\Sigma||F_o| - |F_c||]/\Sigma|F_o|$; $wR2 = \{[\Sigma w[(F_o)^2 - (F_c)^2]^2]/[\Sigma w(F_o^2)^2]\}^{1/2}$; $w = [\sigma^2(F_o)^2 + (AP)^2 + BP]^{-1}$, where $P = [(F_o)^2 + 2(F_c)^2]/3$ and the A and B values are listed in the bottom two rows of the table.

compound	[K(crown)]$_2$[**8**]·py	[K(crown)]$_2$[**11**]	[K(crown)]$_3$[**12**]·py	[K(crypt)][**13**]	[K(crypt)][**14**]·THF
formula	$C_{40}H_{69}K_2N_2O_{13}P_7$	$C_{31}H_{63}K_2N_2O_{12}As_7$	$C_{40}H_{69}K_2N_2O_{13}As_7$	$C_{43}H_{72}KN_4O_6P_7$	$C_{72}H_{114}KN_6O_7P_7$
Fw (g mol^{-1})	1080.96	1258.47	1388.61	996.94	1431.58
crystal system	monoclinic	monoclinic	monoclinic	orthorhombic	monoclinic
space group	$P2_1$	$C2/c$	$P2_1$	$Pna2_1$	$P2_1$
a (Å)	10.3007(1)	50.182(1)	10.3767(1)	20.5480(5)	15.6647(3)
b (Å)	24.3464(3)	9.8621(2)	24.5708(1)	16.9255(3)	15.1270(3)
c (Å)	10.4883(1)	20.3537(4)	10.6999(1)	15.8004(3)	17.1338(4)
α (°)					
β (°)	90.321(1)	104.359(2)	90.289(1)		91.220(2)
γ (°)					
V (Å^3)	2630.27(5)	9758.4(3)	2728.05(4)	5495.1(2)	4059.1(2)
Z	2	8	2	4	2
radiation, λ (Å)	Cu K_α, 1.54178				
T (K)	150(2)				
ρ_{calc} (g cm^{-3})	1.365	1.713	1.690	1.205	1.171
μ (mm^{-1})	4.098	7.432	6.728	3.129	2.280
reflns collected	24917	53390	59081	18599	23963
independent reflns	10184	10178	10934	8402	12512
parameters	578	639	577	614	973
R(int)	0.0191	0.0309	0.0227	0.0496	0.0355
R1/wR2, $I \geq 2\sigma_I$ (%)	2.77/7.22	2.51/6.18	2.62/7.19	4.83/11.71	6.29/17.06
R1/wR2, all data (%)	2.75/7.24	2.85/6.41	2.62/7.19	6.80/13.15	7.49/18.35
GOF	1.043	1.049	1.123	1.071	1.018
A	0.0464	0.0293	0.0468	0.0629	0.1235
B	0.5577	15.5787	1.1587	1.1886	0.8924

[a] $R1 = [\Sigma||F_o| - |F_c||]/\Sigma|F_o|$; $wR2 = \{[\Sigma w[(F_o)^2 - (F_c)^2]^2]/[\Sigma w(F_o^2)^2]\}^{1/2}$; $w = [\sigma^2(F_o)^2 + (AP)^2 + BP]^{-1}$, where $P = [(F_o)^2 + 2(F_c)^2]/3$ and the A and B values are listed in the bottom two rows of the table.

compound	[K(crown)][**15**]·0.65THF ·0.35hexane	[K(crown)][**16**] ·hexane	[K(crypt)][**17**]	[K(crown)][**17**]	[K(crypt)][**18**]
formula	$C_{60.69}H_{104.08}KN_6O_{6.65}P_7$	$C_{56}H_{100}KN_6O_6P_7$	$C_{20}H_{38}KN_2O_6P_3$	$C_{14}H_{26}KO_6P_3$	$C_{20}H_{38}KN_2O_6As_3$
Fw (g mol^{-1})	1280.26	1209.31	534.53	422.36	666.38
crystal system	monoclinic	orthorhombic	monoclinic	monoclinic	monoclinic
space group	$P2_1/n$	$P2_12_12_1$	$P2_1/n$	$P2_1/m$	$P2_1/n$
a (Å)	16.0447(2)	15.9418(2)	9.9714(3)	9.0864(1)	10.0095(1)
b (Å)	26.4964(3)	16.7687(2)	10.8313(2)	15.5733(2)	10.8312(1)
c (Å)	16.9173(1)	26.4606(4)	25.5105(7)	14.6129(2)	25.7344(3)
α (°)					
β (°)	91.488(1)		97.071(3)	99.328(1)	95.621(1)
γ (°)					
V (Å^3)	7189.57(13)	7073.53(16)	2734.26(12)	2040.46(4)	2776.58(5)
Z	4	4	4	4	4
radiation, λ (Å)	Cu K_α, 1.54178				
T (K)	150(2)				
ρ_{calc} (g cm^{-3})	1.183	1.136	1.299	1.375	1.594
μ (mm^{-1})	2.512	2.518	3.662	4.732	5.944
reflns collected	45894	25827	14287	10326	14024
independent reflns	14987	14024	5677	4387	5759
parameters	983	729	289	248	305
R(int)	0.0341	0.0261	0.0220	0.0181	0.0172
R1/wR2, $I \geq 2\sigma_I$ (%)	4.04/10.37	6.31/16.99	3.42/8.95	4.33/11.70	3.27/8.11
R1/wR2, all data (%)	4.98/11.10	7.29/17.99	3.90/9.33	4.50/11.87	3.51/8.30
GOF	1.023	1.034	1.048	1.068	1.032
A	0.0547	0.0985	0.0472	0.0610	0.0378
B	2.2485	3.3702	0.9868	1.4170	2.4945

[a] $R1 = [\Sigma||F_o| - |F_c||]/\Sigma|F_o|$; $wR2 = \{[\Sigma w[(F_o)^2 - (F_c)^2]^2]/[\Sigma w(F_o^2)^2]\}^{1/2}$; $w = [\sigma^2(F_o)^2 + (AP)^2 + BP]^{-1}$, where $P = [(F_o)^2 + 2(F_c)^2]/3$ and the A and B values are listed in the bottom two rows of the table.

compound	[K(crown)][**18**]	[K(crown)(THF)$_2$][**19**]	[K(crypt)][**20a**]	[K(crypt)][**20b**] ·0.5THF	[K(crown)][**22**]·THF
formula	$C_{14}H_{26}KO_6As_3$	$C_{34}H_{50}KO_8P_3$	$C_{32}H_{46}KN_2O_6As_3$	$C_{34}H_{50}KN_2O_{6.50}As_3$	$C_{24}H_{38}KO_7As_3$
Fw (g mol^{-1})	554.21	718.75	818.57	854.62	702.40
crystal system	monoclinic	triclinic	monoclinic	monoclinic	triclinic
space group	$P2_1/m$	$P\bar{1}$	Cc	$P2_1/c$	$P\bar{1}$
a (Å)	9.1068(2)	10.4833(2)	11.4018(1)	20.5579(1)	8.0614(2)
b (Å)	15.6018(4)	11.1755(2)	17.3110(2)	21.2058(1)	10.1857(2)
c (Å)	14.9447(3)	17.2569(3)	18.7984(3)	19.8422(2)	19.1222(4)
α (°)		94.827(2)			94.170(2)
β (°)	98.208(2)	99.635(2)	101.123(1)	115.888(1)	96.314(2)
γ (°)		106.361(2)			106.266(2)
V (Å^3)	2101.63(8)	1894.01(6)	3640.67(8)	7782.09(11)	1489.31(6)
Z	4	2	4	8	2
radiation, λ (Å)	Cu K_α, 1.54178		Mo K_α, 0.71073		Cu K_α, 1.54178
T (K)	150(2)				
ρ_{calc} (g cm^{-3})	1.752	1.260	1.493	1.459	1.566
μ (mm^{-1})	7.683	2.805	2.894	2.712	5.584
reflns collected	11024	39124	7274	29398	32636
independent reflns	4517	7877	7268	17654	6183
parameters	242	444	398	838	401
R(int)	0.0288	0.0228	0.0410	0.0285	0.0221
R1/wR2, $I \geq 2\sigma_I$ (%)	10.12/27.78	3.57/9.15	3.63/8.88	3.81/7.76	2.61/7.08
R1/wR2, all data (%)	11.55/29.29	3.72/9.30	3.90/9.12	6.23/8.72	2.69/7.17
GOF	1.076	1.031	1.037	1.029	1.050
A	0.1448	0.0433	0.0421	0.0307	0.0375
B	17.8392	0.8050	7.8034	6.6096	1.1566

[a] $R1 = [\Sigma||F_o| - |F_c||]/\Sigma|F_o|$; $wR2 = \{[\Sigma w[(F_o)^2 - (F_c)^2]^2]/[\Sigma w(F_o^2)^2]\}^{1/2}$; $w = [\sigma^2(F_o)^2 + (AP)^2 + BP]^{-1}$, where $P = [(F_o)^2 + 2(F_c)^2]/3$ and the A and B values are listed in the bottom two rows of the table.

compound	[Cs(crown)][**23**]	[K(crypt)][**25**]	[K(crown)][**26**]	[K(crown)][**27**]	[K(crown)(THF)][**28**]
formula	$C_{18}H_{28}CsO_6P_3$	$C_{28}H_{52}As_3KN_2O_6Ru$	$C_{17}H_{26}KO_9P_3Mo$	$C_{17}H_{26}KO_9As_3Mo$	$C_{33}H_{42}KO_{10}P_3Mo$
Fw (g mol^{-1})	566.22	877.65	602.33	734.18	826.62
crystal system	orthorhombic	monoclinic	monoclinic	monoclinic	triclinic
space group	$Pna2_1$	$P2_1/n$	$P2_1/n$	$P2_1/n$	$P\bar{1}$
a (Å)	14.9764(2)	11.7391(1)	8.8345(1)	8.8791(1)	10.3755(4)
b (Å)	19.3094(2)	17.4228(1)	16.4513(2)	16.5362(2)	10.8188(4)
c (Å)	8.3324(1)	18.6466(1)	16.9233(2)	17.0138(2)	17.8646(6)
α (°)					78.429(3)
β (°)		107.681(1)	96.7960(1)	96.7470(10)	79.284(3)
γ (°)					73.683(3)
V (Å^3)	2409.61(5)	3633.60(4)	2442.33(5)	2480.78(5)	1867.43(12)
Z	4	4	4	4	2
radiation, λ (Å)	Cu K_α, 1.54178		Mo K_α, 0.71073		Cu K_α, 1.54178
T (K)	150(2)				
ρ_{calc} (g cm^{-3})	1.561	1.604	1.638	1.966	1.470
μ (mm^{-1})	14.127	7.870	0.947	4.710	5.534
reflns collected	51301	78137	10667	10749	16986
independent reflns	5040	7613	5561	5641	7718
parameters	417	388	320	314	470
R(int)	0.0480	0.0248	0.0334	0.0287	0.0195
R1/wR2, $I \geq 2\sigma_I$ (%)	3.14/8.47	1.80/4.94	3.27/7.02	3.27/7.14	2.36/5.91
R1/wR2, all data (%)	3.21/8.56	1.85/4.98	5.11/7.73	4.86/7.64	2.57/6.09
GOF	1.090	1.063	1.008	1.045	1.012
A	0.0564	0.0281	0.0394	0.0373	0.0348
B	1.3552	1.1971	0.0000	0.3721	0.3581

[a] $R1 = [\Sigma||F_o| - |F_c||]/\Sigma|F_o|$; $wR2 = \{[\Sigma w[(F_o)^2 - (F_c)^2]^2]/[\Sigma w(F_o^2)^2]\}^{1/2}$; $w = [\sigma^2(F_o)^2 + (AP)^2 + BP]^{-1}$, where $P = [(F_o)^2 + 2(F_c)^2]/3$ and the A and B values are listed in the bottom two rows of the table.

compound	[K(crypt)][**29**]	[K(crown)][**31**]	[K(crypt)][**32**]	[K(crypt)][**33**]
formula	$C_{35}H_{46}KN_2O_9As_3Mo$	$C_{23}H_{30}KO_9As_3Mo$	$C_{25}H_{41}KN_3O_6P_3$	$C_{28}H_{41}KN_3O_9P_3Mo$
Fw (g mol^{-1})	998.54	810.27	611.62	791.59
crystal system	monoclinic	triclinic	monoclinic	orthorhombic
space group	$P2_1/c$	$P\bar{1}$	$P2_1/c$	$Cmca$
a (Å)	10.9027(2)	8.5753(3)	13.0560(3)	20.7468(4)
b (Å)	37.5485(5)	10.9107(4)	11.9141(2)	16.2409(3)
c (Å)	20.3109(3)	16.9299(4)	20.1168(3)	20.7960(3)
α (°)		97.171(3)		
β (°)	92.785(1)	102.873(3)	101.273(2)	
γ (°)		102.459(3)		
V (Å^3)	8305.1(2)	1482.75(8)	3068.81(10)	7007.1(2)
Z	8	2	4	8
radiation, λ (Å)	Cu K_α, 1.54178			
T (K)	150(2)			
ρ_{calc} (g cm^{-3})	1.597	1.815	1.324	1.501
μ (mm^{-1})	6.563	8.996	3.344	5.873
reflns collected	103347	16074	14416	18413
independent reflns	17327	6139	5394	3745
parameters	919	362	343	231
R(int)	0.0344	0.0302	0.0308	0.0258
R1/wR2, $I \geq 2\sigma_I$ (%)	2.59/5.91	3.35/8.66	4.94/13.83	2.85/7.15
R1/wR2, all data (%)	2.93/6.12	3.54/8.80	5.85/14.56	3.23/7.51
GOF	1.071	1.127	1.081	1.047
A	0.0200	0.0351	0.0874	0.0417
B	7.5475	2.2033	0.9306	8.0167

[a] $R1 = [\Sigma||F_o| - |F_c||]/\Sigma|F_o|$; $wR2 = \{[\Sigma w[(F_o)^2 - (F_c)^2]^2]/[\Sigma w(F_o^2)^2]\}^{1/2}$; $w = [\sigma^2(F_o)^2 + (AP)^2 + BP]^{-1}$, where $P = [(F_o)^2 + 2(F_c)^2]/3$ and the A and B values are listed in the bottom two rows of the table.

compound	[K(crypt)][**34**]·0.5CH_2Cl_2	[K(crypt)][**37**]	[K(crypt)][**39**]	[K(crown)(THF)][**39**–**Mo(CO)$_3$**]	[K(crypt)][**42**]
formula	$C_{29.50}H_{42}ClKN_3O_{10}P_3Mo$	$C_{30}H_{46}KN_2O_6As_3Fe$	$C_{21}H_{41}KN_3O_6As_3$	$C_{22}H_{37}KNO_{10}As_3Mo$	$C_{24}H_{48}KN_2O_6P_5$
Fw (g mol^{-1})	862.06	850.40	695.43	835.33	654.59
crystal system	monoclinic	monoclinic	monoclinic	monoclinic	monoclinic
space group	$P2_1/n$	$P2/c$	$P2_1/c$	$P2_1/c$	$P2_1/c$
a (Å)	11.5991(1)	22.9614(6)	16.8350(7)	9.1706(1)	8.9380(4)
b (Å)	22.5642(1)	8.2165(2)	12.2013(5)	19.3853(2)	26.330(1)
c (Å)	14.9144(1)	19.9711(5)	14.1223(6)	17.8376(2)	14.4129(5)
α (°)					
β (°)	97.71(1)	110.599(3)	92.345(4)	91.579(1)	95.800(4)
γ (°)					
V (Å^3)	3868.18(5)	3526.90(15)	2898.4(2)	3169.87(6)	3374.5(2)
Z	4	4	4	4	4
radiation, λ (Å)	Cu K_α, 1.54178				
T (K)	150(2)				
ρ_{calc} (g cm^{-3})	1.480	1.602	1.594	1.750	1.288
μ (mm^{-1})	6.010	7.958	5.731	8.465	3.931
reflns collected	82775	18565	27387	16262	18210
independent reflns	8092	7284	6022	6584	6992
parameters	473	389	307	374	535
R(int)	0.0291	0.0348	0.0509	0.0362	0.0313
R1/wR2, $I \geq 2\sigma_I$ (%)	2.64/6.89	4.16/11.01	9.03/25.22	5.37/14.80	3.06/7.53
R1/wR2, all data (%)	2.77/7.01	5.09/11.85	9.81/25.72	5.49/14.93	3.65/7.90
GOF	1.029	1.029	1.193	1.121	1.040
A	0.0347	0.0609	0.0804	0.0969	0.0399
B	2.6148	5.2924	38.3743	2.5528	0.5159

[a] $R1 = [\Sigma||F_o| - |F_c||]/\Sigma|F_o|$; $wR2 = \{[\Sigma w[(F_o)^2 - (F_c)^2]^2]/[\Sigma w(F_o^2)^2]\}^{1/2}$; $w = [\sigma^2(F_o)^2 + (AP)^2 + BP]^{-1}$, where $P = [(F_o)^2 + 2(F_c)^2]/3$ and the A and B values are listed in the bottom two rows of the table.

APPENDIX C

Publications

Publications of research described in this thesis:

- "Studies on the Reactivity of Group 15 Zintl Ions with Carbodiimides: Synthesis and Characterization of a Heptaphosphaguanidine Dianion" Turbervill, R. S. P.; Goicoechea, J. M. *Chem. Commun.* **2012**, *48*, 1470–1472.
- "Hydrophosphination of Carbodiimides Using Protic Heptaphosphide Cages: A Unique Effect of the Bimodal Activity of Protonated Group 15 Zintl Ions" Turbervill, R. S. P.; Goicoechea, J. M. *Organometallics* **2012**, *31*, 2452–2462.
- "Synthesis of 1,2,3-Tripnictolide Anions by Reaction of Group 15 Zintl ions with Acetylene. Isolation of $[E_3C_2H_2]^-$ (E = P, As) and Preliminary Reactivity Studies" Turbervill, R. S. P.; Goicoechea, J. M. *Chem. Commun.* **2012**, *48*, 6100–6102.
- "Synthesis and Characterization of Free and Coordinated 1,2,3-Tripnictolide Anions" Turbervill, R. S. P.; Jupp, A. R.; McCullough, P. S. B.; Ergöçmen, D.; Goicoechea, J. M. *Organometallics* **2013**, *32*, 2234–2244.
- "An Asymmetrically Derivatized 1,2,3-Triphospholide: Synthesis and Reactivity of the 4-(2′-Pyridyl)-1,2,3-triphospholide Anion" Turbervill, R. S. P.; Goicoechea, J. M. *Inorg. Chem.* **2013**, *52*, 5527–5534.
- "Hydropnictination Reactions of Carbodiimides and Isocyanates with Protonated Heptaphosphide and Heptaarsenide Zintl Ions" Turbervill, R. S. P.; Goicoechea, J. M. *Eur. J. Inorg. Chem.* **2014**, *2014*, 1660–1668.

Publications of research not described in this thesis:

- "Transition Metal Complexes of Anionic N-Heterocyclic Dicarbene Ligands". Musgrave, R. A.; Turbervill, R. S. P.; Irwin, M.; Goicoechea, J. M. *Angew. Chem., Int. Ed.* **2012**, *51*, 10832–10835.

- “Group 12 Metal Complexes of N-Heterocyclic Ditopic Carbanionic Carbenes”. Waters, J. B.; Turbervill, R. S. P.; Goicoechea, J. M. *Organometallics* **2013**, *32*, 5190–5200.
- “‘Classical’ and ‘Abnormal’ Bonding in Tin (II) N-Heterocyclic Carbene Complexes”. Turbervill, R. S. P.; Goicoechea, J. M. *Aus. J. Chem.* **2013**, *66*, 1131–1137.
- “Iron(II) Complexes of Ditopic Carbanionic Carbenes”. Musgrave, R. A.; Turbervill, R. S. P.; Irwin, M.; Herchel, R.; Goicoechea, J. M. *Dalton Trans.* **2014**, *43*, 4335–4344.